

ALMA MATER STUDIORUM
UNIVERSITÀ DI BOLOGNA

FACOLTÀ DI SCIENZE MATEMATICHE FISICHE E NATURALI
Dipartimento di Astronomia

DOTTORATO DI RICERCA IN ASTRONOMIA
CICLO XXIV (2009-2011)

**Pulsating variable stars as tracers of
galactic structure and interaction
mechanisms**

Tesi di Dottorato
di
MARIA IDA MORETTI

COORDINATORE : **Prof. Lauro MOSCARDINI**
RELATORE : **Prof. Bruno MARANO**
CO-RELATORE : **Dott. Gisella CLEMENTINI**
CO-RELATORE : **Dott. Vincenzo RIPEPI**

Esame Finale Anno 2012

SCUOLA DI DOTTORATO IN SCIENZE MATEMATICHE, FISICHE E
ASTRONOMICHE

Settore Concorsuale: 02/C1 – Astronomia, Astrofisica, Fisica della Terra e dei Pianeti

Settore Scientifico-Disciplinare: FIS/05 – Astronomia e Astrofisica

Contents

Introduzione	3
1 Galaxy formation scenarios	7
1.1 Galaxy formation: Cold Dark Matter theory	7
1.2 Galactic formation	8
1.3 Dwarf Spheroidal galaxies	9
2 Variable stars as tools	13
2.1 Radially pulsating variable stars	14
2.2 δ Scuti and SX Phoenicis stars	15
2.3 RR Lyrae stars	17
2.3.1 Fourier Analysis of the RR Lyrae light curves	18
2.3.2 $M_V - [Fe/H]$ and PL relations for RR Lyrae stars	22
2.4 Classical Cepheid stars	26
2.5 Type II Cepheid stars	28
2.6 Anomalous Cepheid stars	30
3 “Ultra-faint” dwarf spheroidal galaxies	33
3.1 Leo IV	33
3.1.1 Observations and data reduction	34
3.1.2 Identification of variable stars	35
3.1.3 CMD, structure and distance to Leo IV	40
3.2 Hercules	41
3.3 Observations and Data Reduction	43
3.4 Variable Stars	45
3.4.1 Metallicity and reddening from the RR Lyrae stars	48

3.5	CMD, structure and distance	50
3.5.1	A new estimate of the distance to Hercules	53
4	The Magellanic System	59
4.1	The Magellanic System	59
4.2	Optical observations: microlensing surveys	62
4.2.1	EROS-2	64
4.2.2	OGLE III	64
4.3	VISTA telescope and surveys	66
4.4	The VMC survey	70
4.4.1	VMC observations	74
5	Data analysis, and first results for RR Lyrae stars from the VMC survey	81
5.1	Optical data for the LMC RR Lyrae and Cepheids	81
5.2	EROS-2 data in the SEP field: GRATIS analysis	84
5.3	Classification of the RR Lyrae stars	87
5.3.1	Identification of the pulsation mode with the Bailey diagram .	87
5.3.2	Determination of the Fourier parameters	89
5.3.3	Metallicity estimate for RR _{ab} stars	93
5.3.4	Metallicity estimate for the RR _c stars	93
5.4	Determination of the ⟨K _S ⟩ values	98
5.5	Period-Luminosity-metallicity relation	100
5.6	RR Lyrae stars in the 30 Dor region	111
6	First results for Classical Cepheids from the VMC survey	143
6.1	VMC data for the Cepheids	143
6.2	Classical Cepheids in the 30 Dor field	153
6.3	Zero point of the PW and PLC relations, and distance to the LMC .	158
6.3.1	Zero points from the parallax of Galactic Cepheids	158
6.3.2	Zero points from the IRSB Baade-Wesselink method	160
6.3.3	Zero points from the CORS Baade-Wesselink method	160
	Summary and Conclusions	163

Introduction

In the Λ Cold Dark Matter theory the Milky Way and, generally, all massive galaxies, formed at least the external parts, by accreting smaller galaxies. It is thus very important to understand whether, and how the nearby dwarf galaxies surrounding the Milky Way have contributed to the formation of the Galactic halo.

Among the Milky Way satellites are both dwarf irregular and dwarf spheroidal galaxies. The former are rich in gas, have surface brightness $\mu_V \leq 23$ mag arcsec $^{-2}$ and total masses $M_{tot} \leq 10^{10} M_\odot$. Dwarf spheroidal galaxies, instead, are gas-deficient and faint ($\mu_V \geq 22$ mag arcsec $^{-2}$), with mass $M_{tot} \sim 10^7 M_\odot$. The best example of dwarf Irregular satellites of the Milky Way are the Large and Small Magellanic Cloud. They also represent the nearest case of interacting systems. Among dwarf spheroidals are also the so-called “ultra-faint” dwarfs, recently discovered by the Sloan Digital Sky Survey (York et al., 2000). They have ($\mu_V \gtrsim 28$ mag arcsec $^{-2}$) and $M_{tot} \sim 10^7 M_\odot$. They are dark matter dominated and highly distorted in shape. They are among the best candidates of the “building block” of the Galactic halo. In the Milky Way most of the globular clusters hosting RR Lyrae stars divide in two distinct groups (Oosterhoff dichotomy, Oosterhoff 1939) depending on the average period of the fundamental mode RR Lyrae stars, and the relative proportions of fundamental mode and first overtone RR Lyrae stars. We expect the “true” building block candidates to exhibit as well such a dichotomy.

One probe of the structure, formation and evolution history of the Galactic halo is its variable stellar population. Several types of pulsating variable stars exist, all lying in an almost vertical region of the Herzprung-Russel diagram and sharing the same pulsation mechanism. Among them, the RR Lyrae stars trace the oldest stars, the Classical Cepheids trace the young stars, and the Anomalous Cepheids are intermediate-age tracers. Age differences among pulsating stars belonging to

the same stellar system correspond to differences in evolutionary phase, luminosity, pulsation properties, and geometrical distribution within the system. Using the variable stars is therefore possible to study the galaxy structure and get hits on the interaction with other systems (e. g. the Milky Way).

My PhD project has been focused on the study of the pulsating variable stars in two ultra-faint dwarf spheroidal satellites of the Milky Way, namely, Leo IV and Hercules; and in two fields of the Large Magellanic Cloud (namely, the Gaia South Ecliptic Pole calibration field, and the 30 Doradus region) that were repeatedly observed in the K_S band by the VISTA Magellanic Cloud (VMC, PI M.R. Cioni) survey of the Magellanic System.

Our first target has been the Leo IV ultra-faint galaxy. We have obtained the first V , $B - V$ color-magnitude diagram (CMD) of the Leo IV dwarf spheroidal, from B , V time-series photometry collected with the Isaac Newton Telescope, the William Hershel Telescope, and The Southern Astrophysical Research telescope. The CMD reaches about half a magnitude below the Leo IV turnoff, which we have detected at $V = 24.7$ mag. We have identified three fundamental mode RR Lyrae stars, and one SX Phoenicis variable in the galaxy. In the period-amplitude diagram the Leo IV RR Lyrae stars are located close to the loci of Oosterhoff type I systems and evolved fundamental-mode RR Lyrae stars in the Galactic globular cluster M3. However, their mean pulsation period suggests an Oosterhoff type II classification for this galaxy. The RR Lyrae stars trace very well the galaxy horizontal branch (HB), setting its average magnitude at $\langle V_{RR} \rangle = 21.48 \pm 0.03$ mag, and bringing to a distance estimate of 154 ± 5 kpc. One of the RR Lyrae star is located well outside the galaxy half-light radius, still it lies exactly on the HB in the color-magnitude diagram. We conclude that the star belongs to the Leo IV galaxy, and, with its very peripheral location shows that that Leo IV is elongated due to the tidal interaction with the Milky Way.

Hercules is the other ultra-faint dwarf galaxy we have studied in this PhD work. B , V time-series photometry of Hercules was obtained using a variety of different telescopes (the Isaac Newton Telescope, the William Hershell Telescope, the Liverpool Telescope, the Faulkes Telescope and the 2.2 m ESO/MPI telescope). We have identifying 9 RR Lyrae stars and 1 Anomalous Cepheid in Hercules. The average period of the fundamental mode RR Lyrae stars along with the V -band period-

amplitude diagram allow us to firmly classify Hercules as an Oosterhoff II system. We have obtained a color-magnitude diagram of the galaxy, reaching $V \sim 25$ mag, that shows the presence of a population as old and metal poor as the Galactic globular clusters M68 and M15. We also obtained the deepest color-magnitude of Hercules ever presented before, using Hubble Space Telescope (HST) archive data. The detection of an Anomalous Cepheid shows that Hercules hosts also an intermediate-age population component, confirming previous results on the galaxy star formation history. Also in Hercules, the distribution of the RR Lyrae stars suggests an elongated shape due to the interaction with the Milky Way.

Finally, the second part of the PhD thesis was focused on the analysis of RR Lyrae stars and Cepheids located in the South Ecliptic Pole (SEP) field, and in the 30 Doradus (30 Dor) region of the Large Magellanic Cloud, on the basis of infrared Y , J , K_S data obtained with the Visible and Infrared Survey Telescope for Astronomy (VISTA) in the context of the Magellanic Cloud survey VMC. We present the K_S -band light curves of the Classical Cepheids and RR Lyrae stars in SEP and 30 Dor fields, and discuss in detail the procedures that were developed in order to gain information on the distance and 3D-structure of the Magellanic Cloud System from the analysis of the RR Lyrae stars and Cepheids. The VMC K_S light curves of the RR Lyrae stars in the SEP and 30 Dor regions have good photometric quality, with typical errors for the individual data points between ~ 0.02 and 0.05 mag. The Cepheids have excellent light curves with typical errors of ~ 0.01 mag. The averaged K_S magnitudes derived for both types of variables were used to derive PLK_S (for the Cepheids) and $PLK_S Z$ (for the RR Lyrae) relations that are in good agreement and show a smaller scatter than found in previous studies. These relations were used to measure absolute distances to the two fields, thus allowing to show the potential and scientific impact that the VMC survey, once completed, will have on our knowledge of the structure of the Magellanic System.

This PhD thesis is organized as follow: Chapter 1 provides the scientific context of the present study. Chapter 2 gives information on the pulsating stars as tools to study the resolved stellar populations in galaxies. Chapter 3 describes the data analysis and results obtained from the study of the Leo IV and Hercules ultra-faint dwarfs. Chapters 5 and 6 summarize the work done on the RR Lyrae and Classical Cepheids in SEP and 30 Dor regions of the LMC. Conclusions and future

perspectives of the PhD thesis work are presented in Chapter 7.

Chapter 1

Galaxy formation scenarios

1.1 Galaxy formation: Cold Dark Matter theory

The Λ Cold Dark Matter theory (Λ CDM, Blumenthal et al. 1984) predicts that small structures cluster to form bigger objects (Davis et al., 1985). This is the so-called hierarchical model of the Universe. Observations are generally in agreement with the Λ CDM theory (Cole et al. 1994; Kauffmann et al. 1999), however, there are two important discrepancies that could compromise the validity of the Λ CDM paradigm:

- the problem of the cuspy galactic halos: the Λ CDM predictions bring to rotation curves of galactic halos that are more cuspy than observed (Kravtsov et al. 1998; Moore et al. 1999);
- the “missing satellites” problem: the CDM cosmological model predicts that massive galaxies such as the Milky Way (MW) should be surrounded by large numbers of dark matter dominated satellite halos. The relatively modest population of dwarf galaxies observed to surround the MW and the Andromeda (M31) galaxies seems to conflict with this prediction (Kauffmann et al. 1993).

These problems are strictly connected with the study of dwarf galaxies and in particular with the study of the dwarf spheroidal (dSph) (see section 1.3) satellites of the MW. For what concerns the missing dwarf problem, searching for new dSphs is fundamental to fill the gap between theory and observations. The MW Halo is better suited for this kind of search, as dSphs are faint, low surface brightness systems (see section 1.3), hence their detection is easier nearby. We will see in the next

sections that several studies support the accreting model for the building up of the external halo of the MW, in agreement with the CDM predictions.

1.2 Galactic formation

The detailed study of resolved stellar populations in the MW, and in nearby galaxies, is a powerful tool to better understand the processes that may have lead to the formation of the Galactic halo. In this context, the Local Group (see section 1.3) is used as a true laboratory to perform near-field cosmology.

In the second half of the twentieth century, Eggen et al. (1962) proposed the so called *monolithic scenario* for the formation of the Galactic halo: they suggested that the halo formed in a rapid free-fall collapse. Searle & Zinn (1978) pointed out discrepancies between the predictions of the monolithic scenario and the observations, and put forward the idea that the Galactic halo built over an extended period of time by merging of independent fragments.

Zinn (1980) describes as follows this process of *hierarchical accretion*:

“The clouds in the central zone merged to form a large gas cloud that later evolved into the Galactic disk. The clouds in the second zone evolved as isolated systems for various lengths of time up to ~ 5 Gyr, but, eventually, all these clouds collided with the disk and were destroyed. The clouds of the outermost zone have evolved in relative isolation until the present time, and have become the Magellanic Clouds and the dwarf spheroidal galaxies.”

The present picture is that the main body of the MW ($R_{gc} < 10$ kpc) was formed in a monolithic collapse (Sandage, 1990), whereas the region with $R_{gc} > 15$ kpc was mainly assembled by infall and capture of smaller fragments, as explained in the hierarchical model (Chiba & Beers 2000; van den Bergh & Mackey 2004). If this is the case, evidences of the assembling process should be seen in the properties of the halo stellar populations, at least in the outer halo, where the accreting model is supposed to dominate. As originally pointed out by Searl & Zinn, the best candidates for the small fragments that “built up” the external halo of the MW are the dwarf galaxies (see section 1.3). These galaxies are large in number and dSphs in particular are found around both the MW and M31 (despite their number is still lower than expected by the CDM theory).

A clear evidence supporting the merger assembling of the MW halo is the observation of the tidal streams of the Sagittarius galaxy (Ibata et al., 1994). This dSph has left a debris stream fully encircling our Galaxy (e.g. Ibata et al. 2001) and is currently contributing to the assembly of the Galactic halo with both stars and globular clusters (GCs). Like the Sagittarius dSph, also the Canis Major overdensity (Martin et al., 2004) is interacting with the MW and there are several Galactic GCs possibly associated with this system. The “Monoceros Ring” (Newberg et al. 2002; Yanny et al. 2003) is probably the tidal debris of a destroyed dwarf galaxy, whose nucleus lies towards the Canis Major dSph. Not only dSphs are important in this context; another excellent laboratory to study the interaction of galaxies is the system formed by the two Magellanic Clouds (MCs, see section 4.1), that represent the closest prototypes of interacting dwarf irregular galaxies.

A powerful probe of the extended structure of galaxies, their formation and evolution history is their population of variable stars. In this, pulsating stars like the RR Lyrae stars and the Cepheids (see Chapter 2), being excellent distance indicators, and probing old and young/intermediate ages, respectively, provide powerful tools to investigate interaction and merging processes in the MW and in its satellites.

1.3 Dwarf Spheroidal galaxies

As first stated by Hubble (1936), the Local Group (LG) is a small group of galaxies, isolated with respect to the field. Nowadays, we know that this kind of structure is very common in the Universe and this makes the LG an ideal laboratory to check the theory of galactic formation and evolution. The LG contains two big spirals: the MW and M31. Having comparable mass and luminosity they form two subsystems inside the LG. The centre of mass of the LG is situated between them, closer to M31. Another spiral is M33, while the only elliptical galaxy in the LG is M32, a satellite of M31. Among the irregular galaxies are the Large and Small Magellanic Clouds (LMC and SMC respectively; see section 4.1) both satellites of the MW. Despite a general agreement on the number of luminous galaxies that belong to the LG, the census of the dwarf galaxies is still an issue for two main reasons:

- the membership of some galaxies to the LG is still uncertain;

- not all dwarf galaxies of the LG are yet observed (Mateo, 1998). This claim was widely confirmed by the large numbers of new dwarfs discovered by the wide-field surveys of the MW and M31 halos started after 2000, as briefly described in the following.

Dwarf galaxies have $M_V \geq -18$ regardless of the morphological type (Grebel, 2005). The dSphs, in particular, are less luminous than $M_V \sim -11.0$, have surface brightness $\mu_V \geq 22$ mag arcsec 2 , and total mass $M \leq 10^7 M_\odot$. They are found all over the LG, being the dominant population by number. The dSph galaxies are among the darkest objects we know in the Universe, with mass-to-light ratios ranging from $M/L \sim 5$ to $M/L \sim 100$ for galaxies such as Draco and Ursa Minor (Mateo, 1998), respectively. If they are dominated by dark matter they could give a fundamental contribution to the mass of galaxy clusters, and perhaps of the entire Universe.

Before 2005, only 10 dSphs satellite galaxies of the MW were known: Draco, Ursa Minor, Fornax, Carina, Sculptor, LeoI, LeoII, Sextans, Sagittarius, and Canis Major (Mateo 1998; Ibata et al. 1995; Irwin & Hatzidimitriou 1995; Martin et al. 2004). Similarly, only 12 dwarf galaxies were known to be M31 companions until 2004, among which only 6 dSphs.

The MW dSphs, also referred to as “bright” or “classical” dSphs, generally are found to contain stars exhibiting different chemical compositions than the stars in the Galactic halo (e.g. Helmi et al. 2006). Also, when the pulsation properties of their RR Lyrae stars are considered, the classical dSphs do not conform to the subdivision into Oosterhoff types I (Oo I) and II (Oo II; Oosterhoff 1939) observed for field and cluster MW variables. Indeed, in the MW, GCs that contain significant numbers of RR Lyrae stars have fundamental-mode (RR_{ab}) pulsators with mean period ($\langle P_{ab} \rangle$) either around 0.55 days or around 0.65 days, and separate into the so called Oo I and Oo II types (Oosterhoff, 1939). Extragalactic GCs and field RR Lyrae stars in the bright dSphs surrounding the MW instead, generally have $\langle P_{ab} \rangle$ intermediate between the two Oosterhoff types, and are thus classified as “Oosterhoff-intermediate” (Catelan 2009 and references therein). These observational evidences suggest that it is unlikely that the halo of the MW was formed by accretion of objects with properties similar to the present-day “classical” dSphs.

The observations of the *Sloan Digital Sky Survey* (SDSS, York et al. 2000) started in 2005, and have covered so far more than one forth of the sky, centered

around the North Galactic Pole. The SDSS has produced detailed images and created 3-dimensional maps containing more than 930000 galaxies, and more than 120000 quasars. Among other things, the SDSS revolutionized the study of the LG dSphs as it allowed us to detect MW satellites that had not been recognized before because of their low surface brightness: $\mu_V \geq 28$ mag arcsec $^{-2}$ (Belokurov et al., 2007). Indeed, since 2005, 17 new faint dSph satellites of the MW have been discovered, primarily from the analysis of *SDSS* imaging: Willman I, Ursa Major I, Ursa Major II, Bootes I, Coma Berenices (Coma), Segue I, Canes Venatici I (CVn I), Canes Venatici II (CVn II), Leo IV, Hercules, Leo T, Bootes II, Leo V, Bootes III, Segue II, Pisces I and Pisces II (Willman et al. 2005a; Willman et al. 2005b; Zucker et al. 2006a; Zucker et al. 2006b; Grillmair 2006; Grillmair 2009; Belokurov et al. 2006; Belokurov et al. 2007; Belokurov et al. 2008; Belokurov et al. 2009; Irwin et al. 2007; Walsh et al. 2007; Belokurov et al. 2010). Similarly, around M31 19 new satellites were discovered in the last 5 - 6 years, mainly based on the INT and CFHT data (Richardson et al. 2011 and references therein) and, more recently, also from the analysis of the SDSS data (Slater et al. 2011; Bell et al. 2011). These new discoveries have reduced the discrepancy between number of dark matter halos predicted by the CDM theory, and number of dwarf satellites observed around the MW and M31 spirals.

The new MW dSphs are fainter than the previously known spheroidals, with typical surface brightness generally around 28 mag/arcsec 2 or fainter, hence they have been named “ultra-faint” dwarfs (UFDs). Bright dSphs and UFDs lie in two separate regions in the absolute magnitude versus half-light radius plane (see Fig. 3 of Clementini 2010) suggesting that they may belong to different categories of stellar systems. These faint galaxies have high mass-to-light ratios and often distorted morphologies, likely due to the tidal interaction with the MW. They all host an ancient stellar population with chemical properties similar to those of the stars in the external Galactic halo (Simon & Geha 2007; Kirby et al. 2008; Frebel et al. 2009). Several of the faint dSphs have mean metallicities as low or lower than the most metal-poor Galactic GCs and, generally, much lower than those of the classical dSphs. Six of the faint dSphs have been searched for variable stars so far (Bootes I, Dall’Ora et al. 2006; CVn I, Kuehn et al. 2008; CVn II, Greco et al. 2008; Coma, Musella et al. 2009; Leo IV, Moretti et al. 2009; and UMa II, Dall’Ora et al. 2012).

With the exception of only CVn I, all were found to contain RR Lyrae stars with properties resembling those of the MW OoII GCs. All the above characteristics suggest that a much larger population of systems, similar to the presently observed UFDs, may have been the “building blocks” of the halos of large galaxies such as the MW.

In the above framework, this PhD project developed along two main lines: (i) the study of the variable stars and stellar populations in two of the recently discovered “ultra-faint” dwarf spheroidal satellites of the MW, namely the Leo IV and the Hercules UFDs; and (2) the derivation of period luminosity relations in the K band (PL_K) for Cepheids, and PL_K - metallicity ($PL_K Z$) relations for RR Lyrae stars in two 1×1.5 degree² fields of the LMC, based on near-infrared photometry obtained by the VISTA ESO Public Survey on the Magellanic System (LMC, SMC & Bridge) - VMC, (PI: M.-R.L. Cioni, University of Hertfordshire - UK). We focused our attention on the structure of these objects being the deformation in shape a hint of interaction with the MW. The first line of research is part of a wider project aiming at the identification of the possible “building blocks” that contributed to the Galactic halo, by systematically investigating the pulsation properties of the new satellite of the MW, discovered by the *SDSS*. The second line of research is part of a large program aiming at the reconstruction of the 3D-structure of the system formed by LMC, SMC and Bridge between them. As the nearest large, metal-poor interacting satellites of MW the Magellanic Clouds represent in fact, optimal targets for the study of the environmental effects that large galaxies with satellites experience anywhere in the Universe.

Chapter 2

Variable stars as tools

In this Chapter we provide a brief description of the properties and potential of the pulsating variable stars as distance indicators and stellar population tracers.

We can define as *variable* a star that shows a variation in luminosity (ranging from a limit given by the instrument precision to few magnitudes) within a time interval that is small compared with the evolutionary time of that star. There are two main types of variable stars: intrinsic and extrinsic. The former show variability connected with internal physical phenomena, and include pulsating stars and supernovae. The latter show variability due to external causes and include, for example, eclipsing binaries and pulsars. Among the intrinsic periodic variables, an important role is played by the radially pulsating stars that periodically oscillate along a single dimension. They are used in this thesis work as a *tool* to trace the stellar populations and to study the 3-D distribution of stars inside a number of MW satellites. In particular, in this thesis we concentrate on the investigation of the two ultra-faint dSphs: LeoIV and Hercules, and of the Large Magellanic Cloud, our nearest dwarf irregular galaxy.

In the next section we summarize the properties of the classes of radially pulsating variable stars that are used in this thesis work as distance indicators and stellar population tracers.

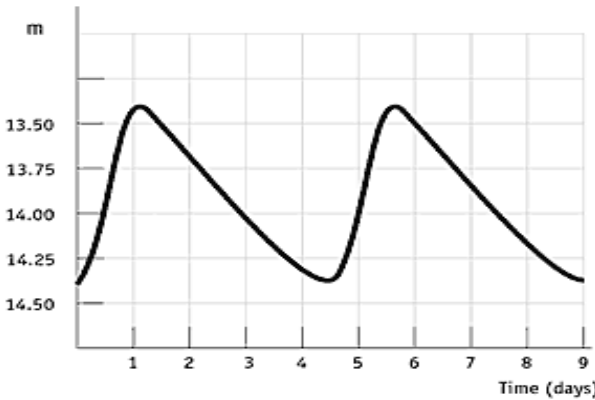


Figure 2.1: Schematic light curve of a Cepheid variable star.

2.1 Radially pulsating variable stars

Radially pulsating variable stars undergo periodic changes in radius and temperature that are responsible for the change in luminosity. The variation of the luminosity against time is called *light curve* (see Fig. 2.1). Often the variation of the luminosity is plotted against the phase of pulsation, defined as $\phi = (t - t_0)/P - \text{int}[(t - t_0)/P]$.

The characteristic time scale of pulsation is related to the stellar mean density according to the so-called period-density relation that can be derived by simple order of magnitude arguments. This ranges from seconds (for white dwarf structures) to hundred of days (for red giant stars). The most important pulsation observables are the period and the amplitude of the luminosity variation, that are both independent of uncertainties on distance and interstellar extinction, and therefore particularly useful, as we will discuss in the following. Since the pioneering paper by Zhevakin (1953), Eddington (1926) and Cox & Whitney (1958), it has become clear that the pulsation mechanism is related to variations of the opacity (the so called κ mechanism) and the adiabatic exponent in the ionization regions of the most abundant elements in the stellar envelopes, namely H, He and He+. As the driving mechanisms of pulsation are active in these external layers, the inner structure is not involved and can be neglected in pulsating models (King & Cox 1968 and references therein).

Radially pulsating stars share this driving mechanism, as demonstrated by the

occurrence of the so-called instability strip, the almost vertical region in the HR diagram where most of the pulsators are located (see Fig. 2.2)

As shown in Fig. 2.2, stars in different evolutionary phases cross the Instability Strip at different luminosity levels so that their observations in Galactic and extra-galactic resolved systems allow us to trace stellar populations of different ages.

In particular: RR Lyrae and Type II Cepheids (*W Virginis stars* in Fig. 2.2) trace the oldest stars ($t > 10$ Gyrs); the Anomalous Cepheids (ACs) trace the intermediate-age population ($\sim 1\text{-}5$ Gyrs); the Classical Cepheids (CC) and δ Scuti stars are the youngest among the radially pulsating variables (50-200 Myrs). Table 2.1 summarizes the main properties of the most known classes of pulsating variable stars.

The quoted period-density relation is at the basis of the use of variable stars as population tracers. Indeed, by combining it with the Stephan Boltzman law, one obtains a relation connecting the period to the mass, the luminosity and the effective temperature, as the one first derived by van Albada & Baker (1971) for RR Lyrae stars. This kind of relations are of crucial importance because they establish a link between the period information and the evolutionary parameters, that in turn are related to age and chemical composition. Moreover, if the mass and the luminosity are related to each other, as for Classical Cepheids, this relation becomes a period-luminosity-color relation that can be used to infer the intrinsic luminosity of each pulsator of known period and color. Neglecting the color dependence, or averaging over the color extension, a statistical period-luminosity relation is obtained. Such a relation for Classical Cepheids is at the basis of the absolute extragalactic distance scale and of the estimate of the Hubble constant by the Hubble Space Telescope Key Project (Freedman et al. 2001) and the Supernova Project (Saha et al. 2001).

2.2 δ Scuti and SX Phoenicis stars

SX Phoenicis are stars with masses in the range $1.5 < M/M_{\odot} < 2.5$ that enter the lower part of the *Instability Strip* either in their core hydrogen burning phase or when they move towards the sub-giant branch during their shell-hydrogen burning phase. Their oscillation periods are in the range $0.02 < P < 0.25$ d, with amplitudes of the order of ~ 0.1 mag in the V band. These variables are the so-called δ Scuti (δ Sct) stars if they are metal rich ($Z > 0.01$) or SX Phoenicis (SX Phe) stars if they are

Type	Period (day)	$\langle M_V \rangle$ (mag)	A_V (mag)	Spectral Type	Pop.	Evol. Phase
δ Scuti	≤ 0.02	$2 \div 3$	≤ 0.5	A-F	I	MS
SX Phoenicis	≤ 0.1	$2 \div 3$	< 1.5	A-F	II	MS
RR Lyrae ab-type	$0.45 \div 1$	$0.0 \div 1.0$	$\geq 0.6 \div 1$	A2-F2	II	HB
RR Lyrae c-type	≤ 0.4	$0.0 \div 1.0$	$0.4 \div 0.6$	A2-F2	II	HB
Anomalous Ceph.s	$0.3 \div 2$	$-2 \div 0$	< 1.5	A-F	?	HB?
W Virginis	$10 \div 50$	$-3 \div -1$	< 1.5	F2-G6(?)	II	post-HB
BL Herculis	$2 \div 10$	$-1 \div 0$	≤ 1.5	F2-G6(?)	II	post-HB
Classical Ceph.s	$1 \div 100$	$-7 \div -2$	≤ 1.5	F6-K2	I	blue loop

Table 2.1: Main pulsation and evolutionary properties of variable stars in the *Instability Strip*.

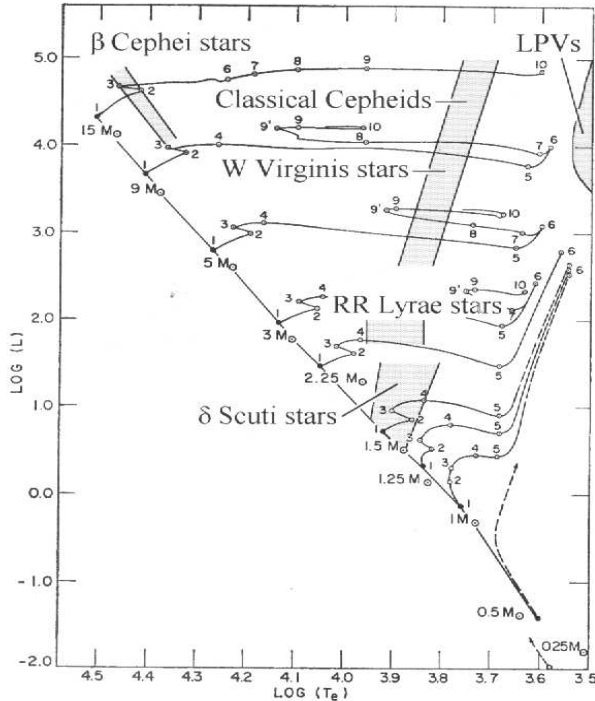


Figure 2.2: Locus of the color magnitude diagram in which lie pulsating variable stars: *Instability Strip*.

metal poor ($Z < 6 \times 10^{-3}$). In the Milky Way there is a physical distinction between δ Sct and SX Phe: the δ Scuti are Population I (Pop. I) stars, while the SX Phoenicis trace the metal poor Population II (Pop. II) stars. Amplitudes of the Pop. I stars can vary from a few 0.001 mag to several 0.1 mag. Even if high-amplitude δ Sct (HADS) stars are generally radial pulsators, several of these variables also exhibit non-radial modes (Poretti, 2003). In similar way, SX Phe stars show a mixture of modes, especially those found in GCs. Therefore, the separation between HADS and SX Phe stars is not easy if no information on the metal abundance is available. Since the light curves of both HADS and SX Phe stars are asymmetrical and resemble those of the Classical Cepheids, and since these variables too do obey to a Period-Luminosity relation, it quite common to group both HADS and SX Phe stars under the common term “Dwarf Cepheids”. Since these variables obey a *PL* relation they can be utilized as standard candles to find distances. Given their intrinsic faintness and the short time scale of their variations, the known samples of δ Scuti stars almost all belong to the Milky Way (Nemec et al. 1994; Rodríguez & López-González 2000) and only few of these variables have been identified in systems external to the Milky Way (Clementini et al. 2003, Di Fabrizio et al. 2005, Kaluzny et al. 2006) and used by McNamara et al. (2007) to define the *PL* relation of the LMC Dwarf Cepheids. Finally, about 90 SX Phe variables have been found in the Fornax dSph galaxy (Poretti et al., 2008).

2.3 RR Lyrae stars

RR Lyrae stars are old ($t > 10$ Gyrs), low mass stars ($M \sim 1M_{\odot}$) during the core Helium burning phase corresponding to the Horizontal Branch (HB) sequence in the H-R diagram. They are among the oldest objects in the Universe.

The prototype star RR Lyr was discovered in 1899 by Williamina Fleming and in the following years a significant number of these pulsators were observed in globular clusters by Bailey, who classified them on the basis of the period and the light curve shape. In particular, the shape of the light curve allows us to divide the RR Lyrae stars into *ab*-type (RR_{ab}), with asymmetric light curves and amplitude decreasing as the period increases from ~ 0.45 to ~ 1 d, and *c*-type (RR_c) with amplitude A_V ranging from 0.2 to 0.6 mag, sinusoidal light curves, and period ranging from ~ 0.2

to ~ 0.4 d. The theory of stellar pulsation has explained the two types as pulsating in the fundamental mode (RR_{ab}) and in the first overtone mode (RR_c). Some RR Lyrae stars show pulsation in both modes and they are called *double mode* or RR_d . These are particularly useful to obtain independent estimates of the stellar mass (Petersen 1973; Bono et al. 1996; Bragaglia et al. 2001).

2.3.1 Fourier Analysis of the RR Lyrae light curves

According to Simon & Teays (1982), the light curve of an RR Lyrae star can be approximated with a Fourier function of the form:

$$m(t) = A_0 + \sum_{i=1}^N A_i \cos[i\omega_0(t - t_0) + \phi_i] \quad (2.1)$$

where $m(t)$ is the star apparent magnitude at time t , A_0 is the average magnitude, N is the number of fitted terms, ω_0 is the angular pulsation frequency of the star ($\omega_0 = 2\pi/P_0$), t is the time of observation, t_0 is the time of maximum light, and A_i and ϕ_i are the amplitude and phase coefficients of the individual Fourier terms. The Fourier analysis of the light curve can be used to classify the RR Lyrae stars, using the A_1 , A_2 amplitudes and the ϕ_{21} , ϕ_{31} phases of the Fourier decomposition (see e.g., Simon & Teays 1982, Cacciari et al. 2005). The Fourier analysis is also used to infer properties of the RR Lyrae stars such as the metal abundance [Fe/H]. In the last thirty years a number of studies on this specific subject have appeared in the literature (see e.g., Jurcsik & Kovács 1996, hereafter JK96, Kovács & Walker 2001, Morgan et al. 2007). In particular, JK96 derived a relation between the Fourier parameter ϕ_{31} ¹ of the V -band light curve, the period, and the metallicity of an *ab*-type RR Lyrae star:

$$[\text{Fe}/\text{H}] = -5.038 - 5.394P + 1.345\phi_{31}. \quad (2.2)$$

that can be used to infer the star metallicity when a spectroscopic measurement is not available, provided that the pulsation period and the V -band light curve of the star are known. In this thesis work we have extensively used JK96 method to estimate the metallicity of the RR Lyrae stars. Therefore, in the following we discuss this relation and its calibration in different metallicity scale in detail. JK96

¹ $\phi_{ij} = j\phi_i - i\phi_j$

introduced the so-called *compatibility condition*: $D_m^2 < 3$, that the star light curve must satisfy, in order to have a reliable estimate of [Fe/H]. However, they also note, that this condition might be too strict, and even for stars with a larger D_m values it may be possible to obtain reliable results. Cacciari et al. (2005) for example, adopt a relaxed compatibility condition, and find that a maximum value of 5 for D_m allows to increase the statistic without changing the results. Kapakos et al. (2011) find that the criterion $D_m < 3$ cannot lead to a robust sample of RR_{ab} stars without taking into consideration the σ_{D_m} . Thus they used RR Lyrae stars with $\sigma_{D_m} < 3$ and $D_m - \sigma_{D_m} < 3$ in their analysis. Di Fabrizio et al. (2005) used the Fourier parameter technique to estimate metallicities for 29 ab-type RR Lyrae stars in two areas close to the bar of the LMC. They compared the “photometric” metallicities derived with this technique with spectroscopic metal abundances derived for the stars by Gratton et al. (2004). They find that the average difference between photometric and spectroscopic metallicities is 0.30 ± 0.07 dex, with the photometric abundances being larger due to differences in the metallicity scales used by “photometric” and spectroscopic techniques (see discussion below).

Morgan et al. (2007) found a relation between [Fe/H], ϕ_{31} and P that holds for first overtone pulsators, by using c-type RR Lyrae stars in a number of Galactic globular clusters:

$$[Fe/H]_{ZW} = 52.466P^2 - 30.075P + 0.131\phi_{31}^2 + 0.982\phi_{31} - 4.198\phi_{31}P + 2.424 \quad (2.3)$$

with a standard deviation of 0.145 dex.

In conclusion, while the spectroscopic metallicities are, in general, to be preferred, the Fourier parameters can be used to infer the mean metallicity of a sample of RR Lyrae stars when the spectroscopic analysis is not feasible. An important issue is the metallicity scale on which the JK96 relation measures the metal abundance. Eq. 2.2 connects the Fourier parameters with metallicity estimates in the Jurcsik (1995, hereafter J95) metallicity scale. J95 metallicity scale is valid both for GCs and field RR Lyrae stars, and is defined by the following relation:

$$[Fe/H]_{J95} = -0.190(\pm 0.007)\Delta S + 0.027(\pm 0.052) \quad (2.4)$$

² $D_F = |F_{obs} - F_{calc}|/\sigma_F$ where F_{obs} is the observed value of the given Fourier parameter, F_{calc} is its predicted value from the other observed parameters, σ_F is the respective standard deviation as listed in Table 6 of JK96. D_m is the maximum of the deviation parameters $\{D_F\}$.

where ΔS is the Preston (1959) index, defined as the difference in tenths of spectral class between the spectral type of an *ab* type RR Lyrae variable at minimum light, estimated from the hydrogen lines [Sp(H)], and that estimated from the intensity of the CaII *K* line [Sp(K)]:

$$\Delta S = 10[Sp(H) - Sp(K)]. \quad (2.5)$$

J95 also gives a linear relation to transform her metallicities to the Zinn & West (1984, hereafter ZW) metallicity scale, which is valid for objects with $[Fe/H]_{ZW} < -1.0$:

$$[Fe/H]_{J95} = 1.431(\pm 0.006)[Fe/H]_{ZW} + 0.880(\pm 0.010). \quad (2.6)$$

Eq. 2.6 can be used to transform the photometric [Fe/H] estimates, obtained with Eq. 2.2, from the J95 to the ZW metallicity scale. More recently, Carretta et al. (2009; hereafter C09) have defined a new metallicity scale based on high resolution spectroscopy abundances, and have provided relations to convert the ZW metallicities to their new metallicity scale:

$$[Fe/H]_{C09} = (-0.413 \pm 0.027) + (0.130 \pm 0.289)[Fe/H]_{ZW} - (0.356 \pm 0.108)[Fe/H]_{ZW}^2 \quad (2.7)$$

that has a $\sigma = 0.119$ dex. Kapakos et al. (2011) found a relation (their eq. 3) that links directly the JK96 and C09 metallicities:

$$[Fe/H]_{C09} = (1.001 \pm 0.0050)[Fe/H]_{JK96} - (0.112 \pm 0.077). \quad (2.8)$$

this relation is valid in the range from -2.31 dex to -0.68 dex on the JK96 scale. Fig. 2.3 shows the [Fe/H] in C09 scale obtained using the two different procedures based on Eqs. 2.6, eq:fromZWtoC09, and Eq. 2.8. Points that are well within the region of validity of both Eq. 2.8 and Eq. 2.6 (black points) lie perfectly on the unity line, indicating that the two methods are in perfect agreement. Points outside this interval are marked with different colours. Red points correspond to objects that have $[Fe/H]_{JK96}$ values outside the region of validity of Eq. 2.8. Yellow points correspond to objects that have $[Fe/H]_{ZW84}$ values obtained by inverting Eq. 2.6, outside its interval of validity. Fig. 2.3 also shows that the errors obtained using Kapakos et al. (2011) direct transformation to the ZW scale are smaller than those obtained through the double transformation from J95 to ZW, and from ZW to C09 scales.

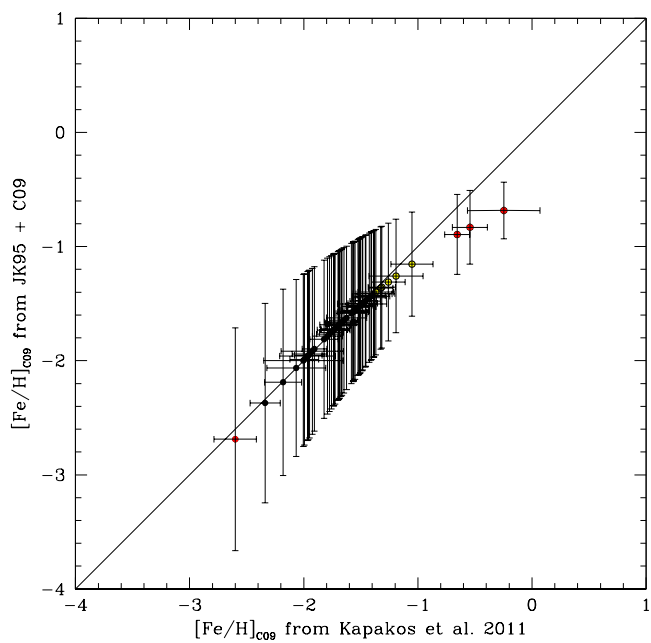


Figure 2.3: Metallicities in C09 scale obtained with different methods (cfr. text). Red and yellow points are values outside the interval of validity of relations 2.8 and 2.6, respectively. The black line is the unity line.

2.3.2 M_V -[Fe/H] and PL relations for RR Lyrae stars

For RR Lyrae stars, the visual absolute magnitude does not vary significantly with the period, because these variables belong the horizontal branch, but has been found and predicted to depend on metallicity according to the relation (Sandage 1981a,b):

$$M_V(RR) = \alpha \times [Fe/H] + \beta. \quad (2.9)$$

In the past decades several authors studied this relation using different methods, including synthetic Horizontal Branch models (Lee et al., 1994) and the Baade-Wesselink method (Fernley et al., 1998). A robust value for the slope α was derived by Clementini et al. (2003) and Gratton et al. (2004), using more than a hundred RR Lyrae stars in the LMC: $\alpha = 0.214 \pm 0.047$ mag/dex. Many estimates of the zero point β can be found in the literature. Cacciari & Clementini (2003) found $\beta = 0.59 \pm 0.03$ for $[F/H]=-1.5$ dex; $\beta = 0.56 \pm 0.09$ for $[Fe/H]=-1.5$ dex, was found by Clementini et al. (2003) on the basis of their distance modulus of the LMC of 18.52 ± 0.09 mag; more recently, Benedict et al. (2011) derived $\beta = 0.45 \pm 0.05$ for $[Fe/H]=-1.5$ dex using HST parallax as for 5 RR Lyrae stars, and adopting the slope by Gratton et al. (2004). The systematic differences up to 0.10-0.15 mag in the zero points derived by different authors remain a major problem in the use of the M_V -[Fe/H] relation.

On the other hand, the dependence of the $V - K$ color on the effective temperature leads to the occurrence of a Period-Luminosity (PL) relation in the K band. This relation is a very promising tool to infer distances because in the near infrared (NIR) bands the effects of reddening and, possibly, metallicity are significantly reduced and the pulsation amplitudes are smaller, allowing us to derive mean magnitudes even from a reduced number of phase points.

Several authors studied this tool both from a theoretical and an observational point of view. Longmore et al. (1986) pioneering work was followed by Liu & Janes (1990), Jones et al. (1996) and Skillen et al. (1993) and a comprehensive analysis of the IR properties of RR Lyrae stars was given by Nemec et al. (1994). From the pulsation theory side, the PL_K properties have been studied by Bono et al. (2001):

$$M_K = 0.139 - 2.071 \times (\log P + 0.30) + 0.167 \times \log Z \quad (2.10)$$

where Z is in the range 0.0001 to 0.006, and by Bono et al. (2003)

$$M_K^F = -0.770(\pm 0.044) - 2.101 \times \log P + 0.231(\pm 0.012) \times [Fe/H]. \quad (2.11)$$

Cassisi et al. (2004) and Catelan et al. (2004) provide evolutionary calibrations of the PL_K relations with slopes and zero-points that vary with the HB morphology type (according to Lee et al. 1994) and with the metallicity.

The PL_K relation was used to infer distance estimates for the Reticulum globular cluster in the LMC (Dall’Ora et al. 2004, Sollima et al. 2006), several Galactic Globular Clusters (Sollima et al. 2006, Coppola et al. 2011), and few fields near the bar of the LMC (Szewczyk et al. 2008, Borissova et al. 2009). As an example we show in Fig. 2.4 (left panel) the empirical relation found by Dall’Ora et al. (2004). It is a very well defined relation for which a linear regression gives:

$$\langle K \rangle = -2.16(\pm 0.09) \times \log P + 17.352(\pm 0.025), \quad (2.12)$$

with a rms of only 0.03 mag.

This is a remarkable result for a standard candle. Using the Eq. 2.11 from Bono et al. (2003), they found a distance estimate for the Reticulum cluster of $\mu_0 = 18.52 \pm 0.005(\text{random}) \pm 0.117(\text{systematic})$ where the error is dominated by the systematic uncertainty affecting the absolute zero-point calibration and the metallicity scale. Similar results are found in other GCs. The right panel of Fig. 2.4 shows an analogous work done by Coppola et al. (2011) for the Galactic GC M5. The linear regression (blue line in Fig. 2.4) is :

$$\langle K \rangle = -2.33(\pm 0.08) \times \log P + 13.28(\pm 0.02), \quad (2.13)$$

with a rms of 0.05 mag. Averaging results coming from the above mentioned theoretical (Bono et al. 2001, Bono et al. 2003, Cassisi et al. 2004, Catelan et al. 2004) and empirical (Sollima et al., 2006) calibrations, they infer a distance estimate for M5 of $\mu_0 = (14.44 \pm 0.02)$ mag.

The extension of this method to RR Lyrae in the LMC is of particular interest because the distance to the LMC is a cornerstone of the extragalactic distance scale. Indeed the two *Hubble Space Telescope (HST)* projects focused on the cosmic distance scale, namely the Key Project (Freedman et al. 2001) and the SNIa project (Saha et al. 2001) assume a distance modulus of the LMC (18.5 mag) and the

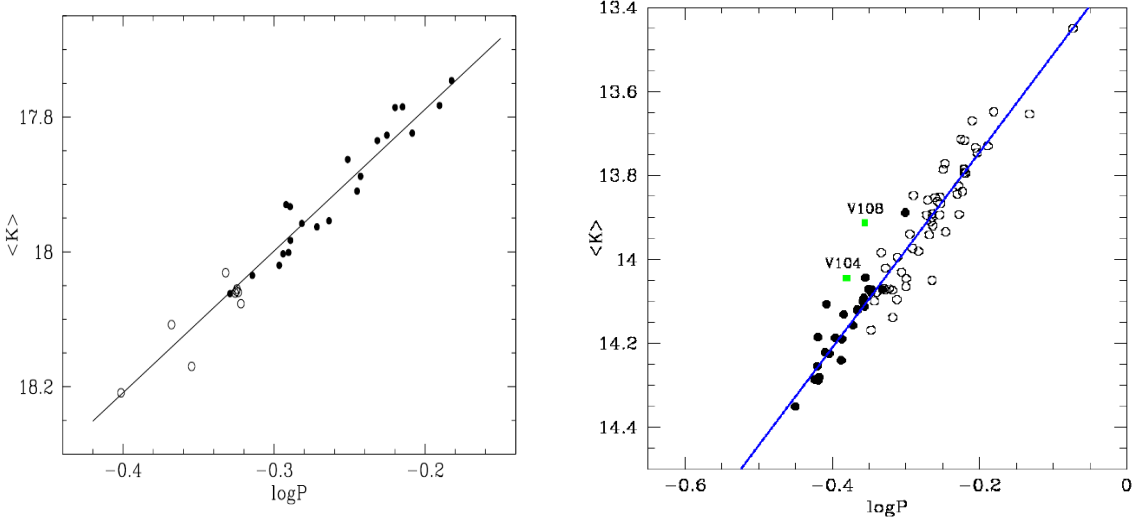


Figure 2.4: *Left:* PL_K relation obtained by Dall’Ora et al. (2004) in the LMC cluster Reticulum. Filled and empty circles correspond to RR_{ab} and RR_c stars, respectively. *Right:* PL_K relation obtained by Coppola et al. (2011) in the Galactic GC M5. Filled and empty circles correspond to RR_c and RR_{ab} stars, respectively. Green points correspond to overluminous stars 3σ outside the linear regression (blue line).

universality of the slope of LMC Cepheid optical PL relations. But there is still a non negligible discrepancy among modern distance determinations to the LMC from different methods (e.g. Benedict et al. 2002; Molinaro et al. 2012 and references therein). Most recent distance determinations to the LMC have clustered around the value of 18.5 mag that was adopted by the Key Project. However, a shorter LMC distance modulus (closer to 18.4 mag) has been obtained for example on the basis of recent exhaustive distance determinations of Galactic Cepheids from the IR surface brightness technique (Fouqué et al., 2007).

Szewczyk et al. (2008) applied the RR Lyrae PL_K relation to five fields of the LMC, and their investigation represents a promising step toward a resolution of the distance discrepancy. Szewczyk et al. (2008) obtain a distance estimate of the LMC corresponding to $\mu = 18.58 \pm 0.03(\text{statistical}) \pm 0.11(\text{systematic})$ mag, where the systematic error takes into account the errors associated with the adopted calibrations, mean metallicity, photometric zero point and absorption correction. Borissova et al. (2009) combined NIR photometry and spectroscopically measured metallicities for 50 RR Lyrae stars in the LMC and found that the metallicity dependence of the

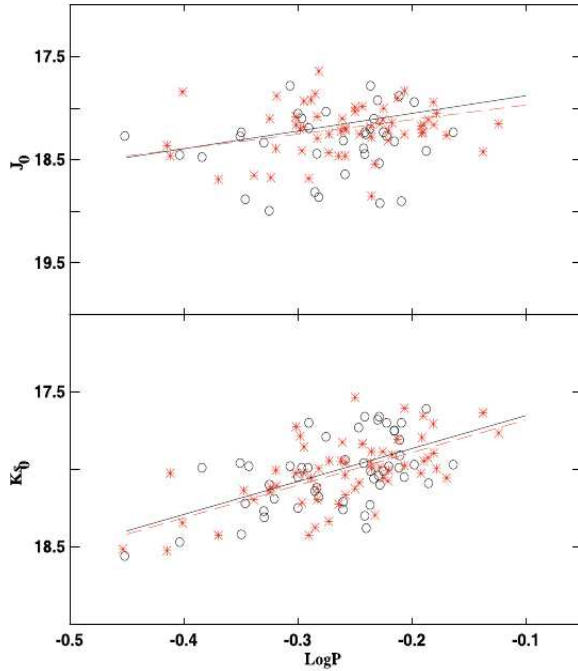


Figure 2.5: Infrared J (upper panel) and K (lower panel) PL relation for RR Lyrae in the LMC. Empty circles correspond to RR Lyrae observed by Borissova et al. (2009); red asterisks are data from Szewczyk et al. (2008). Figure from Borissova et al. (2009).

NIR PL relation is really small:

$$M_{K_s} = 2.11(\pm 0.17) \times \log P + 0.05(\pm 0.07) \times [Fe/H] - 1.05. \quad (2.14)$$

They obtained an estimate of the LMC distance of $\mu_0 = 18.53 \pm 0.13$ mag. Fig 2.5 shows the relation provided by Borissova et al. (2009) combining their data with those by Szewczyk et al. (2008). Comparing Fig. 2.5 with Fig. 2.4, it is clear that the dispersion is significantly larger in the case of LMC field observations. This could suggest that, even if small, the contribution of the metallicity should be taken into account, and/or that there is a depth effect. As already mentioned, differential reddening should not be important in these bands.

The above mentioned studies provided an increasing knowledge of the $PL_K Z$ relation as distance indicator tool. Still, they are based on small samples. A systematic and homogeneous analysis on a wider area is of crucial importance to fully appreciate the capability of such relation. In this context the VMC survey (see section

4.4) will provide to the astronomical community an unprecedented huge amount of K band data that will cast new light on the potential of the PLK_Z relation.

2.4 Classical Cepheid stars

Cepheids are high-luminosity ($-2 > M_V > -7$), radially pulsating variable stars, with periods ranging from 1 to 100 days, and commonly associated with relatively young stellar populations, such as those found in open clusters, disk of spiral galaxies or in irregular galaxies. Their presence in star clusters allow their ages to be estimated, with inferred values up to about $\sim 10^8$ yr. From the stellar evolution point of view, these variables are intermediate-mass ($3 - 12 M_\odot$) stars that cross the instability strip during the helium burning phase. In particular, after the quiescent ignition of He in the core (3α reaction), these stars may make an excursion toward higher effective temperature and, subsequently, come back toward the asymptotic giant branch in the HR diagram. This “loop” may extend to sufficiently high temperature (or blue color) to intersect the instability strip in which case the stars become Classical Cepheids. Their high intrinsic brightness makes them ideal distance indicators on Galactic and extragalactic scales. Indeed, from the space they are observable up to distances of 20-30 Mpc (see e.g. Freedman et al. 2001). The close relationship between period and luminosity which was found by Henrietta S. Leavitt in 1912, has given Classical Cepheids an unique role in establishing the distances to the near galaxies, and hence the distance scale of the Universe. On this basis they provide the absolute calibration of important secondary distance indicators, such as the maximum luminosity of supernovae Ia, the Tully-Fisher relation, surface brightness fluctuations, and the planetary nebulae luminosity function, that are able to reach cosmological distances and in turn to provide an estimate of the Hubble constant (Freedman et al. 2001; Saha et al. 2001). A very debated issue is the universality of the period-luminosity relation and, in particular, the effect of the metallicity on its coefficients, because any systematic error affecting the Cepheid period-luminosity is expected to have relevant consequences on the extragalactic distance scale and on the resulting estimate of the Hubble constant. Cepheids are also good tracers of intermediate mass stars in the Galactic disk (Kraft & Schmidt 1963, Matsunaga et al. 2011), and star-forming regions in extragalactic systems (Elmegreen & Efremov

1996; Efremov 2003; Meschin et al. 2009).

The use of Cepheids as tracers of young stellar populations was supplemented by the evidence that if these objects obey to a PL relation, and to a Mass-Luminosity relation, they also obey to a Period-Age relation. In particular, an increase in period implies an increase in luminosity, i. e., an increase in the stellar mass, and in turn a decrease in the Cepheid age. Therefore they can also be considered age indicators (Bono et al. 2005; Marconi et al. 2006).

PL for Classical Cepheid stars

Henrietta Swan Leavitt (1868-1921) discovered 2400 Classical Cepheids, most of them are located in the Small Magellanic Cloud (cfr. section 4.1). She noted that more luminous Cepheids had longer pulsation cycles, and plotted the apparent magnitudes of these stars against their periods. The resulting plot demonstrated that the apparent magnitude of Classical Cepheids is closely correlated with their period (Leavitt & Pickering, 1912). In 1955 the periods of 550 classical Cepheids in the LMC were published (see Shapley & McKibben Nail 1955). Then a considerable survey for LMC Cepheids was done by Woolley et al. (1962). The catalogue prepared by Payne-Gaposchkin (1971) on the basis of Harvard photographic plates contained about 1100 Cepheids in the LMC. After these early works, several studies succeeded during the last decades of the past century (Freedman & Madore 1990; Madore & Freedman 1991; Laney & Stobie 1994); but the situation really changed when very large catalogs of Cepheids were published as a by-product of the gravitational microlensing surveys: EROS (Beaulieu et al. 1995; see section 4.2.1), MACHO (Welch et al., 1997) and OGLE-II (Udalski et al. 1999; see section 4.2.2). Thanks to these microlensing projects and to infrared surveys such as 2-MASS (Skrutskie et al., 2006) and DENIS (Epchtein et al., 1999), it became possible to begin studying Classical Cepheids on a really statistically significant way (e.g. Groenewegen 2000).

As already stated, the physical basis of Cepheid PL relation is related to the period-density relation coupled with the Stephan-Boltzman law, with the assumption of the mass-luminosity relation predicted by stellar evolution for intermediate mass stars in the central He burning phase. The PL relation for Classical Cepheids is a 2-dimensional projection of the higher-order Period-Luminosity-Color (PLC) relation (Madore & Freedman, 2012). The PLC relation, in turn, is a finite por-

tion of a plane, a so-called strip, embedded in the 3-dimensional space of period, luminosity, and color. It is well known that the intrinsic width of the Cepheid P-L relation decreases as a function of increasing wavelength (e. g. Madore & Freedman 1991; McGonegal et al. 1982; Caputo et al. 2000a). Furthermore, in the infrared bands the reddening becomes less important and the effect of metallicity on the PL seems to be smaller (Groenewegen & Oudmaijer 2000; Caputo et al. 2000a; Marconi et al. 2005).

It is of paramount importance to systematically study the PL_K relation in several different regions of the LMC, not only to improve our knowledge of the distribution of the young stellar component in this galaxy, but also and mainly to check the distance determinations for the LMC, which is the fundamental first step of the cosmological distance ladder. The VMC survey (see section 4.4) with an unprecedented sensitivity and sky coverage will allow us to perform this systematic study over the entire Magellanic Cloud System.

2.5 Type II Cepheid stars

Type II Cepheids originate from hot, low mass stellar structures that started the main central He burning phase on the blue side of the RR Lyrae gap and now evolve toward the asymptotic giant branch crossing the pulsation region with luminosity and effective temperature that increases and decreases, respectively, while decreasing the mass (e.g. Di Criscienzo et al. 2007; Wallerstein 2002). They are believed to be the immediate progeny of low mass HB stars ($M \sim 0.53M_{\odot}$), but with mass still large enough to reach the AGB stage, i.e., blue HB stars. This is supported both by observations, which show that type II Cepheids are present only when a sizeable blue HB component is also present (Wallerstein 1970; Smith & Wehlau 1985; Clement et al. 2001), apparently independently of metallicity (Pritzl et al., 2002), and by theoretical models (Schwarzschild & Harm 1970; Gingold 1976; Marconi & Di Criscienzo 2007 and references therein). Accordingly, detection of type II Cepheids should immediately implies the presence of a sizeable blue HB component.

These pulsating variable stars consist of two subclasses in different evolutionary stages, namely, the BL Herculis (BL Her) and the W Virgins (W Vir). Their evolutionary status can be summarized as follows: stars on the horizontal branch, bluer

than the RR Lyrae gap, evolve toward higher luminosity and larger radius (just like stars leaving the main sequence) as they finish the helium in their cores. In doing so they cross the instability strip at a luminosity that corresponds to a period between roughly 1 and 5 days. This accounts for the short-period group, namely, the BL Her of low metallicity. The origin of BL Her of near-solar metallicity remains uncertain, since they are likely to originate from the red horizontal branch. After reaching the AGB they advance to higher luminosity and begin to suffer helium shell flashes, which cause the star to make an excursion into the instability strip. The luminosity at which this occurs results in stars having periods between 12 and about 20 days. These are the so called W Vir variable stars. The paucity of Type II Cepheids with periods between 5 and 12 days, especially in the GCs, can be understood as the lack of shell flashes until the star's luminosity reaches the value which corresponds to a 12 day period.

PL for Type II Cepheid stars

Until the mid of the 20th century astronomers were not aware that there exist two types of Cepheid variables. Only after the famous distance scale revision done by Baade (1952), it became clear that Population I and II Cepheids follow different period-luminosity relations. On average, type II Cepheids are about 1.5 mag fainter than Classical Cepheids of the same periods. As summarized by Di Criscienzo et al. (2007), Nemec et al. (1994) derived metal-dependent period-luminosity relations in various photometric bands, suggesting that the Type II Cepheids pulsate either in the fundamental or in the first overtone mode, and that the slopes of the *PL* relations are significantly different for the two modes. On the other hand, on the basis of a sample of Type II Cepheids identified in the OGLE-II variable star catalogue for the Galactic bulge fields, Kubiak & Udalski (2003) found that all the observed stars, which have period from ~ 0.7 to about 10 days, follow the same *PL* relation. Similar results were derived by Pritzl et al. (2003) and Matsunaga et al. (2006) for Type II Cepheids in Galactic GCs. Furthermore, these last two studies support the hypothesis that the same *PL* relation holds for BL Her and W Vir stars, without a steepening of the slope for periods longer than $P \sim 10$ days, as earlier suggested by McNamara (1995). More recently, Soszyński et al. (2008b) published a catalogue of 197 Type II Cepheids in the LMC. The sample consists of 64 BL Her, 96 W vir

stars and 37 RV Tau stars. This is the largest sample of such type of variable stars detected anywhere outside the MW. They present V, I, W_I PL relations for the stars that are very important benchmarks for future work. They also notice a significant difference in $(V - I)$ colors among BL Her and W Vir stars, although a subset of their W Vir stars had, on average, colors similar to the BL Her stars.

2.6 Anomalous Cepheid stars

Anomalous Cepheids (ACs) are metal-poor-He-burning stars in the post-turnover portion of the Zero Age Horizontal Branch (ZAHB) evolutionary phase (Bono et al. 1997; Caputo 1998). They have periods between 0.30 d and 2.0 d, and are intrinsically brighter than RR Lyrae stars (between ~ 0.5 mag and ~ 2 mag brighter). They also appear to be significantly brighter than Population II Cepheids at fixed period. Their origin is still debated and two interpretations are presently the most widely accepted: 1) they are young (≤ 5 Gyr) single stars produced by recent star formation; 2) they formed from mass transfer in old binary systems (e.g. Marconi et al. 2004). They are rare in Galactic GCs, whereas they have been observed in several nearby dwarf spheroidal galaxies (Fiorentino & Monelli 2012, and references therein). Soszyński et al. (2008b) found 83 Anomalous Cepheids in the LMC; they are divided into 62 fundamental-mode and 21 first-overtone pulsators. This is the largest sample of ACs ever detected.

PL for Anomalous Cepheid stars

Zinn & Searle (1976) named these variable stars Anomalous Cepheids because they do not follow the period-luminosity relation of Classical and Population II Cepheids. Fig. 2.6 shows the PL relations obtained by Soszyński et al. (2008b) for the LMC Cepheids. It is clear from this figure that the ACs locate themselves between type I and type II Cepheids in the PL diagram, and that their PL relation is well defined in the Wesenheit index, but not so in the V and I bands. On the theoretical side the PL of ACs is predicted to be the extension to short period and low metallicity of the Classical Cepheids PL (see Caputo et al., 2004).

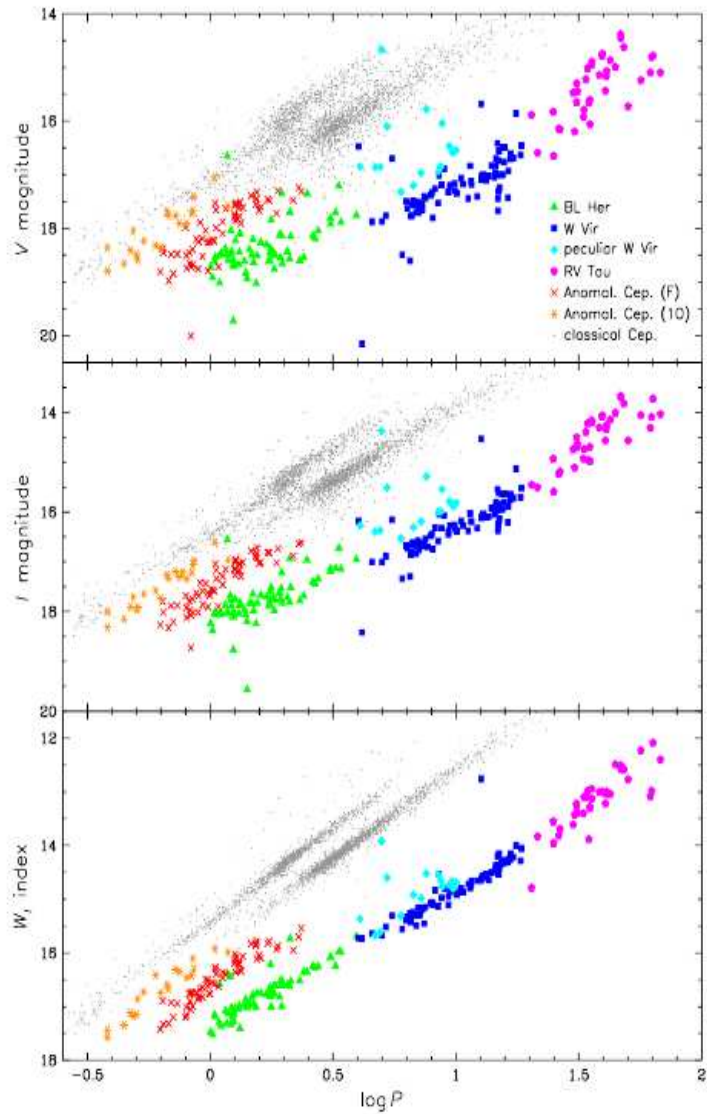


Figure 2.6: Period-luminosity in V , I and Wesenheit index diagrams for Cepheids in the LMC. Symbols and color-coding are described in the figure label. Figure from Soszyński et al. (2008b).

Chapter 3

“Ultra-faint” dwarf spheroidal galaxies

In this Chapter we describe the results that were obtained from the study of the variable stars, stellar populations, and structure of two new "ultra-faint" satellites of the Milky Way: Leo IV and Hercules.

3.1 Leo IV

The Leo IV galaxy (R.A.= $11^h32^m57^s$, DEC.= $-00^\circ32'00''$, J2000.0; $l = 265^\circ.4$, $b=56^\circ.5$) is one of the new faint satellites discovered around the MW by the SDSS. It is a low-mass, $M = (1.4 \pm 1.5) \times 10^6 M_\odot$, system with surface brightness $\mu_V=28.3$ mag arcsec $^{-2}$ (Simon & Geha, 2007), absolute magnitude $M_V = -5.1 \pm 0.6$ mag, and half-light radius $r_h \sim 3.3$ arcmin (Belokurov et al., 2007). It is located at an heliocentric distance of 160_{-14}^{+15} kpc with a position angle of 355° (Belokurov et al., 2007). Its color magnitude diagram (CMD) is more complex than the CMDs of other galaxies discovered by Belokurov et al. (2007), due to the presence of an apparently “thick” red giant branch (RGB) and a blue horizontal branch (HB). The thickness of the RGB suggests the presence of stellar populations of different age/metallicity in this galaxy (Belokurov et al., 2007). The i , $g - i$ CMD of Leo IV, obtained from the SDSS discovery data, reaches $i \sim 22$ mag. No study of the variable stars in the galaxy has yet been performed. Simon & Geha (2007) obtained spectra for 18 bright stars in Leo IV from which they derived an average velocity dispersion of 3.3 ± 1.7 km s $^{-1}$ and an av-

Table 3.1: Instrumental set-up and log of the observations of Leo IV

Dates	Telescope/Instrument	Detector (pixel)	Resolution (" /pixel)	FOV (arcmin ²)	N _B	N _V
Apr. 2007	2.5m INT/WFC	4 of 4k × 2k	0.33	34 × 34	17	18
May 2007	4.2m WHT/Prime Focus Camera	2 of 2k × 4k	0.24	16.2 × 16.2	8	10
Mar.-Apr. 2007	4.1m SOAR/SOI	2 of 4k × 4k	0.077	5.24 × 5.24	12	13

verage metallicity $\langle [Fe/H] \rangle = -2.31 \pm 0.10$ dex with a dispersion $\sigma[Fe/H]=0.15$ dex, on the Zinn & West (1984) metallicity scale (hereafter ZW). Kirby et al. (2008), using Keck DEIMOS spectroscopy coupled with spectral synthesis analysis, measured the metallicity of a subset of 12 stars extracted from the Simon & Geha (2007) sample. They obtained an average metallicity $\langle [Fe/H] \rangle = -2.58 \pm 0.08$, with a dispersion $\sigma[Fe/H]=0.75$ dex and individual metallicities as low as $[Fe/H] \sim -3.0$. The value derived by Kirby et al. (2008) is based on an automated spectroscopic method that is known to provide systematically lower metallicity estimates as discussed by the authors themselves (Kirby et al., 2009, 2010).

In the following we describe the study of Leo IV published in Moretti et al. (2009), where we obtained the first $V, B - V$ CMD of the Leo IV dSph, reaching a depth of $V \sim 25.5$ mag, and identified three fundamental-mode RR Lyrae stars (RR_{ab}) and one SX Phoenicis (SX Phe) variable in the galaxy. We obtained well sampled B, V light curves for each variable star and used the average magnitude of the RR Lyrae stars to estimate the distance to the Leo IV galaxy.

3.1.1 Observations and data reduction

Time series B, V, I photometry of the Leo IV dSph galaxy was collected on 2007 April 20-23 with the Wide Field Camera (WFC), the prime focus mosaic CCD camera of the 2.5 m Isaac Newton Telescope (INT), on 2007 May 11-12, with the Prime Focus Imaging Platform (PFPI) of the 4.2 m William Hershel Telescope (WHT), and on 2007 March-May, with the SOAR Optical Imager (SOI) of the 4.1 m SOUTHERN Astrophysical Research telescope (SOAR). The fields of views covered by the three instruments are 5.24×5.24 arcmin² for SOI at the SOAR telescope, 16.2×16.2 arcmin² for PFPI at the WHT and 33×33 arcmin² for WFC at the INT. Two partially overlapping SOI fields were necessary to cover the galaxy, while just one PFPI field was sufficient, and from the INT data we could also infer

additional information on stars outside the Leo IV half-light radius. We obtained a total number of 37 B , 42 V , and 12 I images of the galaxy. Here we present results from the analysis of the B and V data. Table 3.1 provides informations on the instrumental sep-up and a log of the B , V observations of Leo IV. Images were reduced following standard procedures (bias subtraction and flat-field correction) with IRAF¹. The INT and WHT data were corrected for linearity following recipes provided in the telescope's Web pages. We then performed PSF photometry using the DAOPHOT/ALLSTAR/ALLFRAME packages (Stetson 1987, 1994). Typical internal errors of the B , V single-frame photometry for stars at the HB level range from 0.02 to 0.03 mag for the INT and WHT data, and are of about 0.02 mag for the SOAR data. The absolute photometric calibration was obtained using observations of standard stars in the Landolt (1992) fields SA 101, SA 107, SA110, and PG1323, as extended by P.B. Stetson,² which were observed at the INT during the night of 2007 April 22. Errors of the absolute photometric calibration are $\sigma_B=0.01$ mag, $\sigma_V=0.01$ mag, respectively.

3.1.2 Identification of variable stars

Variable stars were identified using the V and B time-series data separately. First we calculated the Fourier transforms (in the Schwarzenberg-Czerny 1996) of the stars having at least 12 measurements in each photometric band, then we averaged these transforms to estimate the noise and calculated the signal-to-noise ratios (S/Ns). Results from the V and B data sets were cross-correlated, and all stars with $S/N > 5$ in both photometric bands were visually inspected, for a total of about 2000 objects. We also checked whether some of the stars in the Blue Straggler Stars (BSSs) region might be pulsating variables of SX Phe type. The study of the light curves and period derivation were carried out using the Graphical Analyzer of Time Series package (GRaTiS; Clementini et al. 2000). We confirmed the variability and obtained reliable periods and light curves for 3 RR Lyrae stars, all fundamental-mode pulsators (stars: V1, V2 and V3), and for one SX Phe variable (star V4). The identification and

¹IRAF is distributed by the National Optical Astronomy Observatories, which are operated by the Association of Universities for Research in Astronomy, Inc., under cooperative agreement with the National Science Foundation.

²see <http://cadcwwwda.nrc.ca/standards>.

properties of the confirmed variable stars are summarized in Table 3.2, their light curves are shown in Figure 3.1. Stars V1, V2 and V4 lie inside the galaxy half-light radius, while V3 lies outside, at about 12 arcmin from the Leo IV center (see right panel of Figure 3.4). In the CMD, the SX Phe star is located in the region of the BSSs, while all the RR_{ab} stars (V3 included) fall near the galaxy’s HB. We checked the position of V4 on the period-luminosity (PL) relation of the SX Phe stars. Using the star’s period and the absolute magnitude inferred from the apparent magnitude and the distance provided by the RR Lyrae stars (see section 3.1.3), we found that V4 lies very close to the Poretti et al. (2008) PL relation for SX Phe stars, thus confirming the classification as an SX Phe star.

The average pulsation period of the Leo IV RR_{ab} stars is $\langle P_{ab} \rangle = 0.655$ d, and seems to suggest an Oosterhoff type II classification for that Leo IV. Before 2009, only four dSphs of Oosterhoff type II were known, namely, Ursa Minor among the classical dSph companions of the MW, and Bootes I (Dall’Ora et al. 2006), CVn II (Greco et al. 2008), and Coma (Musella et al. 2009), among the ultra-faint SDSS dSphs. On the other hand, in the V -band period-amplitude diagram (see Figure 3.2) the Leo IV RR_{ab} stars fall close to the locus of OoI systems (from Clement & Rowe 2000), with V1 and V3 lying near the distribution of the bona fide regular variables, and V2 lying close to the locus of the well-evolved fundamental-mode RR Lyrae stars in the Galactic GC M3 (from Cacciari et al. 2005). Nevertheless, V2 does not appear to be overluminous in the CMD, as would be required if the star were evolved off the zero-age HB. The ambiguous behavior and the small number of variable stars make the conclusive assignment of an Oosterhoff type to the Leo IV dSph rather difficult.

We used the parameters of the Fourier decomposition of the V -band light curve, along with the Jurcsik & Kovács (1996) method for RR_{ab} stars (see section 2.2.1), to estimate the metallicity on the ZW scale of V1, the only variable of our RR Lyrae sample which satisfies the Jurcsik & Kovács (1996) compatibility condition. For this star we find $[\text{Fe}/\text{H}]_{ZW} = -2.11$ that transformed to Carretta et al. (2009) metallicity scale becomes $[\text{Fe}/\text{H}]_{C09} = -2.27$. The metallicity derived for V1 (see column 11 of Table 3.2) is in good agreement with the spectroscopic metallicity derived for another RR Lyrae star (variable V2) by Kirby et al. (2008) (see last column of Table 3.2).

Name	α (2000)	δ (2000)	Type	P (days)	Epoch (max) (-2450000)	$\langle V \rangle$ (mag)	$\langle B \rangle$ (mag)	A_V (mag)	A_B (mag)	$[Fe/H]_{ZW84}$ (a)
V1	11 32 59.2	-00 34 03.6	RRab	0.61895	4212.453	21.47	21.82	0.73	0.99	-2.11
V2	11 32 55.8	-00 33 29.4	RRab	0.7096	4214.543	21.46	21.86	0.64	0.76	-2.03
V3	11 33 36.6	-00 38 43.3	RRab	0.635	4212.453	21.52	21.81	0.65	0.82	—
V4	11 32 45.4	-00 31 44.4	SX Phe	0.0994	4213.397	22.96	23.34	0.37	0.38	—

Table 3.2: Identification and properties of variable stars in the Leo IV dSph galaxy. Note: (a) The metallicity of star V1 was derived from the Fourier parameters of the V -band light curve. The metallicity of V2 is from Kirby et al. (2008). Table from Moretti et al. (2009)

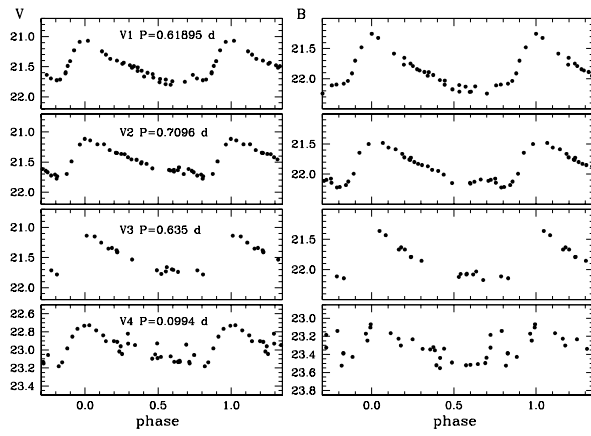


Figure 3.1: V (left panels) and B (right panels) light curves of the variable stars discovered in the Leo IV dSph galaxy. Three upper rows: fundamental-mode RR Lyrae stars; bottom row: SX Phe variable. Figure from Moretti et al. (2009)

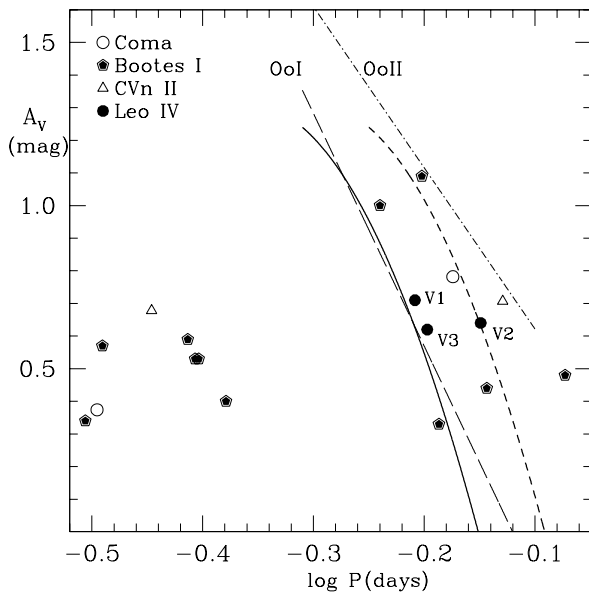


Figure 3.2: V -band period-amplitude diagram of RR Lyrae stars in the Coma, Bootes I, CVn II, and Leo IV dSphs. Variables with $\log P > -0.35$ days are RRab pulsators, those with $\log P < -0.35$ days are first-overtone (RRc) pulsators. Long-dashed and dot-dashed lines show the position of the Oo I and Oo II Galactic GCs, according to Clement & Rowe (2000). Period-amplitude distributions of the *bona fide* regular (*solid curve*) and well evolved (*dashed curve*) RRab stars in M3, from Cacciari et al. (2005), are also shown for comparison. Figure from Moretti et al. (2009)

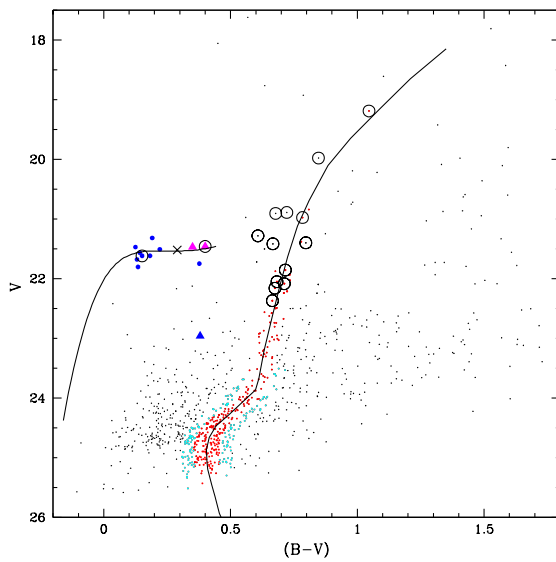


Figure 3.3: V , $B - V$ CMD of the Leo IV dSph obtained by plotting stellar-like objects located within the half-light radius of 3.3 arcmin. Variable stars V1, V2 and V4 are marked by triangles, star V3 by a cross, The solid line is the ridge line of the Galactic GC M15. Red and cyan dots are stars respectively within ± 0.05 mag in $B - V$ and, for $V > 23.5$ mag, from ± 0.05 and ± 0.10 mag in $B - V$ from the ridgeline of M15. Open circles mark member stars of the Leo IV dSph according to Simon & Geha (2007) and Kirby et al. (2008). Figure from Moretti et al. (2009)

3.1.3 CMD, structure and distance to Leo IV

Figure 3.3 shows the V , $B - V$ CMD of the Leo IV dSph obtained by plotting all stellar-like objects located within the half-light radius of 3.3 arcmin from the Belokurov et al. (2007) center of Leo IV. The selection between stars and galaxies, for magnitudes brighter than $V = 22.5$ mag, was done with the software Source Extractor (SExtractor; Bertin & Arnouts 1996). Variables stars are plotted in the CMD according to their intensity-averaged magnitudes and colors (see Table 3.2), using filled triangles for stars V1, V2, and V4, and a cross for star V3. Although well outside the Leo IV half-light radius, V3 appears to be perfectly located on the galaxy’s HB, thus confirming its membership to the galaxy. Non-variable HB stars are marked by (blue) filled circles. The CMD reaches $V \sim 25.5$ mag, and appears to be heavily contaminated at every magnitude level by field objects belonging to the MW. We used the mean ridgeline of the Galactic GC M15 (from Durrell & Harris 1993; solid line) properly shifted in magnitude and color, and selected as stars most likely belonging to the Leo IV galaxy the sources lying within ± 0.05 mag from the ridgeline of M15 (red dots). To allow for the larger photometric errors, for magnitudes fainter than $V = 23.5$ mag, we also considered as belonging to the galaxy stars with $B - V$ color the range from ± 0.05 and ± 0.10 mag from the ridgeline of M15 (cyan dots). The HB of Leo IV shows up quite clearly and along with the galaxy’s RGB, is well reproduced by the ridgeline of M15, implying that Leo IV has an old and metal-poor stellar population with metallicity comparable to that of M15 ($[Fe/H] = -2.5 \pm 0.08$, on the ZW scale). We also note that, by adopting for M15 a reddening value of $E(B - V) = 0.10 \pm 0.01$ mag (Durrell & Harris, 1993), the color shift needed to match the HB and RGB of Leo IV implies for the galaxy a reddening of $E(B - V) = 0.04 \pm 0.01$ mag. For comparison, the reddening in the direction of Leo IV obtained from the Schlegel et al. (1998) maps is 0.025 ± 0.026 mag. The objects marked by the open circles are stars within the Leo IV half-light radius, whose membership to the galaxy was confirmed spectroscopically by Simon & Geha (2007). They include the RR Lyrae star V2 and a number of HB and RGB stars which fall very close to the M15 ridgeline, thus supporting our identification of the Leo IV member stars.

The left panel of Figure 3.4 shows a map of all sources observed in the FOV of the WHT observations that we consider to belong to the Leo IV galaxy, according to their

position with respect to the M15 ridgeline, or with membership spectroscopically confirmed by Simon & Geha (2007, open circles). Symbols and color-coding are the same as in Figure 3.3 and, for nonvariable stars, the symbol sizes are proportional to the star's brightness. The solid circle shows the region corresponding to the half-light radius of Leo IV centered on the Belokurov et al. (2007) coordinates for the galaxy. The right panel of Figure 3.4 shows a map of the sources observed in the INT FOV which lie within ± 0.05 mag in $B - V$ (for $V > 23.5$ mag, within ± 0.10 mag in $B - V$) from the ridgeline of M15. An overdensity of objects rather extended and irregular in shape is visible, corresponding to the region occupied by the Leo IV dSph. The black circle shows the half-light radius of Leo IV, according to Belokurov et al. (2007). The peripheral location of V3 is remarkable, and provides further hints on the elongation and rather deformed morphology of the Leo IV dSph.

The average apparent magnitude of the galaxy's RR Lyrae stars is $\langle V_{RR} \rangle = 21.48 \pm 0.03$ mag (standard deviation of the mean). Assuming $M_V = 0.59 \pm 0.03$ mag for the absolute luminosity of the RR Lyrae stars at $[Fe/H] = -1.5$ (Cacciari & Clementini 2003, but see also the discussion in Sect. 2.3.2), $\Delta M_V / \Delta [Fe/H] = 0.214 \pm 0.047$ mag dex $^{-1}$ for the slope of the luminosity-metallicity relation of RR Lyrae stars (Clementini et al., 2003), $E(B - V) = 0.04 \pm 0.01$ mag and $[Fe/H] = -2.31$ Simon & Geha (2007), the distance modulus of Leo IV is $\mu_0 = 20.94 \pm 0.07$ mag which corresponds to a distance $d = 154 \pm 5$ kpc. The error includes uncertainties in the photometry, reddening, metallicity, and RR Lyrae absolute magnitude, but does not take into account evolution off the zero-age HB which might contribute an additional 0.05 mag uncertainty, bringing the total error budget to 0.09 mag. If we adopt instead $M_V = 0.54$ mag at $[Fe/H] = -1.5$, which is consistent the LMC distance modulus of $\mu_0 = 18.52 \pm 0.09$ mag derived by Clementini et al. (2003) we obtain $\mu_0 = 20.99 \pm 0.07$ mag ($d = 158 \pm 5$ kpc). These new, precise distance estimates agrees very well with the distance of 160^{+15}_{-14} kpc derived by Belokurov et al. (2007).

3.2 Hercules

The Hercules ultra-faint dwarf (R.A.= $16^h 31^m 02.0^s$, Decl.= $12^\circ 47' 29.6''$, J2000.0) was discovered by Belokurov et al. (2007) from the analysis of the SDSS data. Hercules appears to be highly elongated, with an half-light radius of about 9 arcmin

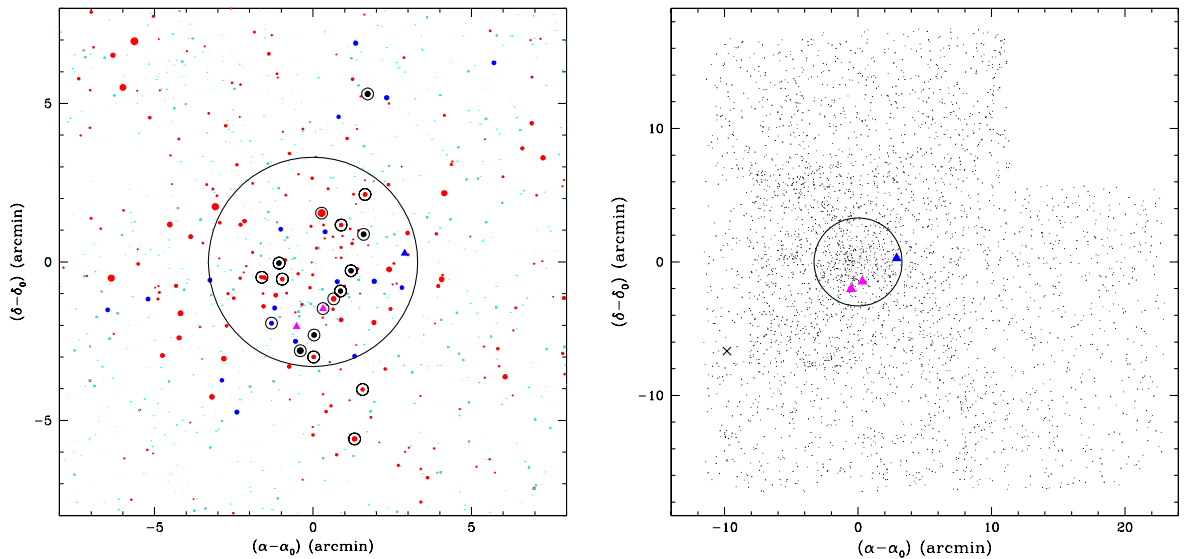


Figure 3.4: *Left panel:* Map of sources in the FOV of the WHT observations, which we consider to belong to the Leo IV galaxy according to the fit with the M15 ridge-line, or with membership spectroscopically confirmed by Simon & Geha (2007, open circles). Symbols and color-coding are the same as in Figure 3.3 and, for non-variable stars, the symbol sizes are proportional to the star’s brightness. *Right panel:* Map of sources observed in the INT field of view which lie within ± 0.05 mag in $B - V$ (for $V > 23.5$ mag, within ± 0.10 mag in $B - V$) from the ridgeline of M15. The symbols and color-coding for the variable stars are the same as in Figure 3.3. In both panels the large circle shows the region corresponding to the half-light radius of Leo IV centered on the Belokurov et al. (2007) coordinates for the galaxy. Figure from Moretti et al. (2009).

Table 3.3: Instrumental set-up and log of the observations of Hercules

Dates	Telescope/Instrument	Detector (pixel)	Resolution ('' /pixel)	FOV	N_B	N_V
Apr. 2007	2.5m INT/Wide Field Camera	4 of $4\text{k} \times 2\text{k}$	0.33	$34' \times 34'$	52	32
May 2007	4.2m WHT/Prime Focus Camera	2 of $2\text{k} \times 4\text{k}$	0.24	$16.2' \times 16.2'$	5	4
Jul. 2007	2.2m ESO/Wide Field Imager	8 of $2\text{k} \times 4\text{k}$	0.238	$34' \times 33'$	7	7
Jul. 2008	2m LT/Ratcam optical CCD camera	$2\text{k} \times 2\text{k}$	0.270 ^a	$4.6' \times 4.6'$	24 ^b	22 ^b
Jan-Jun 2009	2m Faulkes Telescope North/EM01	$2\text{k} \times 2\text{k}$	0.278 ^a	$4.7' \times 4.7'$	14 ^c	7 ^d

^a Binning 2×2 ^b We covered 6 different fields around the galaxy center published by Belokurov et al. (2007)^c We covered 4 different fields around the galaxy center^d We covered 2 different fields around the galaxy center

($r_h \simeq 8.4$ arcmin, for Belokurov et al. 2007; $r_h \simeq 8.6$ arcmin, for Coleman et al. 2007; $r_h \simeq 8.4$ arcmin, for Martin et al. 2008), and ellipticity $\epsilon \sim 0.67$ (Coleman et al., 2007; Martin et al., 2008). Hercules has no evidence of an internal rotation, and a very low velocity dispersion of ~ 5 km s $^{-1}$ for Simon & Geha (2007) or 3.72 km s $^{-1}$ for Adén et al. (2009). The explanation of such a large ellipticity in absence of a rotational support might imply that Hercules is not in dynamical equilibrium due to strong tidal distortions (see discussion in Coleman et al., 2007; Martin et al., 2008). The latest studies estimate for the galaxy distances in the range of ~ 132 kpc to ~ 147 kpc (see e.g., Coleman et al., 2007; Sand et al., 2009; Adén et al., 2011) and a total absolute magnitude ranging from $M_V = 6.2$ mag to $M_V = 6.6$ mag (see e.g. Martin et al., 2008; Sand et al., 2009). In the literature there are several spectroscopic and photometric determinations of the mean metallicity $\langle [\text{Fe}/\text{H}] \rangle$ of Hercules, with values in C09 metallicity scale ranging from about -2.3 to -2.7 dex (Koch et al., 2008; Adén et al., 2009; Kirby et al., 2008; Simon & Geha, 2007).

3.3 Observations and Data Reduction

Time-series observations in B and V of the Hercules UFD were obtained over the period 2007 April, to 2009 June, using a number of different telescopes. The collected data and related telescopes/instrumental set-ups are summarized in Table 3.3, where N_B and N_V are the number of frames in the B and V bands, respectively.

Table 3.4: Identification and properties of variable stars in the Hercules UFD galaxy

Name ^a	α (2000)	δ (2000)	Type	P (days)	Epoch ^b (-2450000)	$\langle V \rangle$ (mag)	$\langle B \rangle$ (mag)	A_V (mag)	A_B (mag)
V1	16:31:02.17	+12:47:33.7	RRab	0.639206	4870.149	21.27	21.68	1.06	1.16
V2	16:31:02.91	+12:45:48.5	AC	0.53777	4614.590	20.72	21.14	0.45	0.59
V3	16:30:54.93	+12:47:04.2	RRc	0.39997	4614.6767	21.32	21.72	0.48	0.61
V4	16:30:56.14	+12:48:29.2	RRc	0.39576	4612.5745	21.23	21.59	0.58	0.69
V5	16:30:52.28	+12:49:12.0	RRc	0.40183	4212.699	21.30	21.64	0.47	0.61
V6	16:30:52.41	+12:49:60.0	RRab	0.69981	4232.700	21.35	21.76	0.90	1.19
V7	16:31:29.48	+12:47:34.9	RRab	0.67799	4613.456	21.22	21.65	0.81	1.03
V8	16:31:27.20	+12:44:16.7	RRab	0.66234	4613.497	21.25	21.69	0.90	1.09
V9	16:31:29.50	+12:40:03.1	RRab	0.72939	4214.6101	21.18	21.60	0.0	1.00
V10 ^c	16:30:03.96	+12:52:06.3	RRab	0.6616	4210.679	21.28	21.69	1.17	1.32

^a We have named the variable stars with an increasing number starting from Martin et al. (2008) center for Hercules

^b Epoch corresponds to the time of maximum light.

^c This star has very scattered light curves

Pre-reduction of the images was performed by following standard procedures (bias subtraction and flat-field correction) with IRAF. We then performed PSF photometry using the DAOPHOT IV/ALLSTAR/ALLFRAME packages (Stetson 1987, 1994). After an accurate evaluation of the PSF of each individual frame, a reference image was built by averaging all the available frames and a source catalogue was extracted from the stacked image. The source list was then passed to ALLFRAME, in order to obtain a homogeneous photometry of all images simultaneously, thus providing catalogues of the b and v instrumental magnitudes for each telescope, separately. Typical internal errors of the single-frame photometry for stars at the magnitude level of the horizontal branch (HB; $V \sim 21.3$ mag) are of about 0.01 mag in both bands.

The absolute photometric calibration was derived using observations of standard stars in the Landolt fields SA 101, SA 107, SA 110 and PG1323 (Landolt 1992), as extended by P.B. Stetson³, which were obtained at the INT during the night of 2007 April 22. Errors of the absolute photometric calibration are $\sigma_B = 0.01$ and $\sigma_V = 0.01$ mag, respectively. As the various telescopes we used to observe Hercules define slightly different photometric systems, each individual dataset was tied to the INT standard calibration independently.

³see <http://cadcwwwda.nrc.ca/standards>.

3.4 Variable Stars

Variable stars were identified from the B and V time-series data, independently, using the *ad hoc* procedure based on the calculation of Fourier transforms that we have already described in Sect. 3.1.2. Even if we expected to mainly find variables of RR Lyrae type in Hercules, we also checked whether any of the stars in the Blue Straggler region might be a pulsating variable of SX Phoenicis (SX Phe) type. We identified a total number of 10 candidate variables in Hercules. To study their light curves and derive their periods we used the software GRATiS (see e.g., Clementini et al. 2000), that, beyond confirming the variability also provided periods accurate to 4-6 decimal places for all of them. The Hercules variables include 1 Anomalous Cepheid (AC) and 9 RR Lyrae stars, of which 6 are fundamental-mode (RRab) and 3 are first-overtone (RRc) pulsators.

Classification and properties of the confirmed variable stars are summarized in Table 3.4, their light curves are shown in Figs. 3.5 and 3.6. We have assigned to the variables increasing numbers starting from the galaxy center that was set at R.A.= $16^h31^m05.2^s$, Decl.= $12^\circ47'29.6''$, J2000.0 (Martin et al., 2008). Time-series data for the variable stars are provided in Table 3.5. The light curves are very well sampled, and show very little scatter, except for star V10. We suspect that this RR Lyrae star might be affected by the Blazhko effect (Blažko, 1907).

We note that, according to the period, variable V2 could be as well a fundamental mode RR Lyrae star. However, the star average magnitude is about 0.4-0.5 mag brighter than the HB level. This occurrence together with a too small amplitude for the star short period, suggest that the variable either suffers from blending by a contaminant star or is, instead, an AC. On the other hand, visual inspection of the star images seems to exclude the presence of possible companions, thus favoring the classification as AC for this variable star. As described in Section 3.5, the AC classification is further confirmed by the comparison with evolutionary tracks.

The AC, all the RRc variables and four of the RRab stars lie inside the half-light radius of the Hercules galaxy ($r_h \simeq 8.6$ arcmin, for Martin et al. 2008). The remaining two RRab stars lie slightly outside this region, with the farthest from the center being confirmed as member by Adén et al. (2009) on the basis of both radial velocity and Strömgren photometry (see Section 3.5 and Fig. 3.8 for details). All

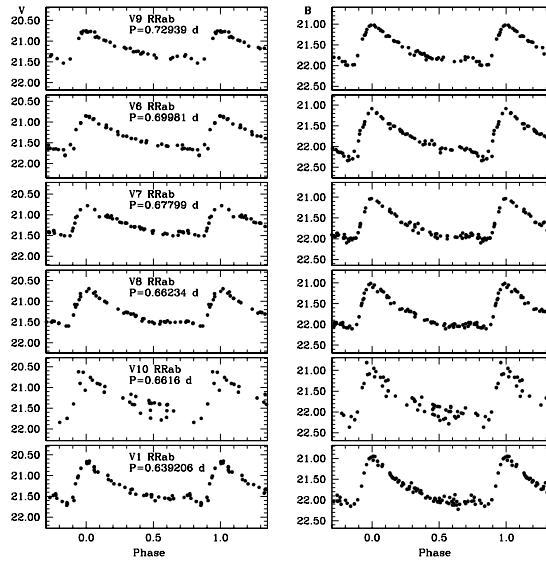


Figure 3.5: Light curves of Hercules fundamental mode RR Lyrae stars. Variables are ordered by decreasing period.

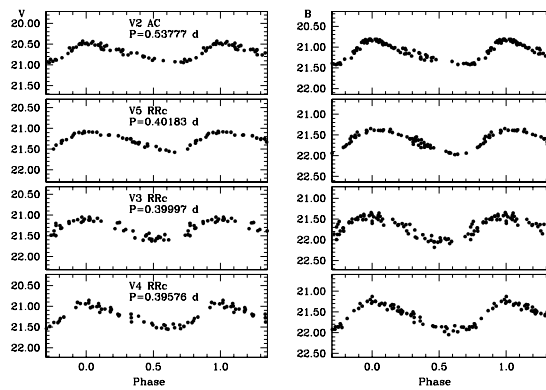


Figure 3.6: Light curves of Hercules AC (top panel), and first overtone RR Lyrae stars. Variables are ordered by decreasing period.

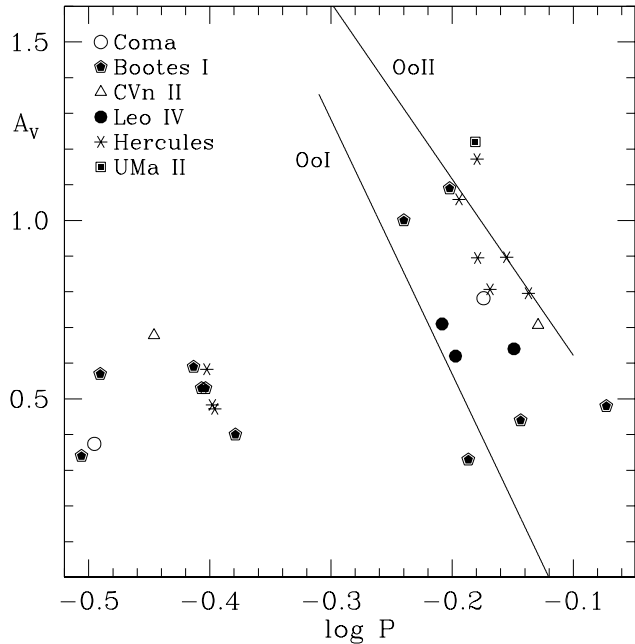


Figure 3.7: V -band period-amplitude diagram of the RR Lyrae stars in the UFDs studied so far for variability: Coma, Boo I, CVn II, Leo IV, UMa II and Hercules UFDs. Solid lines are the positions of the Oo I and II Galactic GCs, from Clement & Rowe (2000).

the RR Lyrae stars fall on the HB of the Hercules UFD, and their mean magnitude is consistent, within the errors, with the average luminosity of the HB inferred by fitting the galaxy CMD with the ridge line of the GGC M68 (see section 3.5 for details).

The mean period of the RRab stars is $\langle P \rangle = 0.68$ d ($\sigma = 0.03$ d) thus firmly classifying Hercules as an Oosterhoff type-II system. Fig. 3.7 shows the position of the Hercules RR Lyrae stars on the V -band period-amplitude (Bailey) diagram. We have also reported in this figure the RR Lyrae stars identified in the other MW UFDs we have studied so far, for comparison. Hercules' RRab stars (star symbols) lie closer to the loci of the Oo II systems (from Clement & Rowe, 2000, solid line) and the RRc stars fall on the long-period tail of the bell-shaped distribution defined by RRc stars in Oo II systems.

Table 3.5: B, V photometry of the variable stars detected in the Hercules UFD

Hercules - Star V8 - RRab					
HJD (-2454211)	V (mag)	σ_V (mag)	HJD (-2454211)	B (mag)	σ_B (mag)
0.652005	21.26	0.02	0.640218	21.69	0.02
0.676609	21.31	0.02	0.664420	21.72	0.02
0.702719	21.34	0.02	0.728613	21.89	0.02
0.741483	21.42	0.02	1.682154	22.10	0.02
1.693693	21.59	0.02	1.705106	22.00	0.02
1.717861	21.33	0.01	1.730836	21.49	0.01
2.646191	21.27	0.01	2.634102	21.69	0.02
2.686550	21.36	0.02	2.658033	21.75	0.02
2.722461	21.42	0.02	2.734216	21.94	0.02
3.610141	21.48	0.02	3.621931	22.01	0.02

Table 3.5 is published in its entirety in the electronic edition of Musella et al. (2012). A portion is shown here for guidance regarding its form and content.

3.4.1 Metallicity and reddening from the RR Lyrae stars

We have Jurcsik & Kovács (1996) method to estimate the metallicity of the Hercules RR Lyrae stars. We have first performed a Fourier decomposition of the V -band light curves, and calculated amplitude ratios A_{n1} and phase differences ϕ_{n1} . We list in Table 3.6 these quantities till to the term $n=3$. The Fourier parameters were used along with the formulae provided by Jurcsik & Kovács (1996) and Morgan et al. (2007) for ab- and c-type RR Lyrae stars, respectively, to obtain individual metallicities for the Hercules RR Lyrae stars, except for V10 whose light curve is too noisy for a reliable application of Jurcsik & Kovacs method. The metallicity estimates obtained with this technique are reported in column 2 of Table 3.7, they are in ZW scale. They were transformed to the Carretta et al. (2009) metallicity scale (see Column 3 of Table 3.7) using the relations provided in Sect. 2.3.1 and then averaged (weighted average) to obtain our best estimate for the metallicity of the Hercules old population: $\langle [Fe/H]_{RR,C09} \rangle = -2.30 \pm 0.15$ dex.

The metal abundance we have derived from the RR Lyrae stars is in excellent agreement with measurements by Simon & Geha (2007), Coleman et al. (2007),

Table 3.6: Fourier parameters of the V -band light curve for variable stars in Hercules

Name	Type	A_{21}	A_{31}	ϕ_{21}	$err\phi_{21}$	ϕ_{31}	$err\phi_{31}$
$V1$	RRab	0.49917	0.36365	3.64547	0.09703	1.44958	0.13949
$V2$	AC	0.29909	0.15253	4.57133	0.14328	1.99718	0.26515
$V3$	RRc	0.03663	0.09088	4.43201	1.46807	3.03154	0.61169
$V4$	RRc	0.27846	0.11197	4.42430	0.21027	2.31475	0.48194
$V5$	RRc	0.22652	0.08833	5.09514	0.12519	3.59738	0.30253
$V6$	RRab	0.54905	0.34341	4.05899	0.12258	2.13826	0.18946
$V7$	RRab	0.39660	0.32364	3.97741	0.07756	1.82471	0.10378
$V8$	RRab	0.44746	0.34821	3.73524	0.07124	1.59599	0.09866
$V9$	RRab	0.44564	0.39424	3.97431	0.07633	1.74252	0.09976
$V10$	RRab	0.50604	0.37673	4.28900	0.31261	2.83362	0.44539

Table 3.7: Individual metallicities and reddening values derived for the RR Lyrae stars in Hercules (see text for details).

Name	$[Fe/H]_{ZW} \pm \sigma_{[Fe/H]_{ZW}}$	$[Fe/H]_{C09} \pm \sigma_{[Fe/H]_{C09}}$	$E(B - V)$
$V1$	-2.23 ± 0.13	-2.4 ± 0.2	0.10
$V3$	-2.12 ± 0.06	-2.29 ± 0.13	---
$V4$	-2.13 ± 0.04	-2.31 ± 0.12	---
$V5$	-2.03 ± 0.07	-2.14 ± 0.14	---
$V6$	-1.81 ± 0.18	-1.8 ± 0.3	0.06
$V7$	-2.02 ± 0.10	-2.13 ± 0.19	0.08
$V8$	-2.18 ± 0.10	-2.36 ± 0.19	0.12
$V9$	-2.29 ± 0.10	-2.52 ± 0.19	0.08

Koch et al. (2008) and Adén et al. (2009), but is about 0.4 dex higher than derived by Kirby et al. (2008). However, the value of $[Fe/H] \sim -2.7$ (on C09 scale) derived for the galaxy by Kirby et al. (2008) is based on an automated spectroscopic method that is likely to provide systematically lower metallicity estimates as discussed by the authors themselves (Kirby et al., 2009, 2010). More recently, Adén et al. (2011) found a large metallicity spread ($-3.2 < [Fe/H] < -2.0$ dex) in Hercules, from the analysis of medium-high resolution spectra of 11 red giant branch (RGB) stars in the galaxy. However, if the average is computed only on the red giants with metallicity measured from a significant number of iron lines (≥ 5 ; four stars according to Adén et al. Table 6), we obtain an average value of $\langle [Fe/H] \rangle = -2.3 \pm 0.2$ dex, in excellent agreement with the value we have derived from the RR Lyrae stars. We used the RR Lyrae stars also to estimate a reddening value for Hercules. From the relation by Piersimoni et al. (2002), that holds for RRab stars, and connects the color excess, to the light curve amplitude in the B band, the logarithm of the period, and the star metallicity we obtain a mean color excess $E(B - V)_{RRab} = 0.09 \pm 0.02$ mag, where we have adopted the individual metallicities on Carretta et al. (2009) scale listed in Table 3.7. This estimate is in very good agreement with the value of 0.084 ± 0.026 mag derived from the Schlegel et al. (1998) maps. In the following we adopt for Hercules the average metallicity, $\langle [Fe/H]_{RR,C09} \rangle = -2.30 \pm 0.15$ dex, and the reddening value $E(B - V) = 0.09 \pm 0.02$ mag that were derived from the RR Lyrae stars.

3.5 CMD, structure and distance

Fig. 3.8 shows the $V, B - V$ CMD of Hercules obtained in the present study. We used the CHI and SHARP parameters provided by the ALLFRAME package to select only the stellar-like objects (grey dots) present in our total FOV of about $40' \times 40'$. The selection is reliable for magnitude brighter than $V \sim 24$ mag, while uncertainty increases at fainter magnitudes. In the left panel we plot stellar-like objects within in the galaxy half light radius (8.6 arcmin, Martin et al., 2008), in the right panel instead we show objects outside this region. The CMD reaches $V \sim 25$ mag and appears to be heavily contaminated at each magnitude level by field objects belonging to the MW halo and disk, as well as by background galaxies. The main

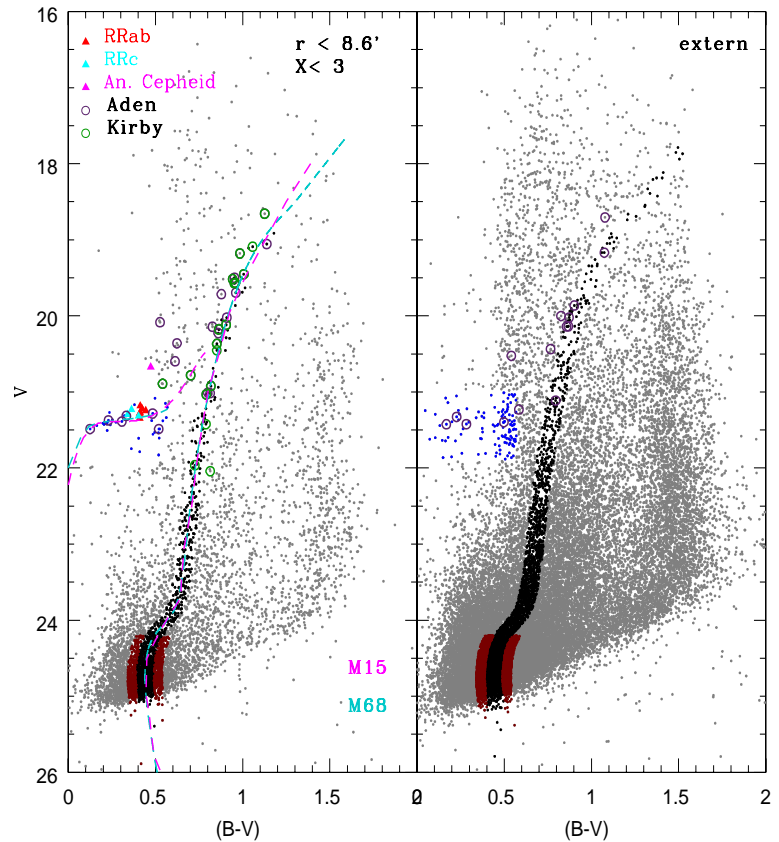


Figure 3.8: *Left:* $V, B - V$ CMD of the Hercules UFD, drawn from all the stellar-like objects within the galaxy half-light radius ($r_h \simeq 8.6$ arcmin, Coleman et al. 2007). Dashed cyan and magenta lines are the ridgelines of the Galactic GCs M 68 and M 15, respectively. Black and red dots are stars respectively within ± 0.05 mag in $B - V$ and from ± 0.05 to ± 0.1 mag from the ridgelines of M 68. Blue dots are non-variable stars on the HB. Variable stars are marked by filled triangles, cyan: RRc stars, red: RRab stars, magenta: Anomalous Cepheid. Green and violet open circles mark member stars of the Hercules UFD identified spectroscopically by Kirby et al. (2008) and spectro-photometrically by Adén et al. (2009), respectively (see text for details). *Right:* $V, B - V$ CMD of the stellar-like objects outside the Hercules half-light radius.

branches of the Hercules CMD are barely distinguishable, due to the overwhelming contamination by the MW field stars. To identify stars belonging to Hercules we applied the method that we have already successfully used for Leo IV, and in our previous papers (see e.g., Musella et al. 2009; Moretti et al. 2009). Specifically, we used the mean ridgelines of the Galactic GC M68 (NGC 4590; dashed cyan lines in Figure 3.8), obtained from Walker (1994) B, V photometry, and shifted them by $\Delta V = +5.68$ mag in magnitude, and $\Delta(B - V) = +0.02$ mag in color, to match the HB and RGB of the Hercules UFD. M68 is well suited for identifying members of the Hercules UFD because, like Hercules, is very metal-poor. Its metallicity, $[Fe/H]_{M68} = -2.27 \pm 0.04$ dex (Carretta et al., 2009), is in very good agreement with the mean metallicity obtained in section 3.4.1 from the RR Lyrae stars. The cluster has also a well defined and tight RGB, as well as an extended HB including stars both redder and bluer than the RR Lyrae instability strip (Walker 1994). With this procedure we selected as most probable members of the Hercules galaxy the sources lying within ± 0.05 mag in $B - V$ from the ridgelines of M 68 (black dots in the left panel of Figure 3.8). To account for the larger photometric errors, below $V = 24.2$ mag we also considered as belonging to the galaxy stars with colors within ± 0.05 and ± 0.10 mag from the ridgelines of M 68 (red dots). Adopting for M68 a reddening value of $E(B - V) = 0.07 \pm 0.01$ mag (Walker, 1994) the color shifts needed to match the HB and RGB of Hercules imply a reddening of $E(B - V) = 0.09 \pm 0.01$ mag for the galaxy, in excellent agreement with the value obtained from Hercules $RRab$ stars (see Section 3.4.1). In the left panel of Fig. 3.8 we also show the ridgelines of the Galactic GC M15 (NGC 7078, dashed magenta lines), taken from Durrell & Harris (1993) and shifted by $\Delta V = +5.5$ mag in magnitude, and $\Delta(B - V) = -0.02$ mag in color, to match the HB and RGB of Hercules. M15 is slightly more metal-poor than M 68 with $[Fe/H]_{M15} = -2.33 \pm 0.02$ dex (Carretta et al., 2009), and matches equally well the main branches of the Hercules CMD. Finally, we have compared the CMD of Hercules with the ridgelines of the metal-intermediate GC M3 (Ferraro et al., 1997; Johnson & Bolte, 1998). However, the RGB ridgeline of M3 is too red and would require a negative reddening to match Hercules RGB.

With the help of the M68 ridgelines, it is possible to determine the average luminosity of Hercules HB in the region of the so-called RR Lyrae gap ($< V_{HB} > = 21.30 \pm 0.02$ mag), and to locate the galaxy main-sequence turnoff at $V \sim 24.4$ mag.

Our identification of the Hercules member stars finds an excellent confirmation in the spectroscopic study by Kirby et al. (2008, 20 stars represented by the green open circles in Fig. 3.8) and in the spectrophotometric analysis by Adén et al. (2009, 47 stars represented by the violet open circles in Fig. 3.8), with membership to the Hercules UFD confirmed by radial velocity measurements and, for Adén et al. (2009)'s sample also by Strömgren photometry. The impressive agreement between these studies and our results supports the reliability of the procedure we have used to select Hercules member stars and to identify the HB.

Fig. 3.8 shows an overabundance of stars above the HB ($V \sim 20.5$ mag). These stars were already identified by Adén et al. (2009), who investigated whether they might represent variable stars brighter than the RR Lyrae stars. We also searched for candidate variables this region of the CMD, but, as already discussed in Section 3, we found only one AC variable, star V2 (filled magenta triangle in Fig. 3.8).

Fig. 3.9 shows the position of the stars we consider to be members of the Hercules galaxy in our FOV. Symbols and color-coding are the same as in Fig. 3.8, and symbol size is proportional to the object's magnitude. The black ellipse corresponds to the half light radius, the angle position and the ellipticity obtained for Hercules by Martin et al. (2008). This map confirms that the galaxy is elongated and has an irregular and extended shape. Likely, Hercules was tidally disrupted and is now embedded in the MW halo. Our discovery of two RRab variables outside the half light radius, together with the spectrophotometric identification in the same external region of some stars with confirmed membership by Adén et al. (2009), support the tidal interaction scenario.

3.5.1 A new estimate of the distance to Hercules

The RR Lyrae detected in Hercules offer the opportunity to estimate an accurate distance to this galaxy.

The position of the RR Lyrae stars is in satisfactory agreement with the M68 HB fiducial line, although with some spread. Two of the Hercules variables (V9 and V10) are located outside the galaxy half light radius (see Fig. 3.9), and V10, has very noisy light curves. We suspect it might be affected by Blazhko effect (Blazhko 1907). The measure the distance we have used only the RR Lyrae lying inside the galaxy half light radius. Their average apparent magnitude is: $\langle V_{RR} \rangle = 21.28 \pm 0.05$ mag

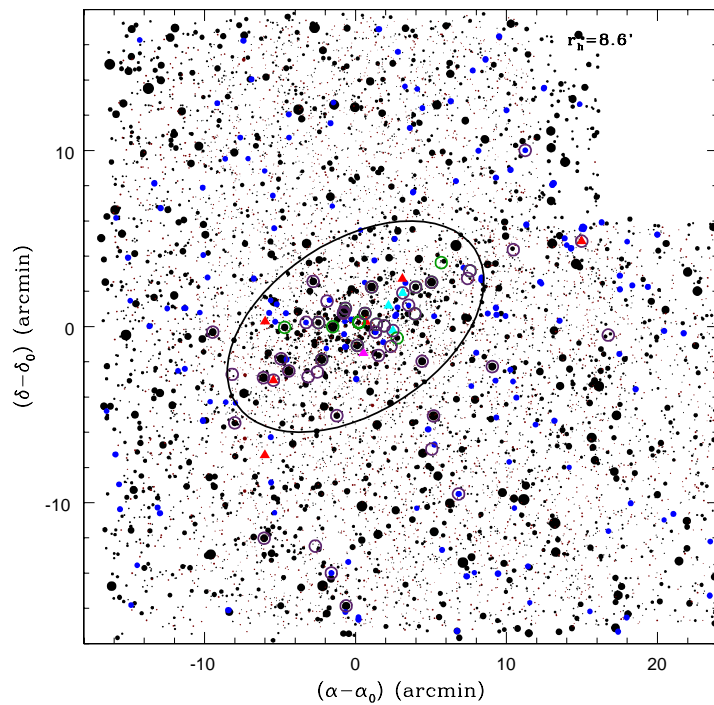


Figure 3.9: Map of the stars we consider to belong to the Hercules galaxy in the FOV of our observations. Symbols and color coding are the same as in Fig. 3.8. Symbol sizes are proportional to the object’s magnitudes. A black ellipse describes the half-light region of the galaxy, for the angle position and ellipticity obtained for Hercules by Martin et al. (2008).

(where the error is the standard deviation of the average).

Assuming $M_V = 0.59 \pm 0.03$ mag for the absolute visual magnitude of the RR Lyrae stars at $[Fe/H]=-1.5$ (Cacciari & Clementini 2003, but see also the discussion in Sect. 2.3.2), $\Delta M_V/\Delta[Fe/H] = 0.214 \pm 0.047$ mag dex $^{-1}$ for the slope of the luminosity-metallicity relation of RR Lyrae stars (Clementini et al., 2003), $< [Fe/H]_{RR,C09} > = -2.30 \pm 0.15$ dex, and $E(B - V) = 0.09 \pm 0.02$ from the RR Lyrae stars, the distance modulus of Hercules is $\mu_0 = 20.58 \pm 0.08$ mag which corresponds to a distance $d = 131 \pm 5$ kpc, where the error includes the contribution of the uncertainties on the metallicity, the reddening, the adopted slope of the $M_V - [Fe/H]$ relation and the average apparent visual magnitude of Hercules RR Lyrae stars. If we adopt instead $M_V = 0.54$ mag at $[Fe/H]=-1.5$, which is consistent with the LMC distance modulus of $\mu_0 = 18.52 \pm 0.09$ mag derived by Clementini et al. (2003) we obtain a true distance modulus of 20.63 ± 0.08 mag ($d = 134 \pm 5$ kpc).

Our distance determinations are in statistical agreement with previous estimates by Belokurov et al. (2007), Coleman et al. (2007) and Adén et al. (2009).

An additional distance estimate based on the RR Lyrae stars can be obtained using the theoretical Wesenheit relation in the B, V bands as defined by Di Criscienzo et al. (2004) with the assumption of a suitable evolutionary mass for the metallicity of Hercules. The resulting distance modulus is: 20.60 ± 0.10 mag, in very good agreement with the values obtained from the absolute magnitude-metallicity relation.

Finally, in Fig. 3.10 we show a zoom of the HB region of the CMD in Fig. 3.8 (with the same color-coding) where we have reported (solid lines) the helium burning evolutionary tracks from the stellar model database BaSTI⁴ (Pietrinferni et al., 2006), for stellar masses ranging from 0.7 to $1.4 M_\odot$ (with a step of $0.1 M_\odot$) and $Z = 0.0001$. In particular, the red and blue lines are the HB evolutionary tracks for 0.7 and $0.8 M_\odot$ respectively, whereas the black lines are for $M \geq 0.9 M_\odot$ including the range of masses corresponding to the HB turnover (Caputo & degl'Innocenti, 1995). The blue dashed line represents the Zero Age Horizontal Branch (ZAHB) for the same chemical composition. The location of the RR Lyrae stars is consistent with the model predictions and suggests an evolutionary effect for some of them. On the other hand, the AC (star V2) is, as expected, consistent with the evolution

⁴BaSTI database official site: <http://www.oa-teramo.inaf.it/BASTI>

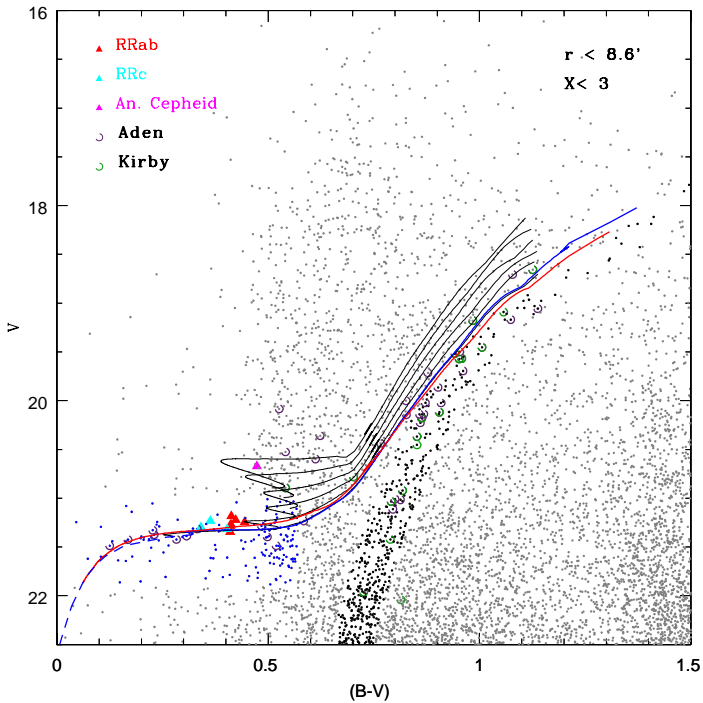


Figure 3.10: Zoom of the HB region of the CMD in the Fig. 3.8 with same symbols and color-coding. Solid lines represent the HB evolutionary tracks for $Z = 0.0001$ and stellar masses from 0.7 to $1.4 M_{\odot}$ (with a step of $0.1 M_{\odot}$). Red and blue lines are the HB evolutionary tracks for 0.7 and $0.8 M_{\odot}$ respectively, whereas the black lines are for $M \geq 0.9 M_{\odot}$ including the range of masses corresponding to the HB turnover (Caputo & degl’Innocenti, 1995). The blue dashed line represents the ZAHB location for the same chemical composition.

of a $M \sim 1.35 M_{\odot}$ from the turnover region of the ZAHB, confirming the presence of an intermediate-age stellar population $\sim 2 - 3$ Gyr old in Hercules.

HST data

The ground-based data of Hercules were complemented by times series observations in the F606W and F814W filters obtained with the Wide Field Planetary Camera 2 (WFPC2) on board the Hubble Space Telescope (HST). These data were obtained on 2007 February 26, as part of GO11084 (PI:Zucker) and are available on the HST archive. They consist of 3 F606W, and 5 F814W images, respectively, each obtained with an exposure lenght of 1200 sec. We adopted the HSTphot package (Dolphin, 2000), a PSF-fitting photometry package specifically designed for the treatment of

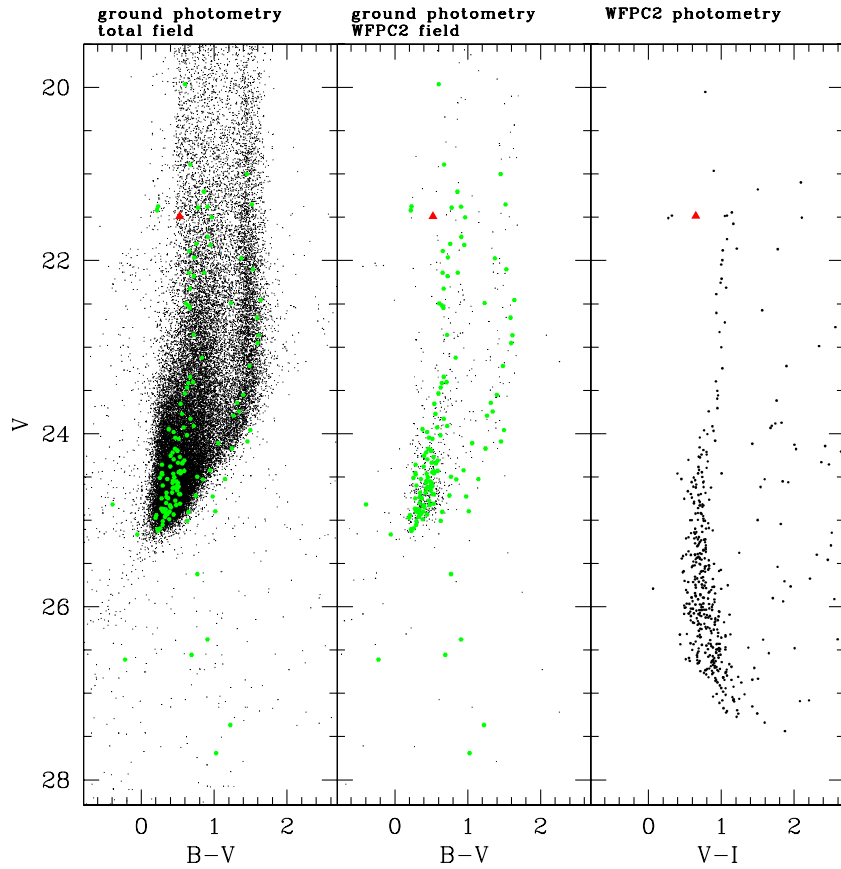


Figure 3.11: *Right Panel:* $V, V - I$ CMD of Hercules obtained from the WFPC2 HST photometry; *Left panel:* $V, B - V$ CMD of Hercules UFD from our ground-based photometry. All stellar-like objects measured in the total field of view ($40' \times 40'$) of the ground-based observations, are plotted (back points). Green dots show stars observed from the ground that have a counterpart in our HST dataset. Central Panel: ground-based $V, B - V$ CMD of sources in the FOV covered by the WFPC2 observations, and, marked in green objects that have a counterpart in the HST catalogue. The red triangles in all panel is the only RR Lyrae star falling in the WFPC2 FOV.

the HST WFPC2 images, to reduce and calibrate the data to the standard Johnson-Cousins photometric system. The right panel of Fig. 3.11 shows the V , $V - I$ CMD obtained from the WFPC2 HST photometry, where we have plotted only objects with $\chi^2 \leq 1.5$, sharpness values between -0.3 or 0.3 (see Dolphin 2000 for details), and photometric errors ≤ 0.015 mag, in both V and I bands. The HST CMD is exquisitely deep and well defined, reaching $V \sim 27.5$ mag, i.e. more than 3 magnitudes below the turnoff (TO) of Hercules ($V_{TO} \sim 24.4$ mag), that is now clearly detected in the HST photometry, that has errors of $\sigma_V = 0.03$ mag, $\sigma_I = 0.041$ mag, for $V = 25.098$ mag and $I = 24.457$ mag, respectively. For comparison, the left panel of Fig. 3.11 shows the V , $B - V$ CMD of Hercules UFD obtained with our ground-based photometry. All stellar-like objects measured in the total field of view ($40' \times 40'$ covered by our ground-based observations, were plotted (back points). Green dots show stars observed from the ground that have a counterpart in our HST dataset. The FOV covered by the HST observations is $2.5' \times 2.5'$, and only one of the RR Lyrae (red triangle in Fig. 3.11) falls in the area of Hercules observed with the HST. The central panel of Fig. 3.11 shows the ground-based V , $B - V$ CMD of sources in the FOV covered by the WFPC2 observations, and, marked in green objects that have a counterpart in the HST catalogue.

Chapter 4

The Magellanic System

In this Chapter we present the second part of the PhD project, that was focussed on the analysis of the LMC RR Lyrae stars and Cepheids, based on the near infrared data of the VMC survey.

4.1 The Magellanic System

Historical view

The Magellanic Clouds have been known for thousands of years to the inhabitants of the southern hemisphere. Many of the Middle Age sailors noted the two Clouds. As described in Westerlund 1997, the Clouds became connected with the name of the Portuguese seafarer Magalhaes through Antonio Pigafetta's description of the first circumnavigation of the globe in 1519-1522: "The Antarctic Pole is not so marked by stars as the Arctic. You can see there are several small stars clustered together, in the manner of two clouds a little separated one another and somewhat dim." Their nature as the two nearest external galaxies was pointed out by Abbe (1867): "The visible universe is composed of systems, of which the *Via Lactea*, the two *Nubeculae*, and the *Nebulae*, are the individuals, and which are themselves composed of stars (either simple, multiple, or in clusters) and of gaseous bodies of both regular and irregular outlines." Detailed investigations of the two Clouds began when the Harvard College Observatory established its southern station at Arequipa in Perù (1889-1927) and at Bloemfontain in South Africa. The most relevant result provided by early observations was the period-luminosity (PL) relation for Cepheid

variables described in the *Harvard Circular N.* 173, 1912. One hundred years separate us from this famous discovery by Leavitt & Pickering (1912); during this time several fundamental results concerning the Magellanic Clouds were achieved bringing us to the global picture of the system we have now.

Present picture

The Magellanic System lies at a distance of ~ 57 Kpc (e.g. Cioni et al. 2000b) and is formed by: the Large Magellanic Cloud (LMC), the Small Magellanic Cloud (SMC), the Bridge between them and the Stream, a trailing HI component (Mathewson et al. 1974). The LMC is a face-on (van der Marel & Cioni, 2001) dwarf irregular galaxy, also referred to as a late type spiral galaxy. It hosts several different populations of stars: old, intermediate-age, young, as well as star forming regions. The SMC is a highly inclined dwarf galaxy sometimes referred to as a dwarf Spheroidal galaxy (Zaritsky et al., 2000). Both MCs have a bar but while the LMC's is supposed to be just a few Kpc thick, the SMC's may extend up to 20 Kpc through the line of sight. The metallicity of the LMC, SMC and the Bridge are 1/2, 1/4 and 1/10 of the solar metallicity, respectively. The interaction between the MCs could be responsible for the formation of the Bridge (Irwin et al., 1985), several episodes of star formation (Zaritsky & Harris, 2004) and the creation of the Stream (Besla et al., 2010). As Besla et al. (2010) pointed out, the Magellanic Clouds are the closest near-equal-mass interacting pair of galaxies. The optical and infrared surveys of the system show the Clouds as two distinct objects separated in space by a projected distance of ~ 20 kpc. The HI distribution, however, shows a different picture. The Clouds are connected by a low-metallicity bridge of gas and share a common gaseous envelope (Putman et al. 2003; Brüns et al. 2005). The existence of such features suggests that the two Clouds are a binary interacting pair. The Bridge in particular indicates that they have had a close encounter in the recent past. Toomre & Toomre (1972) demonstrate that two isolated galaxies are capable of removing substantial amounts of material via tides, forming pronounced features such as bridges and tails. The Stream is a filamentary feature of HI gas (no stars; Guhathakurta & Reitzel 1998) that trails behind the Clouds for at least 150° across the sky (Braun & Thilker 2004; Nidever et al. 2010). The Stream has historically been explained as the product of a tidal and/or hydrodynamic interaction between the Clouds and

the Milky Way (Gardiner & Noguchi 1996; Connors et al. 2006; Mastropietro et al. 2005). This picture is based on the belief that the Clouds have experienced multiple close passages near our Galaxy. However, recent *Hubble Space Telescope (HST)* proper motion measurements of the Clouds (Kallivayalil et al. 2006a; Kallivayalil et al. 2006b), independently confirmed by Piatek et al. (2008), have challenged this picture. These studies suggest instead that the Clouds have, at best, completed one orbit around the MW, or may even be still on their first passage (Besla et al., 2007). This occurs if either the MW's mass were higher ($\sim 2 \times 10^{12} M_{\odot}$; Besla et al. 2007), or if the velocity inferred from the proper motion measurements were substantially lower, e.g. if the velocity at the solar circle were higher (Shattow & Loeb 2009; Reid et al. 2009). In this case, the only previous pericentric passage around the Galaxy would be ~ 6 Gyr ago and the apocenter of the orbit would be ~ 400 kpc (i.e. larger than the virial radius of the MW). These values are lower limits since these studies assume that the MW's mass is constant over time, whereas in the current Λ CDM paradigm our Galaxy is believed to have been half as massive ~ 8 Gyr ago (Wechsler et al., 2002). Depending on the mass evolution of the MW it may be impossible for the Clouds to have completed multiple passages. Independently of which scenario is the correct one, there is no orbital solution that brings the Clouds near the MW over the past 3 Gyr. On the other hand, there is strong evidence that the Stream is a young feature (1-2 Gyr). Estimates of the survivability of high velocity clouds by Heitsch & Putman (2009) and Kereš & Hernquist (2009) make it improbable for the Stream to have survived much longer. The lifetime of the Stream poses a problem for all past numerical models, which invoke some combination of MW tides and/or ram pressure stripping to form the Stream. These models require at least one complete orbit around the MW, implying an incompatible age of at least 6 Gyr. As such, regardless of whether the Clouds are on their first or second passage to the MW, in the context of the origin of the Stream we are left with the same doubt: how can the Stream have formed without a complete orbit about the MW? Or, more generically, how can a pronounced tail be formed from a pair of dwarfs on their first infall toward a massive host?

The knowledge of the Magellanic System (MS) structure is of crucial importance to better understand its evolution and in turn improve our knowledge of the formation of the MW. This is one of the main purposes of the VISTA Y, J, K_S survey of

the MS (VMC, see section 4.4). Started in November 2009, and extending over a ~ 5 yrs time span the VMC survey will indeed study the stellar 3-D structure and the star formation history of the LMC, SMC, Bridge and of a small piece of the Stream, thus providing new observational constraints on the near-field cosmology scenario.

In the framework of the VMC collaboration, in this PhD thesis we have developed, tested and fine tuned the procedures necessary to derive information on distance and 3D-structure of the Magellanic Cloud System from the analysis of the MC RR Lyrae stars and Cepheids, and have then applied them to two LMC fields completely observed by VMC. These procedures represent now the basic instrument to extend the analysis to the fields that the VMC survey will observe until the completion of the entire project.

4.2 Optical observations: microlensing surveys

In the last couple of decades a number of different microlensing surveys have provided tens of millions light curves for objects in the Large and Small Magellanic Clouds. Despite these data were not obtained with the aim of studying variable stars, they allowed to detect and derive the period of variability for tens of thousands MC variables among which, most noteworthy, RR Lyrae stars, Classical Cepheids (CC), binaries, and Long Period Variables (LPV). The most extended of these surveys are: MACHO (Alcock et al., 2000), EROS (Tisserand et al., 2007), and OGLE (Udalski et al., 1997).

In this PhD thesis we have used identification, coordinates and pulsation properties (period, epoch of maximum light, parameters of the Fourier decomposition of the visual light curves) of the LMC RR Lyrae stars and Cepheids extracted from the microlensing catalogues of variable stars (see sections 4.2.1 and 4.2.2) to build infrared K -band light curves for the variables observed by the VMC survey. The average magnitudes in the K -band have then been used to construct period-luminosity relations from which to derive distances for the variable stars and information on the 3-D structure of the LMC.

In Figure 4.1 we show a map with the distribution of candidate RR Lyrae stars in the LMC according to the EROS-2 survey (black points), with superimposed the VMC tiles (black squares), the OGLE III fields (in red), and the MACHO fields (in

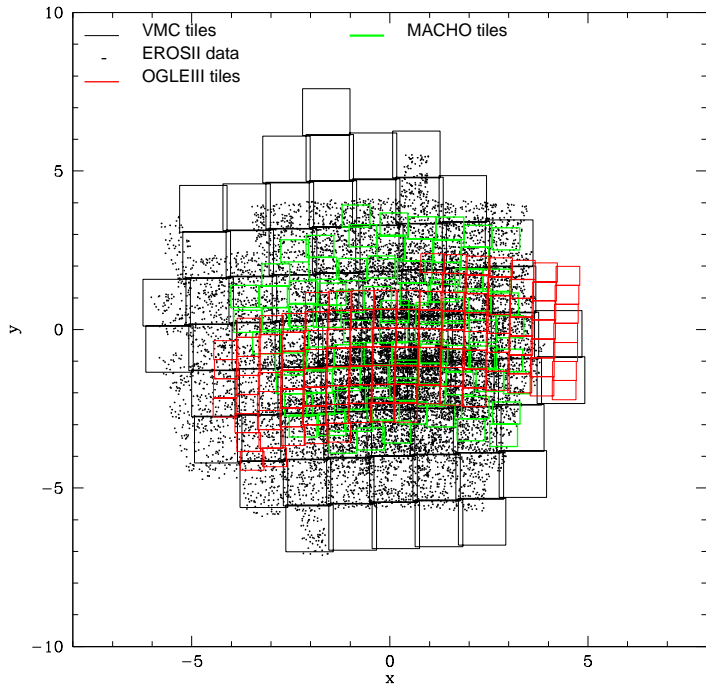


Figure 4.1: Map of candidate RR Lyrae stars in the LMC, according to the EROS-2 survey (black points), with superimposed the VMC tiles (black squares), the OGLE III fields (in red), and the MACHO fields (in green). $x = \alpha - \alpha_0$ and $y = \delta - \delta_0$ where $\alpha_0 = 81^\circ$ and $\delta_0 = -69^\circ$

green). The largest coverage of the LMC is provided by the EROS-2 data. However, EROS-2 as well as MACHO used non conventional filters. In particular, EROS’ *blue* channel, $\lambda \in (420\text{-}720 \text{ nm})$, overlaps to the *V* and *R* standard bands, while EROS’ *red* channel, $\lambda \in (620\text{-}920 \text{ nm})$, roughly matches the mean wavelength of the Cousins *I* band (Tisserand et al. 2007). OGLE used instead B_{Johnson} (B_J), V_{Johnson} (V_J) and I_{Cousins} (I_C) filters. For these reasons we used the OGLE-III data whenever available (e.g., in the centre of the LMC), and the EROS-2 data in the outer parts of the LMC that are not covered by other surveys. A number of most external VMC tiles are not covered by any of the previous microlensing surveys, however, the OGLE-IV survey, started in 2010, is in progress, and, once completed will cover the entire field of view of the VMC survey.

4.2.1 EROS-2

EROS-2 (*Expérience pour la Recherche d’Objets Sombres*) is a second generation microlensing experiment (Tisserand et al., 2007) that monitored 93 deg² in the Magellanic Clouds, 63 deg² in the Galactic Bulge, and 28 deg² in the spiral arms of the Milky Way. The EROS-2 observations were performed between 1996 July, and 2003 February. EROS-2 used the Marly 1 meter telescope at ESO, La Silla. The telescope was equipped with two 0.95 deg² CCD mosaics; each CCD has 2048 × 2048 pixels of 15 × 15 μm^2 size.

Images were taken simultaneously in two wide passbands, the so-called R_{EROS} centered close to the I_C standard band, and the B_{EROS} , which is intermediate between the standard V and R bands. Almost all of the EROS-2 fields were calibrated using stars from the catalogs of the Magellanic Cloud Photometric Survey (Zaritsky et al., 2004). For 4.5 deg², the calibration was checked with the OGLE-II catalog. To a precision of ∼0.1 mag, the EROS magnitudes satisfy the following transformation equations:

$$R_{EROS} = I_C; B_{EROS} = V_J - 0.4(V_J - I_C). \quad (4.1)$$

EROS-2 has, so far, the best coverage of the MCs. Data from this survey are widely used in this thesis work.

4.2.2 OGLE III

The Optical Gravitational Lensing Experiment (OGLE) is a wide-field sky survey started in 1992 and originally motivated by the search for microlensing events (Soszyński et al. 2008a, and references therein). The observing strategy of the project originally proposed by Paczynski (1986), was to regularly monitor the brightness of about 200 million stars in the Magellanic Clouds and Galactic bulge on time-scales of at least two years, in order to observe lensing events connected with “dark halo” objects with masses ranging from $10^{-6}M_\odot$ to 10^2M_\odot . It was clear immediately that such a kind of observations would have provided an enormous database of photometric measurements as a byproduct. The first phase of the project (OGLE I) started in 1992 and observations were continued until 1995 using the 1m Swope telescope at the Las Campanas Observatory, Chile (Udalski et al., 1992). The project

was very successful (Udalski et al., 1993) but it suffered from limited availability of telescope time, the observations were confined to the Galactic bulge, and the area covered on the sky was relatively small. The second phase of the project (OGLE-II) was conducted between 1997 and 2000 and the observations were collected with the new 1.3 m Warsaw Telescope dedicated for massive photometric surveys of dense stellar fields (Udalski et al., 1997). As a byproduct, catalogues of thousands of Cepheids, RR Lyrae stars, eclipsing binaries, and long period variables in the Galactic Bulge and the two Magellanic Clouds were produced (Szymanski, 2005). The OGLE-III phase started on 2001 June and used the 1.3-m Warsaw telescope equipped with the new eight 2048×4096 CCD detector mosaic camera at the Las Campanas Observatory, Chile (Udalski, 2003). The OGLE project allowed to discover tens of thousands of new variable stars in the LMC and SMC. In particular, the OGLE III catalogues contain:

- 3361 CCs in the LMC, of which almost 1000 are new identifications (Soszyński et al., 2008a).
- 24906 RR Lyrae stars in the LMC, of which 42 are in common with the General Catalogue of Variable Stars (GCVS), 8745 are in common with the MACHO catalogue, and 7407 are in common with the OGLE II catalogue, hence providing ~ 8700 new identifications (Soszyński et al., 2009).
- 4630 CCs in the SMC, of which ~ 2049 are in common with the OGLE II catalogue (Udalski et al., 1999), and ~ 160 in common with the EROS-2 catalogue Marquette (1999), hence providing ~ 2421 new identifications (Soszyński et al., 2010).
- 2475 RR Lyrae stars in the SMC, of which 558 in common with the OGLE II catalogue (Soszynski et al., 2002), 27 in common with the GCVS, and 19 in common with the list of RR Lyrae stars in the vicinity of 47 Tuc published by Weldrake et al. (2004), hence providing ~ 1871 new identifications (Soszyński et al., 2010).
- 197 Type II Cepheids in the LMC, of which 125 are identified for the first time Soszyński et al. (2008b).

- 43 Type II Cepheids in the SMC, of which 11 are in common with the OGLE II catalogue, providing 32 new identifications (Soszyński et al., 2010c).
- 83 new Anomalous Cepheids in the LMC identified in the OGLE III catalogue (Soszyński et al., 2010c).

Most of the observations were obtained in the I photometric band which closely resembles the Johnson-Cousins standard filter. All fields were also observed in the V band with a frequency of about 10% the I -band coverage (Udalski et al., 2008). The data were calibrated to the standard system using hundreds of thousands stars observed during the OGLE-II project (1997-2000) and in common with the OGLE-III observations (Soszyński et al. 2008a, and references therein). The accuracy of the photometric calibrations is better than 0.02 mag.

The observing material collected during the OGLE-III phase is a unique dataset that can be used in a large variety of astrophysical applications. During this thesis work we massively used the OGLE-III data.

4.3 VISTA telescope and surveys

VISTA, the Visible and Infrared Survey Telescope for Astronomy, is a 4 m telescope situated at the ESO's Paranal Observatory in Chile (see Fig. 4.2 and Table 4.1). It is the biggest near-IR wide field imaging telescope and is designed¹ to perform six public surveys. The VISTA infrared camera (VIRCAM, Dalton et al. 2006) has a set of broad-band filters: Z, Y, J, H, K_S and a narrow-band filter at $\lambda = 1.18\mu$ (see Table 4.2). VIRCAM uses an array of 16 2048x2048 20 μm pixel detectors with a mean pixel size of 0.339'' and a total field of view of 1.65 deg².

The physical space among detectors (see Fig. 4.3, left panel) produces gaps in a single exposure image (see Fig. 4.3, right panel). A number of basic actions are executed during the near-infrared observations in general, and during the VIRCAM/VISTA operation in particular. Here we give the definition of these actions

¹75% of the VISTA time available to ESO will be available for large scale public surveys and the remaining 25% for smaller proprietary surveys. On the assumption that VISTA is unavailable ~ 10 nights a year for maintenance, the corresponding numbers of nights per year are ~ 236 nights (Public Surveys) and ~ 78 nights (Proprietary Surveys).

Name	Visible and Infrared Survey Telescope for Astronomy (VISTA)
Location	Paranal (Chile)
Start of operations	2009
Type	near-infrared survey telescope
Wavelength range	(0.84 - 2.5) μm
Aperture	4.1 m
Optical design	modified Ritchey Chrétien with corrector
Mounting	altazimuth fork
Housing	conventional rotating dome

Table 4.1: Informations on the VISTA telescope. Table adapted from <http://www.eso.org/public/teles-instr/surveylelescopes/vista.html>



Figure 4.2: Left: Picture of the Paranal mountains in the Atacama desert (Chile) where are located both VISTA (down) and the VLTs (up). Right: VISTA enclosure. Figures from Emerson et al. (2006)

in order to make the following discussion more understandable².

- An “integration” is a simple snapshot of a specified elapse of time. This elapsed time is known as the Detector Integration Time - DIT (secs).
- An “exposure” is the stored product of N individual integrations. Each exposure is associated with an exposure time equal to NDIT \times DIT, where NDIT is the number of DIT.
- A “microstep (pattern)” is a pattern of exposures at positions each shifted by a very small amount (< 3 arcsec) from the reference position.

²see the VISTA user manual at <http://www.eso.org/sci/facilities/paranal/instruments/vircam/doc/>

- A “jitter (pattern)” is a pattern of exposures at positions each shifted by an amount (< 30 arcsec) from the reference position. Each position of a jitter pattern can contain a microstep pattern.
- A “pawprint” is the ensemble of 16 non-contiguous images of the sky produced by the VISTA IR camera, with its 16 non-contiguous detectors. The name “pawprint” is from the similarity to the prints made by the padded paw of an animal (see Fig. 4.3).
- A “tile” is a filled area of the sky fully sampled by combining multiple pawprints. Six pawprints are required to survey a contiguous area of 1.5 deg^2 . Three steps in the Y direction and 2 steps in the X direction (see Fig. 4.4) provide a fully covered image. The field of view of a single tile is indeed the result of the combination of the field of view of the six pawprint that form the tile. The field of view of the pawprints overlap; this implies that a VISTA tile observes at least twice each portion of the sky, except for two edge strips in the extreme “Y” directions of the array.

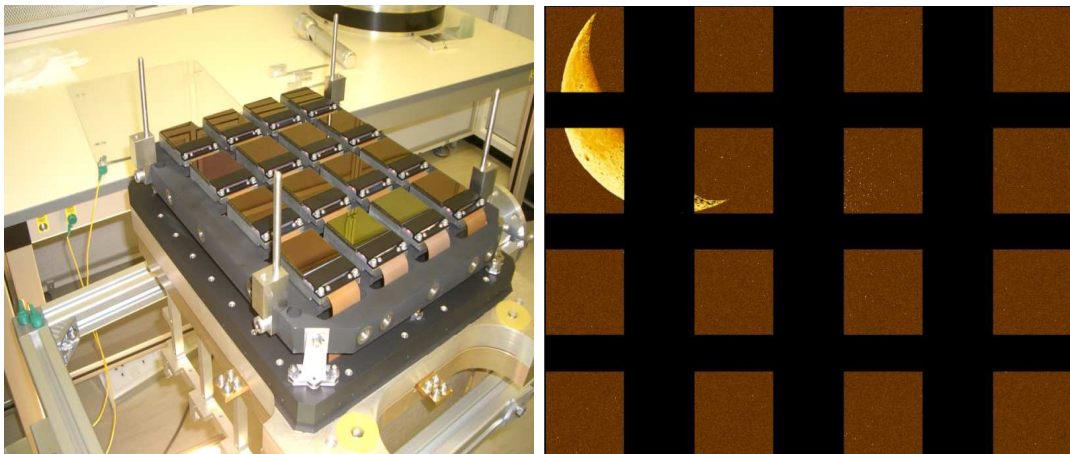


Figure 4.3: *Left:* Picture of VIRCAM. *Right:* Example of a “pawprint” image showing the Moon. (Figures taken from <http://www.vista.ac.uk/>)

Filter	Z	Y	J	H	K_S	NB1.18
Central wavelength (μm)	0.88	1.02	1.25	1.65	2.15	1.18
FWHM (μm)	0.12	0.10	0.18	0.30	0.30	0.01

Table 4.2: Characteristics of the filters used by VIRCAM

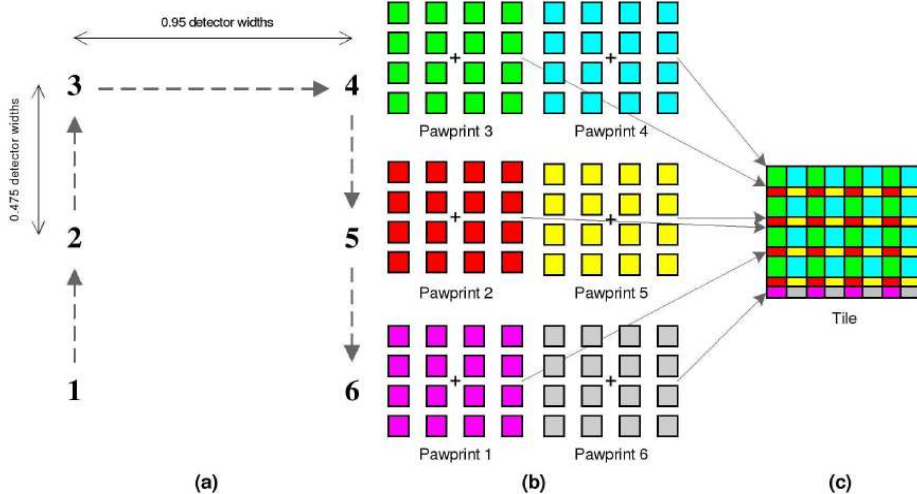


Figure 4.4: Contiguous tile formed from the combination of six overlapping pawprints. Panel (a): three shifts in the Y direction and two shifts in the X direction allow to fill the field. Panel (b): six pawprints that form a tile; Panel (c): Tile resulting from the combination of pawprints shown in panel (b) using the path shown in panel (a). Figures from <http://www.vista.ac.uk/>

The VISTA Telescope is specifically designed to perform large surveys in the infrared (Emerson, 2001). In fall 2009 VISTA obtained the first observations of six ESO large public surveys³, namely:

- UltraVista;
- VISTA kilo-Degree Infrared Galaxy Survey (VIKING);
- VISTA Magellanic Survey (VMC);
- VISTA Variables in the Via Lactea (VVV);
- VISTA Hemisphere Survey (VHS);
- VISTA Deep Extragalactic Survey (VIDEO).

³For a detailed description of the surveys see <http://www.eso.org/sci/observing/policies/PublicSurveys/sciencePublicSurveys.html>.

Among these surveys we briefly describe VVV that, similarly to VMC, targets variable stars. The VVV (P.I. Dante Minniti, Catolica) survey will observe the Galactic bulge and a portion of the adjacent plane in the Z , Y , J , H , and K_S filters. VVV covers a total area of 520 square degrees containing 355 open and 33 globular clusters. The VVV is multi-epoch in nature in order to detect a large number of variable objects and will provide > 100 carefully spaced observations of each tile. A catalog with $\sim 10^9$ point sources including $\sim 10^6$ variable objects is expected. These will be used to create a 3-dimensional map of the Bulge from well-understood distance indicators such as the RR Lyrae stars. Other science drivers include the derivation of ages of the stellar populations, study of globular cluster evolution, as well as of the stellar initial mass function.

4.4 The VMC survey

VISTA Y , J , K_S survey for Magellanic Clouds (VMC; P.I. Maria-Rosa Cioni, Hertfordshire University, UK) will observe 184 deg^2 of the Magellanic System (MS) in the Y , J , and K_S wavebands reaching an expected sensitivity limit of Vega magnitudes $Y=21.9$ mag, $J = 21.4$ mag and $K_S=20.3$ mag with S/N=10 (Cioni et al., 2011). The main goals of the survey are to study the star formation history (SFH) of the Magellanic System as well as to trace its three-dimensional structure. The SFH of the entire MS will be studied from color magnitude diagrams and simulations of the resolved stellar populations. The 3-D geometry of the MS will be inferred exploiting a number of different distance indicators among which the luminosity of the red clump stars, and the Cepheid and RR Lyrae period-luminosity, period-luminosity-colour and Wasenheit relations. The VMC K_S -band data are taken in time series mode down to ~ 20 mag. Each time series is composed by 12 individual epochs. This gives the possibility to study the K_S infrared light curves of variable stars belonging to the different stellar populations in the Magellanic System. Previous infrared surveys such as 2MASS (Skrutskie et al., 2006) and DENIS (Cioni et al., 2000a) were much shallower. They allowed to study the Cepheids but not the RR Lyrae stars.

The VMC survey covers the LMC area (116 deg^2) with 68 tiles, while 27 tiles cover the SMC (45 deg^2), and 13 cover the Bridge (20 deg^2), see Fig. 4.5. Addition-

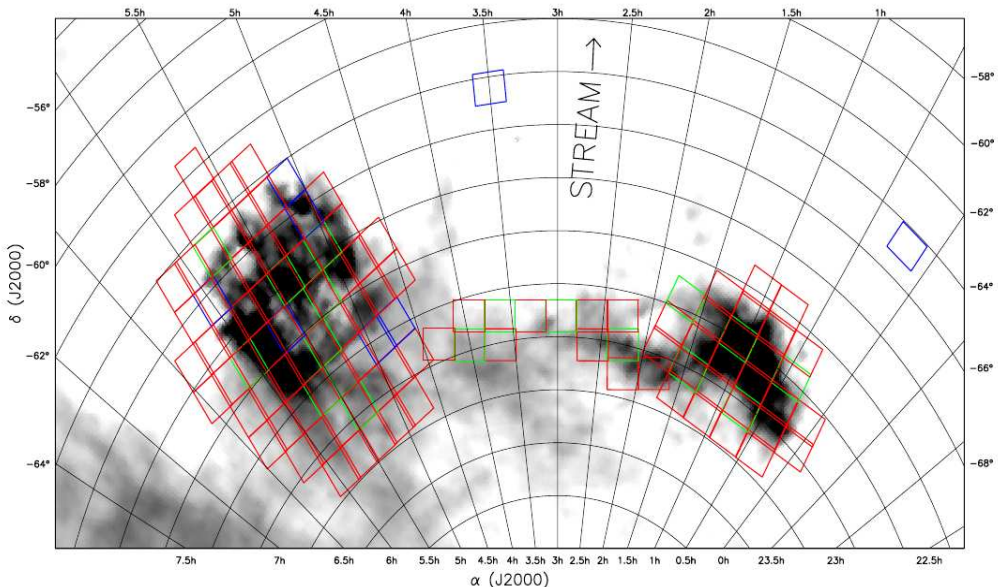


Figure 4.5: Sky coverage of the VMC survey. The underlying image shows the HI distribution according to McClure-Griffiths et al. (2009). The VISTA tiles are colour coded as follows: blue rectangles represent tiles for which observations started during the dry-runs and in the ESO period P85, green rectangles are for tiles observed in P86, and red tiles are observations that did not start until P87 (see Section 4.4.1 for details on the observation periods). Figure from Cioni et al. (2011).

ally, 2 tiles (3 deg^2) are positioned on the Stream, one approximately to the North of the centre of the Bridge and the other one to the North of the SMC, corresponding respectively to a dense area of gas and to a dense area of stars, following the simulations by Mastropietro (2009). Each tile is identified by two numbers: the first number indicates the row and the second the column of the mosaic that covers the system. Note that a separate tiling pattern has been defined for each region. Fig. 4.6 shows the tiles distribution in the LMC region. Row numbers increase from South to North and column numbers increase from West to East. Tiles covering the LMC are oriented at a position angle of $+90$ deg. The default orientation (position angle = 0) points the “*Y*” axis to the North and the “*X*” axis to the West. The position angle is defined to increase from minimum number of tiles and maximum area, increasing the efficiency of the survey. The overlap between the doubly-covered sky areas in adjacent tiles corresponds to 60 arcsec in both “*X*” and “*Y*” directions. The LMC mosaic was created using the Survey Area Definition Tool (SADT - Arnaboldi et al. 2008). A geodesic rectangle centered at $\alpha = 05^h : 35^m : 50^s$, $\delta = -69^\circ : 27' : 12''$ (J2000), with width=11.8 deg and height=15.9 deg, was created as the basis of the tiling process. Outer tiles were removed leading to the patterns shown in Figs. 4.5 and 4.6. The area covered by the tiles was checked against the distribution of stellar associations, carbon stars and other stellar objects using Aladin (Bonnarel et al., 2000). The centre of the rectangle was adjusted to include the 30 Doradus nebulosity within a single tile and similarly, the field in the direction of the South Ecliptic Pole (SEP) that the future space mission Gaia⁴ will repeatedly observe for calibration. Guide stars were assigned automatically to each tile using the GCS-2 reference catalogue (Lasker et al. 2008).

The SMC is covered using tiles placed at a position angle of 0 deg, with the wide tile-edge approximately along the right ascension direction in order to maximize the coverage with that number of tiles. The geodesic rectangle is centered at $\alpha = 00^h : 50^m : 00^s$, $\delta = -73^\circ : 00' : 00''$ (J2000), with width=8.0 deg and height=8.0 deg. The position of the centre of the rectangle was tuned to match the area that will be observed in the optical domain by the VLT Survey Telescope (VST) as part of the STEP survey (P.I. Ripepi; Capaccioli et al. 2005) and to provide sufficient overlap for a consistent calibration with the Bridge area.

⁴<http://sci.esa.int/science-e/www/area/index.cfm?fareaid=26>

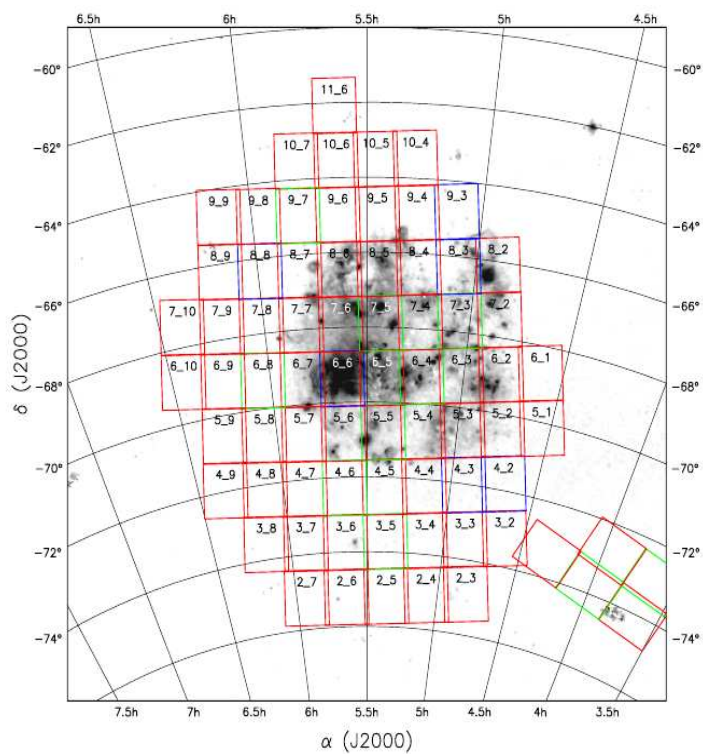


Figure 4.6: Tiles distribution in the LMC area (from Cioni et al. 2011). Tiles are color-coded as in Fig. 4.5.

The VMC tiles in the Bridge are chosen in order to have a good sampling of the stellar population following a continuous pattern (Cioni et al., 2011). In this case the geodesic rectangle was drawn with centre at $\alpha = 03^h : 00^m : 00^s$, $\delta = -74^\circ : 30' : 00''$ (J2000) and with width 13.5 deg and height 3 deg.

The two tiles positioned in the Stream region were prepared using the same parameters as for the LMC tiles, except for the position angle set to 0 deg. In these cases the geodesic rectangles are respectively coincident with the two tiles.

The next section describes the strategy and the status of the VMC survey as of the time of writing this PhD thesis.

4.4.1 VMC observations

The first VMC data were obtained during the Science Verification observations (15-31 October 2009) and the so called dry-run period (1 November 2009-31 March 2010) when VISTA was tested and survey operations were still being defined. The bulk of the VMC observations is carried out during the even-numbered ESO periods starting in October every year and ending in March the following year because of the seasonal observability of the Magellanic system.

Observations of the VISTA Public Surveys are obtained in service mode by the ESO staff. The requested observing conditions for the VMC survey are summarized in Table 4.3. Tiles centered on the most crowded regions, i.e. 30 Dor and the central regions of both LMC and SMC, have more stringent seeing conditions. This is necessary to prevent confusion in the bluest bands, while K_S band observations will not be limited by confusion for a seeing $\leq 0.9''$. The best $FWHM_S$ in the VISTA images are 0.6-0.7'' and undersampling, with respect to a pixel size of 0.339'', is not a cause of concern in the data treatment.

The Magellanic system never rises above 50° from the horizon. Therefore, a compromise had to be made between observing at reasonable airmass and achieving continuous observability over about five months for the monitoring process. The maximum airmass constraints were optimized as a function of the tile declination, as shown in Table 4.3.

Table 4.4 describes the main parameters of the VMC observations. The total exposure time is calculated as follows: (number of epochs) \times 2 \times (number of jitters) \times (number of DITs) \times DIT. The factor of two comes from the tiling pattern, during

Band	Seeing (arcsec) uncrowded	Seeing (arcsec) crowded
Y	1.2	1.0
J	1.1	0.9
K_s	1.0	0.8
Field	Tile row	Airmass
LMC	2 , 3, 4	1.7
LMC	5, 6, 7	1.6
LMC	8, 9, 10, 11	1.5
Stream	1,2	1.5
SMC	2 , 3, 4, 5	1.7
SMC	6, 7	1.6
Bridge	1, 2, 3	1.7

Table 4.3: Observing conditions requested for the VMC survey (from Cioni et al. 2011).

which most points of the sky are observed twice (on average). For the K_S band the total exposure time is: $12 \times 2 \times 5 \times 15 \times 5 = 9000$ s.

Each VMC Observing Block (OB) includes only one filter. OBs were prepared using a new version of the Phase II Proposal Preparation tool especially revised for Public Surveys with the VISTA and VST telescopes. It allows the user to have more control over the survey execution with new high-level tools called *scheduling containers* (Arnaboldi et al., 2008). Three types of container were available: *concatenations* (grouping together OBs for back-to-back execution), *time-links* (imposing time constraints for the execution of OBs, including execution of OBs in a user-defined sequence), and *groups* (that improve the prioritization of OBs to ensure the completion of one set of OBs before another set is started). Each time-link sequence can start at any time, i.e. a $TK1$ OB can be observed on the same night as an OB in the Y, J or K_S filter taken as part of a concatenation or a group. Once started, the next observation of a TKn OB, in a time-link sequence, is obtained at intervals equal or larger than: 1, 3, 5 and 7 days for epochs 2 to 5, respectively, and thereafter at least 17 days from each previous observation (epochs 6 to 11). Some OBs in the time-link sequence were also repeated. Table 4.5 summarize time-link sequences where 11 individual K_S band OBs are associated with each LMC field.

Filter	Y	J	Ks
Central wavelength	1.02	1.25	2.15
Bandwidth	0.10	0.18	0.30
Detector Integration Time DIT (s)	20	10	5
Number of DITs	4	8	15
Number of exposures	1	1	1
Micro-stepping	1	1	1
Number of Jitters	5	5	5
Paw-prints in tile	6	6	6
Pixel size (arcsec)	0.339	0.339	0.339
System FWHM	0.51	0.51	0.51
Exposure time per epoch (s)	800	800	750
Number of epochs	3	3	12
Total exposure time (s)	2400	2400	9000
Predicted sensitivity per epoch (Vega mag)	21.3	20.8	18.9
Signal-to-noise per epoch at depth required	5.7	5.9	2.9
Total predicted sensitivity (Vega mag)	21.9	21.4	20.3
Total signal-to-noise at depth required	10	10	10
Saturation limit (Vega mag)	12.9	12.7	11.4
Area (square degrees)	184	184	184
Number of tiles	110	110	110

Table 4.4: Parameters of the VMC survey (from Cioni et al. 2011).

Table 4.5: LMC epochs: time linked (T) Ks-band monitoring. Table adapted and updated from Cioni et al. (2011).

Tile	TK1	TK2	TK3	TK4	TK5	TK6	TK7	TK8	TK9	TK10	TK11
3_5	01.12.10	10.12.10 06.12.10 ^a 06.12.10 ^b	20.02.11	02.09.11 04.09.11 ^b 02.09.11 ^a	13.09.11	02.10.11	06.11.11	23.11.11	16.01.12	05.02.12	
4_2	14.12.09	17.12.09	5.01.10	14.01.10	22.01.10	21.01.12					
4_3	10.12.09	17.12.09	21.12.09	27.12.09	18.01.10	25.01.12					
5_5	26.10.10	28.10.10	11.11.10	26.11.10 16.11.10 ^b	09.12.10	27.12.10 02.01.11	26.01.11	10.10.11	31.10.11	22.11.11	
6_4	27.10.10	29.10.10	11.11.10	28.11.10 27.11.10	13.12.10	03.01.11	22.02.11	18.09.11	08.10.11	01.11.11	23.11.11
6_6	8.11.09 6.11.09 ^a	12.11.09	17.11.09	29.11.09	7.12.09	26.12.09	13.01.10 ^a	31.01.10	19.02.10	11.03.10	10.11.10
6_8	15.01.12										
7_3	29.01.11	01.01.12 20.02.11 ^{a4}	20.01.12	27.01.12 01.02.12							
7_5	01.03.11 ^{a2}										
8_3	3.12.09	6.12.09	22.12.09	28.12.09	14.01.10	31.01.10	22.02.10	25.10.10	14.11.10 ^b 05.09.11	27.09.11	07.11.11 08.11.11
8_8	14.11.09	19.11.09	25.11.09	30.11.09	7.12.09 ^b 26.10.10	25.12.09	14.01.10	31.01.10	19.02.10	07.03.10	26.11.10 16.11.10 ^b
9_3	4.12.09	9.12.09	19.12.09	23.01.10 16.01.10 ^b	31.01.10	24.02.10 20.02.10 ^b	15.09.10	11.10.11 ^b 16.01.12	02.02.12		
9_7	02.03.11										

^a Reduced number of jitters and/or paw-prints

^{an} ^an Reduced number of jitters and/or paw-prints for a number of n OBs during the same night;

^b Seeing and/or ellipticity too high.

The preliminary results of the survey and its strategy are described in Cioni et al. (2011); results on star formation history, AGN stars and planetary nebulae studies are presented in Rubele et al. (2011), Gullieuszik et al. (2011) and Miszalski et al. (2011), respectively.

Data reduction and archiving

The raw VISTA images acquired for the VMC survey are reduced by the VISTA Data Flow System (VDFS, Irwin et al. 2004) pipeline at the Cambridge Astronomical Survey Unit (CASU). The VDFS pipeline is specifically designed for reducing VISTA data and is used to process up to 250 GB/night of data. The VMC data are reduced together with other VISTA data on a weekly basis. Prior to this science reduction the data are checked at the observatory site (ESO Chile) using a simplified version of the VDFS pipeline. The data are subsequently checked at ESO in Garching to monitor the instrumental performance and to feed updated information back to the observatory (Cioni et al., 2011). The most relevant VDFS steps for the reduction of the VMC data are the reset, dark, linearity, flat and sky background corrections; jittered and paw-print stacking; points source extraction; astrometric and photometric calibration; bad pixel handling, propagation of uncertainties and effective exposure times by use of confidence maps; nightly extinction measurements.

A tile image is produced by combining 96 different images (16 detector images per each of 6 pawprints).

The data reduced by the VDFS pipeline at CASU are ingested into the VISTA Science Archive (VSA) at the Wide Field Astronomy Unit (WFAU) in Edinburgh which is similar to the WFCAM Science Archive (Hambly et al., 2008). There are three main types of VSA tables that are important for the VMC survey (Cioni et al. 2011, Cross et al. 2009):

- vmcDetection table: it contains the catalogues corresponding to individual observations;
- vmcSource table: it contains the list of sources obtained from deep stack images and each source is matched in the three VMC bands;
- vmcSynoptic tables: contain the colour information and the multi-epoch information for individual observations.

VSA releases before September 2011 had some problems with the Julian Day of the observation (see section 5.4). A very large fraction of my work inside the VMC project was devoted to check the quality of the first data obtained with VISTA. These checks slowed down the scientific work and results, nonetheless they were necessary steps of the data analysis in general, and of the VMC data in particular.

The latest release of VMC data from the VSA (VMCv20120126) occurred on January 26th, 2012. This release included completely observed (the whole 12 epoch time-series), reduced and catalogued VMC data for two tiles in the LMC, tile 6_6 and tile 8_8, (see Table 4.5). The fields covered by these two tiles are very important for astronomical reasons:

- tile 8_8 covers the South Ecliptic Pole (hereinafter SEP) region that the Gaia astrometric satellite (Lindegren & Perryman 1996; Lindegren 2010) will repeatedly observe at the beginning of the mission for calibration purposes. It is an external tile that lies in an uncrowded, peripheral area of the LMC. Information on the variable stars in this area comes only from the optical data in non conventional filters of the EROS-2 survey;
- tile 6_6 is centered on the well known 30 Doradus (hereinafter 30 Dor) star forming region. It lies in the central part of the LMC and is a very crowded

area. Optical time-series data in the V_J and $I_{cousins}$ filters are available here, from the OGLE III survey.

The very different location and crowding conditions of these two fields gave us the possibility to test and fine tune our strategy for the analysis of the variable stars observed by the VMC survey.

Chapter 5

Data analysis, and first results for RR Lyrae stars from the VMC survey

We have used the identification, the period, and the epoch of maximum light of the RR Lyrae stars and Cepheids identified in the Large Magellanic Cloud (LMC) by the optical microlensing surveys (see section 4.2), to fold the K_S -band light curves produced by VMC (see section 4.4) and derive average K_S magnitudes for these variables. In this Chapter we present the work done on the visual light curves of both RR Lyrae stars and Cepheids, and present results from the analysis of the RR Lyrae stars contained in the first two “tiles” completely observed by the VMC survey, namely tiles 8_8 and 6_6. These two tiles are centered respectively on the South Ecliptic Pole (SEP) field and on the well known 30 Doradus (30 Dor) star forming region of the LMC.

5.1 Optical data for the LMC RR Lyrae and Cepheids

Fig. 5.1 shows the distribution of RR Lyrae stars (left) and Classical Cepheids (right) identified in the LMC by the OGLE III survey (Soszyński et al. 2009, and Soszyński et al. 2008a, respectively). As expected, the two distributions are very different. The RR Lyrae stars have a larger density in the central region of the LMC, however, they are still present in the external areas, their distribution is smooth and traces a spheroid corresponding to the LMC halo. On the other hand, the Classical Cepheids are strongly concentrated towards the LMC bar and almost disappear in

the external regions. Fig. 5.2 shows the distribution of EROS-2 candidate RR Lyrae stars (left) and Cepheids (right) in the LMC area. Black boxes show the VMC tiles on the LMC, red boxes correspond to the LMC fields observed by OGLE III, green boxes represent the VMC tiles with the complete 12-epoch time-series already available, and the magenta rectangle shows the South Ecliptic Pole (SEP) field that the Gaia satellite (Lindegren & Perryman 1996; Lindegren 2010) will repeatedly observe at the beginning of the mission for calibration purposes. Fig. 5.2 shows that EROS-2 coverage of the LMC is much larger than OGLE III coverage, but is still smaller than the VMC coverage. The wider area of the LMC covered by EROS-2 allows to better study the distribution of both RR Lyrae stars and Cepheids in the LMC. The comparison of the two panels in Fig. 5.2 further highlights the difference between RR Lyrae and Cepheid distributions pointed out by the OGLE III data (see Fig. 5.1), but also reveals a feature not observed before because of the smaller field of view sampled by OGLE III: as already noted in Clementini (2011), the distribution of EROS-2 candidate Cepheids (right panel of Fig. 5.2) suggests the existence in the LMC of a second bar running almost parallel above the first main LMC bar. We expect that the VMC data, combined with the microlensing data, both EROS-2, OGLE III and OGLE IV, which is in progress (see section 4.2.2), will allow us to confirm the existence and fully characterize this second bar as well as to significantly improve our knowledge of the geometrical structure of the entire Magellanic System.

Four VMC fields of the LMC have already been completely observed (green rectangles in Fig. 5.2) they correspond the tiles: 6_6 (middle left), 8_8 (top left), 6_4 (middle right,) and 8_3 (top right). However, as anticipated in section 4.4.1, at the time of writing this PhD Thesis, only data corresponding to tiles 6_6 (30 Dor field) and 8_8 (SEP field) had been fully reduced and catalogued. The data for tiles 6_4 and 8_3 have been fully reduced, but not yet completely catalogued by the VSA, thus they were released in the last VSA internal release of January 26th, 2012. We expect them to be made available in the next VSA internal release on July 2012. The work described here is indeed part of a bigger project that aims at studying systematically the infrared properties of the pulsating variable stars in each of the 68 tiles that cover the LMC, as well as in each of the 27 tiles that cover the SMC (see section 4.4.1). The result will be an improved knowledge of the geometrical distribution of the stars in the MS.

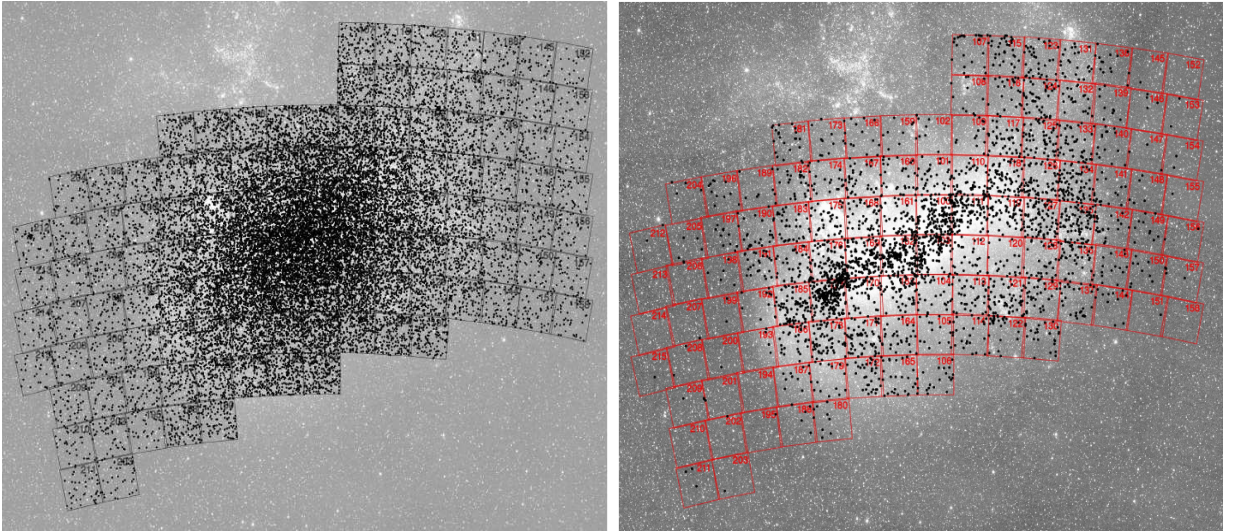


Figure 5.1: Distribution of the OGLE III fields (black and red boxes, respectively) in the LMC field. Black points represent RR Lyrae stars (left panel), and Cepheids (right panel), respectively. The background image of the LMC is originated from the ASAS sky survey Pojmanski (1997). Figures from Soszyński et al. (2009), and Soszyński et al. (2008a), respectively.

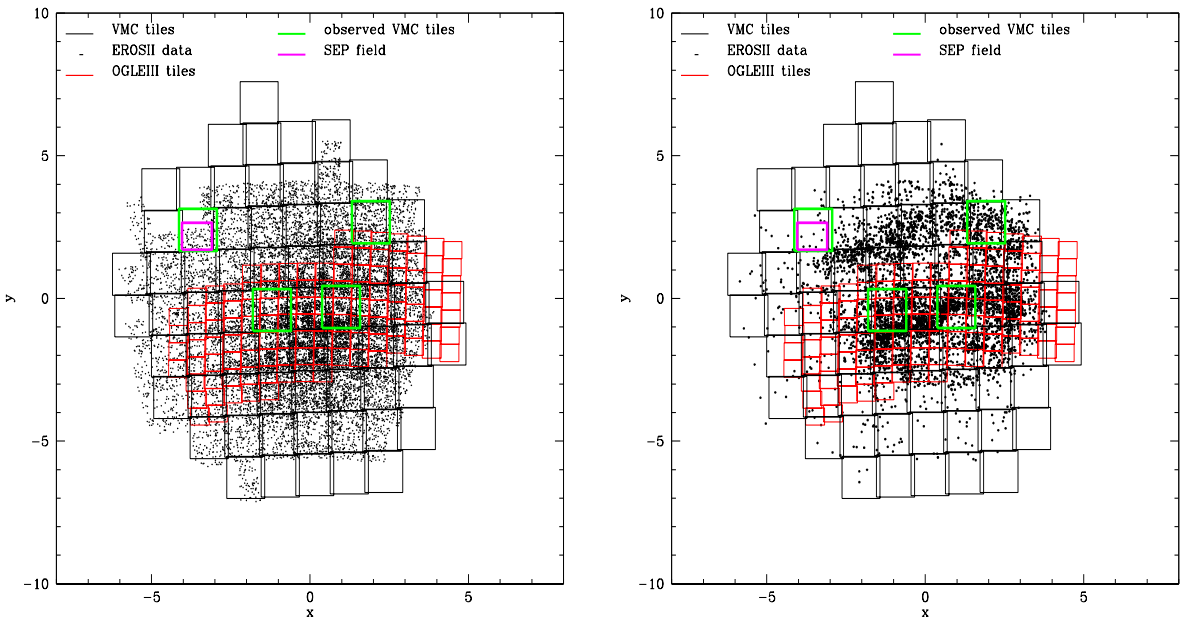


Figure 5.2: Distribution of the EROS-2 RR Lyrae (left) and Cepheid (right) candidates (black points) in the LMC. Black boxes represent the VMC tiles, green boxes represent VMC tiles completely observed (full 12-epoch time series), red boxes are the OGLE III fields and magenta box represent the Gaia SEP calibration field.

Given its location on the periphery of the LMC, tile 8_8 only overlaps with EROS-2. Coordinates, periods and optical light-curves of RR Lyrae stars and Cepheids in the SEP field were taken from the EROS-2 catalogue and cross-matched to the VMC data using TOPCAT¹ (Tool for OPerations on Catalogues And Tables). The 30 Dor field is covered by both EROS-2 and OGLE III, as well as by MACHO, but for the present analysis we only employed periods and optical (Johnson-Cousins, V, I bands) light-curves from OGLE III.

5.2 EROS-2 data in the SEP field: GRATIS analysis

In this work we extensively used the EROS-2 data for the LMC RR Lyrae stars and Cepheids (see section 4.2), which were kindly provided by the EROS collaboration. Fig. 5.3 shows the ($B_{EROS}, B_{EROS} - R_{EROS}$) color magnitude diagram obtained from the EROS-2 catalogue of the LMC sources (red points). The blue points correspond to candidate RR Lyrae stars: all objects with B_{EROS} magnitude between 18.46 and 20.03 mag, and $B_{EROS} - R_{EROS}$ colour between 0.05 and 0.58 mag in the EROS-2 catalogue were considered candidate RR Lyrae stars. Fig. 5.4 shows the (P, B_{EROS}) diagram obtained from the EROS-2 catalogue of the LMC sources (red points). The blue points correspond to candidate Classical Cepheids (CCs): all objects with B_{EROS} magnitude between 13.39 mag and 17.82 mag, and Period between 0.89 d and 15.85 d were considered CC candidates. These selections returned lists of 16337 RR Lyrae, and 5800 Cepheid candidates over the whole field of the LMC covered by EROS-2.

We first selected the EROS-2 candidate RR Lyrae stars and Cepheids in the SEP field, by extracting all objects within $87.8464 < \text{RA(deg)} < 91.8464$ and $-67.3413 < \text{DEC(deg)} < -65.3413$, in EROS-2 catalogues of candidate RR Lyrae and Cepheids. We then matched the EROS-2 catalogues with the VMC data, using the VSA utilities (see section 4.4.1). In the SEP field we found 117 candidate RR Lyrae stars, and 21 CC candidates in common between the EROS-2 and the VMC catalogues. To study the light curves of these objects we used the GRaphical Analyser of TIme Series

¹see <http://www.star.bris.ac.uk/~mbt/topcat/>

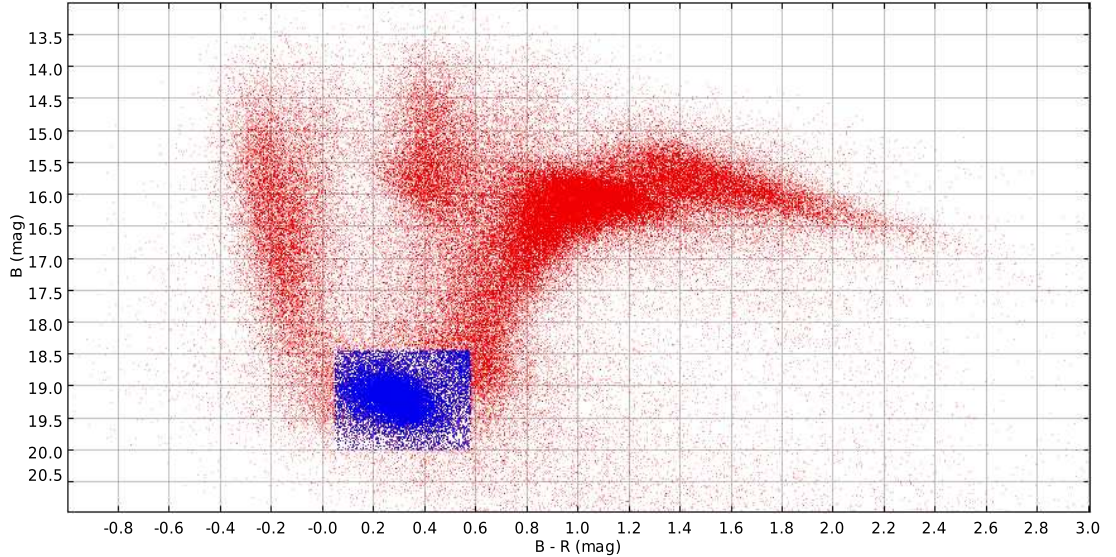


Figure 5.3: B_{EROS} , $B_{EROS} - R_{EROS}$ color magnitude diagram of the LMC from the EROS-2 data (red points). The blue box marks the region corresponding to candidates RR Lyrae stars.

(GRATIS) software developed at the Bologna Observatory by P. Montegriffo (see e.g., Clementini et al. 2000). We checked the EROS-2 Period (P_{EROS2}) for a sub-sample of 24 RR Lyrae stars in the SEP field, by obtaining our own estimate for the period (P_{GRATIS}). We found a very good agreement between P_{EROS2} and P_{GRATIS} , with difference, on average, on the fifth decimal place, thus adopted P_{EROS2} for the remaining stars. Although we did not calculate P_{GRATIS} for all candidates in the SEP, we analyzed the light-curves for all of them with the GRATIS package using P_{EROS2} as input period. In this way we used GRATIS not to search the Period, but to visually check the light-curves of the RR Lyrae and Cepheid candidates. Thanks to this visual inspection it was possible to clean the samples of RR Lyrae and Cepheids from spurious sources and/or wrong periods, as in the case of star id_{EROS2}=B0383l16657, for which P_{EROS2} is twice the actual period.

Fig. 5.5 shows the light curve of a confirmed RR Lyrae star on the left, and the light curve of a transient source, misclassified as RR Lyrae star, on the right. Of the 116 RR Lyrae candidates, 107 were confirmed by the analysis with Gratias, while the

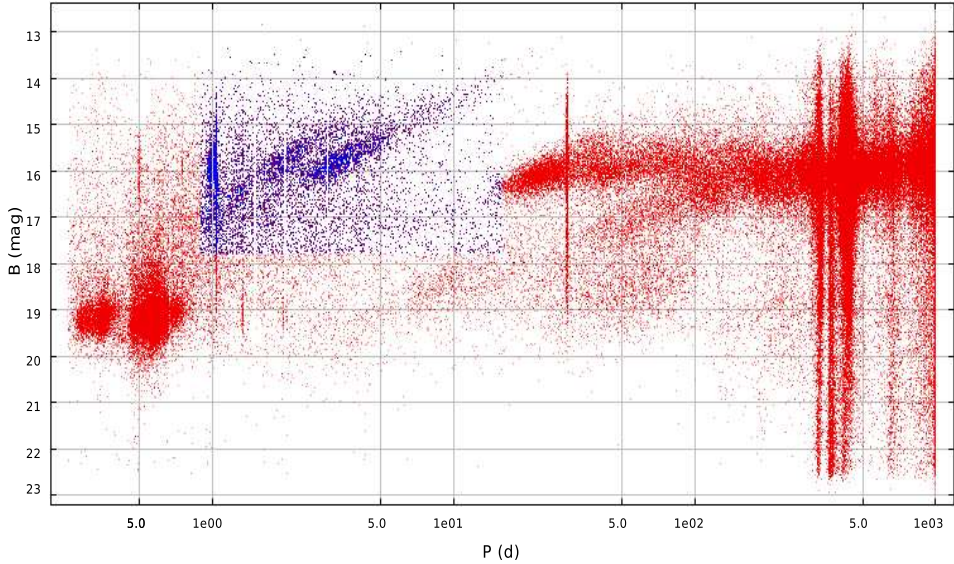


Figure 5.4: Distribution of EROS-2 data (red points) for the LMC field in the (P , B_{EROS}) plane. The blue box marks the region corresponding to candidate Classical Cepheids. The Period axis is in logarithmic scale.

remaining 9 were rejected (see below). Table 5.6 summarized main informations on the confirmed RR Lyrae stars. Also for the CCs we analysed the light curves using GRATIS; out of the 21 CC candidates, 12 were confirmed, while 10 were rejected.

Thanks to the analysis with GRATIS, we also determined the epoch of maximum light for each B_{EROS} band light curve. Moreover, we were able to make a first distinction between RR_{ab} and RR_c pulsators, by simply checking the shape of the light curves. The classification in pulsation mode of the RR Lyrae stars was also carefully studied using the Bailey diagram and the Fourier parameters of the light curve decomposition (see 5.3.1).

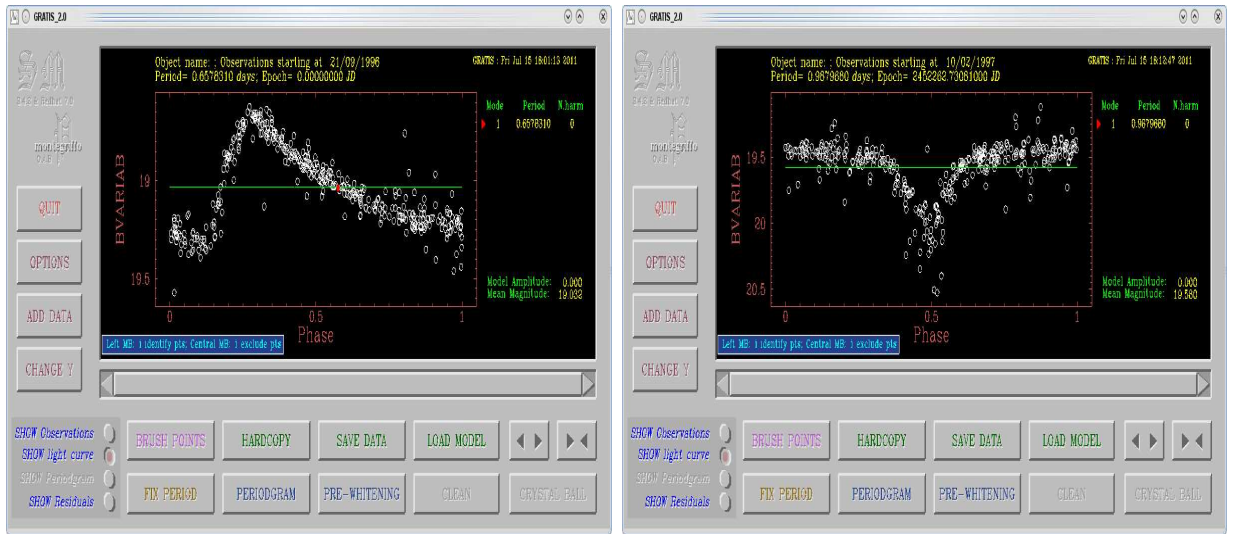


Figure 5.5: Light curves of two RR Lyrae candidates. *Left*: typical light curve of a confirmed RR Lyrae star; *Right*: light curve of a source misclassified as RR Lyrae star, that likely is a transient object.

5.3 Classification of the RR Lyrae stars

5.3.1 Identification of the pulsation mode with the Bailey diagram

We discuss in this paragraph the classification of the RR Lyrae stars made using the Bailey diagram ($\log P$, A_V). Light curves in the Johnson V_J band are needed to apply the Bailey analysis. We therefore transformed each B_{EROS} and R_{EROS} light curve to the V_J and I_C bands using equation 4 from Tisserand et al. (2007):

$$R_{EROS} = I_C; \quad (5.1)$$

$$B_{EROS} = V_J - 0.4(V_J - I_C). \quad (5.2)$$

We transformed the light curves of all 116 SEP RR Lyrae stars to the V_J band and then studied the light curves (cfr. section 5.2) with GRATIS. This analysis was necessary to check the quality of the V_J light curves obtained with the Eqs. 5.1 and 5.2. From this analysis we also inferred the amplitude A_V of the light curve. A_V is extremely important both to classify the RR Lyrae stars in type (Bailey 1902) and to study the K band light curve using the template fitting method (cfr. 5.4).

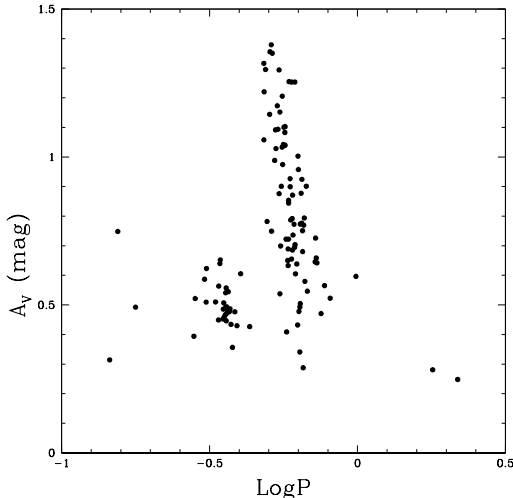


Figure 5.6: Bailey diagram of the RR Lyrae stars in the SEP field.

Fig. 5.6 shows the distribution of the SEP RR Lyrae stars in the Bailey diagram. In this plot we can distinguish the following groups:

- $\log P < -0.6$ and $\log P > 0.2$: these objects are non RR Lyrae stars;
- $-0.6 \leq \log P \leq -0.3$ and $A_V \leq 0.7$ mag: first-overtone (RR_c) RR Lyrae stars;
- $-0.3 \simeq \log P \simeq 0.1$: fundamental mode (RR_{ab}) RR Lyrae stars.

The classification through the Bailey diagram (see fig. 5.6) is generally in good agreement with the classification obtained through the visual inspection of the light curve with GRATIS. The points outside both the RR_c and the RR_{ab} loci in fig. 5.6 are: lm0370n7027, lm0373l7929, lm0505l9240, lm0373n18084 (that were already classified as non-RR by the GRATIS analysis) and lm0371n18417. They were all discarded. Two further objects (idEROS-2: lm0385k3074 and lm0507k19195) are classified respectively as RR_c and RR_{ab} with the Bailey diagram, but after the analysis with GRATIS were discarded, as they likely are binary systems. This underlines the importance of the visual inspection of the light curves for objects that have period and amplitude of the light curve compatible with an RR Lyrae star but have a completely different shape of the light curve. Three objects were not successfully classified with GRATIS but they are classified by the Bailey diagram. These

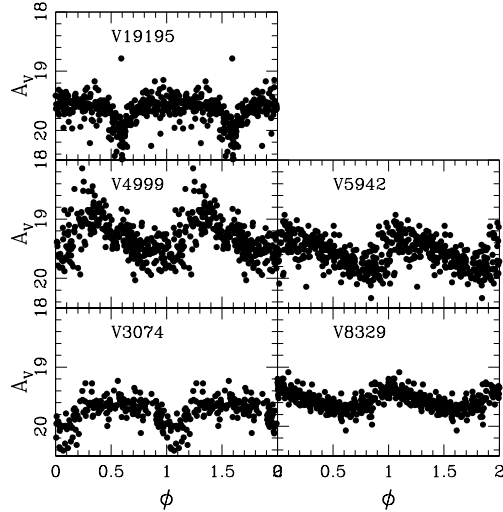


Figure 5.7: Light curves of variable stars classified as RR Lyrae from the Bailey diagram but not/not successfully in the GRATIS analysis.

sources have idEROS-2=lm0373m4999, lm0371l5942 and lm0381l8329. Light curves for all the five sources for which there is disagreement between the two methods of classification are showed in Fig.5.7. All these objects were dropped in the following analysis.

Indeed, we have used in the following analysis only sources that were classified, without any doubts, as RR Lyrae stars both by the visual analysis with GRATIS, and by the Bailey diagram. This method may sound a bit restrictive, but gave us a very reliable sample of 106 RR Lyrae stars in the SEP field. The final catalogue of the SEP RR Lyrae stars contains 30 RR_c and 76 RR_{ab} variables. Table 5.6 summarizes main informations on these confirmed RR Lyrae stars. An alternative way to classify the RR Lyrae stars in types is to use the Fourier parameters of the light curve. We have used this method to further checked the classification of the 106 SEP RR Lyrae stars (see 5.3.2).

5.3.2 Determination of the Fourier parameters

In order to obtain reliable values for the Fourier parameters, we first cleaned the V_J -band light curves from possible outliers, according to the following iterative procedure:

- we discarded all points with residual > 0.200 mag from GRATIS best fit model of the light curve;
- we checked the standard deviation σ of the distribution of residuals:
 - if $\sigma < 0.070$ mag we stopped the cleaning operation;
 - if $\sigma > 0.070$ mag, we discarded also data points with residuals $\in (0.150, 0.200)$ mag from the best fit model.
- we again checked the standard deviation σ of the distribution of residuals:
 - if $\sigma < 0.070$ mag we stopped the cleaning operation;
 - if $\sigma > 0.070$ mag , we discarded also data points with residual $\in (0.100, 0.150)$ mag from the best fit model.

Note that all light curves, after this cleaning still have more than 83 data points. The discard operation was successful for most of the RR Lyrae stars but not all of them. We were able to obtain reliable Fourier parameters using a sine Fourier decomposition for a final catalogue of 81 RR Lyrae stars, of which 56 are RR_{ab} 's and 25 are RR'_c s. For each star we obtained $A(i)$, $\phi(i)$ with i from 1 to 10. The Fourier parameters are summarized in Table 5.1.

Fig 5.8 shows the plot of A_{21}^2 against ϕ_{21} ; almost all the points are split into two separate regions of the plot: in the upper region are points representing RR_{ab} stars, while the RR_c stars concentrate themselves in the lower region, (e.g. Cacciari et al. 2005). There are at least four stars with Fourier parameters out of the expected loci; namely, idEROS-2: lm0380k19902, lm0371m5148, lm0506n12471, and lm0383l15644. These stars had no particular problems during the GRATIS analysis of the light curve, and are well inside the Bailey RR Lyrae loci; we thus decided to retain them. Fig.5.9 shows ϕ_{31} against $\log P$. The presence of a relation between ϕ_{31} and $\log P$ for the RR_{ab} stars (empty circles) is very clear. This is not the case of the RR_c stars (filled black circles), that also have extremely large errors. This is caused by the high number (10) of harmonics used in the Fourier decomposition. This number is too high for c-type RR Lyrae stars. We therefore repeated the Fourier analysis of the RRc stars using only 3 harmonic (see section 5.3.4).

² $A_{ij} = A_i/A_j$

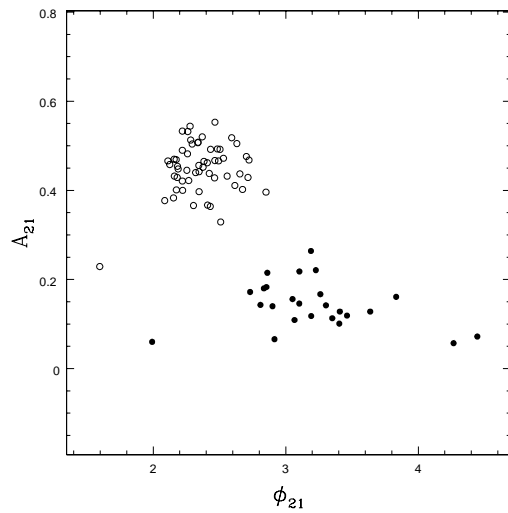


Figure 5.8: A_{21} values against ϕ_{21} . Empty circles are RR_{ab} stars; filled circles are RR_c stars. We do not show errors in the plot, but they are provided in Table 5.1.

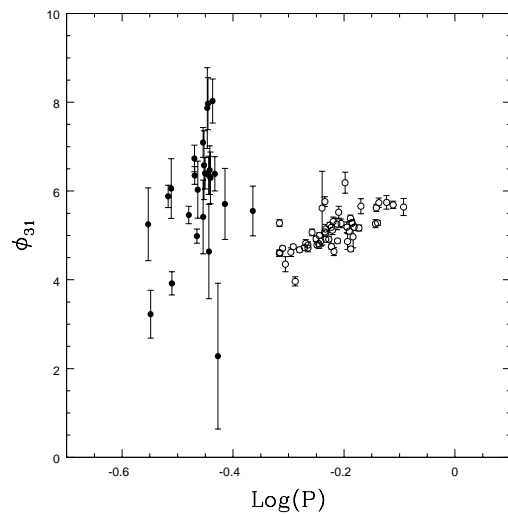


Figure 5.9: $\log P$ values against ϕ_{31} . Empty circles are RR_{ab} stars; filled circles are RR_c stars.

92Data analysis, and first results for RR Lyrae stars from the VMC survey

id_{EROS}	RRtype	P_{EROS}	ϕ_{21}	$\text{err}_{\phi_{21}}$	ϕ_{31}	$\text{err}_{\phi_{31}}$	A_{21}	$\text{err}A_{21}$	D_m
10234	0	0.482726	2.47	0.05	5.28	0.08	0.6	0.4	5.97
10498	0	0.594565	2.11	0.05	5.23	0.06	0.5	0.3	10.69
10748	1	0.360168	3.8	0.3	4.64	1.06	0.2	0.2	41.08
10812	1	0.354487	3.64	0.19	6.4	0.4	0.1	0.2	72.32
10894	0	0.655036	2.41	0.15	5.0	0.2	0.4	0.1	26.19
1127	0	0.584708	2.32	0.07	5.05	0.07	0.4	0.4	4.04
11492	0	0.552641	2.12	0.05	5.07	0.08	0.5	0.4	6.35
11722	0	0.648894	2.28	0.05	4.69	0.05	0.5	0.4	7.32
11777	1	0.279836	2.83	0.17	5.2	0.8	0.2	0.2	78.74
12246	0	0.773581	2.72	0.05	5.69	0.08	0.5	0.2	12.79
12471	1	0.351672	4.3	0.6	5.4	0.8	0.1	0.2	115.36
13140	1	0.304106	3.10	0.11	5.9	0.3	0.2	0.3	28.50
13678	0	0.505996	2.15	0.06	4.62	0.10	0.4	0.5	18.44
13919	1	0.307907	3.5	0.2	6.1	0.7	0.1	0.3	22.39
14070	1	0.282675	3.19	0.09	3.2	0.5	0.3	0.3	53.80
14083	0	0.524842	2.17	0.04	4.68	0.05	0.5	0.4	3.37
14319	0	0.568044	2.16	0.04	4.82	0.06	0.5	0.4	5.58
14454	1	0.352939	3.3	0.2	6.6	0.8	0.1	0.2	81.56
14455	0	0.564069	2.26	0.04	4.79	0.05	0.5	0.4	3.25
14988	0	0.543303	2.16	0.06	4.72	0.09	0.4	0.4	6.08
15364	0	0.592290	2.34	0.05	4.92	0.06	0.5	0.3	4.26
15448	1	0.362432	3.35	0.18	6.3	0.6	0.1	0.2	27.48
15514	0	0.753009	2.71	0.07	5.74	0.15	0.4	0.2	11.29
15574	0	0.601586	2.46	0.07	5.12	0.10	0.5	0.3	10.39
15644	1	0.43207	4.4	0.5	5.6	0.6	0.1	0.2	37.98
15662	1	0.342598	3.05	0.16	4.98	0.16	0.2	0.3	17.12
15888	1	0.357676	2.8	0.2	7.9	0.9	0.1	0.2	55.21
15972	0	0.543127	2.34	0.05	4.78	0.07	0.5	0.5	4.41
16071	0	0.657831	2.38	0.05	5.18	0.07	0.5	0.3	1.73
16710	0	0.603013	2.62	0.07	5.31	0.10	0.4	0.4	4.44
16908	0	0.598866	2.19	0.04	4.75	0.06	0.4	0.5	4.81
16920	0	0.721478	2.63	0.06	5.62	0.08	0.5	0.3	36.17
16928	0	0.582626	2.41	0.07	5.08	0.09	0.5	0.3	3.33
16999	0	0.582837	2.70	0.07	5.76	0.11	0.5	0.3	30.26
17115	0	0.598345	2.48	0.07	5.18	0.11	0.5	0.3	4.15
1765	1	0.343763	3.23	0.12	6.0	0.6	0.2	0.3	43.31
17861	0	0.725348	2.53	0.04	5.28	0.06	0.5	0.3	2.82
18337	0	0.569036	2.28	0.05	4.78	0.07	0.5	0.4	5.73
18477	1	0.358804	3.1	0.2	8.0	0.6	0.1	0.3	57.13
18546	1	0.361223	2.85	0.18	6.5	0.6	0.2	0.2	122.69
18737	0	0.584510	2.27	0.07	5.14	0.11	0.4	0.3	8.56
19172	0	0.573327	2.22	0.08	4.87	0.11	0.4	0.3	6.80
19178	0	0.651892	2.49	0.05	5.29	0.08	0.5	0.3	3.13
19248	0	0.494594	2.09	0.06	4.35	0.17	0.4	0.4	6.81
19850	0	0.535519	2.22	0.03	4.72	0.04	0.5	0.4	3.73
19902	0	0.515216	1.60	0.15	3.96	0.10	0.2	0.4	21.28
19933	1	0.339066	2.9	0.4	6.7	0.3	0.1	0.2	28.27
20171	1	0.331325	2.86	0.14	5.5	0.2	0.2	0.3	23.23
20205	0	0.671272	2.34	0.05	5.17	0.07	0.5	0.3	5.18
20208	0	0.575952	2.43	0.15	5.6	0.8	0.4	0.2	42.00
21063	0	0.718701	2.46	0.05	5.26	0.09	0.4	0.3	5.97
21254	1	0.359865	3.26	0.14	6.4	0.4	0.2	0.3	18.73
21390	1	0.369042	3.2	0.2	6.4	0.4	0.1	0.2	79.47
22456	0	0.538300	2.35	0.06	4.82	0.08	0.4	0.4	37.22
23417	0	0.569449	2.26	0.05	5.00	0.06	0.5	0.4	5.00
24832	0	0.648020	2.50	0.05	5.38	0.07	0.5	0.3	7.66
2508	1	0.308761	2.9	0.3	3.9	0.3	0.1	0.3	25.07
2684	0	0.614284	2.22	0.03	4.88	0.04	0.5	0.5	3.78
3518	0	0.808167	2.85	0.09	5.64	0.19	0.4	0.2	4.86
4000	0	0.482372	2.22	0.06	4.60	0.07	0.4	0.5	8.34
4284	0	0.729118	2.65	0.07	5.74	0.11	0.4	0.3	45.51
4670	1	0.339586	2.73	0.12	6.4	0.2	0.2	0.3	25.74
4863	0	0.612503	2.43	0.07	5.26	0.13	0.5	0.3	10.79
5148	1	0.373764	2.0	0.6	2.3	1.6	0.1	0.2	45.57
5441	0	0.633687	2.56	0.08	6.2	0.2	0.4	0.2	18.58
5500	0	0.584960	2.18	0.04	4.91	0.05	0.4	0.3	3.24
5838	0	0.617036	2.59	0.06	5.52	0.13	0.5	0.2	7.29
5990	0	0.644776	2.37	0.04	5.10	0.06	0.5	0.3	5.50
6036	0	0.511104	2.25	0.04	4.75	0.04	0.4	0.5	2.18
6235	0	0.488967	2.18	0.03	4.71	0.05	0.5	0.5	1.99
6601	0	0.623342	2.38	0.07	5.27	0.10	0.5	0.3	3.89
6636	1	0.351408	3.41	0.19	7.1	0.3	0.1	0.2	67.76
6674	0	0.483525	2.17	0.04	4.61	0.06	0.4	0.5	4.10
7107	0	0.676837	2.67	0.09	5.66	0.17	0.4	0.3	8.07
7473	0	0.638708	2.51	0.09	5.18	0.12	0.3	0.2	24.00
7752	0	0.640428	2.35	0.10	4.86	0.18	0.4	0.2	6.73
8204	0	0.561825	2.29	0.04	4.92	0.06	0.5	0.4	2.96
8721	1	0.384920	3.10	0.15	5.7	0.8	0.1	0.2	104.82
8769	0	0.605180	2.30	0.07	4.64	0.09	0.4	0.3	4.70
8898	0	0.652404	2.42	0.06	5.27	0.08	0.4	0.3	11.14
9603	1	0.365587	3.4	0.2	8.0	0.5	0.1	0.3	49.00

Table 5.1: Fourier parameters of the RR Lyrae stars in the SEP field. Column 1 gives the RR Lyrae type with zero and one corresponding to fundamental mode and first overtone pulsators, respectively

5.3.3 Metallicity estimate for RR_{ab} stars

We have estimated the metallicity of the SEP RR_{ab} stars using the Fourier parameters of their V-band light curves and Jurksic & Kovács (1996; hereafter JK96) relation (see section 2.3.1). We applied equation 2.2 to the 56 RR_{ab} stars in the SEP field obtaining a metallicity estimate for each of them in the J95 scale. Following Cacciari et al. (2005), we considered all the objects with $D_m < 5$, because in our sample only 5 stars have $D_m < 3$. Using eq. 2.8 we then transformed the J95 metallicities to the C09 metallicity scale. The top panel of Fig 5.10 shows the [Fe/H]_{C09} values, and their errors, obtained with this procedure plotted against the pulsation period. In this plot the blue points are stars with $D_m < 5$, they are much scattered than the other points, thus showing the importance of considering only objects with small D_m to infer reliable metallicity estimates. The lower panel of Fig 5.10 shows the metallicity distribution of the SEP RR_{ab} stars. Black, blue, and green lines represent the histogram of all objects, objects with $D_m < 5$, and objects with $D_m < 3$, respectively. The three distributions peak for the same [Fe/H]_{C09} value. In the black histogram, metallicities that differ significantly from the central peak value correspond to stars with high D_m values.

We list in Table 5.2 the individual [Fe/H] values derived with this procedure for the SEP RR_{ab} stars with $D_m < 5$. The weighted mean metallicity of these objects is: $\langle [Fe/H]_{C09} \rangle = (-1.65 \pm 0.02)$ dex, with $\sigma = 0.2$. Some stars have an [Fe/H] value out of the range of validity of equation 2.8 ($-2.31 < [Fe/H]_{JK96} < -0.68$). All these stars have $D_m \geq 5$, hence they were not used to derive the average metallicity.

5.3.4 Metallicity estimate for the RR_c stars

We have used Eq. 2.3 from Morgan et al. (2007) to obtain metallicity estimates for the RR_c stars in the SEP field. This relation provides metallicities in the ZW84 scale. To transform them to the C09 scale we used the relation 2.7 given in Carrereta et al. (2009). Morgan et al. (2007) use a cosine Fourier decomposition. We therefore derived the Fourier parameters of the c-type RR Lyrae stars using a cosine decomposition. Given the symmetric shape of the light curve of the c-type RR Lyrae, we used only 3 harmonics for the light curve decomposition. Fig 5.11 shows the [Fe/H]_{C09} values of the RR_c stars, and their errors, obtained with this proce-

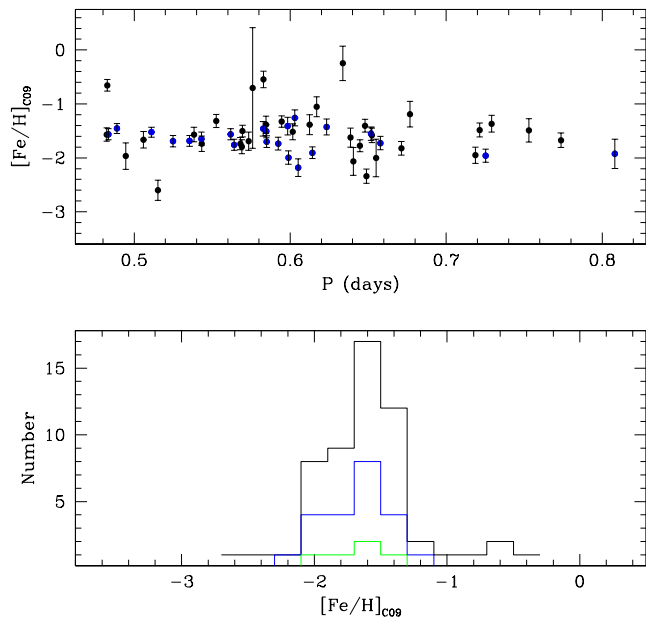


Figure 5.10: *Top panel:* $[Fe/H]$ values of the RR_{ab} stars (black points) in the SEP field plotted against the pulsation period. In blue are points corresponding to stars with $D_m < 5$. *Lower panel:* metallicity distribution of the RR_{ab} stars. The different histograms correspond to: the distribution obtained from all the RR_{ab} stars (black line), the distribution of the RR_{ab} stars with $D_m < 5$ (blue line), and the RR_{ab} stars with $D_m < 3$ (green line).

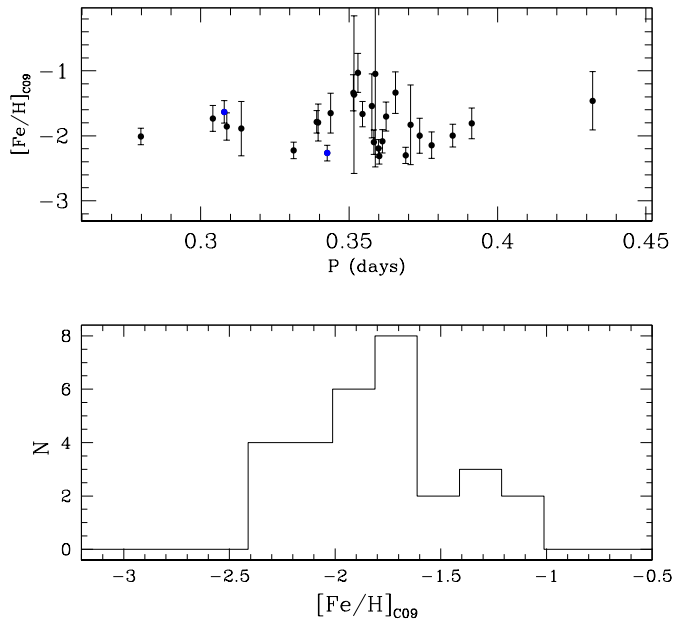


Figure 5.11: *Top panel:* $[Fe/H]$ values for the RR_c (black points) in the SEP field plotted against the pulsation period. In blue are points corresponding to stars with $err\phi_{31} < 0.3$. *Lower panel:* metallicity distribution of the RR_c stars. All the RR_c stars in the SEP are plotted.

VMC name	id-1	[Fe/H] _{C09} dex	err[Fe/H] _{C09} dex	D _m	P (days)	ϕ ₃₁	errϕ ₃₁
VMC90.01699_66.36999	16071	-1.73	0.12	1.73	0.657831	5.18	0.07
VMC89.01188_66.79188	6235	-1.46	0.09	1.99	0.488967	4.71	0.05
VMC90.26666_66.46120	6036	-1.52	0.09	2.18	0.511104	4.75	0.04
VMC90.50615_66.90768	17861	-1.96	0.12	2.82	0.725348	5.28	0.06
VMC89.14485_65.82450	8204	-1.56	0.10	2.96	0.561825	4.92	0.06
VMC89.29626_67.08839	19178	-1.55	0.12	3.13	0.651892	5.29	0.08
VMC88.81756_65.79473	5500	-1.70	0.11	3.24	0.584960	4.91	0.05
VMC89.18743_66.69605	14455	-1.76	0.10	3.25	0.564069	4.79	0.05
VMC90.14881_66.94333	16928	-1.46	0.13	3.33	0.582626	5.08	0.08
VMC90.04898_66.86007	14083	-1.69	0.10	3.37	0.524842	4.68	0.05
VMC91.19125_66.88860	19850	-1.68	0.10	3.73	0.535519	4.72	0.05
VMC88.66768_65.75290	2684	-1.91	0.11	3.78	0.614284	4.88	0.05
VMC90.00150_66.29262	6601	-1.42	0.15	3.89	0.623342	5.27	0.10
VMC90.60471_66.28531	1127	-1.51	0.12	4.04	0.584708	5.05	0.07
VMC88.69875_65.81397	6674	-1.56	0.10	4.10	0.483525	4.61	0.06
VMC88.62716_66.07124	17115	-1.41	0.16	4.15	0.598345	5.18	0.11
VMC88.95860_65.65705	15364	-1.74	0.12	4.26	0.592290	4.92	0.06
VMC90.43995_66.58296	15972	-1.65	0.12	4.41	0.543127	4.78	0.07
VMC89.21644_67.07065	16710	-1.26	0.15	4.44	0.603013	5.31	0.10
VMC88.91820_66.65638	8769	-2.18	0.16	4.70	0.605180	4.64	0.09
VMC88.75765_66.36566	16908	-2.00	0.12	4.81	0.598866	4.75	0.06
VMC90.09496_66.62618	3518	-1.9	0.3	4.86	0.808167	5.64	0.19

Table 5.2: Metallicity values obtained for the RR_{ab} stars in the SEP field. The columns are: 1) EROS-2 identification number; 2) metallicity value in the C09 scale; 3) metallicity error; 4) JK96 regularity value; 5) P_{EROS-2} ; 6) ϕ_{31} Fourier parameter; 7) ϕ_{31} error.

dure plotted against the pulsation period. Blue points are stars with $\text{err}\phi_{31} \leq 0.07$. The weighted mean metallicity of these objects is: $\langle [\text{Fe}/\text{H}]_{\text{C09}} \rangle = -2.07$ dex, with $\sigma = 0.3$.

There is a systematic difference of ~ 0.4 dex between the average metallicity of RR_{ab} and RR_c stars, with the former being more metal rich. A similar difference was also found by Kapakos et al. (2011). Although we do not have a clear explanation for this shift, we suspect it might be caused by some systematics in the calibration of the different relations used to estimate the metallicity of the RR_{ab} and RR_c stars.

VMC name	id_{EROS}	P (days)	$[\text{Fe}/\text{H}]_{C09}$ dex	$\text{err}[\text{Fe}/\text{H}]_{C09}$ dex	ϕ_{31}	$\text{err}\phi_{31}$
VMC89.05881_65.62997	11777	0.2798360	-2.0	0.1	1.0	0.6
VMC88.54182_67.04457	13140	0.3041060	-1.7	0.2	2.6	0.4
VMC90.63806_66.84103	13919	0.3079070	-1.6	0.2	2.9	0.3
VMC90.61131_66.97001	2508	0.3087610	-1.9	0.2	2.5	0.5
VMC88.58812_66.39030	20171	0.3313250	-2.2	0.1	1.9	0.4
VMC89.38447_66.88713	19933	0.3390660	-1.8	0.2	3.3	0.3
VMC90.70238_66.62708	4670	0.3395860	-1.8	0.3	3.3	0.6
VMC90.18475_66.87184	15662	0.3425980	-2.3	0.1	2.1	0.2
VMC90.85286_66.43754	1765	0.3437630	-1.7	0.3	3.6	0.6
VMC90.04089_66.99461	6636	0.3514080	-1.3	0.3	4.2	0.4
VMC88.48468_66.13947	12471	0.3516720	-1.4	1.2	4.1	2.0
VMC88.42676_66.00653	14454	0.3529390	-1.0	0.3	4.6	0.4
VMC88.46714_66.59529	10812	0.3544870	-1.7	0.2	3.7	0.3
VMC88.83012_66.51167	15888	0.3576760	-1.5	0.5	4.0	0.9
VMC88.94167_66.43547	5942	0.3583190	-2.1	0.2	3.0	0.5
VMC89.06184_66.07770	18477	0.3588040	-1.0	1.4	4.7	2.0
VMC89.47125_66.74303	21254	0.3598650	-2.2	0.1	2.8	0.3
VMC88.89312_66.82638	10748	0.3601680	-2.3	0.1	1.8	0.6
VMC88.97116_66.20557	18546	0.3612230	-2.1	0.2	3.1	0.5
VMC91.17422_66.70195	15448	0.3624320	-1.7	0.2	3.8	0.4
VMC90.80177_66.66222	9603	0.3655870	-1.3	0.3	4.4	0.5
VMC90.10844_66.41316	21390	0.3690420	-2.3	0.1	2.5	0.4
VMC89.37604_66.35017	5148	0.3737640	-2.0	0.3	3.5	0.7
VMC88.44221_66.46144	8721	0.3849200	-2.0	0.2	3.7	0.4
VMC91.18246_66.56863	9807	0.3913350	-1.8	0.2	4.1	0.5
VMC90.46352_66.91447	15644	0.4320700	-1.5	0.4	1.1	0.8
VMC89.06472_65.76323	3849	0.3777840	-2.1	0.2	1.4	0.7
VMC89.31884_66.75497	22698	0.3707080	-1.8	0.6	0.6	1.4
VMC89.76387_66.52093	15111	0.3136930	-1.9	0.4	0.0	1.2

Table 5.3: Metallicity values obtained for the RR_c stars in the SEP field. The columns are: 1) VMC name; 2) EROS-2 identification number; 3) P_{EROS-2} ; 4) metallicity value in the C09 scale; 5) metallicity error; 6) ϕ_{31} parameter in the cosine decomposition; 7) ϕ_{31} error.

5.4 Determination of the $\langle K_S \rangle$ values

In this section we focus on the determination of the mean magnitudes in the K_S band ($\langle K_S \rangle$) for the RR Lyrae stars in the SEP field. We used as a reference the catalogue of confirmed RR Lyrae stars obtained from the EROS-2 catalogue (see 5.2). For these stars we used the K_S light curves made available to us at the beginning of Sept. 2011, by the VSA release: VMCv20110909. It should be noted that the work on the K_S light curves was significantly delayed by problems occurred with the Julian Day of the tile cataloguing procedure applied by the VSA. As described in (Cioni et al. 2011, see section 4.4.1), the observation time of a pawprint is of the order of \sim 10 minutes, while the observation time of a tile is of the order of 1h. In the VSA releases before September 2011, the JD associated with the tile observations corresponded to the middle of the tile exposures. This is a good estimate of the time of observation for objects that are observed in the middle of the pawprints. However, for stars observed, for instance, only in the first pawprint of a tile, this procedure provides a wrong estimate of the time of observation. Fig 5.12 shows, as an example, the differences in JD obtained respectively with the tile data using as time of observation the mean JD of all pawprints (black points), and the tile data after in the VSA were introduced the start and end time of observation for each star (green points), with respect to the pawprint data (long shaded line). We also note that for “concatenated observations” differences are clearly smaller. This is because the exposure length of a “concatenation” is smaller (\sim 30 minutes).

In order to have reliable JDs before September 2011, we could use only VSA data available in pawprint version. This implied that for each night of observation we had to average the K_S measurements to reach almost the same S/N value that is provided by the tile observations. This problem was sorted out with the VMCv20110909 release, thanks to the checks made during this thesis work. Indeed an important by-product of this work in the first stages of the VMC project, was to improving the pipeline reduction procedures, or as in this case, the cataloguing procedures.

The K_S light curves of the RR Lyrae stars in the SEP field presented in this thesis work are the final results, after two years spent on the analysis of VMC preliminary data. The LMC RR Lyrae stars are much fainter, hence have lower S/N light curves, than the LMC Cepheids. The SEP field is an uncrowded region, thus this is not a

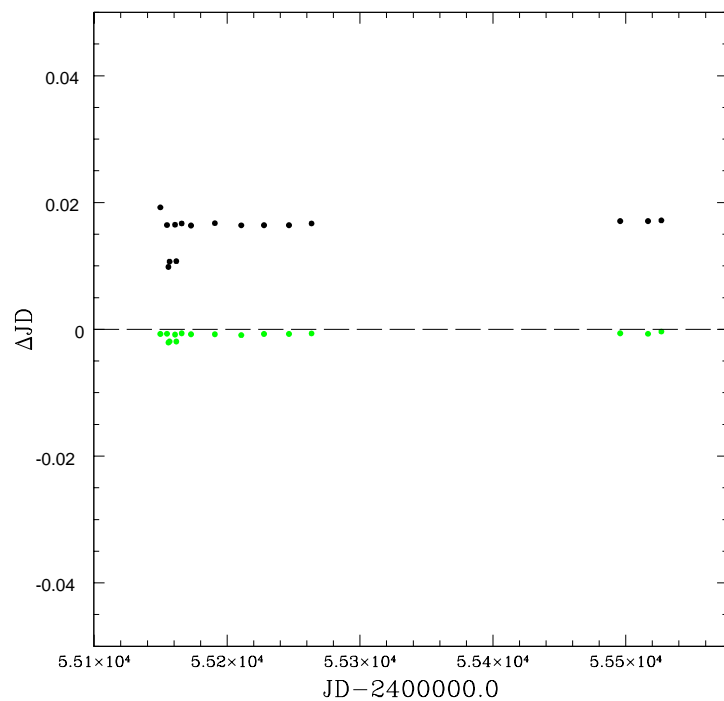


Figure 5.12: Differences in the JD estimates for star VMC88.46714_66.59529, using different observation times. The reference value (long dashed line) is that of the pawprint data. Black points correspond to tile data for which the mean JD of all pawprint JDs is used; green points correspond to tile data in which to each star is associated a JD obtained averaging only the JDs of the pawprints in which that star was observed.

big problem, while it becomes an issue in the 30 Dor field (see section 5.6).

Figs. from 5.13 to 5.19 show the K_S light curves overplotted by the K -band templates of (Jones et al., 1996), that we adopted to fit the K_S light curves, and thus infer average K_S magnitudes for the SEP RR Lyrae stars. Jones et al. (1996) provide different templates depending on the type of variability (RR_{ab} or RR_c type), and on the B -amplitude of the variable star. They described each of these templates as a Fourier decomposition. This method needs a precise knowledge of the star ephemeris as well as the amplitudes in the V or the B band. We have applied the template fitting method to the SEP RR Lyrae stars using pulsation properties derived from the EROS-2 data. Table 5.6 summarizes the resulting $\langle K_S \rangle$ values and their errors. According to Jones et al. (1996), the mean K_S values inferred with this procedure have errors less than 0.03 mag. We then used the $\langle K_s \rangle$ to study the $PL_K Z$ relation (see section 5.5).

5.5 Period-Luminosity-metallicity relation

The Period- K -band Luminosity-Metallicity relation for RR Lyrae stars is a most powerful distance indicator for Population II systems. In the context of the VMC survey, we will apply the $PL_K Z$ relation to each VMC tile, separately. This will allow us to infer an estimate of the distance to each tile and, in turn, to study the structure of the Magellanic Clouds. We can also derive our own $PL_K Z$ relation, from the VMC data, to compare with the literature relations, thus improving our knowledge on this very promising tool.

In the following we describe the results obtained from the application of the $PL_K Z$ relation to the RR Lyrae stars in the SEP field of the LMC. Once we have the period (cfr. 5.2 and Tab.5.6) and the $\langle K_s \rangle$ values (cfr. 5.4 and Tab.5.6) for each RR Lyrae star, we can plot the PL relation. This is shown in Fig. 5.20, where filled circles are the RR_{ab} , and open circles are the RR_c stars in the SEP field, respectively. The $PL_K Z$ relation obtained with this procedure is: $K_s = (17.351 \pm 0.035) - 2.450 \pm 0.133 \times \log P$, with rms=0.082. This relation was derived by considering only objects that lie within 3σ from the best fit line.

A number of different $PL_K Z$ relations exist in the literature (see Section 2.3.2): Bono et al. (2003) (see eq. 5.5), Dall’Ora et al. (2004) (see eq. 5.6), Sollima et al.

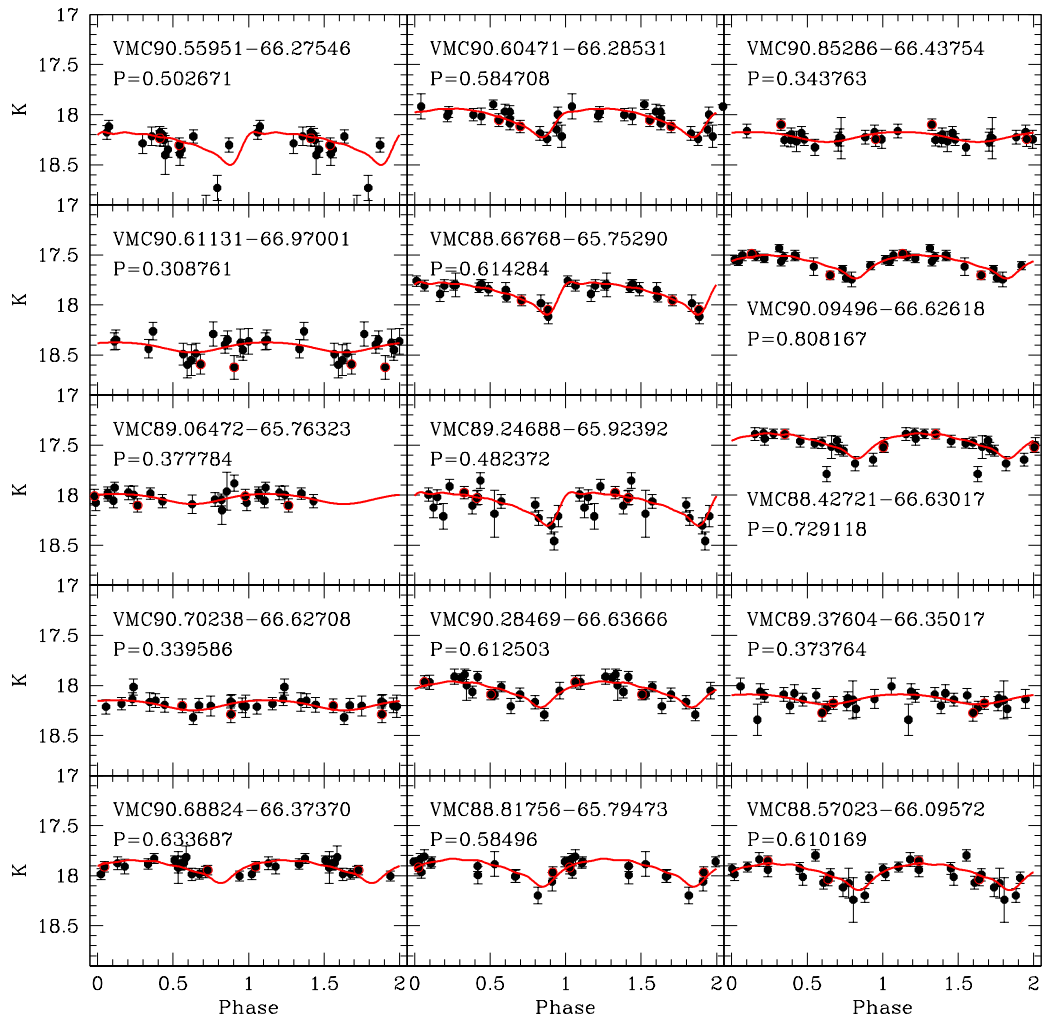


Figure 5.13: K_s light curves for RR Lyrae stars in the SEP field, overplotted by the templates that we used to estimate the $\langle K_s \rangle$ magnitude for each star. Red circles mark the observations out of constraints (see Table 4.3).

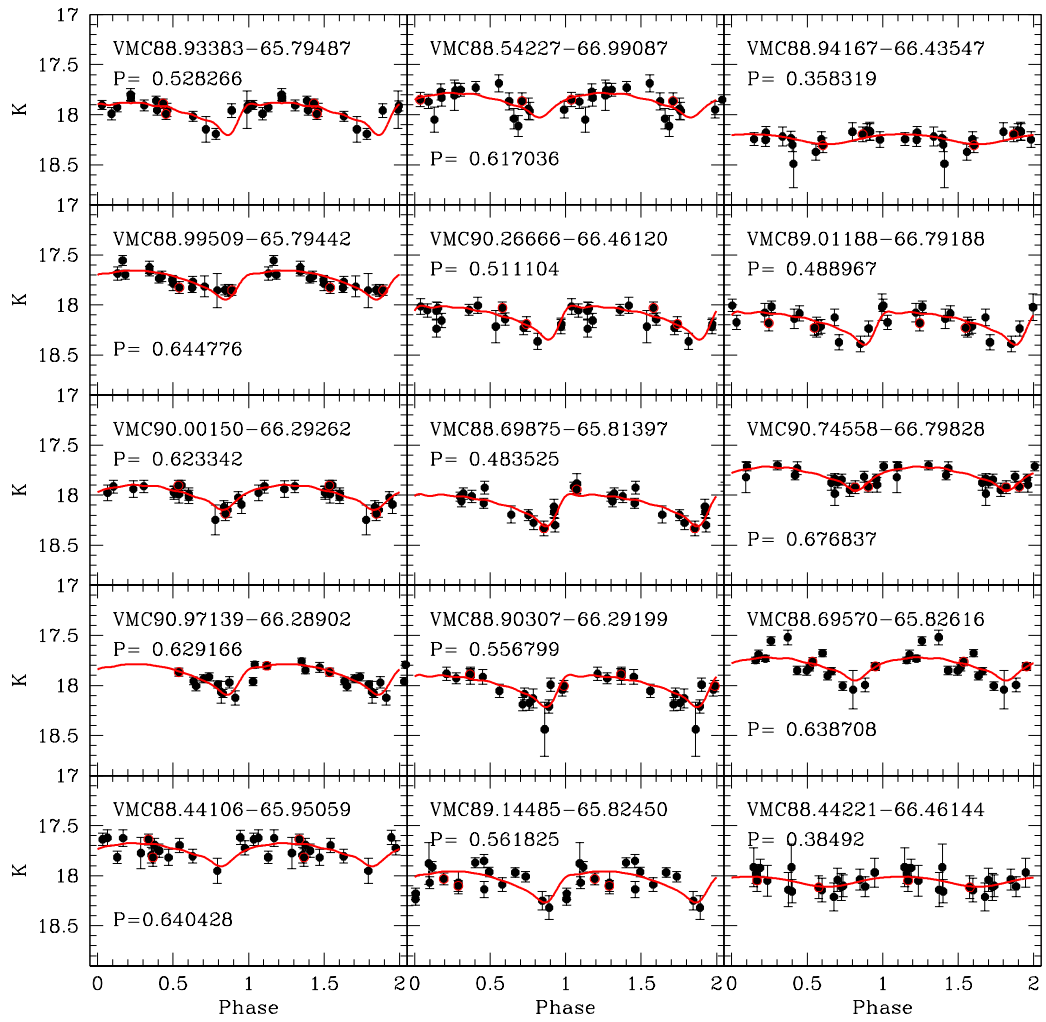


Figure 5.14: K_s light curves for RR Lyrae stars in the SEP field, overplotted by the templates that we used to estimate the $\langle K_s \rangle$ magnitude for each star. Red circles mark the observations out of constraints (see Table 4.3).

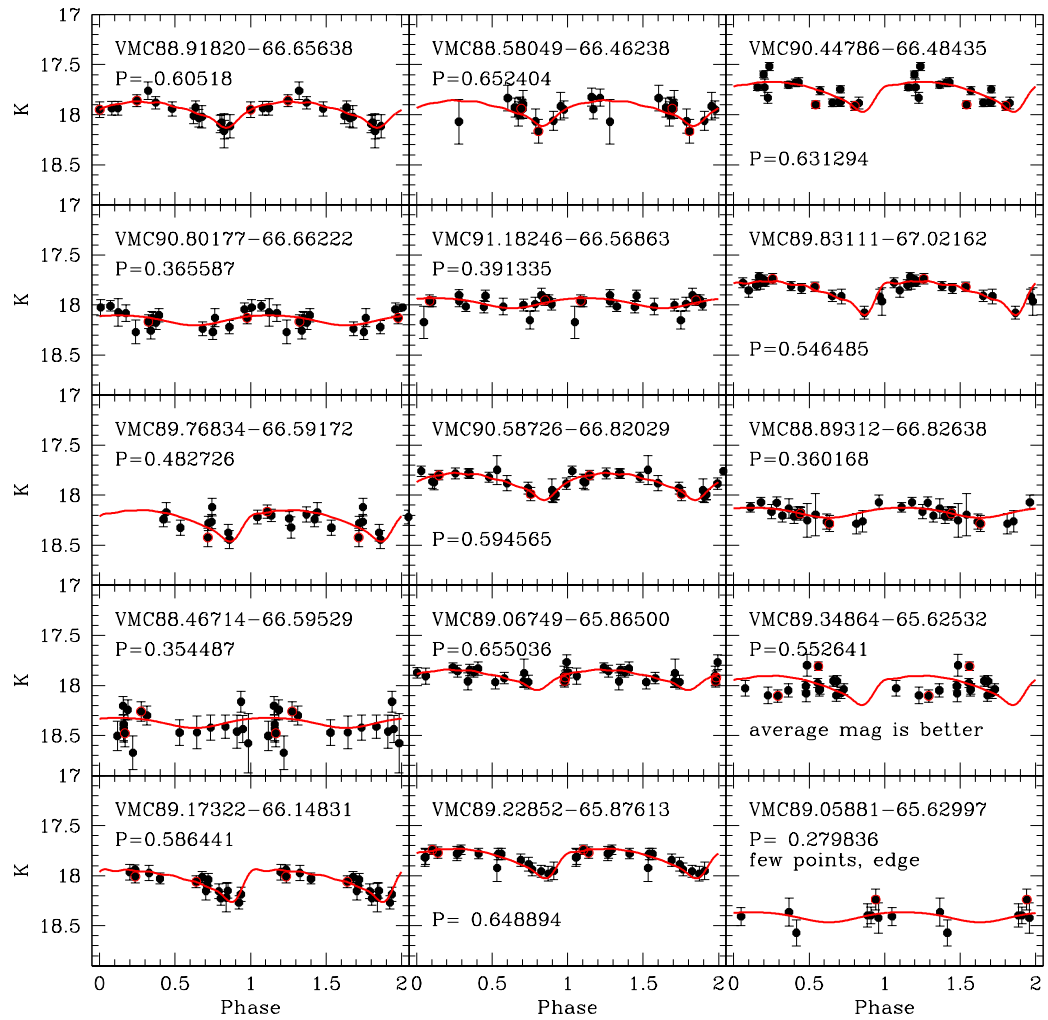


Figure 5.15: K_s light curves for RR Lyrae stars in the SEP field, overplotted by the templates that we used to estimate the $\langle K_s \rangle$ magnitude for each star. Red circles mark the observations out of constraints (see Table 4.3).

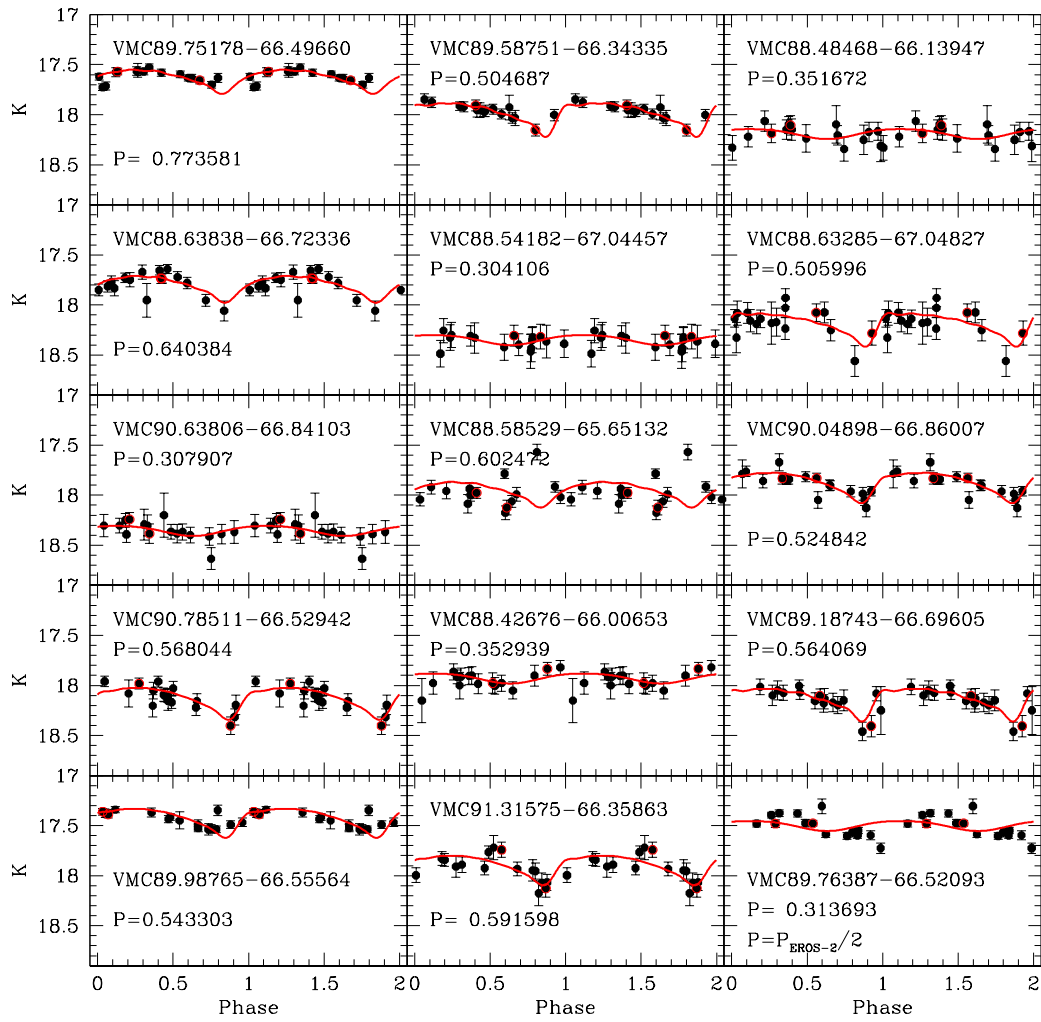


Figure 5.16: K_s light curves for RR Lyrae stars in the SEP field, overplotted by the templates that we used to estimate the $\langle K_s \rangle$ magnitude for each star. Red circles mark the observations out of constraints (see Table 4.3).

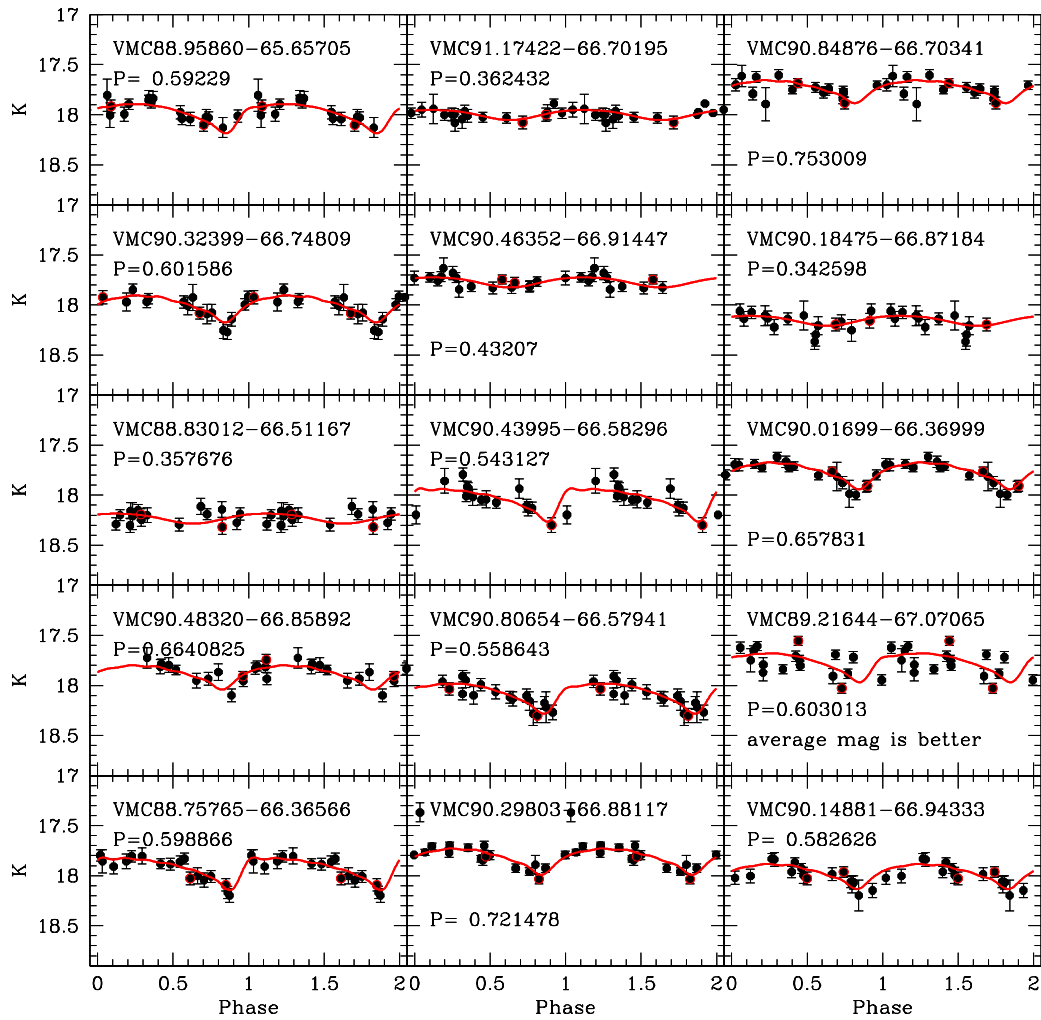


Figure 5.17: K_s light curves for each RR Lyrae star in the SEP field, overplotted by the templates that we used to estimate the $\langle K_s \rangle$ magnitude for each star. Red circles mark the observations out of constrains (see Table 4.3).

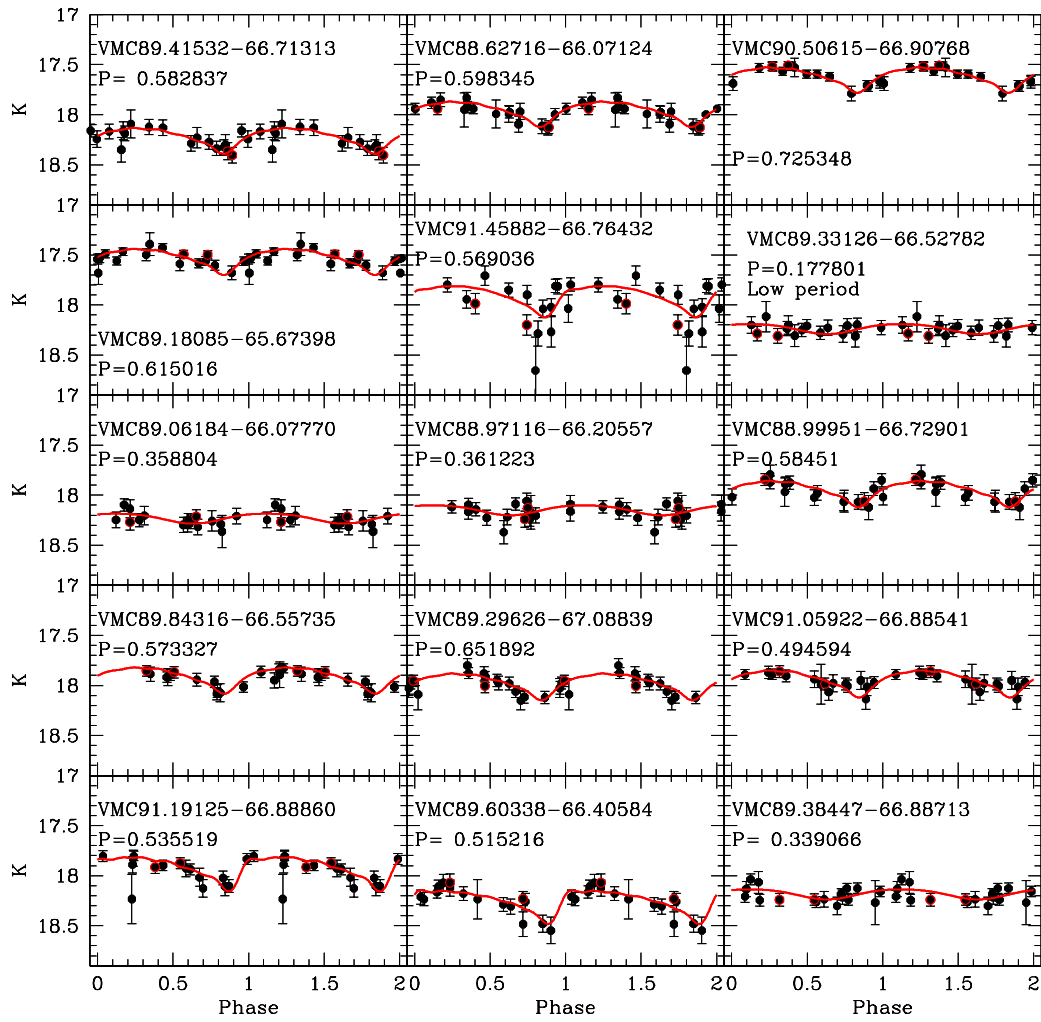


Figure 5.18: K_s light curves for RR Lyrae stars in the SEP field, overplotted by the templates that we used to estimate the $\langle K_s \rangle$ magnitude for each star. Red circles mark the observations out of constraints (see Table 4.3).

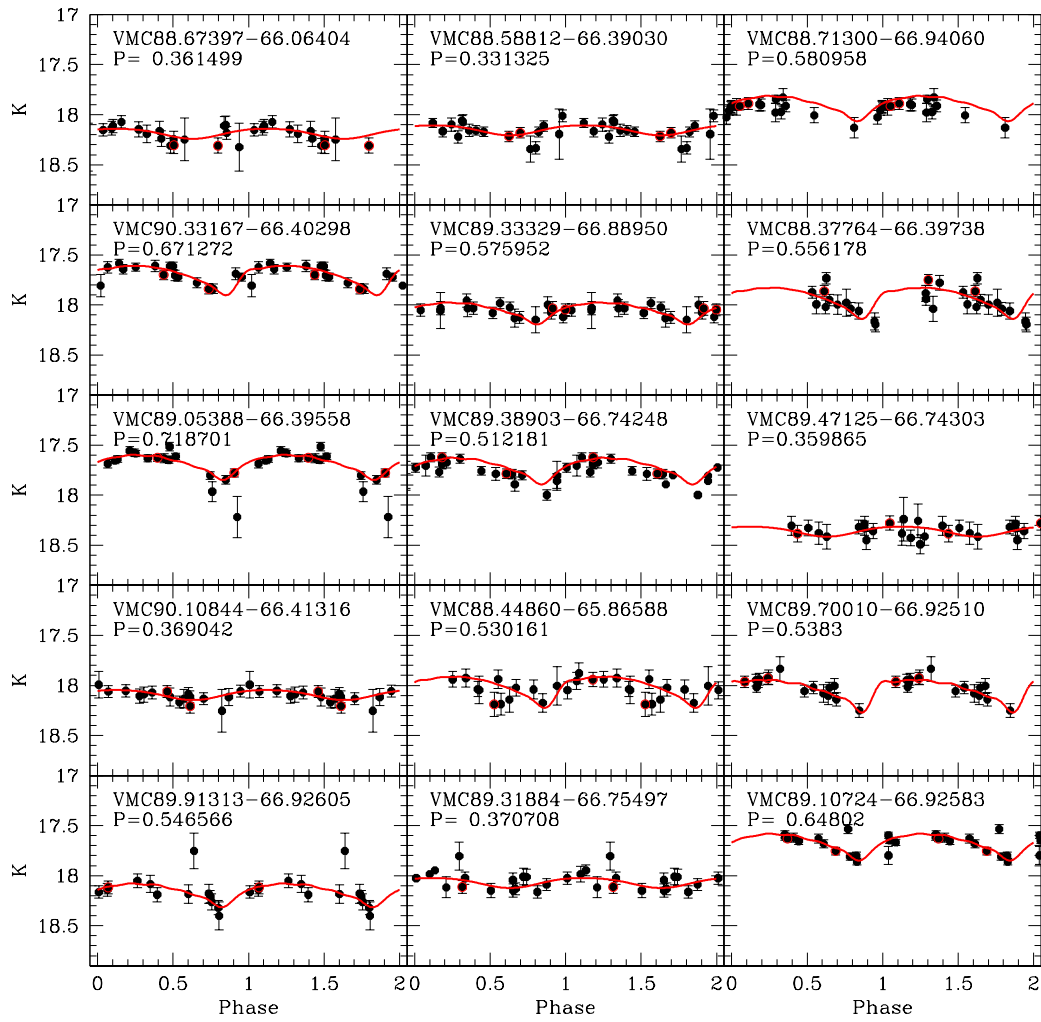


Figure 5.19: K_s light curves for RR Lyrae stars in the SEP field, overplotted by the templates that we used to estimate the $\langle K_s \rangle$ magnitude for each star. Red circles mark the observations out of constrains (see Table 4.3).

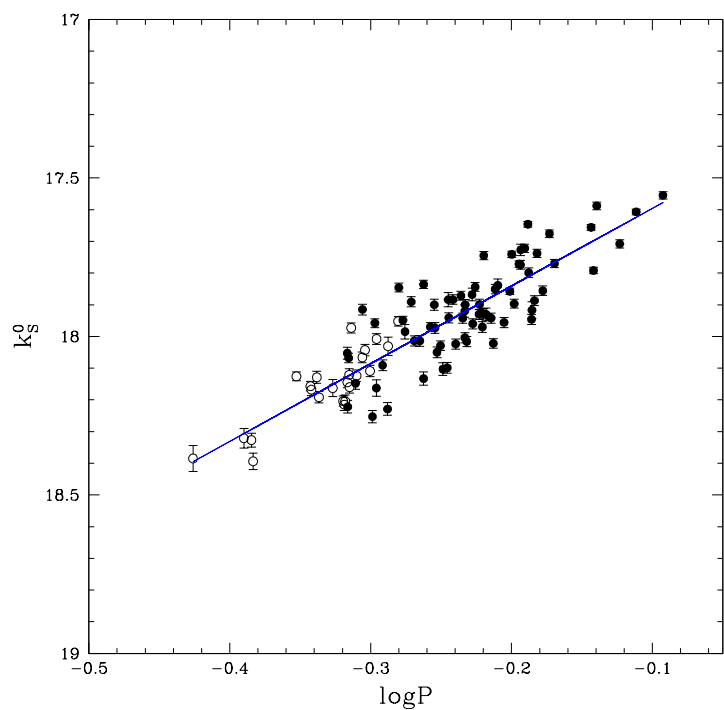


Figure 5.20: Dereddened mean K_s magnitudes against LogP, for RR Lyrae stars in the SEP field. Empty and filled circles represent c- and ab-type RR Lyrae stars, respectively. The periods of the RRc stars were fundamentalized by adding 0.127 to the $\log P$.

(2006) (see eq. 5.4), Sollima et al. (2008) (see eq. 5.3), Del Principe et al. (2006) (see eq. 5.7), Borissova et al. (2009) (see eq. 5.8). Some of them are based on RR Lyrae stars in the field and globular clusters of the LMC. Benedict et al. (2011) have estimated new zero points for these different PL_KZ relations, on the basis of new *HST* trigonometric parallaxes for five Galactic field RR Lyrae stars:

$$M_K = (-2.38 \pm 0.04)(\log P + 0.28) + (0.08 \pm 0.11)([Fe/H] + 1.58) + a_1, \quad (5.3)$$

$$M_K = (-2.38 \pm 0.04)(\log P + 0.28) + a_2, \quad (5.4)$$

$$M_K = -2.101(\log P + 0.28) + (0.231 \pm 0.012)([Fe/H] + 1.58) + a_3, \quad (5.5)$$

$$M_K = (-2.16 \pm 0.09)(\log P + 0.28) + a_4, \quad (5.6)$$

$$M_K = (-2.71 \pm 0.12)(\log P + 0.28) + (0.12 \pm 0.04)([Fe/H] + 1.58) + a_5 \quad (5.7)$$

$$M_K = (-2.11 \pm 0.17)(\log P + 0.28) + (0.05 \pm 0.07)([Fe/H] + 1.58) + a_6 \quad (5.8)$$

where the a_1 - a_6 values are, respectively: -0.56 , -0.57 , -0.58 , -0.56 , -0.57 , and -0.56 (see Benedict et al. 2011). These different relations are based on a number of different metallicity scales. In particular, Bono et al. (2003) and Del Principe et al. (2006) use the ZW metallicity scale. Sollima et al. (2008), use the Carretta & Gratton (1997) metallicity scale. The relation from Dall’Ora et al. (2004) has no metallicity term., as also does, according to Benedict et al. (2011), the relation derived by Sollima et al. (2006). Finally, Borissova et al. (2009) use the so called Harris metallicity scale, that they consider to be ~ 0.06 more metal than ZW metallicity scale.

To estimate distance moduli for the SEP field we entered the above relations using: pulsation periods for the SEP RR Lyrae stars taken from the EROS-2 catalogue; $\langle K_S \rangle$ magnitudes derived applying the template fitting procedure to the VMC20110909 VSA release time series dereddened according to Rubele et al. (2011), and metallicities obtained by the Fourier analysis of the V band light curves³ (see section 5.3.3 and 5.3.4).

In order to properly take into account the systematic difference of ~ 0.4 dex in the mean metallicity of $RRab$ and RRc stars (see section 5.3.3 and 5.3.3), we followed 3 different approaches for the metallicity term:

³Obtained by the B_{EROS} and R_{EROS}

- A: average of the metallicities of all RR Lyrae stars;
- B: average of the metallicities of *RRab* stars only;
- C: average of the metallicities of *RRc* stars only.

Details of method A

We used just one value for the metallicity, obtained by averaging the photometric metallicity estimates of both *RRab* and *RRc* stars. We associated to this mean value an error corresponding to the standard deviation of the distribution: $\langle [\text{Fe}/\text{H}]_{\text{ZW}} \rangle = -1.8$; $\sigma_{[\text{Fe}/\text{H}]_{\text{ZW}}} = 0.3$. This allowed us to use all the 106 stars simultaneously to estimate the distance modulus. The majority of the above *PLZ* relations use the ZW metallicity scale. We therefore transformed the *RRab* metallicities from JK96 to the ZW scale, using Eq. 2.6. Eq. 2.3 for the c-type RR Lyrae stars provides metallicities directly on the ZW scale. Only Sollima et al. (2008) uses the Carretta & Gratton (1997) metallicity scale; we then used the relation given by Carretta & Gratton (1997) to transform them to ZW:

$$[\text{Fe}/\text{H}]_{\text{CG97}} = (-0.618 \pm 0.083) - (0.097 \pm 0.189)[\text{Fe}/\text{H}]_{\text{ZW}} - (0.352 \pm 0.067)[\text{Fe}/\text{H}]_{\text{ZW}}^2. \quad (5.9)$$

Each of the above relations was used to infer an M_K absolute magnitude for each RR Lyrae star. The M_K value was combined with the dereddened apparent K magnitude (using A_K values based on Rubele et al. 2011) providing a μ_0 estimate for each individual star. Average μ_0 values and related standard error inferred from the different PL_KZ relations are summarized in Column 4 of Table 5.4.

Details of method B

We used the mean metallicity derived by averaging the photometric metallicities obtained only from the *RRab* stars. We associated to this mean value an error corresponding to the standard deviation of the average: $\langle [\text{Fe}/\text{H}]_{\text{ZWab}} \rangle = -1.7$; $\sigma_{[\text{Fe}/\text{H}]_{\text{ZWab}}} = 0.2$, and inferred distance moduli from the above *PLZ* relations for each of the 76 ab-type RR Lyrae stars. The average distance moduli μ_0 and related standard errors obtained the different PL_KZ relations are summarized in Column 2 of Table 5.4.

PL_K -relation	$\mu_{<ab>}$	$\mu_{<c>}$	$\mu_{<ab+c>}$
Bono et al 2003	18.594 ± 0.015	18.71 ± 0.03	18.635 ± 0.014
Dall’Ora et al. 2004	18.551 ± 0.015	18.57 ± 0.03	18.557 ± 0.014
Sollima et al. 2008	18.553 ± 0.015	18.59 ± 0.03	18.566 ± 0.014
Sollima et al. 2006	18.573 ± 0.015	18.57 ± 0.03	18.573 ± 0.014
Del Principe et al. 2006	18.603 ± 0.015	18.62 ± 0.03	18.611 ± 0.014
Borissova et al. 2009	18.552 ± 0.015	18.60 ± 0.03	18.566 ± 0.014
average	18.57 ± 0.02	18.61 ± 0.05	18.58 ± 0.03

Table 5.4: Distance moduli for the LMC SEP obtained applying different PL_KZ relations to the SEP RR Lyrae stars. Column 1: Reference of the PL_KZ relation; Column 2: distance modulus obtained using only RR_{ab} stars; Column 3: distance modulus obtained using only RR_c stars; Column 4: distance modulus obtained using all the RR Lyrae stars. See text for details.

Details of method C

We used the mean metallicity derived by averaging the photometric metallicities obtained only from the RR_c stars. We associated to this mean value an error corresponding to the standard deviation of the average: $\langle [\text{Fe}/\text{H}]_{\text{ZW}_c} \rangle = -2.07$; $\sigma_{[\text{Fe}/\text{H}]_{\text{ZW}_c}} = 0.12$, and inferred distance moduli from the above PL_Z relations for each of the 30 c-type RR Lyrae stars. The average distance moduli μ_0 and related standard errors inferred from the different PL_KZ relations are summarized in Column 2 of Table 5.4.

5.6 RR Lyrae stars in the 30 Dor region

The 30 Dor field is a very crowded star forming region in the central part of the LMC. Its location on a map of the VMC tiles on the LMC is shown in Fig 5.21.

A number of different studies have targeted the RR Lyrae stars in regions close to the 30 Dor field. Clementini et al. (2003) and Gratton et al. (2004) presented photometry and spectroscopy for more than a hundred RR Lyrae stars in two fields located close to bar of the LMC (blue rectangles in Fig. 5.21). They measured average magnitudes, local reddening, and individual metallicities for the RR Lyrae stars from which they derived the slope of the RR Lyrae luminosity-metallicity relation, and an estimate of the distance to the LMC. In particular, they inferred

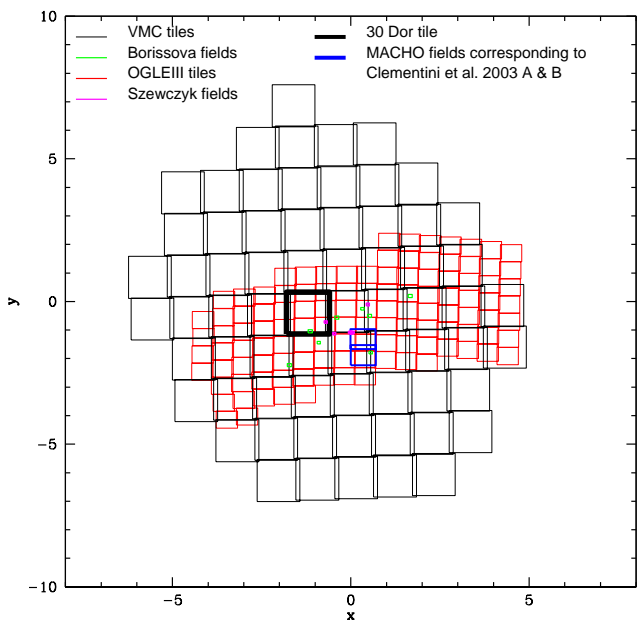


Figure 5.21: Location of the 30 Dor field (black thick rectangle) on the map of VMC tiles (black thin rectangles) covering the LMC. Blue rectangles mark the MACHO fields in which lie the LMC regions studied by Clementini et al. (2003) and Gratton et al. (2004). Green and magenta rectangles mark fields studied by Borissova et al. (2004, 2006, 2009) and Szewczyk et al. (2008), respectively. See text for details.

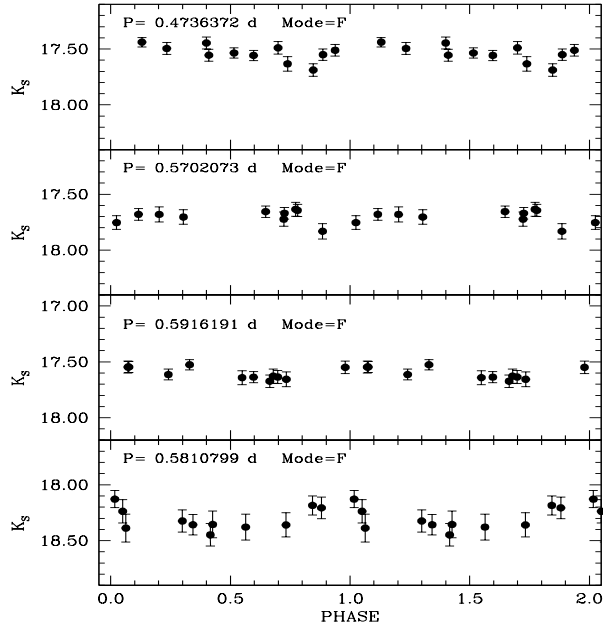


Figure 5.22: K_S light curves of RR Lyrae stars in the 30 Dor field.

a mean metallicity for the RR Lyrae stars in this region of the LMC of $[Fe/H] = -1.48 \pm 0.03$ dex, with $\sigma = 0.29$ dex on the Harris (1996) metallicity scale. This scale is, on average, 0.06 dex more metal-rich than the ZW scale. Borissova et al. (2006) measured radial velocities for 87 LMC RR Lyrae stars and metallicities for 78 RR Lyrae stars. These targets are located in 10 fields (green rectangles in Fig. 5.21) covering a wide range of distances, out to 2.5 degrees from the center of the LMC. One of the Borissova et al. fields is contained in the 30 Dor tile. They inferred a mean metallicity value $[Fe/H] = -1.53 \pm 0.02$ dex⁴ with a dispersion of $\sigma = 0.20 \pm 0.02$ dex in agreement with Gratton et al. (2004) results, and showing that the LMC RR Lyrae stars form a rather homogeneous metal-poor population.

Infrared PL relations for the RR Lyrae stars in the central part of the LMC have been obtained by a number of different authors (see section 2.3.2). Szewczyk et al. (2008) obtained deep infrared J and K band observations of five fields located in the LMC bar (magenta rectangles in fig. 5.21). They found consistent values for the distance modulus of the LMC using a number of different theoretical and empirical calibrations of the PL_KZ relation, and adopt as their final value

⁴Metallicities in Borissova et al. (2009) are measured using the Gratton et al. 2004 method.

18.58 ± 0.03 (statistical) $\pm (0.11)$ (systematic) mag, in good agreement with most independent determinations of the distance to this galaxy. Borissova et al. (2009) investigated the metallicity dependence of the infrared PL relation for RR Lyrae stars combining near-IR photometry and spectroscopically measured metallicities for 50 RR Lyrae stars within nine fields in the central region of the LMC. They found a very mild dependence on metallicity of the PL in the K band, and inferred from their near-IR $PL_K Z$ relation, an LMC distance modulus of 18.53 ± 0.13 mag. They point out that their distance modulus relies on the trigonometric parallax of the star RR Lyrae. The 30 Doradus field (thick black rectangle in fig. 5.21) is one of the VMC fields completely observed, reduced and catalogued. This field has been covered by the OGLE III survey (<http://ogle.astrowu.edu.pl/>), which thus provides the reference catalogue for the variable stars. For the analysis of the 30 Dor variables we adopted the periods and mode classification provided by the OGLE III team, without performing a new analysis of the light curves with GRATIS. The severe crowding conditions makes the analysis of the RR Lyrae stars in the 30 Dor field much more complicated and time consuming than in the SEP and any other field of the LMC. To mitigate the crowding problems, we used for the RR Lyrae stars in the 30 Dor region the PSF photometry kindly provided by Stefano Rubelle. By cross-matching the OGLE III catalogue of RR Lyrae stars in the 30 Dor region against the VSA and the PSF-photometry catalogues we obtained a list of 1241 RR Lyrae stars. Fig. 5.22 shows examples of the K_S light curves for fundamental mode RR Lyrae stars in the 30 Dor field. Table 5.7 summarizes the properties (Id, coordinates, type, period, time of maximum light, and average magnitudes) of the 30 Dor RR Lyrae stars. A proper analysis of the 30 Dor RR Lyrae stars using templates to fit the K_S -band light curves, and the Fourier parameters to estimate individual metallicities, as we have done for the SEP variables, is in progress. Here, we summarize preliminary results on the PL_K relations that we obtained by simply intensity-averaging the individual K_S time series and neglecting the metallicity dependence. To account for the variable reddening that characterizes the 30 Dor region, we adopted the recent evaluations by Haschke et al. (2011). Fig. 5.23 shows the PL_{K_S} relation we have obtained for the 30 Dor RR Lyrae stars using this simplified procedure. In the figure open circles are $RRab$ stars and filled circles are RRc stars, periods for the latter were fundamentalized by adding 0.127 to the $\log P$. The

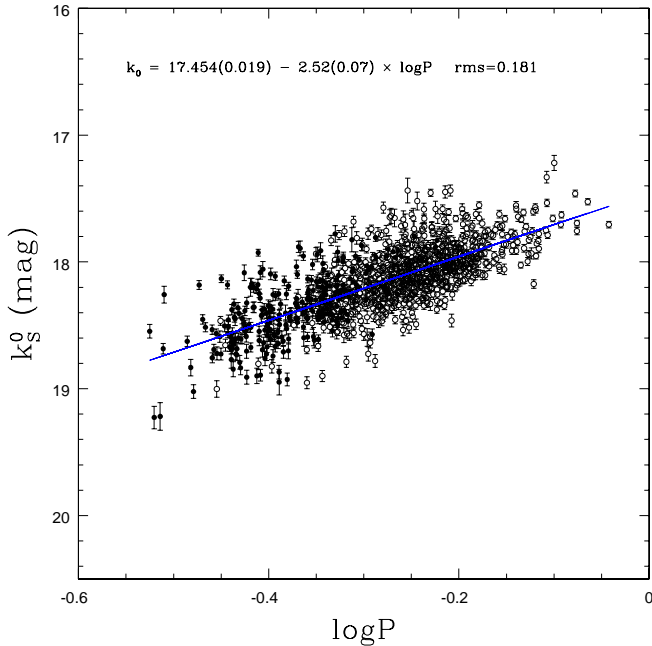


Figure 5.23: Dereddened mean K_s magnitudes against $\log P$, for RR Lyrae stars in the 30 Dor field. Empty and filled circles represent c- and ab-type RR Lyrae stars, respectively. The periods of the RRc stars were fundamentalized by adding 0.127 to the $\log P$.

PL_K relation obtained with this procedure is:

$$k_0 = (17.454 \pm 0.019) - 2.51 \pm 0.06 \times \log P \quad (5.10)$$

with an r.m.s. of 0.181 mag. This relation was derived by discarding objects 3σ outside the best fit linear regression (blue line).

The PL_K relation in Fig. 5.23 is much more scattered than the PL_K relation found for the SEP field and has a significantly fainter zero point. Using then the same approach described in Section 5.5 and adopting for the metallicity the mean metal abundance $[\text{Fe}/\text{H}] = -1.53 \pm 0.02$ dex derived for the LMC RR Lyrae stars by Borissova et al. (2006), we have obtained the distance moduli summarized in Table 5.5. These distance moduli do not agree with the results obtained by (Szewczyk et al., 2008; Borissova et al., 2009) using the same method (i.e. the PL_K of the RR Lyrae stars).

Clearly, these are very preliminary and rather puzzling results. Much more work is needed to improve the analysis of the 30 Dor RR Lyrae stars. As a first attempt

PL_K -relation	μ_0
Bono et al 2003	18.736 ± 0.005
Dall’Ora et al. 2004	18.712 ± 0.005
Sollima et al. 2008	18.699 ± 0.005
Sollima et al. 2006	18.727 ± 0.005
Del Principe et al. 2006	18.733 ± 0.005
Borissova et al. 2009	18.711 ± 0.005
average	18.720 ± 0.005

Table 5.5: Distance moduli for the 30 Dor field obtained applying different $PL_K Z$ relations to the 30 Dor RR Lyrae stars.

to check whether there is some trend in the PL when moving along the 30 Dor field, we divided the 30 Dor RR Lyrae stars into nine subfields of equal area (see left panel of Figure 5.24) in order to calculate independent PL_K relations for each of these 9 subfields, starting from the two subfields marked in red in the right panel of Figure 5.24.

The PL_K relation derived from the RR Lyrae stars contained in the upper-left subregion (subregion 1) is:

$$K_0 = 17.42 \pm 0.06 - 2.7 \pm 0.2 \times \log P \quad (5.11)$$

with an rms= 0.143. This PL_K is shown in Fig. 5.25. Crosses mark stars which are more than 3σ from the linear regression (blue line) and were discarded.

The PL_K relation derived from the RR Lyrae stars contained in the lower-right subregion (subregion 9) is:

$$K_0 = 17.45 \pm 0.05 - 2.5 \pm 0.2 \times \log P \quad (5.12)$$

with an rms=0.201. This PL_K is shown in Fig. 5.26.

The PL_K relations in the two subregions are indistinguishable within the errors. This seems to rule out a trend in the PL in the 30 Dor field. If we blindly rely on the results obtained from the PL_K relations of SEP ($\mu_0 = 18.58 \pm 0.03$ mag) and 30 Dor ($\mu_0 \sim 18.72 \pm 0.01$ mag) RR Lyrae stars we should conclude that the 30 Dor RR Lyrae are at larger distance than the SEP variables. On the other hand, the results of the PL for Classical Cepheids, that will be presented in the next Chapter, leading to a shorter distance modulus of $\mu_0 = 18.46 \pm 0.03$ mag (see section 6.2) further complicates the interpretation of the RR Lyrae results.

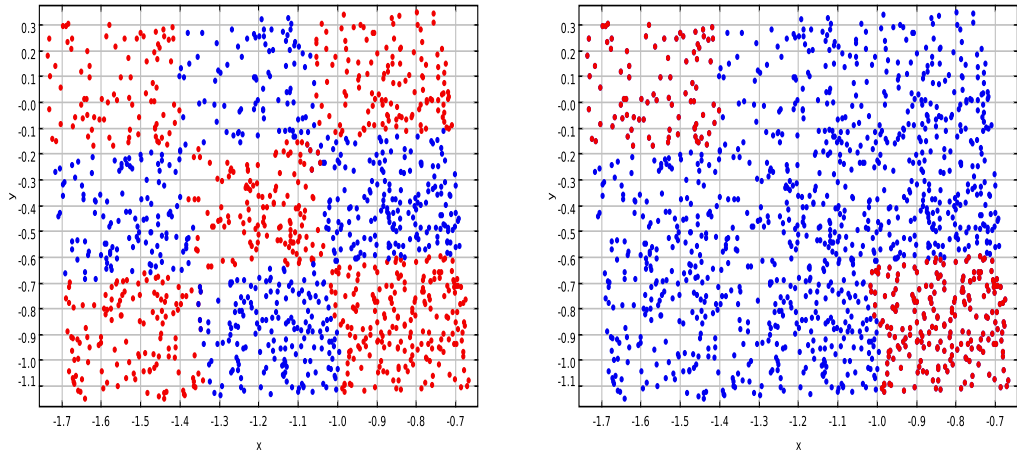


Figure 5.24: *Left Panel:* RR Lyrae stars (solid points) in the 30 Dor region divided into 9 subregions of equal area. *Right Panel:* RR Lyrae stars (red solid points) of the two subregions that we have started to analyze. See text for details.

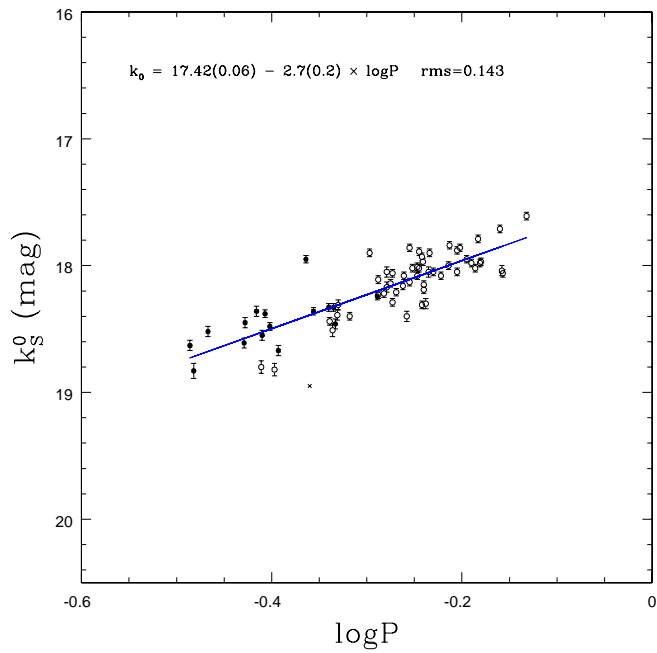


Figure 5.25: PL_K relation defined by the RR Lyrae stars in the subregion 1. Empty circles are RR_{ab} stars, filled circles are RR_c stars. Crosses are stars which are more than 3σ from the linear regression (blue line).

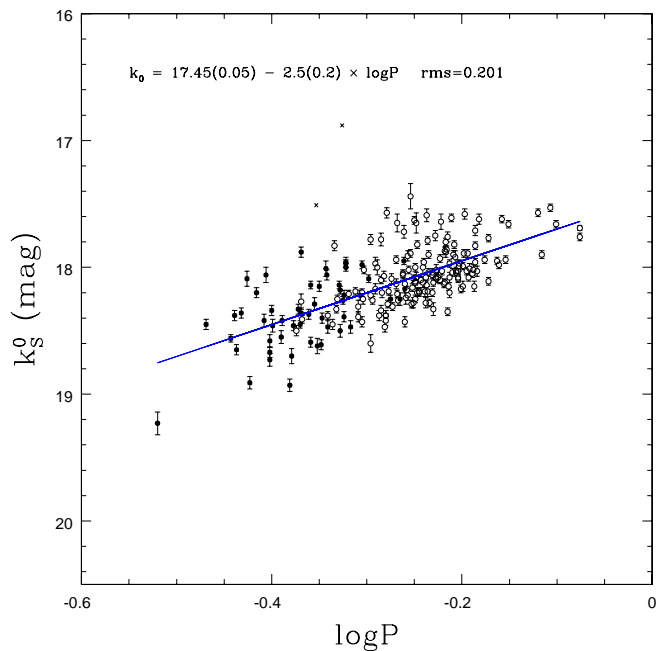


Figure 5.26: PL_K relation defined by the RR Lyrae stars in the subregion 9. Empty circles are RR_{ab} stars, filled circles are RR_c stars. Crosses are stars which are more than 3σ from the linear regression (blue line).

5.6 RR Lyrae stars in the 30 Dor region

VSA id	id-1	α (2000)	δ (2000)	RR	P (days)	Epoch(max) (JD-2450000)	$\langle B_{EROS} \rangle$ (mag)	A_V (mag)	$\langle K_s \rangle$ (mag)	$\sigma_{\langle K_s \rangle}$ (mag)	
VMC89.05881	65.62997	11777	89.05881	-65.62997	c	0.279836	2652.64817	19.055	0.39	18.43	0.04
VMC88.54182	67.04457	13140	88.54182	-67.04457	c	0.304106	1381.58947	19.192	0.58	18.34	0.02
VMC90.63806	66.84103	13919	90.63806	-66.84103	c	0.307907	1908.62017	19.185	0.50	18.36	0.02
VMC90.61131	66.97001	2508	90.61131	-66.97001	c	0.308761	1221.65639	19.137	0.62	18.39	0.02
VMC89.76387	66.52093	15111	89.76387	-66.52093	c	0.313693	2184.83767	19.109	0.43	17.500	0.011
VMC88.58812	66.39030	20171	88.58812	-66.3903	c	0.33125	2165.83235	19.047	0.51	18.170	0.019
VMC89.38447	66.88713	19933	89.38447	-66.88713	c	0.339066	2248.63538	19.078	0.44	18.215	0.019
VMC90.70238	66.62708	4670	90.70238	-66.62708	c	0.339586	1510.78566	19.169	0.56	18.185	0.019
VMC90.18475	66.87184	15662	90.18475	-66.87184	c	0.342598	1454.89457	19.046	0.63	18.153	0.019
VMC90.85286	66.43754	1765	90.85286	-66.43754	c	0.343763	1435.80988	19.231	0.65	18.222	0.019
VMC90.04089	66.99461	6636	90.04089	-66.99461	c	0.351408	0775.75636	19.074	0.45	17.948	0.016
VMC88.48468	66.13947	12471	88.48468	-66.13947	c	0.351672	1504.75912	18.971	0.48	18.166	0.018
VMC88.42676	66.00653	14454	88.42676	-66.00653	c	0.352939	2317.72252	18.903	0.50	17.933	0.016
VMC88.46714	66.59529	10812	88.46714	-66.59529	c	0.354487	2051.51101	19.280	0.45	18.34	0.02
VMC88.83012	66.51167	15888	88.83012	-66.51167	c	0.357676	0403.65860	19.390	0.46	18.227	0.019
VMC89.06184	66.07770	18477	89.06184	-66.07770	c	0.358804	2264.66450	19.083	0.49	18.231	0.019
VMC89.47125	66.74303	21254	89.47125	-66.74303	c	0.359865	1773.86766	19.122	0.55	18.36	0.02
VMC88.89312	66.82638	10748	88.89312	-66.82638	c	0.360168	2186.82044	19.194	0.44	18.177	0.019
VMC88.97116	66.20557	18546	88.97116	-66.20557	c	0.361223	1568.69875	19.172	0.49	18.146	0.018
VMC88.67397	66.06404	20120	88.67397	-66.06404	c	0.361499	1834.86629	19.187	0.48	18.172	0.019
VMC91.17422	66.70195	15448	91.17422	-66.70195	c	0.362432	2581.80256	18.948	0.47	18.008	0.016
VMC90.80177	66.66222	9603	90.80177	-66.66222	c	0.365587	1433.85859	19.128	0.54	18.129	0.018
VMC90.10844	66.41316	21390	90.10844	-66.41316	c	0.369042	0384.66456	19.141	0.47	18.063	0.017
VMC89.31884	66.75497	22698	89.31884	-66.75497	c	0.370708	1905.63006	19.109	0.48	18.080	0.019
VMC89.37604	66.35017	5148	89.37604	-66.35017	c	0.373764	0856.75824	19.024	0.43	18.132	0.018
VMC89.06472	65.76323	3849	89.06472	-65.76323	c	0.377784	1661.56158	99.999	0.35	18.042	0.016
VMC88.44221	66.46144	8721	88.44221	-66.46144	c	0.384942	0404.76630	19.123	0.47	18.057	0.017
VMC91.18246	66.55863	9807	91.18246	-66.55863	c	0.391335	1635.53733	19.043	0.42	17.981	0.016
VMC90.46352	66.91447	15644	90.46352	-66.91447	c	0.43207	1878.74046	18.762	0.42	17.766	0.013
VMC89.24688	65.92392	4000	89.24688	-65.92392	ab	0.482372	1502.75022	18.914	1.31	18.083	0.018
VMC89.76834	66.59172	10234	89.76834	-66.59172	ab	0.482726	1654.58824	19.375	1.05	18.26	0.02
VMC88.69875	65.81397	6674	88.69875	-65.81397	ab	0.483525	1968.69418	18.974	1.22	18.099	0.018
VMC89.01188	66.79188	6235	89.01188	-66.79188	ab	0.488967	1167.60566	19.151	1.29	18.125	0.019
VMC91.05922	66.88541	19248	91.05922	-66.88541	ab	0.494594	0411.72916	18.966	0.78	17.957	0.016
VMC90.55951	66.27546	663	90.55951	-66.27546	ab	0.502671	1522.73976	19.410	1.27	18.18	0.02
VMC89.58751	66.34335	12420	89.58751	-66.34335	ab	0.504687	1476.82046	19.508	1.14	17.888	0.015
VMC88.63285	67.04827	13678	88.63285	-67.04827	ab	0.505996	1950.68154	19.217	1.35	18.090	0.019
VMC90.26666	66.46120	6036	90.26666	-66.46120	ab	0.511104	1570.72598	19.343	1.37	18.102	0.018
VMC89.38903	66.74248	21067	89.38903	-66.74248	ab	0.512181	1840.83142	18.882	0.74	17.758	0.013
VMC89.60338	66.40584	19902	89.60338	-66.40584	ab	0.515216	1566.73078	19.532	1.35	18.157	0.019
VMC90.04898	66.86007	14083	90.04898	-66.86007	ab	0.524842	1897.65806	18.903	0.98	17.854	0.015
VMC88.93383	65.79487	5559	88.93383	-65.79487	ab	0.528266	1658.58260	18.963	1.09	17.947	0.016
VMC88.44860	65.86588	21824	88.4486	-65.86588	ab	0.530161	1236.73959	19.001	1.02	17.980	0.017
VMC91.19125	66.88860	19850	91.19125	-66.88860	ab	0.535519	2581.80256	19.025	1.17	17.895	0.016
VMC89.70010	66.92510	22456	89.7001	-66.9251	ab	0.5383	1843.87176	19.220	1.09	17.985	0.017
VMC90.43995	66.55826	15972	90.43995	-66.55826	ab	0.543127	1958.76520	19.301	1.29	18.015	0.016
VMC89.98765	66.55564	14988	89.98765	-66.55564	ab	0.543303	1872.78084	19.138	0.87	17.436	0.010
VMC89.83111	67.02162	9897	89.83111	-67.02162	ab	0.546485	0835.80158	18.903	1.15	17.714	0.014
VMC89.91313	66.92605	22582	89.91313	-66.92605	ab	0.546566	1866.72666	19.259	0.53	18.17	0.02
VMC89.34864	65.62532	11492	89.34864	-65.62532	ab	0.552641	1566.70416	19.044	0.90	18.053	0.016
VMC88.37764	66.39738	20974	88.37764	-66.39738	ab	0.556178	0399.79420	19.117	1.03	17.897	0.016
VMC88.90307	66.29199	7407	88.90307	-66.29199	ab	0.556799	2301.78814	19.306	1.20	17.971	0.016
VMC90.80654	66.57941	16708	90.80654	-66.57941	ab	0.558643	2662.72348	19.292	0.97	18.059	0.018
VMC89.14485	65.82450	8204	89.14485	-65.8245	ab	0.561825	2236.63572	19.083	1.04	18.068	0.018
VMC89.18743	66.69605	14455	89.18743	-66.69605	ab	0.564069	2165.83235	19.167	1.10	18.053	0.018

120 *Data analysis, and first results for RR Lyrae stars from the VMC survey*

VMC90.78511	-66.52942	14319	90.78511	-66.52942	ab	0.568044	1502.77046	19.365	1.08	18.080	0.018
VMC91.45882	-66.76432	18337	91.45882	-66.76432	ab	0.569036	2254.67274	18.936	1.03	17.928	0.015
VMC88.78716	-66.71886	23417	88.78716	-65.71886	ab	0.569449	2619.64881	19.033	1.10	17.916	0.016
VMC89.84316	-66.55735	19172	89.84316	-66.55735	ab	0.573327	1443.80388	19.123	0.72	17.883	0.015
VMC89.33329	-66.88950	20208	89.33329	-66.8895	ab	0.575952	2574.77742	19.315	0.40	18.045	0.017
VMC88.71300	-66.94060	20193	88.713	-66.9406	ab	0.580958	2003.58706	19.091	0.65	17.966	0.016
VMC90.14881	-66.94333	16928	90.14881	-66.94333	ab	0.582626	1954.70090	18.974	0.63	17.921	0.016
VMC89.41532	-66.71313	16999	89.41532	-66.71313	ab	0.582837	1439.81465	19.308	0.68	18.22	0.02
VMC88.99951	-66.72901	18737	88.99951	-66.72901	ab	0.58451	1464.78763	19.097	0.72	17.923	0.015
VMC90.60471	-66.28531	1127	90.60471	-66.28531	ab	0.584708	0400.71316	19.313	0.85	18.008	0.017
VMC88.81756	-65.79473	5500	88.81756	-65.79473	ab	0.58496	2000.60142	18.984	0.84	17.969	0.016
VMC89.17322	-66.14831	11644	89.17322	-66.14831	ab	0.586441	1828.82309	18.966	1.25	18.058	0.017
VMC91.31575	-66.35863	15027	91.31575	-66.35863	ab	0.591598	1563.77261	19.228	0.92	17.886	0.015
VMC88.95860	-65.65705	15364	88.9586	-65.65705	ab	0.59229	1469.73869	19.017	0.89	17.974	0.016
VMC90.58726	-66.82029	10498	90.58726	-66.82029	ab	0.594565	2266.75986	19.020	0.78	17.848	0.014
VMC88.62716	-66.07124	17115	88.62716	-66.07124	ab	0.598345	2225.84181	19.117	0.65	17.967	0.016
VMC88.75765	-66.36566	16908	88.75765	-66.36566	ab	0.598866	1641.55387	19.051	1.25	17.932	0.015
VMC90.32399	-66.74809	15574	90.32399	-66.74809	ab	0.601586	2581.80256	19.219	0.79	18.011	0.016
VMC88.58529	-65.65132	13995	88.58529	-65.65132	ab	0.602472	1837.79110	19.131	0.68	17.993	0.017
VMC89.21644	-67.07065	16710	89.21644	-67.07065	ab	0.603013	1590.67784	19.550	0.87	17.759	0.014
VMC89.91820	-66.65638	8769	88.9182	-66.65638	ab	0.60518	1952.68464	19.169	0.73	17.934	0.015
VMC88.57023	-66.09572	5521	88.57023	-66.09572	ab	0.610169	2637.80939	19.057	0.77	17.954	0.016
VMC90.28469	-66.63666	4863	90.28469	-66.63666	ab	0.612503	1451.85267	19.401	0.69	18.037	0.016
VMC88.66768	-65.75290	2684	88.66768	-65.7529	ab	0.614284	2236.63572	18.781	1.25	17.828	0.015
VMC89.18085	-65.67398	17942	89.18085	-65.67398	ab	0.615016	1556.81167	19.130	0.70	17.551	0.011
VMC88.54227	-66.99087	5838	88.54227	-66.99087	ab	0.617036	1625.66665	19.070	0.60	17.814	0.015
VMC90.00150	-66.29262	6601	90.0015	-66.29262	ab	0.623342	2401.55234	19.289	0.63	17.944	0.016
VMC90.97139	-66.28902	7254	90.97139	-66.28902	ab	0.629166	0396.82836	19.164	1.00	17.899	0.015
VMC90.44786	-66.48435	9162	90.44786	-66.48435	ab	0.631294	1481.79696	19.050	0.95	17.789	0.013
VMC90.68824	-66.37370	5441	90.68824	-66.3737	ab	0.633687	2026.55644	19.278	0.47	17.877	0.015
VMC88.69570	-65.82616	7473	88.6957	-65.82616	ab	0.638708	2228.69562	18.937	0.49	17.794	0.014
VMC88.63838	-66.72336	13082	88.63838	-66.72336	ab	0.640384	0383.77552	19.052	0.77	17.751	0.013
VMC88.44106	-65.95059	7752	88.44106	-65.95059	ab	0.640428	1499.73922	18.965	0.50	17.753	0.013
VMC88.99509	-65.79442	5990	88.99509	-65.79442	ab	0.644776	2245.86102	18.738	0.87	17.761	0.013
VMC89.10724	-66.92583	24832	89.10724	-66.92583	ab	0.64802	1443.79465	18.844	0.77	17.661	0.012
VMC89.22852	-65.87613	11722	89.22852	-65.87613	ab	0.648894	1241.74438	18.930	0.92	17.810	0.014
VMC89.29626	-67.08839	19178	89.29626	-67.08839	ab	0.651892	0332.82646	19.127	0.75	17.960	0.016
VMC88.58049	-66.46238	8898	88.58049	-66.46238	ab	0.652404	1566.70864	19.152	0.68	17.893	0.015
VMC89.06749	-65.86500	10894	89.06749	-65.865	ab	0.655036	1658.58360	19.075	0.28	17.885	0.015
VMC90.01699	-66.36999	16071	90.01699	-66.36999	ab	0.657831	0932.49584	19.033	0.76	17.715	0.013
VMC90.48320	-66.85892	16657	90.4832	-66.85892	ab	0.6640825	1940.78649	19.083	0.57	17.849	0.014
VMC90.33167	-66.40298	20205	90.33167	-66.40298	ab	0.671272	1892.72546	18.944	0.90	17.651	0.012
VMC90.74558	-66.79828	7107	90.74558	-66.79828	ab	0.676837	1908.62017	19.013	0.54	17.825	0.014
VMC89.05388	-66.39558	21063	89.05388	-66.39558	ab	0.718701	2255.70817	18.950	0.64	17.676	0.012
VMC90.29803	-66.88117	16920	90.29803	-66.88117	ab	0.721478	2000.62653	19.032	0.72	17.816	0.014
VMC90.50615	-66.90768	17861	90.50615	-66.90768	ab	0.725348	2003.60763	18.846	0.65	17.564	0.012
VMC88.42721	-66.63017	4284	88.42721	-66.63017	ab	0.729118	2262.73526	18.886	0.64	17.489	0.011
VMC90.84876	-66.70341	15514	90.84876	-66.70341	ab	0.753009	1493.82836	18.992	0.47	17.708	0.013
VMC89.75178	-66.49660	12246	89.75178	-66.4966	ab	0.773581	0457.76997	18.992	0.56	17.601	0.011
VMC90.09496	-66.62618	3518	90.09496	-66.62618	ab	0.808167	2240.69776	18.995	0.52	17.527	0.011

Table 5.6: Properties of confirmed RR Lyrae stars in the SEP field. Column 1: star id in the VMC catalogue; Column 2: EROS-2 id (only the last 4-5 digits); Columns 3,4: RA,DEC from the EROS-2 catalogue; Column 5: RR type; Column 6: EROS-2 period (except for star 16657 where we used the half of the EROS-2 period); Column 7: time of maximum light; Column 8: $\langle B_{EROS} \rangle$ mag, as obtained from the analysis with GRATIS; Column 9: A_V as obtained from the analysis with GRATIS; Column 10: $\langle K_S \rangle$ as obtained with the template's method; Column 11: error in $\langle K_S \rangle$.

5.6 RR Lyrae stars in the 30 Dor region

121

idOGLE	id	RA	DECdeg	type	I	V	P	dP	Epoch	k ₀	err(k ₀)	
OGLE-LMC-RRLYR-21877	VMC85.627035	68.636900	85.627035	-68.636900	RRab	18.912	19.573	0.547263700	1.4E-6	2187.42858	18.16	0.03
OGLE-LMC-RRLYR-19454	VMC83.700990	68.643240	83.700990	-68.643240	RRab	18.891	19.434	0.499421000	7.0E-7	2167.53753	17.86	0.05
OGLE-LMC-RRLYR-18653	VMC83.191185	68.642660	83.191185	-68.642660	RRc	18.904	19.389	0.335900800	7.0E-7	2167.70320	18.33	0.04
OGLE-LMC-RRLYR-20280	VMC84.275670	68.649040	84.275670	-68.649040	RRab	18.857	19.561	0.592429400	1.1E-6	2187.44302	18.10	0.03
OGLE-LMC-RRLYR-21907	VMC85.662660	68.642780	85.662660	-68.642780	RRab	19.376	19.928	0.388219500	4.0E-7	2187.43562	18.80	0.05
OGLE-LMC-RRLYR-20020	VMC84.092445	68.649600	84.092445	-68.649600	RRc	19.015	19.416	0.280158700	6.0E-7	2187.50418	18.54	0.03
OGLE-LMC-RRLYR-21888	VMC85.642455	68.644560	85.642455	-68.644560	RRab	19.162	19.846	0.458133100	6.0E-7	2187.77089	18.44	0.03
OGLE-LMC-RRLYR-21598	VMC85.341090	68.647210	85.341090	-68.647210	RRab	18.794	19.366	0.533937300	1.6E-6	2187.32005	18.06	0.03
OGLE-LMC-RRLYR-18463	VMC83.075460	68.647720	83.075460	-68.647720	RRab	18.825	19.315	0.450714800	2.0E-7	2167.55651	18.12	0.03
OGLE-LMC-RRLYR-18851	VMC83.315400	68.650390	83.315400	-68.650390	RRab	18.934	19.559	0.558726500	6.0E-7	2167.85023	18.06	0.03
OGLE-LMC-RRLYR-18933	VMC83.372790	68.659490	83.372790	-68.659490	RRab	19.099	19.717	0.515377900	5.0E-7	2167.48725	18.33	0.03
OGLE-LMC-RRLYR-19990	VMC84.071730	68.670760	84.071730	-68.670760	RRab	18.642	19.307	0.707276600	1.9E-6	2187.70851	17.86	0.03
OGLE-LMC-RRLYR-21091	VMC84.905730	68.669360	84.905730	-68.669360	RRc	18.905	19.308	0.302158200	5.0E-7	2187.60200	18.27	0.03
OGLE-LMC-RRLYR-19706	VMC83.860395	68.676360	83.860395	-68.676360	RRab	18.999	19.616	0.574046100	1.4E-6	2187.69299	18.12	0.04
OGLE-LMC-RRLYR-21164	VMC84.970485	68.675480	84.970485	-68.675480	RRc	18.686	19.162	0.364415000	7.0E-7	2187.67560	18.05	0.03
OGLE-LMC-RRLYR-21220	VMC85.024215	68.680730	85.024215	-68.680730	RRab	19.130	19.362	0.504584900	5.0E-7	2187.70253	17.90	0.03
OGLE-LMC-RRLYR-19300	VMC83.588355	68.682350	83.588355	-68.682350	RRab	18.950	19.570	0.597524100	8.0E-7	2167.41658	17.92	0.04
OGLE-LMC-RRLYR-18470	VMC83.080230	68.682800	83.080230	-68.682800	RRab	20.126	21.409	0.598200000	1.7E-6	2167.70288	18.38	0.03
OGLE-LMC-RRLYR-20571	VMC84.489390	68.687410	84.489390	-68.687410	RRc	18.393	18.846	0.384976500	1.1E-6	2193.72177	17.81	0.03
OGLE-LMC-RRLYR-18917	VMC83.360595	68.684020	83.360595	-68.684020	RRc	19.344	19.784	0.284344100	5.0E-7	2167.76675	18.20	0.07
OGLE-LMC-RRLYR-21348	VMC85.128195	68.685220	85.128195	-68.685220	RRab	18.798	19.488	0.624507500	2.6E-6	2187.31111	17.88	0.03
OGLE-LMC-RRLYR-20277	VMC84.270390	68.690080	84.270390	-68.690080	RRab	18.674	19.309	0.676827400	4.4E-6	2187.31691	17.87	0.02
OGLE-LMC-RRLYR-18650	VMC83.190300	68.687890	83.190300	-68.687890	RRab	19.055	19.808	0.613213500	1.5E-6	2167.88250	18.12	0.03
OGLE-LMC-RRLYR-20194	VMC83.217440	68.691860	84.217440	-68.691860	RRab	18.831	19.409	0.581596300	9.0E-7	2187.69219	18.01	0.03
OGLE-LMC-RRLYR-19375	VMC83.640420	68.691730	83.640420	-68.691730	RRab	18.629	19.455	0.571297100	1.1E-6	2167.84239	17.91	0.05
OGLE-LMC-RRLYR-19268	VMC83.571540	68.691600	83.571540	-68.691600	RRab	18.884	19.464	0.509701400	1.6E-6	2186.76992	18.15	0.03
OGLE-LMC-RRLYR-20962	VMC84.799605	68.693300	84.799605	-68.693300	RRab	18.974	19.548	0.497205300	6.0E-7	2187.71398	18.30	0.03
OGLE-LMC-RRLYR-20842	VMC84.699420	68.695140	84.699420	-68.695140	RRab	19.163	19.918	0.566930100	9.0E-7	2187.60169	18.24	0.04
OGLE-LMC-RRLYR-22017	VMC85.769835	68.688610	85.769835	-68.688610	RRab	18.859	19.583	0.659508900	3.0E-6	2187.28516	17.98	0.03
OGLE-LMC-RRLYR-21634	VMC85.372665	68.692220	85.372665	-68.692220	RRab	19.202	19.837	0.526649400	6.0E-7	2187.62371	18.17	0.04
OGLE-LMC-RRLYR-19491	VMC83.725185	68.696530	83.725185	-68.696530	RRc	19.121	19.558	0.273957000	6.0E-7	2167.70977	18.61	0.05
OGLE-LMC-RRLYR-20007	VMC84.083160	68.695120	84.083160	-68.695120	RRab	18.824	19.469	0.616755100	2.0E-6	2187.50744	18.00	0.03
OGLE-LMC-RRLYR-21867	VMC85.609365	68.693900	85.609365	-68.693900	RRe	19.142	19.647	0.278604900	8.0E-7	2187.72533	18.45	0.04
OGLE-LMC-RRLYR-20083	VMC84.135780	68.699820	84.135780	-68.699820	RRc	18.867	19.272	0.351665500	9.0E-7	2187.67885	17.99	0.04
OGLE-LMC-RRLYR-2162	VMC84.968835	68.699930	84.968835	-68.699930	RRab	18.925	19.546	0.537568600	5.0E-7	2187.50594	18.12	0.04
OGLE-LMC-RRLYR-21331	VMC85.109295	68.698810	85.109295	-68.698810	RRab	18.839	19.460	0.548572200	7.0E-7	2187.43400	18.08	0.03
OGLE-LMC-RRLYR-19661	VMC83.831625	68.704070	83.831625	-68.704070	RRab	19.348	20.163	0.524175300	1.4E-6	2187.58241	18.18	0.05
OGLE-LMC-RRLYR-21497	VMC85.246110	68.701950	85.246110	-68.701950	RRab	18.917	19.547	0.530866400	2.1E-6	2187.73181	18.14	0.03
OGLE-LMC-RRLYR-20371	VMC84.341640	68.707870	84.341640	-68.707870	RRab	18.887	19.361	0.475208700	4.0E-7	2187.73356	18.08	0.03
OGLE-LMC-RRLYR-21396	VMC85.162995	68.705420	85.162995	-68.705420	RRab	18.937	19.675	0.637726700	3.9E-6	2187.39808	17.95	0.03
OGLE-LMC-RRLYR-18625	VMC83.172885	68.708010	83.172885	-68.708010	RRc	19.038	19.424	0.280615100	5.0E-7	2167.80590	18.50	0.05
OGLE-LMC-RRLYR-20039	VMC84.107415	68.713440	84.107415	-68.713440	RRab	18.933	19.508	0.534417300	1.2E-6	2187.57616	18.15	0.03
OGLE-LMC-RRLYR-21892	VMC85.646970	68.707880	85.646970	-68.707880	RRab	19.207	20.094	0.533551600	1.4E-6	2187.63700	18.29	0.03
OGLE-LMC-RRLYR-21092	VMC84.906135	68.711550	84.906135	-68.711550	RRc	18.918	19.460	0.355597300	1.0E-6	2187.58149	18.18	0.03
OGLE-LMC-RRLYR-21133	VMC84.935805	68.715020	84.935805	-68.715020	RRab	18.903	19.680	0.728335000	2.9E-6	2187.73523	17.64	0.04
OGLE-LMC-RRLYR-20276	VMC84.270150	68.716940	84.270150	-68.716940	RRc	18.951	19.417	0.325182400	8.0E-7	2187.44648	18.36	0.03
OGLE-LMC-RRLYR-20317	VMC84.302685	68.717410	84.302685	-68.717410	RRab	18.759	19.583	0.652776700	3.6E-6	2187.26201	17.82	0.03
OGLE-LMC-RRLYR-19182	VMC83.512005	68.716370	83.512005	-68.716370	RRab	18.751	19.473	0.747400800	5.6E-6	2167.67122	17.83	0.03
OGLE-LMC-RRLYR-20354	VMC84.331965	68.718300	84.331965	-68.718300	RRab	18.874	19.513	0.616046400	2.0E-6	2187.73085	18.01	0.04
OGLE-LMC-RRLYR-19165	VMC83.500770	68.717960	83.500770	-68.717960	RRab	18.782	19.462	0.595386200	7.0E-7	2167.74503	18.01	0.03
OGLE-LMC-RRLYR-20444	VMC84.389460	68.721690	84.389460	-68.721690	RRab	19.312	19.812	0.400552500	4.0E-7	2187.60980	18.51	0.04
OGLE-LMC-RRLYR-21571	VMC85.313295	68.730640	85.313295	-68.730640	RRe	19.683	20.456	0.286193400	1.2E-6	2187.64603	18.36	0.04
OGLE-LMC-RRLYR-20696	VMC84.605220	68.734790	84.605220	-68.734790	RRab	19.224	19.877	0.496695200	1.7E-6	2187.50557	18.24	0.04
OGLE-LMC-RRLYR-20059	VMC84.121185	68.736790	84.121185	-68.736790	RRc	19.279	19.849	0.300248000	7.0E-7	2187.75061	18.74	0.05
OGLE-LMC-RRLYR-21210	VMC85.016355	68.732750	85.016355	-68.732750	RRab	19.090	19.961	0.646300500	3.2E-6	2187.63001	17.98	0.03

122Data analysis, and first results for RR Lyrae stars from the VMC survey

OGLE-LMC-RRLYR-19762	VMC83.908230	68.737070	83.908230	-68.737070	RRab	19.120	19.993	0.536416300	1.3E-6	2187.62307	18.06	0.03
OGLE-LMC-RRLYR-21876	VMC85.626945	-68.734890	85.626945	-68.734890	RRab	19.079	19.777	0.515880300	6.0E-7	2187.72447	18.11	0.03
OGLE-LMC-RRLYR-19246	VMC83.555700	-68.740300	83.555700	-68.740300	RRab	18.831	19.418	0.514648500	5.0E-7	2167.84510	18.03	0.04
OGLE-LMC-RRLYR-19975	VMC84.059520	-68.744050	84.059520	-68.744050	RRab	18.901	19.437	0.512686800	4.0E-7	2187.29475	18.18	0.04
OGLE-LMC-RRLYR-21198	VMC85.005615	-68.743380	85.005615	-68.743380	RRe	19.164	19.651	0.254999800	1.3E-6	2187.72519	18.52	0.04
OGLE-LMC-RRLYR-19461	VMC83.705130	-68.743920	83.705130	-68.743920	RRab	18.900	19.486	0.505894500	5.0E-7	2167.56130	18.23	0.04
OGLE-LMC-RRLYR-18923	VMC83.364600	-68.741320	83.364600	-68.741320	RRab	18.467	19.061	0.750322700	1.2E-6	2167.40153	17.81	0.03
OGLE-LMC-RRLYR-20269	VMC84.266670	-68.748110	84.266670	-68.748110	RRab	18.823	19.469	0.534921700	5.0E-7	2187.47387	18.07	0.03
OGLE-LMC-RRLYR-19758	VMC83.906475	-68.748680	83.906475	-68.748680	RRc	18.803	19.231	0.322238800	9.0E-7	2187.66988	18.32	0.04
OGLE-LMC-RRLYR-20523	VMC84.460965	-68.750100	84.460965	-68.750100	RRab	19.117	19.880	0.613905200	2.0E-6	2187.16729	18.01	0.03
OGLE-LMC-RRLYR-21769	VMC85.516830	-68.744360	85.516830	-68.744360	RRab	18.900	19.630	0.611569100	1.3E-6	2187.59020	18.00	0.03
OGLE-LMC-RRLYR-19982	VMC84.066750	-68.757110	84.066750	-68.757110	RRab	18.951	19.599	0.539460000	8.0E-7	2187.68858	18.28	0.04
OGLE-LMC-RRLYR-19933	VMC84.032730	-68.758570	84.032730	-68.758570	RRab	19.102	19.777	0.504270000	5.0E-7	2187.72414	18.20	0.03
OGLE-LMC-RRLYR-22041	VMC85.797780	-68.753850	85.797780	-68.753850	RRab	19.031	19.773	0.568088000	1.7E-6	2187.49089	18.02	0.03
OGLE-LMC-RRLYR-18610	VMC83.167860	-68.754000	83.167860	-68.754000	RRab	19.142	19.740	0.540985600	1.0E-6	2167.35333	18.32	0.04
OGLE-LMC-RRLYR-21242	VMC85.045785	-68.763280	85.045785	-68.763280	RRab	19.104	19.943	0.623667900	2.1E-6	2187.28671	18.05	0.03
OGLE-LMC-RRLYR-20030	VMC84.098595	-68.770760	84.098595	-68.770760	RRc	18.864	19.332	0.341342400	9.0E-7	2187.56435	18.26	0.03
OGLE-LMC-RRLYR-19673	VMC83.841330	-68.771850	83.841330	-68.771850	RRab	18.913	19.503	0.520188700	6.0E-7	2187.25645	18.13	0.03
OGLE-LMC-RRLYR-20233	VMC84.242100	-68.772270	84.242100	-68.772270	RRab	19.036	19.587	0.465786900	4.0E-7	2187.36644	18.22	0.03
OGLE-LMC-RRLYR-19026	VMC83.421735	-68.774650	83.421735	-68.774650	RRab	19.256	20.195	0.661663300	4.7E-6	2167.75844	18.09	0.03
OGLE-LMC-RRLYR-18856	VMC83.318865	-68.777270	83.318865	-68.777270	RRab	18.942	19.559	0.558969400	5.0E-7	2167.42670	18.16	0.03
OGLE-LMC-RRLYR-21483	VMC85.235715	-68.778370	85.235715	-68.778370	RRab	18.786	19.415	0.559362300	6.0E-7	2187.68269	18.02	0.03
OGLE-LMC-RRLYR-18861	VMC83.322225	-68.779960	83.322225	-68.779960	RRab	18.952	19.639	0.611266000	1.4E-6	2167.47452	18.07	0.03
OGLE-LMC-RRLYR-20191	VMC84.216030	-68.771700	84.216030	-68.771700	RRab	18.792	19.516	0.653812800	5.4E-6	2187.74689	17.90	0.03
OGLE-LMC-RRLYR-20904	VMC84.746025	-68.785890	84.746025	-68.785890	RRab	19.288	20.101	0.568044000	8.0E-7	2187.50676	18.02	0.03
OGLE-LMC-RRLYR-19458	VMC83.702430	-68.775370	83.702430	-68.775370	RRe	19.122	19.493	0.230198200	8.0E-7	2167.76437	18.68	0.04
OGLE-LMC-RRLYR-18378	VMC83.029620	-68.784370	83.029620	-68.784370	RRc	18.829	19.276	0.339405000	7.0E-7	2167.85546	18.24	0.03
OGLE-LMC-RRLYR-20495	VMC84.439755	-68.792250	84.439755	-68.792250	RRab	19.464	20.273	0.276555700	1.3E-6	2187.51749	18.41	0.04
OGLE-LMC-RRLYR-21229	VMC85.033035	-68.789370	85.033035	-68.789370	RRab	19.530	20.465	0.514830500	1.0E-6	2187.30452	18.23	0.03
OGLE-LMC-RRLYR-19833	VMC83.957835	-68.795740	83.957835	-68.795740	RRab	18.550	19.068	0.629177900	9.0E-7	2187.46268	17.91	0.03
OGLE-LMC-RRLYR-18724	VMC83.231685	-68.794140	83.231685	-68.794140	RRab	18.714	19.280	0.637263400	1.0E-6	2167.26307	17.70	0.03
OGLE-LMC-RRLYR-21329	VMC85.107900	-68.796640	85.107900	-68.796640	RRab	18.989	19.716	0.589531300	1.0E-6	2187.43607	18.05	0.03
OGLE-LMC-RRLYR-21137	VMC84.939255	-68.798290	84.939255	-68.798290	RRab	18.832	19.414	0.549448000	6.0E-7	2187.41238	17.99	0.03
OGLE-LMC-RRLYR-19772	VMC83.914830	-68.800350	83.914830	-68.800350	RRc	19.085	19.548	0.304159700	7.0E-7	2187.73504	18.45	0.04
OGLE-LMC-RRLYR-19142	VMC83.488710	-68.794650	83.488710	-68.794650	RRab	18.866	19.459	0.545384500	6.0E-7	2167.62690	17.98	0.03
OGLE-LMC-RRLYR-21996	VMC85.752030	-68.794250	85.752030	-68.794250	RRc	19.340	19.995	0.295908900	9.0E-7	2187.75256	18.48	0.03
OGLE-LMC-RRLYR-19581	VMC83.780430	-68.802920	83.780430	-68.802920	RRab	19.027	19.589	0.514528200	1.4E-6	2187.70798	18.30	0.04
OGLE-LMC-RRLYR-21760	VMC85.509915	-68.803940	85.509915	-68.803940	RRab	19.456	20.139	0.401189500	5.0E-7	2187.45237	18.82	0.05
OGLE-LMC-RRLYR-18446	VMC83.066940	-68.803790	83.066940	-68.803790	RRab	19.081	19.758	0.544715900	1.1E-6	2167.42634	18.17	0.03
OGLE-LMC-RRLYR-20969	VMC84.809160	-68.809480	84.809160	-68.809480	RRab	18.990	-99.99	0.558497700	5.0E-6	299.85580	18.0	0.03
OGLE-LMC-RRLYR-18944	VMC83.378940	-68.812670	83.378940	-68.812670	RRab	18.936	19.566	0.565201200	5.0E-7	2167.43411	18.13	0.03
OGLE-LMC-RRLYR-20635	VMC84.544185	-68.819290	84.544185	-68.819290	RRab	19.131	20.002	0.648469500	4.7E-6	2187.49296	17.99	0.03
OGLE-LMC-RRLYR-19447	VMC83.694480	-68.820000	83.694480	-68.820000	RRab	19.576	20.426	0.458894000	1.0E-6	2167.60804	18.38	0.05
OGLE-LMC-RRLYR-18638	VMC83.180280	-68.822400	83.180280	-68.822400	RRab	18.899	19.448	0.556320600	6.0E-7	2167.41938	18.14	0.03
OGLE-LMC-RRLYR-21052	VMC84.873885	-68.825260	84.873885	-68.825260	RRab	19.045	19.791	0.590729600	1.0E-6	2187.53269	18.15	0.03
OGLE-LMC-RRLYR-19992	VMC84.074715	-68.827640	84.074715	-68.827640	RRab	19.208	19.728	0.454786800	5.0E-7	2187.34458	18.52	0.04
OGLE-LMC-RRLYR-19768	VMC83.912325	-68.827550	83.912325	-68.827550	RRab	18.611	19.194	0.657990300	1.5E-6	2187.39543	17.79	0.03
OGLE-LMC-RRLYR-21833	VMC85.576395	-68.821110	85.576395	-68.821110	RRab	18.576	19.126	0.611720000	8.0E-7	2187.34203	17.84	0.03
OGLE-LMC-RRLYR-20082	VMC84.135480	-68.832120	84.135480	-68.832120	RRab	18.879	19.491	0.580931300	1.0E-6	2187.74980	18.18	0.03
OGLE-LMC-RRLYR-19214	VMC83.535045	-68.830950	83.535045	-68.830950	RRab	18.991	19.653	0.579848600	1.2E-6	2167.77487	18.13	0.04
OGLE-LMC-RRLYR-19356	VMC83.621475	-68.829520	83.621475	-68.829520	RRab	19.076	19.724	0.536226800	5.0E-7	2167.52276	18.20	0.03
OGLE-LMC-RRLYR-19619	VMC83.807295	-68.836830	83.807295	-68.836830	RRc	18.868	19.321	0.341276900	9.0E-7	2187.74111	18.16	0.05
OGLE-LMC-RRLYR-18952	VMC83.384130	-68.837350	83.384130	-68.837350	RRab	19.254	20.020	0.530376200	1.0E-6	2167.37860	18.36	0.03
OGLE-LMC-RRLYR-18872	VMC83.329335	-68.838200	83.329335	-68.838200	RRc	19.106	19.559	0.273941600	5.0E-7	2167.71246	18.45	0.05
OGLE-LMC-RRLYR-19887	VMC83.999055	-68.842290	83.999055	-68.842290	RRc	19.127	19.566	0.301345500	1.1E-6	2187.67175	18.58	0.04
OGLE-LMC-RRLYR-20706	VMC84.613830	-68.843290	84.613830	-68.843290	RRab	19.127	19.924	0.567393400	1.0E-6	2187.52746	18.08	0.03
OGLE-LMC-RRLYR-22040	VMC85.797105	-68.836420	85.797105	-68.836420	RRab	18.425	19.096	0.737662300	2.5E-6	2187.44954	17.61	0.03
OGLE-LMC-RRLYR-18340	VMC83.010270	-68.839860	83.010270	-68.839860	RRab	18.726	19.334	0.577986900	9.0E-7	2167.79714	17.89	0.05

5.6 RR Lyrae stars in the 30 Dor region

123

OGLE-LMC-RRLYR-19012	VMC83.414745	68.844540	83.414745	-68.844540	RRab	19.106	19.702	0.532377600	6.0E-7	2167.46161	18.33	0.04
OGLE-LMC-RRLYR-18592	VMC83.149275	68.844140	83.149275	-68.844140	RRab	18.783	19.425	0.617181800	1.1E-6	2167.50613	17.99	0.03
OGLE-LMC-RRLYR-21770	VMC85.518825	68.845700	85.518825	-68.845700	RRab	18.986	19.733	0.575156300	1.0E-6	2187.54007	18.15	0.03
OGLE-LMC-RRLYR-20688	VMC84.599130	68.852080	84.599130	-68.852080	RRab	19.294	20.256	0.667875100	3.3E-6	2187.53037	18.10	0.04
OGLE-LMC-RRLYR-21552	VMC85.299705	68.852920	85.299705	-68.852920	RRab	18.938	19.563	0.555949600	6.0E-7	2187.63983	18.13	0.03
OGLE-LMC-RRLYR-21482	VMC85.233555	68.853940	85.233555	-68.853940	RRab	20.045	21.073	0.436739000	1.6E-6	2187.66550	18.95	0.05
OGLE-LMC-RRLYR-20260	VMC84.261720	68.857290	84.261720	-68.857290	RRe	18.892	19.285	0.259118200	1.2E-6	2187.68257	18.53	0.04
OGLE-LMC-RRLYR-18443	VMC83.065125	68.854270	83.065125	-68.854270	RRab	18.992	19.705	0.603040500	1.4E-6	2167.68955	18.32	0.03
OGLE-LMC-RRLYR-21073	VMC84.890400	68.858680	84.890400	-68.858680	RRab	19.484	20.389	0.540508700	1.0E-6	2187.38662	18.33	0.04
OGLE-LMC-RRLYR-19462	VMC83.706270	68.861680	83.706270	-68.861680	R Rc	18.826	19.605	0.364017000	9.0E-7	2167.73195	17.28	0.06
OGLE-LMC-RRLYR-21029	VMC84.857580	68.863670	84.857580	-68.863670	R Rc	19.803	20.634	0.323257800	1.4E-6	2187.45023	18.51	0.04
OGLE-LMC-RRLYR-19019	VMC83.418765	68.868310	83.418765	-68.868310	R Rc	18.840	19.448	0.396892000	1.2E-6	2167.84883	17.90	0.04
OGLE-LMC-RRLYR-20388	VMC84.354450	68.873980	84.354450	-68.873980	RRab	19.062	19.810	0.557262900	9.0E-7	2187.49785	18.15	0.03
OGLE-LMC-RRLYR-20253	VMC84.253005	68.873000	84.253005	-68.873000	RRab	18.338	18.690	0.580268200	2.0E-6	2187.44986	17.66	0.04
OGLE-LMC-RRLYR-20403	VMC84.365700	68.874670	84.365700	-68.874670	R Rc	18.638	19.084	0.351800500	8.0E-7	2187.44914	18.11	0.04
OGLE-LMC-RRLYR-19257	VMC83.564145	68.872910	83.564145	-68.872910	RRab	18.565	19.041	0.600685800	1.3E-6	2167.29235	17.90	0.03
OGLE-LMC-RRLYR-19068	VMC83.446425	68.876620	83.446425	-68.876620	RRab	18.228	18.509	0.554178100	7.0E-7	2167.66787	17.83	0.03
OGLE-LMC-RRLYR-20383	VMC84.351030	68.880620	84.351030	-68.880620	RRab	19.038	19.638	0.508663900	7.0E-7	2187.40456	18.21	0.04
OGLE-LMC-RRLYR-21287	VMC85.078890	68.879020	85.078890	-68.879020	R Rc	20.066	21.130	0.301867700	1.3E-6	2187.47775	18.67	0.04
OGLE-LMC-RRLYR-19358	VMC83.624130	68.884090	83.624130	-68.884090	RRab	18.834	19.406	0.569120700	1.4E-6	2167.57624	17.95	0.03
OGLE-LMC-RRLYR-18785	VMC83.268285	68.882230	83.268285	-68.882230	R Rc	18.952	19.408	0.310155400	6.0E-7	2167.88151	18.25	0.04
OGLE-LMC-RRLYR-21972	VMC85.730535	68.880560	85.730535	-68.880560	RRab	19.034	19.716	0.538729900	8.0E-7	2187.58989	18.21	0.03
OGLE-LMC-RRLYR-20743	VMC84.640245	68.881420	84.640245	-68.881420	RRab	19.352	20.481	0.504690800	1.0E-6	2190.50029	18.16	0.05
OGLE-LMC-RRLYR-18646	VMC83.182365	68.889520	83.182365	-68.889520	RRab	18.935	19.577	0.522815400	6.0E-7	2167.84702	18.28	0.04
OGLE-LMC-RRLYR-19083	VMC83.456700	68.893320	83.456700	-68.893320	R Re	18.615	18.961	0.268939200	7.0E-7	2167.69623	18.18	0.03
OGLE-LMC-RRLYR-19369	VMC83.631465	68.893550	83.631465	-68.893550	RRab	18.679	18.869	0.522912100	4.0E-7	2167.52091	17.79	0.04
OGLE-LMC-RRLYR-18635	VMC83.177970	68.895060	83.177970	-68.895060	R Rc	18.635	19.152	0.402091000	8.0E-7	2167.56308	18.03	0.03
OGLE-LMC-RRLYR-18450	VMC83.070630	68.896200	83.070630	-68.896200	RRab	18.717	19.114	0.602567600	1.3E-6	2167.78846	17.95	0.04
OGLE-LMC-RRLYR-19693	VMC83.853240	68.900000	83.853240	-68.900000	RRab	19.423	20.266	0.552391500	1.7E-6	2187.73055	18.33	0.03
OGLE-LMC-RRLYR-21256	VMC85.058145	68.900330	85.058145	-68.900330	R Rc	18.511	18.853	0.323173700	1.0E-6	2187.48553	17.95	0.03
OGLE-LMC-RRLYR-19810	VMC83.945220	68.905090	83.945220	-68.905090	RRab	19.013	19.911	0.678896700	1.9E-6	2187.20037	18.04	0.03
OGLE-LMC-RRLYR-18831	VMC83.2299185	68.904810	83.2299185	-68.904810	RRab	18.548	19.163	0.739795700	2.2E-6	2167.83075	17.76	0.03
OGLE-LMC-RRLYR-18958	VMC83.387145	68.914400	83.387145	-68.914400	RRab	18.940	19.478	0.589581500	8.0E-7	2167.70192	18.15	0.03
OGLE-LMC-RRLYR-18899	VMC83.345385	68.915940	83.345385	-68.915940	RRab	18.743	19.414	0.649184000	1.7E-6	2167.48258	17.94	0.03
OGLE-LMC-RRLYR-21620	VMC85.361370	68.915660	85.361370	-68.915660	RRab	19.238	20.137	0.574971600	2.8E-6	2187.30947	18.19	0.03
OGLE-LMC-RRLYR-21359	VMC85.135455	68.917700	85.135455	-68.917700	RRab	19.841	20.880	0.578728500	2.3E-6	2187.38823	18.30	0.04
OGLE-LMC-RRLYR-18734	VMC83.028645	68.915800	83.028645	-68.915800	RRab	19.871	20.946	0.555939300	1.6E-6	2167.68704	18.24	0.04
OGLE-LMC-RRLYR-20325	VMC84.307755	68.920720	84.307755	-68.920720	RRab	18.817	19.442	0.592398000	8.0E-7	2187.58938	17.88	0.04
OGLE-LMC-RRLYR-20048	VMC84.114645	68.922510	84.114645	-68.922510	RRab	19.239	19.953	0.522330900	1.5E-6	2187.38578	18.35	0.04
OGLE-LMC-RRLYR-19363	VMC83.627730	68.926980	83.627730	-68.926980	RRab	18.823	19.559	0.631011400	2.0E-6	2167.85418	17.89	0.03
OGLE-LMC-RRLYR-21830	VMC85.572195	68.928200	85.572195	-68.928200	RRab	19.242	20.154	0.525582200	8.0E-7	2187.62863	18.05	0.04
OGLE-LMC-RRLYR-21506	VMC85.255770	68.931700	85.255770	-68.931700	RRab	18.631	19.134	0.572924400	6.0E-7	2187.27885	17.93	0.03
OGLE-LMC-RRLYR-21813	VMC85.557585	68.930830	85.557585	-68.930830	R Rc	19.644	20.624	0.346461000	2.0E-6	2187.51952	18.46	0.04
OGLE-LMC-RRLYR-20097	VMC84.143520	68.936550	84.143520	-68.936550	RRab	19.572	20.686	0.555409500	1.9E-6	2187.49598	18.00	0.04
OGLE-LMC-RRLYR-20053	VMC84.119535	68.936470	84.119535	-68.936470	RRab	19.837	21.024	0.598669600	3.5E-6	2187.46061	18.26	0.04
OGLE-LMC-RRLYR-21706	VMC85.451085	68.934040	85.451085	-68.934040	RRab	19.329	20.233	0.695502700	3.1E-6	2187.35141	18.04	0.04
OGLE-LMC-RRLYR-19503	VMC83.735715	68.940260	83.735715	-68.940260	RRab	19.428	20.252	0.491801400	5.0E-7	2167.66537	18.34	0.03
OGLE-LMC-RRLYR-18641	VMC83.181225	68.940650	83.181225	-68.940650	RRab	18.707	19.290	0.614159800	7.0E-7	2167.47344	17.96	0.03
OGLE-LMC-RRLYR-21605	VMC85.347975	68.941550	85.347975	-68.941550	RRab	18.951	19.708	0.650949100	5.1E-6	2187.74682	18.02	0.03
OGLE-LMC-RRLYR-19218	VMC83.538780	68.948240	83.538780	-68.948240	RRab	18.803	19.457	0.595896200	4.0E-7	2167.55680	17.92	0.03
OGLE-LMC-RRLYR-21297	VMC85.084395	68.948670	85.084395	-68.948670	RRab	19.494	20.432	0.551878000	1.0E-6	2187.39896	18.40	0.04
OGLE-LMC-RRLYR-19799	VMC83.936355	68.950950	83.936355	-68.950950	RRab	19.019	19.884	0.724928400	3.6E-6	2187.46299	17.91	0.03
OGLE-LMC-RRLYR-18740	VMC83.242605	68.950090	83.242605	-68.950090	R Rc	18.646	19.071	0.378571200	8.0E-7	2167.62349	18.07	0.03
OGLE-LMC-RRLYR-21328	VMC85.105410	68.950410	85.105410	-68.950410	R Rc	19.301	20.174	0.383625600	1.3E-6	2187.68501	18.24	0.03
OGLE-LMC-RRLYR-21668	VMC85.411230	68.949250	85.411230	-68.949250	RRab	18.882	19.566	0.556302900	6.0E-7	2187.56223	17.86	0.03
OGLE-LMC-RRLYR-19150	VMC83.494425	68.953030	83.494425	-68.953030	RRab	18.647	19.090	0.581072100	1.2E-6	2167.71961	17.91	0.03
OGLE-LMC-RRLYR-18336	VMC83.005620	68.952860	83.005620	-68.952860	RRab	19.588	20.471	0.488061700	4.0E-7	2167.46535	18.40	0.04
OGLE-LMC-RRLYR-19490	VMC83.725095	68.956860	83.725095	-68.956860	RRab	19.123	19.943	0.606692500	1.3E-6	2167.64967	18.16	0.04

124Data analysis, and first results for RR Lyrae stars from the VMC survey

OGLE-LMC-RRLYR-20877	VMC84.726330	68.957000	84.726330	-68.957000	RRab	19.394	20.129	0.473998100	1.5E-6	2187.75970	18.42	0.05
OGLE-LMC-RRLYR-21856	VMC85.599780	68.952980	85.599780	-68.952980	RRab	19.361	20.435	0.696444800	2.6E-6	2187.33152	18.06	0.03
OGLE-LMC-RRLYR-20384	VMC84.352560	68.961880	84.352560	-68.961880	RRab	18.951	19.895	0.907203500	8.6E-6	2186.86960	17.71	0.03
OGLE-LMC-RRLYR-21488	VMC85.239690	68.960130	85.239690	-68.960130	RRc	19.024	19.442	0.277861100	8.0E-7	2187.71729	18.61	0.04
OGLE-LMC-RRLYR-20184	VMC84.207285	68.963370	84.207285	-68.963370	RRab	19.564	20.529	0.536653000	9.0E-7	2187.28941	18.04	0.05
OGLE-LMC-RRLYR-18410	VMC83.049075	68.960300	83.049075	-68.960300	RRab	19.038	19.894	0.662660600	1.5E-6	2167.45952	17.65	0.05
OGLE-LMC-RRLYR-20932	VMC84.768975	68.968580	84.768975	-68.968580	RRab	19.214	19.867	0.525523200	1.5E-6	2187.24475	18.29	0.03
OGLE-LMC-RRLYR-22069	VMC85.832610	68.962210	85.832610	-68.962210	RRab	18.850	19.459	0.566191100	8.0E-7	2187.46241	18.01	0.03
OGLE-LMC-RRLYR-21142	VMC84.948360	68.969170	84.948360	-68.969170	RRab	19.030	19.874	0.633420100	2.0E-6	2187.31713	18.00	0.03
OGLE-LMC-RRLYR-19200	VMC83.522445	68.970750	83.522445	-68.970750	RRab	18.898	19.495	0.544953300	7.0E-7	2167.54183	18.23	0.04
OGLE-LMC-RRLYR-18312	VMC82.997475	68.969010	82.997475	-68.969010	RRc	19.004	19.503	0.346867600	1.6E-6	2167.82412	18.42	0.03
OGLE-LMC-RRLYR-20407	VMC84.371295	68.975360	84.371295	-68.975360	RRab	19.138	19.835	0.554148000	2.3E-6	2187.32164	18.25	0.04
OGLE-LMC-RRLYR-20775	VMC84.660090	68.975180	84.660090	-68.975180	RRab	18.766	19.302	0.558832900	7.0E-7	2193.54380	18.01	0.04
OGLE-LMC-RRLYR-20679	VMC84.590940	68.977600	84.590940	-68.977600	RRab	18.389	19.107	0.794743500	3.1E-6	2187.15490	17.22	0.06
OGLE-LMC-RRLYR-20094	VMC84.141660	68.980000	84.141660	-68.980000	RRab	19.591	20.403	0.505247200	1.8E-6	2187.26317	18.44	0.05
OGLE-LMC-RRLYR-19067	VMC83.445600	68.978450	83.445600	-68.978450	RRe	19.026	19.311	0.264750900	8.0E-7	2167.74996	18.73	0.05
OGLE-LMC-RRLYR-19113	VMC83.474865	68.979310	83.474865	-68.979310	RRab	19.036	19.587	0.478389800	3.0E-7	2167.51302	18.22	0.04
OGLE-LMC-RRLYR-18560	VMC83.129730	68.978260	83.129730	-68.978260	RRab	18.953	19.679	0.665935200	1.7E-6	2167.80250	17.94	0.03
OGLE-LMC-RRLYR-18601	VMC83.159205	68.979580	83.159205	-68.979580	RRc	19.491	20.240	0.353157400	1.3E-6	2167.83884	18.26	0.04
OGLE-LMC-RRLYR-18535	VMC83.118525	68.980800	83.118525	-68.980800	RRab	18.928	19.796	0.765725500	2.7E-6	2167.76705	17.78	0.03
OGLE-LMC-RRLYR-18465	VMC83.077605	68.982550	83.077605	-68.982550	RRab	19.422	20.143	0.337277800	1.2E-6	2167.79285	18.41	0.03
OGLE-LMC-RRLYR-18327	VMC83.003310	68.980620	83.003310	-68.980620	RRc	19.116	19.543	0.296301800	1.1E-6	2167.63000	18.51	0.04
OGLE-LMC-RRLYR-19846	VMC83.968635	68.989900	83.968635	-68.989900	RRab	19.304	20.026	0.338426900	1.1E-6	2187.54125	18.29	0.03
OGLE-LMC-RRLYR-19507	VMC83.737755	68.990970	83.737755	-68.990970	RRab	19.030	19.695	0.530509000	6.0E-7	2167.73955	18.24	0.03
OGLE-LMC-RRLYR-21097	VMC84.910395	68.990750	84.910395	-68.990750	RRab	18.591	19.349	0.862058600	4.0E-6	2187.10632	17.53	0.02
OGLE-LMC-RRLYR-19008	VMC83.411760	68.991380	83.411760	-68.991380	RRab	19.023	19.705	0.625601400	1.8E-6	2167.50199	18.20	0.03
OGLE-LMC-RRLYR-19754	VMC83.905080	68.992760	83.905080	-68.992760	RRab	19.421	20.311	0.593111800	2.3E-6	2187.34571	18.26	0.04
OGLE-LMC-RRLYR-18603	VMC83.160465	68.990920	83.160465	-68.990920	RRe	19.693	20.399	0.277569200	1.4E-6	2167.68732	18.84	0.05
OGLE-LMC-RRLYR-19110	VMC83.473215	68.995260	83.473215	-68.995260	RRab	18.861	19.554	0.643157500	2.8E-6	2167.43524	18.03	0.03
OGLE-LMC-RRLYR-20342	VMC84.318585	68.996840	83.418585	-68.996840	RRab	19.081	19.871	0.571084000	1.9E-6	2187.52192	18.05	0.04
OGLE-LMC-RRLYR-20546	VMC84.474420	68.996800	84.474420	-68.996800	RRc	19.133	19.693	0.326112700	2.1E-6	2187.71206	18.29	0.04
OGLE-LMC-RRLYR-20431	VMC84.382230	68.999330	84.382230	-68.999330	RRab	18.578	19.102	0.600250400	6.0E-7	2187.65360	17.94	0.03
OGLE-LMC-RRLYR-19223	VMC83.542170	69.000100	83.542170	-69.000100	RRab	19.093	19.877	0.595752000	1.3E-6	2167.88194	18.17	0.03
OGLE-LMC-RRLYR-20343	VMC84.320745	69.000970	84.320745	-69.000970	RRab	19.031	19.749	0.470396500	1.2E-6	2187.58920	18.27	0.03
OGLE-LMC-RRLYR-21824	VMC85.568010	68.992560	85.568010	-68.992560	RRab	18.696	19.303	0.692365300	1.2E-6	2187.55302	17.71	0.03
OGLE-LMC-RRLYR-20565	VMC84.485730	69.002290	84.485730	-69.002290	RRab	19.338	20.048	0.492330900	6.0E-7	2187.66430	18.30	0.03
OGLE-LMC-RRLYR-18398	VMC83.042445	68.999080	83.042445	-68.999080	RRab	19.279	20.016	0.553612700	2.1E-6	2167.70626	18.30	0.03
OGLE-LMC-RRLYR-18674	VMC83.202120	69.000500	83.202120	-69.000500	RRab	19.195	19.939	0.567523100	2.3E-6	2167.56269	18.24	0.03
OGLE-LMC-RRLYR-21898	VMC85.655865	68.998180	85.655865	-68.998180	RRc	19.278	19.963	0.344957900	1.3E-6	2187.55897	18.33	0.03
OGLE-LMC-RRLYR-18930	VMC83.369625	69.005070	83.369625	-69.005070	RRab	18.917	19.467	0.510462400	7.0E-7	2167.58622	18.20	0.03
OGLE-LMC-RRLYR-21860	VMC85.602030	69.005580	85.602030	-69.005580	RRab	19.050	19.916	0.599766000	1.4E-6	2187.78544	18.08	0.03
OGLE-LMC-RRLYR-21440	VMC85.201575	69.010610	85.201575	-69.010610	RRab	19.240	19.984	0.480823300	1.8E-6	2187.57458	18.40	0.03
OGLE-LMC-RRLYR-21729	VMC85.481820	69.010270	85.481820	-69.010270	RRc	19.151	19.750	0.328939000	1.7E-6	2187.52369	18.36	0.03
OGLE-LMC-RRLYR-21711	VMC85.453650	69.012010	85.453650	-69.012010	RRab	19.143	20.029	0.659893700	2.3E-6	2187.75892	17.97	0.03
OGLE-LMC-RRLYR-21076	VMC84.892050	69.018780	84.892050	-69.018780	RRab	18.944	19.637	0.559051600	1.5E-6	2187.76797	18.08	0.04
OGLE-LMC-RRLYR-18703	VMC83.216925	69.017570	83.216925	-69.017570	RRc	19.127	19.697	0.317922600	7.0E-7	2167.80262	18.29	0.04
OGLE-LMC-RRLYR-19284	VMC83.579175	69.022170	83.579175	-69.022170	RRab	19.012	19.663	0.546583700	1.7E-6	2167.84068	18.08	0.04
OGLE-LMC-RRLYR-18477	VMC83.082540	69.024210	83.082540	-69.024210	RRab	19.026	19.735	0.595339100	8.0E-7	2167.60238	18.10	0.03
OGLE-LMC-RRLYR-22009	VMC85.762275	69.023090	85.762275	-69.023090	RRab	19.522	20.719	0.572251000	1.2E-6	2187.50299	18.31	0.03
OGLE-LMC-RRLYR-20341	VMC84.317415	69.031650	84.317415	-69.031650	RRab	19.253	20.091	0.530734300	1.9E-6	2187.37703	18.11	0.03
OGLE-LMC-RRLYR-19695	VMC83.853495	69.033140	83.853495	-69.033140	RRab	19.608	20.820	0.652492600	3.0E-6	2187.21007	18.12	0.03
OGLE-LMC-RRLYR-19915	VMC84.021375	69.033860	84.021375	-69.033860	RRab	20.066	21.348	0.528720600	2.5E-6	2187.52614	18.41	0.03
OGLE-LMC-RRLYR-19064	VMC83.443290	69.034080	83.443290	-69.034080	RRab	19.182	19.749	0.453970900	4.0E-7	2167.54980	18.45	0.04
OGLE-LMC-RRLYR-18391	VMC83.038860	69.033220	83.038860	-69.033220	RRc	19.043	19.620	0.356342400	9.0E-7	2167.67147	18.27	0.04
OGLE-LMC-RRLYR-19049	VMC83.438625	69.037950	83.438625	-69.037950	RRab	18.873	19.601	0.646169000	1.3E-6	2167.46447	17.95	0.03
OGLE-LMC-RRLYR-19951	VMC84.044985	69.038150	84.044985	-69.038150	RRe	19.984	21.031	0.290453500	1.5E-6	2187.54862	18.62	0.04
OGLE-LMC-RRLYR-18777	VMC83.263770	69.036980	83.263770	-69.036980	RRab	19.679	20.771	0.618530000	2.9E-6	2167.77229	18.20	0.03
OGLE-LMC-RRLYR-21150	VMC84.954060	69.039300	84.954060	-69.039300	RRab	18.917	19.616	0.585496800	1.9E-6	2187.21321	18.04	0.05

5.6 RR Lyrae stars in the 30 Dor region

125

OGLE-LMC-RRLYR-18914	VMC83.358780	69.039920	83.358780	-69.039920	RRab	19.076	19.737	0.542292000	6.0E-7	2167.73891	18.14	0.03
OGLE-LMC-RRLYR-21298	VMC85.084500	69.040020	85.084500	-69.040020	RRab	19.498	20.329	0.467919800	2.1E-6	2187.47815	18.31	0.04
OGLE-LMC-RRLYR-20000	VMC84.079650	69.040460	84.079650	-69.040460	RRab	19.534	20.613	0.596976800	2.1E-6	2193.25562	18.05	0.04
OGLE-LMC-RRLYR-20768	VMC84.655425	69.039720	84.655425	-69.039720	RRab	19.662	20.158	0.565382100	2.0E-6	2187.30682	18.15	0.03
OGLE-LMC-RRLYR-18894	VMC83.343975	69.047160	83.343975	-69.047160	RRab	18.589	19.206	0.557740100	6.0E-7	2167.47906	17.86	0.03
OGLE-LMC-RRLYR-18414	VMC83.049300	69.047100	83.049300	-69.047100	RRab	18.914	19.711	0.610726000	1.3E-6	2167.88934	17.92	0.03
OGLE-LMC-RRLYR-18796	VMC83.272215	69.048530	83.272215	-69.048530	RRab	19.034	19.662	0.466599600	3.0E-7	2167.44760	18.02	0.03
OGLE-LMC-RRLYR-21317	VMC85.096020	69.051200	85.096020	-69.051200	RRe	19.061	19.368	0.244033400	1.3E-6	2187.73194	18.63	0.04
OGLE-LMC-RRLYR-21801	VMC85.545585	69.048480	85.545585	-69.048480	RRab	19.116	19.913	0.574518300	9.0E-7	2187.60345	17.97	0.03
OGLE-LMC-RRLYR-18951	VMC83.382615	69.054270	83.382615	-69.054270	RRe	19.101	19.646	0.280567900	7.0E-7	2167.63827	18.39	0.04
OGLE-LMC-RRLYR-18848	VMC83.311980	69.055090	83.311980	-69.055090	RRab	18.938	19.617	0.549491000	6.0E-7	2167.55903	18.18	0.03
OGLE-LMC-RRLYR-21312	VMC85.094535	69.056270	85.094535	-69.056270	RRab	19.217	20.080	0.565951800	1.1E-6	2187.43611	18.08	0.03
OGLE-LMC-RRLYR-19782	VMC83.925405	69.059060	83.925405	-69.059060	RRab	19.720	20.926	0.604754400	3.8E-6	2187.72801	18.17	0.03
OGLE-LMC-RRLYR-19043	VMC83.435565	69.056760	83.435565	-69.056760	RRab	18.981	19.681	0.622039300	1.0E-6	2167.41531	18.07	0.03
OGLE-LMC-RRLYR-21523	VMC85.274550	69.058690	85.274550	-69.058690	RRab	18.835	19.537	0.583370500	3.6E-6	2187.33968	17.90	0.03
OGLE-LMC-RRLYR-19279	VMC83.575785	69.069020	83.575785	-69.069020	RRab	19.200	20.086	0.617814600	1.3E-6	2167.79387	18.07	0.03
OGLE-LMC-RRLYR-19584	VMC83.782350	69.070060	83.782350	-69.070060	RRab	19.626	20.795	0.533838700	1.0E-6	2167.38428	17.65	0.06
OGLE-LMC-RRLYR-19842	VMC83.966265	69.067490	83.966265	-69.067490	RRab	19.174	20.020	0.577960600	1.2E-6	2187.33619	17.75	0.06
OGLE-LMC-RRLYR-19118	VMC83.476980	69.070330	83.476980	-69.070330	RRe	19.256	19.863	0.293944800	1.3E-6	2167.80910	18.37	0.04
OGLE-LMC-RRLYR-19216	VMC83.538270	69.074280	83.538270	-69.074280	RRab	19.212	20.043	0.657178400	2.1E-6	2167.42285	18.09	0.03
OGLE-LMC-RRLYR-18399	VMC83.042730	69.066740	83.042730	-69.066740	RRe	19.107	19.522	0.269552800	6.0E-7	2167.65579	18.46	0.04
OGLE-LMC-RRLYR-21467	VMC85.219035	69.075790	85.219035	-69.075790	RRab	19.243	20.021	0.522455900	6.0E-7	2187.29099	18.22	0.03
OGLE-LMC-RRLYR-21193	VMC84.998700	69.078280	84.998700	-69.078280	RRab	18.698	19.433	0.677025400	1.9E-6	2187.53733	17.75	0.03
OGLE-LMC-RRLYR-20677	VMC84.589725	69.080470	84.589725	-69.080470	RRab	19.624	20.045	0.537265800	9.0E-7	2187.60585	18.15	0.04
OGLE-LMC-RRLYR-20591	VMC84.506400	69.081330	84.506400	-69.081330	RRe	19.288	19.180	0.320690600	1.6E-6	2187.65124	17.89	0.06
OGLE-LMC-RRLYR-20089	VMC84.140415	69.081250	84.140415	-69.081250	RRe	19.958	20.876	0.363522400	3.4E-6	2187.71469	17.83	0.10
OGLE-LMC-RRLYR-21840	VMC85.581315	69.077680	85.581315	-69.077680	RRab	18.675	19.324	0.656178400	1.1E-6	2187.38766	17.79	0.03
OGLE-LMC-RRLYR-18953	VMC83.385990	69.082170	83.385990	-69.082170	RRe	19.281	19.827	0.307994000	9.0E-7	2167.67328	18.71	0.05
OGLE-LMC-RRLYR-19351	VMC83.619315	69.083550	83.619315	-69.083550	RRab	19.113	19.964	0.673158700	1.6E-6	2167.58369	18.01	0.03
OGLE-LMC-RRLYR-20141	VMC84.172305	69.084250	84.172305	-69.084250	RRab	19.563	20.344	0.465502600	1.0E-6	2187.67179	18.40	0.04
OGLE-LMC-RRLYR-20192	VMC84.216510	69.084670	84.216510	-69.084670	RRab	19.513	20.550	0.639869800	2.6E-6	2187.16996	18.14	0.03
OGLE-LMC-RRLYR-18684	VMC83.207340	69.080310	83.207340	-69.080310	RRab	19.022	19.858	0.761693200	4.2E-6	2167.23047	17.86	0.03
OGLE-LMC-RRLYR-20058	VMC84.121155	69.086300	84.121155	-69.086300	RRe	19.333	19.946	0.317858700	2.0E-6	2187.49008	18.04	0.05
OGLE-LMC-RRLYR-22071	VMC85.834365	69.078790	85.834365	-69.078790	RRab	19.084	19.830	0.582069600	9.0E-7	2187.35702	18.05	0.04
OGLE-LMC-RRLYR-18285	VMC82.989660	69.083090	82.989660	-69.083090	RRe	19.072	19.634	0.376199100	1.6E-6	2167.56968	18.29	0.05
OGLE-LMC-RRLYR-19093	VMC83.462415	69.086050	83.462415	-69.086050	RRe	19.471	20.300	0.322717600	8.0E-7	2167.86246	18.38	0.05
OGLE-LMC-RRLYR-21333	VMC85.094850	69.086180	85.094850	-69.086180	RRab	19.774	20.975	0.461643300	7.0E-7	2187.31068	18.51	0.05
OGLE-LMC-RRLYR-20596	VMC84.509865	69.088940	84.509865	-69.088940	RRe	19.399	20.122	0.339024900	1.1E-6	2187.67386	18.15	0.07
OGLE-LMC-RRLYR-21685	VMC85.426620	69.084740	85.426620	-69.084740	RRe	19.483	20.002	0.246063100	1.7E-6	2187.57616	18.83	0.06
OGLE-LMC-RRLYR-19974	VMC84.059490	69.090040	84.059490	-69.090040	RRe	19.389	20.041	0.298181300	1.0E-6	2187.48736	18.61	0.06
OGLE-LMC-RRLYR-19341	VMC83.613270	69.089870	83.613270	-69.089870	RRab	19.359	20.106	0.475793000	1.0E-6	2167.82378	18.45	0.04
OGLE-LMC-RRLYR-18373	VMC83.028300	69.087340	83.028300	-69.087340	RRab	18.958	19.655	0.644864900	2.6E-6	2167.52938	18.11	0.04
OGLE-LMC-RRLYR-19906	VMC84.014310	69.091940	84.014310	-69.091940	RRe	19.372	20.313	0.593058000	2.8E-6	2187.68616	18.04	0.03
OGLE-LMC-RRLYR-21538	VMC85.286340	69.086510	85.286340	-69.086510	RRab	18.781	19.483	0.628496400	1.9E-6	2187.18450	17.86	0.03
OGLE-LMC-RRLYR-19637	VMC83.818950	69.093650	83.818950	-69.093650	RRab	19.956	21.140	0.555128700	2.4E-6	2187.51450	18.30	0.04
OGLE-LMC-RRLYR-19560	VMC83.767725	69.094140	83.767725	-69.094140	RRab	19.783	20.953	0.589503500	4.6E-6	2248.28695	18.13	0.03
OGLE-LMC-RRLYR-22048	VMC85.809435	69.087360	85.809435	-69.087360	RRe	19.216	19.930	0.340953700	1.3E-6	2187.74472	18.33	0.03
OGLE-LMC-RRLYR-18626	VMC83.173230	69.092130	83.173230	-69.092130	RRab	19.254	19.995	0.500799900	1.5E-6	2167.46862	18.31	0.03
OGLE-LMC-RRLYR-20637	VMC84.545955	69.096450	84.545955	-69.096450	RRab	19.144	19.99	0.544612800	4.6E-6	2187.51531	17.89	0.04
OGLE-LMC-RRLYR-21250	VMC85.052940	69.093730	85.052940	-69.093730	RRab	18.776	19.398	0.568557800	9.0E-7	2187.41952	17.89	0.03
OGLE-LMC-RRLYR-18337	VMC83.008665	69.093610	83.008665	-69.093610	RRab	18.608	19.323	0.689194700	3.0E-6	2193.23943	17.75	0.03
OGLE-LMC-RRLYR-20413	VMC84.372930	69.100670	84.372930	-69.100670	RRab	18.700	19.337	0.631214300	2.9E-6	2193.64697	17.90	0.03
OGLE-LMC-RRLYR-18852	VMC83.315835	69.100120	83.315835	-69.100120	RRe	19.413	20.100	0.338742600	1.3E-6	2167.81930	18.43	0.03
OGLE-LMC-RRLYR-18680	VMC83.206080	69.100850	83.206080	-69.100850	RRab	18.925	19.528	0.495772800	5.0E-7	2167.53491	18.11	0.03
OGLE-LMC-RRLYR-19586	VMC83.783385	69.104200	83.783385	-69.104200	RRab	20.052	21.405	0.497754000	2.8E-6	2167.62495	18.46	0.04
OGLE-LMC-RRLYR-18409	VMC83.048805	69.102970	83.048805	-69.102970	RRab	18.906	19.473	0.535786200	4.0E-7	2167.42774	17.90	0.04
OGLE-LMC-RRLYR-21548	VMC85.295265	69.105140	85.295265	-69.105140	RRab	19.001	19.863	0.716773800	2.7E-6	2187.68832	17.82	0.03
OGLE-LMC-RRLYR-19386	VMC83.648085	69.108140	83.648085	-69.108140	RRab	19.204	20.059	0.540637200	3.0E-6	2167.53580	18.12	0.03

126 Data analysis, and first results for RR Lyrae stars from the VMC survey

OGLE-LMC-RRLYR-20051	VMC84.117945	69.106570	84.117945	-69.106570	RRab	19.363	20.125	0.512686900	2.1E-6	2187.31970	18.37	0.04
OGLE-LMC-RRLYR-21285	VMC85.077870	69.108340	85.077870	-69.108340	RRc	19.052	19.393	0.381886400	3.0E-6	2187.42570	18.57	0.04
OGLE-LMC-RRLYR-21305	VMC85.090740	69.107580	85.090740	-69.107580	RRab	18.628	19.164	0.525099300	1.0E-6	2187.25414	17.95	0.03
OGLE-LMC-RRLYR-20036	VMC84.105450	69.109840	84.105450	-69.109840	RRab	19.376	20.112	0.475512200	1.1E-6	2187.53125	18.48	0.04
OGLE-LMC-RRLYR-20551	VMC84.477600	69.091310	84.477600	-69.091310	RRc	19.092	19.738	0.372013100	1.8E-6	2187.58670	17.87	0.04
OGLE-LMC-RRLYR-19719	VMC83.875995	69.116810	83.875995	-69.116810	RRab	19.607	20.673	0.649840100	5.6E-6	2187.72684	17.97	0.04
OGLE-LMC-RRLYR-19995	VMC84.078495	69.117130	84.078495	-69.117130	RRe	18.820	19.207	0.290434800	7.0E-7	2187.68120	18.25	0.03
OGLE-LMC-RRLYR-19353	VMC83.620425	69.116270	83.620425	-69.116270	RRab	19.216	20.051	0.550053100	1.1E-6	2167.44389	18.08	0.03
OGLE-LMC-RRLYR-21806	VMC85.549875	69.113000	85.549875	-69.113000	RRab	19.751	21.000	0.637289300	9.6E-6	2187.24784	18.15	0.03
OGLE-LMC-RRLYR-21664	VMC85.409190	69.115590	85.409190	-69.115590	RRc	19.631	20.604	0.350887000	2.2E-6	2187.76749	18.45	0.03
OGLE-LMC-RRLYR-21219	VMC85.024095	69.119960	85.024095	-69.119960	RRc	19.326	20.083	0.344529900	1.5E-6	2187.76394	18.30	0.04
OGLE-LMC-RRLYR-18949	VMC83.381055	69.120040	83.381055	-69.120040	RRab	19.083	19.910	0.642171400	2.5E-6	2167.60770	18.01	0.03
OGLE-LMC-RRLYR-20919	VMC84.758370	69.116170	84.758370	-69.116170	RRab	19.975	-99.99	0.576375700	3.9E-6	2187.35594	18.07	0.06
OGLE-LMC-RRLYR-19519	VMC83.743980	69.122140	83.743980	-69.122140	RRab	19.684	20.880	0.686427800	5.2E-6	2167.64040	18.00	0.03
OGLE-LMC-RRLYR-19179	VMC83.508975	69.120580	83.508975	-69.120580	RRab	19.367	20.177	0.507869600	9.0E-7	2167.85435	18.07	0.04
OGLE-LMC-RRLYR-19402	VMC83.659875	69.124320	83.659875	-69.124320	RRab	18.759	19.438	0.606956900	1.3E-6	2167.86549	18.01	0.03
OGLE-LMC-RRLYR-21072	VMC84.890250	69.122580	84.890250	-69.122580	RRc	19.567	20.030	0.285239100	8.0E-7	2187.58493	18.17	0.05
OGLE-LMC-RRLYR-18731	VMC83.238375	69.123360	83.238375	-69.123360	RRe	18.814	19.278	0.338443400	8.0E-7	2167.67712	18.20	0.03
OGLE-LMC-RRLYR-20142	VMC84.172590	69.129720	84.172590	-69.129720	RRe	19.796	20.481	0.228516200	1.0E-6	2187.66576	19.22	0.11
OGLE-LMC-RRLYR-19979	VMC84.064065	69.131360	84.064065	-69.131360	RRab	19.206	20.060	0.606566500	1.1E-6	2187.42422	18.02	0.04
OGLE-LMC-RRLYR-20587	VMC84.502305	69.123720	84.502305	-69.123720	RRe	18.991	19.363	0.273546200	1.9E-6	2187.62206	18.44	0.04
OGLE-LMC-RRLYR-20024	VMC84.095325	69.132480	84.095325	-69.132480	RRab	19.478	20.334	0.502795400	8.0E-7	2187.48186	18.35	0.03
OGLE-LMC-RRLYR-19157	VMC83.497380	69.136310	83.497380	-69.136310	RRe	19.079	19.444	0.336955500	1.0E-6	2167.75042	18.15	0.05
OGLE-LMC-RRLYR-19502	VMC83.735190	69.137380	83.735190	-69.137380	RRab	19.342	20.178	0.462491000	5.0E-7	2167.73937	18.11	0.03
OGLE-LMC-RRLYR-19087	VMC83.458905	69.137400	83.458905	-69.137400	RRe	18.918	19.687	0.638510300	1.9E-6	2167.85436	18.04	0.03
OGLE-LMC-RRLYR-19923	VMC84.025545	69.140460	84.025545	-69.140460	RRab	18.966	19.769	0.670314700	1.6E-6	2187.67139	17.80	0.02
OGLE-LMC-RRLYR-19435	VMC83.684550	69.141360	83.684550	-69.141360	RRe	18.981	19.688	0.439998200	2.5E-6	2167.72691	18.06	0.03
OGLE-LMC-RRLYR-18499	VMC83.098635	69.138400	83.098635	-69.138400	RRe	19.000	19.519	0.350097500	8.0E-7	2167.79049	18.19	0.03
OGLE-LMC-RRLYR-18583	VMC83.141220	69.140830	83.141220	-69.140830	RRab	19.063	19.695	0.501282000	5.0E-7	2167.60595	18.27	0.03
OGLE-LMC-RRLYR-20967	VMC84.805740	69.143360	84.805740	-69.143360	RRab	18.762	19.339	0.572688000	9.0E-7	2187.69721	18.09	0.03
OGLE-LMC-RRLYR-21134	VMC84.935940	69.144320	84.935940	-69.144320	RRab	19.581	20.520	0.622054900	3.7E-6	2187.73621	18.09	0.03
OGLE-LMC-RRLYR-19786	VMC83.927910	69.146810	83.927910	-69.146810	RRe	20.135	21.116	0.272737200	1.2E-6	2187.75701	18.85	0.06
OGLE-LMC-RRLYR-21130	VMC84.933270	69.148520	84.933270	-69.148520	RRab	18.769	19.485	0.614106100	1.8E-6	2187.74485	17.92	0.03
OGLE-LMC-RRLYR-21371	VMC85.143180	69.150550	85.143180	-69.150550	RRe	19.471	19.824	0.308616200	1.0E-6	2187.51524	18.15	0.04
OGLE-LMC-RRLYR-18557	VMC83.128515	69.151460	83.128515	-69.151460	RRab	18.811	19.475	0.601541300	8.0E-7	2167.55690	17.94	0.03
OGLE-LMC-RRLYR-21469	VMC85.219845	69.156510	85.219845	-69.156510	RRe	19.382	19.934	0.260217300	9.0E-7	2187.65685	18.69	0.04
OGLE-LMC-RRLYR-19682	VMC83.844360	69.160740	83.844360	-69.160740	RRab	19.545	20.624	0.653098700	5.5E-6	2187.74440	17.98	0.03
OGLE-LMC-RRLYR-21268	VMC85.066230	69.159810	85.066230	-69.159810	RRab	19.904	20.804	0.436640100	1.0E-6	2187.69253	18.69	0.03
OGLE-LMC-RRLYR-20175	VMC84.197820	69.165900	84.197820	-69.165900	RRab	19.256	20.192	0.619733600	2.3E-6	2187.38581	17.99	0.03
OGLE-LMC-RRLYR-20246	VMC84.249855	69.167350	84.249855	-69.167350	RRab	19.536	20.701	0.610393200	1.8E-6	2187.30597	18.08	0.03
OGLE-LMC-RRLYR-20108	VMC84.148320	69.170800	84.148320	-69.170800	RRe	19.241	19.978	0.338759100	1.1E-6	2187.68573	18.37	0.05
OGLE-LMC-RRLYR-19827	VMC83.952960	69.171410	83.952960	-69.171410	RRab	20.166	21.422	0.448474200	1.8E-6	2187.69045	18.66	0.04
OGLE-LMC-RRLYR-18451	VMC83.071290	69.168070	83.071290	-69.168070	RRab	19.031	19.672	0.542047200	2.0E-6	2167.44563	18.05	0.03
OGLE-LMC-RRLYR-21556	VMC85.302780	69.168970	85.302780	-69.168970	RRe	19.864	21.342	0.528232800	1.1E-6	2187.34091	18.40	0.04
OGLE-LMC-RRLYR-18878	VMC83.332095	69.170310	83.332095	-69.170310	RRab	18.808	19.448	0.568543100	6.0E-7	2167.80487	17.98	0.04
OGLE-LMC-RRLYR-21589	VMC85.333245	69.171290	85.333245	-69.171290	RRe	19.583	20.665	0.557443800	1.1E-6	2187.74609	18.07	0.03
OGLE-LMC-RRLYR-20961	VMC84.799065	69.172820	84.799065	-69.172820	RRab	18.744	19.587	0.759972600	2.9E-6	2187.54910	17.59	0.03
OGLE-LMC-RRLYR-21464	VMC85.217310	69.172200	85.217310	-69.172200	RRab	19.151	20.123	0.566897000	1.2E-6	2187.33115	17.79	0.04
OGLE-LMC-RRLYR-21005	VMC84.840390	69.174380	84.840390	-69.174380	RRab	20.164	21.977	0.484008300	1.2E-6	2187.46214	18.58	0.04
OGLE-LMC-RRLYR-20138	VMC84.168600	69.176520	84.168600	-69.176520	RRe	19.240	19.735	0.335173000	1.0E-6	2187.53442	18.20	0.05
OGLE-LMC-RRLYR-19997	VMC84.079305	69.178260	84.079305	-69.178260	RRab	19.176	20.097	0.656908500	1.7E-6	2187.55019	18.00	0.03
OGLE-LMC-RRLYR-21916	VMC85.669065	69.172260	85.669065	-69.172260	RRe	18.757	19.419	0.624222400	1.9E-6	2187.29415	17.86	0.03
OGLE-LMC-RRLYR-19039	VMC83.432520	69.176400	83.432520	-69.176400	RRe	19.316	19.943	0.270404900	1.2E-6	2167.87004	18.67	0.03
OGLE-LMC-RRLYR-21665	VMC85.409670	69.174370	85.409670	-69.174370	RRe	19.464	20.368	0.563486800	1.0E-6	2187.32447	18.15	0.03
OGLE-LMC-RRLYR-21139	VMC84.943290	69.178880	84.943290	-69.178880	RRab	19.828	21.311	0.606056000	3.5E-6	2187.54940	18.17	0.04
OGLE-LMC-RRLYR-18828	VMC83.293440	69.179150	83.293440	-69.179150	RRe	18.597	19.232	0.696573600	1.1E-6	2167.83505	17.72	0.03
OGLE-LMC-RRLYR-20256	VMC84.258090	69.178620	84.258090	-69.178620	RRab	19.474	20.359	0.518356500	1.9E-6	2187.64433	18.38	0.05
OGLE-LMC-RRLYR-19146	VMC83.491545	69.180770	83.491545	-69.180770	RRab	19.014	19.784	0.598345300	8.0E-7	2167.81979	18.22	0.03

5.6 RR Lyrae stars in the 30 Dor region

127

OGLE-LMC-RRLYR-19599	VMC83.790120	69.185120	83.790120	-69.185120	RRab	19.922	20.981	0.555203700	1.9E-6	2167.72136	18.47	0.03
OGLE-LMC-RRLYR-21274	VMC85.070895	69.182490	85.070895	-69.182490	RRc	18.850	19.385	0.357286500	9.0E-7	2187.61305	18.22	0.02
OGLE-LMC-RRLYR-19215	VMC83.536740	69.188620	83.536740	-69.188620	RRab	18.662	19.208	0.540911200	8.0E-7	2167.68403	18.05	0.03
OGLE-LMC-RRLYR-21959	VMC85.714770	69.183250	85.714770	-69.183250	RRab	18.401	19.055	0.808980100	1.3E-6	2187.58371	17.63	0.02
OGLE-LMC-RRLYR-21621	VMC85.361460	69.186540	85.361460	-69.186540	RRab	19.746	20.980	0.525098000	2.7E-6	2187.42680	18.44	0.03
OGLE-LMC-RRLYR-21580	VMC85.324215	69.190180	85.324215	-69.190180	RRc	19.603	20.638	0.569349800	1.9E-6	2187.76268	18.29	0.03
OGLE-LMC-RRLYR-18449	VMC83.068710	69.191610	83.068710	-69.191610	RRab	19.156	20.197	0.303142600	6.0E-7	2167.64585	17.05	0.03
OGLE-LMC-RRLYR-21320	VMC85.101660	69.194310	85.101660	-69.194310	RRab	19.695	20.656	0.469564500	6.0E-7	2187.68865	18.55	0.05
OGLE-LMC-RRLYR-20890	VMC84.733305	69.199020	84.733305	-69.199020	RRab	19.125	20.104	0.659952300	2.9E-6	2187.64117	17.97	0.03
OGLE-LMC-RRLYR-18890	VMC83.336265	69.198540	83.336265	-69.198540	RRab	19.283	20.126	0.583664500	2.7E-6	2167.54214	18.31	0.04
OGLE-LMC-RRLYR-21561	VMC85.304820	69.197510	85.304820	-69.197510	RRab	19.325	20.121	0.454079400	5.0E-7	2187.72076	18.37	0.03
OGLE-LMC-RRLYR-21212	VMC85.018350	69.199790	85.018350	-69.199790	RRab	20.229	21.618	0.515147900	2.3E-6	2187.37804	18.78	0.05
OGLE-LMC-RRLYR-22046	VMC85.805385	69.195070	85.805385	-69.195070	RRab	18.844	19.359	0.510577900	5.0E-7	2187.59102	18.18	0.03
OGLE-LMC-RRLYR-20697	VMC84.606885	69.202290	84.606885	-69.202290	RRc	19.396	20.230	0.346901600	1.8E-6	2187.57006	18.54	0.05
OGLE-LMC-RRLYR-20004	VMC84.081330	69.205630	84.081330	-69.205630	RRc	19.495	20.277	0.300785700	9.0E-7	2187.50239	18.57	0.04
OGLE-LMC-RRLYR-19631	VMC83.816190	69.205420	83.816190	-69.205420	RRab	19.692	20.777	0.559519500	1.0E-6	2167.67775	18.33	0.05
OGLE-LMC-RRLYR-21623	VMC85.362750	69.202870	85.362750	-69.202870	RRab	19.565	20.515	0.553007000	2.5E-6	2187.72638	18.03	0.04
OGLE-LMC-RRLYR-21542	VMC85.290540	69.204970	85.290540	-69.204970	RRe	19.008	19.476	0.272163500	1.0E-6	2187.57838	18.56	0.04
OGLE-LMC-RRLYR-19304	VMC83.590680	69.208460	83.590680	-69.208460	RRab	18.595	19.378	0.589302600	8.0E-7	2167.75424	17.45	0.03
OGLE-LMC-RRLYR-19130	VMC83.480640	69.210330	83.480640	-69.210330	RRab	19.587	20.739	0.584377100	1.4E-6	2167.40006	18.21	0.03
OGLE-LMC-RRLYR-20448	VMC84.392730	69.212980	84.392730	-69.212980	RRab	19.816	20.972	0.579814400	3.4E-6	2187.29773	18.34	0.03
OGLE-LMC-RRLYR-19767	VMC83.910900	69.212910	83.910900	-69.212910	RRab	19.821	20.801	0.541774800	1.2E-6	2187.43638	18.26	0.03
OGLE-LMC-RRLYR-19806	VMC83.941380	69.214620	83.941380	-69.214620	RRab	18.685	19.356	0.616703900	2.0E-6	2187.42219	17.73	0.03
OGLE-LMC-RRLYR-19617	VMC83.807100	69.214630	83.807100	-69.214630	RRab	19.391	20.279	0.536108000	5.0E-7	2167.71792	18.36	0.04
OGLE-LMC-RRLYR-22078	VMC85.841190	69.204920	85.841190	-69.204920	RRab	19.285	19.999	0.494404100	8.0E-7	2187.37119	18.37	0.04
OGLE-LMC-RRLYR-19779	VMC83.922765	69.212640	83.922765	-69.212640	RRab	19.814	20.845	0.560086800	1.7E-6	2187.61795	18.33	0.03
OGLE-LMC-RRLYR-19967	VMC84.057150	69.216540	84.057150	-69.216540	RRc	19.508	20.290	0.331112700	1.5E-6	2187.69865	18.59	0.07
OGLE-LMC-RRLYR-20531	VMC84.464340	69.212940	84.464340	-69.212940	RRab	18.723	19.267	0.608965700	1.4E-6	2187.74001	17.82	0.04
OGLE-LMC-RRLYR-21638	VMC85.388315	69.215740	85.388315	-69.215740	RRab	19.845	21.089	0.536920100	2.2E-6	2187.39931	18.30	0.03
OGLE-LMC-RRLYR-21836	VMC85.578315	69.215390	85.578315	-69.215390	RRab	19.120	20.099	0.764680800	6.1E-6	2187.35321	17.83	0.03
OGLE-LMC-RRLYR-19192	VMC83.518140	69.219230	83.518140	-69.219230	RRab	18.870	19.512	0.571348800	6.0E-7	2167.76327	17.99	0.03
OGLE-LMC-RRLYR-18412	VMC83.049240	69.217070	83.049240	-69.217070	RRab	18.784	19.242	0.570404300	1.4E-6	2167.86728	17.52	0.07
OGLE-LMC-RRLYR-20663	VMC84.581130	69.223400	84.581130	-69.223400	RRab	18.953	19.591	0.511405800	6.0E-7	2187.54314	18.32	0.03
OGLE-LMC-RRLYR-19252	VMC83.561250	69.220020	83.561250	-69.220020	RRab	18.711	19.142	0.572162600	1.5E-6	2167.76580	17.79	0.03
OGLE-LMC-RRLYR-21314	VMC85.095045	69.222340	85.095045	-69.222340	RRab	18.899	19.544	0.496471200	4.0E-7	2187.57218	18.06	0.04
OGLE-LMC-RRLYR-18717	VMC83.224950	69.222630	83.224950	-69.222630	RRc	19.155	19.652	0.304113800	7.0E-7	2167.77440	18.64	0.04
OGLE-LMC-RRLYR-18711	VMC83.2220015	69.223630	83.2220015	-69.223630	RRab	19.040	19.656	0.488491400	5.0E-7	2167.41984	18.49	0.04
OGLE-LMC-RRLYR-20535	VMC84.465255	69.227940	84.465255	-69.227940	RRab	19.374	20.279	0.522774700	2.1E-6	2187.74159	18.23	0.03
OGLE-LMC-RRLYR-21176	VMC84.981045	69.229310	84.981045	-69.229310	RRab	19.472	20.348	0.627279400	3.8E-6	2187.23585	17.99	0.03
OGLE-LMC-RRLYR-19553	VMC83.763630	69.231630	83.763630	-69.231630	RRab	19.040	19.810	0.588607600	2.2E-6	2167.83563	17.99	0.03
OGLE-LMC-RRLYR-20674	VMC84.589530	69.231200	84.589530	-69.231200	RRab	18.781	19.474	0.667584400	7.0E-6	2187.46801	17.70	0.03
OGLE-LMC-RRLYR-19680	VMC83.844045	69.232500	83.844045	-69.232500	RRab	19.002	19.834	0.699754400	1.2E-6	2167.52580	17.92	0.03
OGLE-LMC-RRLYR-18707	VMC83.218635	69.230870	83.218635	-69.230870	RRc	19.023	19.435	0.283399000	5.0E-7	2167.85844	18.50	0.05
OGLE-LMC-RRLYR-20656	VMC84.568800	69.236100	84.568800	-69.236100	RRc	18.951	19.561	0.351282500	1.1E-6	2187.76429	18.23	0.05
OGLE-LMC-RRLYR-20534	VMC84.464790	69.236380	84.464790	-69.236380	RRab	19.817	21.367	0.756243200	8.0E-6	2187.76261	18.17	0.03
OGLE-LMC-RRLYR-21948	VMC85.702755	69.232590	85.702755	-69.232590	RRab	19.544	20.347	0.442364400	6.0E-7	2187.53954	18.48	0.05
OGLE-LMC-RRLYR-18579	VMC83.139090	69.236820	83.139090	-69.236820	RRab	18.621	19.211	0.656631500	1.3E-6	2167.82783	17.84	0.03
OGLE-LMC-RRLYR-19989	VMC84.008085	69.240390	84.008085	-69.240390	RRe	18.519	18.879	0.289719900	1.4E-6	2187.67117	17.93	0.03
OGLE-LMC-RRLYR-18506	VMC83.102220	69.240630	83.102220	-69.240630	RRab	18.797	19.258	0.502461800	4.0E-7	2167.72943	18.24	0.03
OGLE-LMC-RRLYR-19463	VMC83.706435	69.245890	83.706435	-69.245890	RRab	18.629	19.195	0.650409300	8.0E-6	2227.39747	17.73	0.03
OGLE-LMC-RRLYR-20228	VMC84.239685	69.249490	84.239685	-69.249490	RRab	19.521	-99.99	0.545388300	8.3E-6	300.02266	18.24	0.03
OGLE-LMC-RRLYR-19171	VMC83.504490	69.244730	83.504490	-69.244730	RRab	18.894	19.527	0.610119900	1.9E-6	2167.29704	18.01	0.03
OGLE-LMC-RRLYR-20694	VMC84.602295	69.252530	84.602295	-69.252530	RRab	19.405	20.400	0.545863100	2.2E-6	2193.67816	18.10	0.05
OGLE-LMC-RRLYR-20075	VMC84.132270	69.253310	84.132270	-69.253310	RRab	19.629	20.594	0.591280700	2.9E-6	2193.38531	18.21	0.04
OGLE-LMC-RRLYR-19155	VMC83.496285	69.254170	83.496285	-69.254170	RRab	19.028	19.685	0.548259300	6.0E-7	2167.71523	18.21	0.03
OGLE-LMC-RRLYR-18837	VMC83.304585	69.254560	83.304585	-69.254560	RRe	19.178	19.752	0.296564600	9.0E-7	2167.68665	18.55	0.04
OGLE-LMC-RRLYR-22026	VMC85.782720	69.248690	85.782720	-69.248690	RRe	18.972	-99.99	0.297890600	1.2E-6	300.01397	18.39	0.03
OGLE-LMC-RRLYR-18931	VMC83.371470	69.256170	83.371470	-69.256170	RRe	18.888	19.436	0.345639500	6.0E-7	2167.74349	18.34	0.04

128Data analysis, and first results for RR Lyrae stars from the VMC survey

OGLE-LMC-RRLYR-21433	VMC85.196325	69.253200	85.196325	-69.253200	RRc	19.474	20.062	0.279962400	8.0E-7	2187.76579	18.48	0.04
OGLE-LMC-RRLYR-20821	VMC84.687105	69.260000	84.687105	-69.260000	RRe	19.041	19.821	0.264968100	6.0E-7	2187.68766	18.13	0.03
OGLE-LMC-RRLYR-22039	VMC85.796580	69.254740	85.796580	-69.254740	RRc	19.658	20.734	0.359407600	2.8E-6	2187.67236	18.41	0.04
OGLE-LMC-RRLYR-18903	VMC83.350365	69.260950	83.350365	-69.260950	RRc	18.999	19.521	0.344619200	8.0E-7	2167.74375	18.19	0.04
OGLE-LMC-RRLYR-21333	VMC85.111635	69.264410	85.111635	-69.264410	RRab	19.293	20.262	0.557950700	7.0E-7	2187.70923	18.14	0.03
OGLE-LMC-RRLYR-20766	VMC84.654990	69.268440	84.654990	-69.268440	RRab	19.790	21.010	0.610477400	3.0E-6	2187.51333	18.30	0.03
OGLE-LMC-RRLYR-21905	VMC85.659465	69.264910	85.659465	-69.264910	RRab	19.123	19.875	0.495827100	5.0E-7	2187.64323	18.17	0.03
OGLE-LMC-RRLYR-18249	VMC82.981485	69.269180	82.981485	-69.269180	RRab	18.974	19.352	0.453351700	3.0E-7	2167.79127	18.32	0.04
OGLE-LMC-RRLYR-20519	VMC84.455220	69.274420	84.455220	-69.274420	RRc	19.254	19.845	0.342464100	1.3E-6	2187.74143	18.37	0.05
OGLE-LMC-RRLYR-21281	VMC85.072125	69.277650	85.072125	-69.277650	RRab	18.441	19.081	0.733986200	1.7E-6	2187.13651	17.66	0.03
OGLE-LMC-RRLYR-18865	VMC83.131620	69.277170	83.131620	-69.277170	RRc	18.743	19.136	0.351847600	7.0E-7	2167.88878	18.30	0.04
OGLE-LMC-RRLYR-20461	VMC84.406770	69.282640	84.406770	-69.282640	RRab	19.184	19.813	0.489693900	1.0E-6	2187.28816	18.00	0.05
OGLE-LMC-RRLYR-20044	VMC84.111015	69.286260	84.111015	-69.286260	RRc	18.664	19.210	0.349039500	1.0E-6	2187.49406	17.78	0.07
OGLE-LMC-RRLYR-20561	VMC84.483030	69.290730	84.483030	-69.290730	RRab	19.475	20.381	0.536586800	1.0E-6	2187.70074	18.36	0.04
OGLE-LMC-RRLYR-19285	VMC83.579445	69.291780	83.579445	-69.291780	RRab	18.904	19.485	0.519150900	5.0E-7	2167.72583	18.29	0.04
OGLE-LMC-RRLYR-20490	VMC84.436185	69.291370	84.436185	-69.291370	RRab	19.364	20.327	0.533251700	2.2E-6	2187.42943	18.15	0.04
OGLE-LMC-RRLYR-19139	VMC83.487300	69.293210	83.487300	-69.293210	RRab	18.768	19.336	0.496874100	4.0E-7	2167.55978	18.13	0.03
OGLE-LMC-RRLYR-20278	VMC84.271785	69.299120	84.271785	-69.299120	RRab	18.961	19.632	0.563252000	1.1E-6	2187.42748	18.07	0.03
OGLE-LMC-RRLYR-20550	VMC84.477465	69.302420	84.477465	-69.302420	RRc	19.365	19.976	0.304776600	1.0E-6	2187.75434	18.95	0.10
OGLE-LMC-RRLYR-20579	VMC84.492765	69.302170	84.492765	-69.302170	RRab	19.122	19.784	0.519038400	7.0E-7	2187.66374	18.19	0.05
OGLE-LMC-RRLYR-19976	VMC84.061680	69.303520	84.061680	-69.303520	RRab	20.078	21.194	0.501150100	2.1E-6	2187.71350	18.57	0.05
OGLE-LMC-RRLYR-21636	VMC85.377795	69.300510	85.377795	-69.300510	RRab	18.844	19.639	0.590616800	1.9E-6	2187.70501	17.73	0.04
OGLE-LMC-RRLYR-22045	VMC85.805280	69.297600	85.805280	-69.297600	RRab	19.272	19.615	0.502392400	8.0E-7	2187.62689	17.95	0.03
OGLE-LMC-RRLYR-19228	VMC83.543895	69.302990	83.543895	-69.302990	RRab	18.684	19.279	0.580166800	1.9E-6	2167.44276	17.72	0.04
OGLE-LMC-RRLYR-21900	VMC85.656765	69.299150	85.656765	-69.299150	RRab	19.454	20.043	0.529183200	3.2E-6	2187.43834	17.75	0.04
OGLE-LMC-RRLYR-21793	VMC85.535910	69.302330	85.535910	-69.302330	RRab	19.279	20.083	0.563109000	4.6E-6	2187.44907	18.40	0.04
OGLE-LMC-RRLYR-19085	VMC83.458140	69.306470	83.458140	-69.306470	RRab	18.583	19.233	0.719129600	7.0E-7	2167.70295	17.80	0.03
OGLE-LMC-RRLYR-18424	VMC83.054985	69.301320	83.054985	-69.301320	RRab	18.689	19.310	0.642436800	1.2E-6	2167.37540	17.93	0.03
OGLE-LMC-RRLYR-18637	VMC83.178270	69.307840	83.178270	-69.307840	RRab	18.542	19.098	0.640045300	6.0E-7	2167.70131	17.93	0.03
OGLE-LMC-RRLYR-20528	VMC84.462555	69.311540	84.462555	-69.311540	RRe	19.657	20.418	0.281416900	1.3E-6	2187.60214	18.59	0.04
OGLE-LMC-RRLYR-20284	VMC84.279090	69.315120	84.279090	-69.315120	RRab	18.965	19.771	0.732948800	5.2E-6	2187.06104	18.03	0.02
OGLE-LMC-RRLYR-18243	VMC82.979730	69.315960	82.979730	-69.315960	RRab	18.963	19.571	0.527748800	5.0E-7	2167.41222	18.27	0.04
OGLE-LMC-RRLYR-18562	VMC83.131215	69.317410	83.131215	-69.317410	RRab	18.847	19.387	0.542650000	7.0E-7	2167.85415	18.05	0.04
OGLE-LMC-RRLYR-18482	VMC83.084805	69.320320	83.084805	-69.320320	RRab	18.917	19.405	0.487844500	3.0E-7	2167.58032	18.31	0.04
OGLE-LMC-RRLYR-19318	VMC83.600655	69.322650	83.600655	-69.322650	RRab	18.913	19.528	0.548106100	6.0E-7	2167.83673	18.13	0.04
OGLE-LMC-RRLYR-21911	VMC85.665300	69.318870	85.665300	-69.318870	RRab	18.714	19.670	0.780341400	3.8E-6	2187.59268	17.33	0.05
OGLE-LMC-RRLYR-21160	VMC84.967215	69.325170	84.967215	-69.325170	RRe	18.907	19.394	0.376881300	1.0E-6	2187.60530	18.03	0.03
OGLE-LMC-RRLYR-21444	VMC85.203780	69.324200	85.203780	-69.324200	RRab	18.875	19.590	0.529825400	6.0E-7	2187.37465	18.01	0.03
OGLE-LMC-RRLYR-19088	VMC83.460660	69.325840	83.460660	-69.325840	RRab	18.802	19.471	0.582208100	7.0E-7	2167.70607	17.98	0.03
OGLE-LMC-RRLYR-18937	VMC83.375700	69.326860	83.375700	-69.326860	RRe	18.836	19.257	0.337219400	8.0E-7	2186.54550	18.14	0.05
OGLE-LMC-RRLYR-21841	VMC85.582230	69.323440	85.582230	-69.323440	RRab	18.947	19.618	0.570120500	7.0E-7	2187.64594	18.08	0.03
OGLE-LMC-RRLYR-18585	VMC83.145285	69.326620	83.145285	-69.326620	RRab	18.952	19.471	0.485457800	4.0E-7	2167.48211	18.32	0.04
OGLE-LMC-RRLYR-21494	VMC85.245210	69.326870	85.245210	-69.326870	RRab	18.798	19.469	0.595094800	9.0E-7	2187.57717	17.95	0.03
OGLE-LMC-RRLYR-20457	VMC84.403230	69.331010	84.403230	-69.331010	RRab	18.781	19.545	0.662957600	5.2E-6	2187.41343	17.94	0.04
OGLE-LMC-RRLYR-21744	VMC85.495965	69.328340	85.495965	-69.328340	RRe	18.687	19.039	0.251155900	1.3E-6	2187.55721	18.18	0.03
OGLE-LMC-RRLYR-19587	VMC83.783760	69.322980	83.783760	-69.322980	RRab	18.945	19.480	0.466749100	3.0E-7	2167.72410	18.21	0.04
OGLE-LMC-RRLYR-20344	VMC84.321300	69.334330	84.321300	-69.334330	RRab	18.915	19.620	0.606230200	1.3E-6	2187.22997	17.98	0.03
OGLE-LMC-RRLYR-21838	VMC85.579605	69.329400	85.579605	-69.329400	RRab	18.766	19.255	0.482972000	4.0E-7	2187.42643	18.01	0.03
OGLE-LMC-RRLYR-19311	VMC83.597280	69.334520	83.597280	-69.334520	RRe	19.181	19.606	0.259254600	1.0E-6	2167.72936	18.76	0.04
OGLE-LMC-RRLYR-20174	VMC84.196740	69.335640	84.196740	-69.335640	RRab	19.253	20.098	0.598482600	1.3E-6	2187.41561	18.31	0.03
OGLE-LMC-RRLYR-18644	VMC83.182275	69.334250	83.182275	-69.334250	RRab	18.641	19.304	0.601733300	1.0E-6	2167.44229	17.76	0.04
OGLE-LMC-RRLYR-20419	VMC84.375840	69.338060	84.375840	-69.338060	RRab	19.236	20.055	0.583050700	1.4E-6	2187.51150	18.28	0.03
OGLE-LMC-RRLYR-21001	VMC84.835455	69.337110	84.835455	-69.337110	RRab	18.931	19.387	0.456073400	5.0E-7	2187.43294	18.23	0.03
OGLE-LMC-RRLYR-21100	VMC84.911190	69.337120	84.911190	-69.337120	RRe	19.279	19.835	0.284477800	8.0E-7	2187.65835	18.52	0.04
OGLE-LMC-RRLYR-21040	VMC84.864825	69.337900	84.864825	-69.337900	RRab	18.715	19.518	0.778995600	2.9E-6	2187.75177	17.75	0.03
OGLE-LMC-RRLYR-19168	VMC83.502420	69.343590	83.502420	-69.343590	RRe	19.077	19.598	0.306785500	4.0E-7	2167.61459	18.59	0.05
OGLE-LMC-RRLYR-19903	VMC84.011385	69.349080	84.011385	-69.349080	RRab	18.996	19.496	0.463770200	4.0E-7	2187.67857	18.29	0.03
OGLE-LMC-RRLYR-21416	VMC85.180830	69.346730	85.180830	-69.346730	RRab	19.419	20.231	0.479154700	1.0E-6	2187.75302	18.33	0.04

5.6 RR Lyrae stars in the 30 Dor region

129

OGLE-LMC-RRLYR-18533	VMC83.118060	69.347100	83.118060	-69.347100	RRc	18.693	19.156	0.363817100	8.0E-7	2167.58055	18.08	0.03
OGLE-LMC-RRLYR-18487	VMC83.091690	69.346620	83.091690	-69.346620	RRc	19.006	19.388	0.282137800	7.0E-7	2167.72844	18.52	0.04
OGLE-LMC-RRLYR-19383	VMC83.646240	69.351300	83.646240	-69.351300	RRc	19.092	19.593	0.311923800	6.0E-7	2167.67864	18.61	0.04
OGLE-LMC-RRLYR-18371	VMC83.027685	69.349080	83.027685	-69.349080	RRab	18.771	19.269	0.524811600	4.0E-7	2167.39625	18.33	0.04
OGLE-LMC-RRLYR-18374	VMC84.491295	69.356240	84.491295	-69.356240	RRab	18.809	19.487	0.586601700	1.0E-6	2187.21711	17.99	0.03
OGLE-LMC-RRLYR-19740	VMC83.891415	69.358480	83.891415	-69.358480	RRab	18.993	19.606	0.504781900	5.0E-7	2187.27839	18.15	0.03
OGLE-LMC-RRLYR-18364	VMC83.025465	69.355250	83.025465	-69.355250	RRab	18.992	19.423	0.275110500	1.5E-6	2186.75724	18.73	0.05
OGLE-LMC-RRLYR-19666	VMC83.834355	69.357000	83.834355	-69.357000	RRab	18.809	19.483	0.621706000	1.4E-6	2167.68372	18.02	0.03
OGLE-LMC-RRLYR-21190	VMC84.994155	69.360310	84.994155	-69.360310	RRab	18.824	19.526	0.659979000	1.3E-6	2187.16290	17.95	0.03
OGLE-LMC-RRLYR-19020	VMC83.419575	69.361460	83.419575	-69.361460	RRc	19.141	19.612	0.274386100	6.0E-7	2167.85333	18.73	0.05
OGLE-LMC-RRLYR-19052	VMC83.439285	69.362040	83.439285	-69.362040	RRc	18.334	18.508	0.301914200	6.0E-7	2167.61716	18.11	0.03
OGLE-LMC-RRLYR-19746	VMC83.897745	69.364450	83.897745	-69.364450	RRab	19.103	19.753	0.556019800	1.8E-6	2187.66695	18.28	0.03
OGLE-LMC-RRLYR-18803	VMC83.278425	69.362250	83.278425	-69.362250	RRab	18.903	19.421	0.487909300	1.2E-6	2167.83637	18.30	0.04
OGLE-LMC-RRLYR-20314	VMC84.296640	69.364090	84.296640	-69.364090	RRab	18.628	19.251	0.665895500	2.3E-6	2187.51236	17.89	0.03
OGLE-LMC-RRLYR-20205	VMC84.224805	69.366250	84.224805	-69.366250	RRab	18.968	19.618	0.518407400	2.0E-6	2187.71253	18.10	0.04
OGLE-LMC-RRLYR-19178	VMC83.508510	69.365580	83.508510	-69.365580	RRc	19.024	19.520	0.304918100	8.0E-7	2167.72875	18.42	0.04
OGLE-LMC-RRLYR-20808	VMC84.678000	69.369870	84.678000	-69.369870	RRab	18.912	19.593	0.617384600	2.1E-6	2187.16326	18.01	0.03
OGLE-LMC-RRLYR-19357	VMC83.622990	69.366080	83.622990	-69.366080	RRab	18.716	19.285	0.578571400	7.0E-7	2167.60983	17.99	0.03
OGLE-LMC-RRLYR-22080	VMC85.846050	69.365030	85.846050	-69.365030	RRc	19.609	20.551	0.393190000	3.4E-6	2187.49106	18.22	0.04
OGLE-LMC-RRLYR-20426	VMC84.379620	69.376480	84.379620	-69.376480	RRab	19.045	19.683	0.549267100	9.0E-7	2187.31280	18.08	0.04
OGLE-LMC-RRLYR-18857	VMC83.318880	69.374520	83.318880	-69.374520	RRab	19.098	19.569	0.630549600	3.5E-6	2167.56753	17.88	0.03
OGLE-LMC-RRLYR-20052	VMC84.118515	69.376710	84.118515	-69.376710	RRab	18.888	19.392	0.518818500	8.0E-7	2187.69110	18.35	0.04
OGLE-LMC-RRLYR-21196	VMC85.338990	69.372280	85.338990	-69.372280	RRab	18.879	19.451	0.539690600	9.0E-7	2187.34297	17.97	0.03
OGLE-LMC-RRLYR-21846	VMC85.592025	69.371680	85.592025	-69.371680	RRab	18.831	19.495	0.612733000	1.1E-6	2187.37443	18.04	0.03
OGLE-LMC-RRLYR-21629	VMC85.367970	69.373640	85.367970	-69.373640	RRc	18.855	19.570	0.444978000	3.4E-6	2187.51340	17.88	0.03
OGLE-LMC-RRLYR-18963	VMC83.388420	69.375940	83.388420	-69.375940	RRab	18.811	19.508	0.671565700	1.8E-6	2167.88422	17.93	0.03
OGLE-LMC-RRLYR-20381	VMC84.348990	69.378480	84.348990	-69.378480	RRab	18.841	19.567	0.675204800	2.2E-6	2187.75912	18.01	0.03
OGLE-LMC-RRLYR-18670	VMC83.199270	69.377350	83.199270	-69.377350	RRc	19.128	19.503	0.262193700	1.3E-6	2167.66825	18.72	0.05
OGLE-LMC-RRLYR-18779	VMC83.264490	69.377650	83.264490	-69.377650	RRab	18.760	19.376	0.600855600	1.2E-6	2167.29197	17.86	0.04
OGLE-LMC-RRLYR-20559	VMC84.481905	69.382390	84.481905	-69.382390	RRab	19.011	19.779	0.528272100	1.9E-6	2187.31540	17.86	0.04
OGLE-LMC-RRLYR-21243	VMC85.046280	69.381240	85.046280	-69.381240	RRab	19.041	19.980	0.460350400	5.0E-7	2187.41794	16.66	0.03
OGLE-LMC-RRLYR-19749	VMC83.899275	69.385060	83.899275	-69.385060	RRab	18.741	19.397	0.636974000	2.4E-6	2187.71944	17.94	0.03
OGLE-LMC-RRLYR-22087	VMC85.854855	69.378470	85.854855	-69.378470	RRab	19.321	20.267	0.594988700	3.6E-6	2187.44638	18.13	0.03
OGLE-LMC-RRLYR-19183	VMC83.512200	69.386280	83.512200	-69.386280	RRab	18.853	19.409	0.551584200	6.0E-7	2167.63915	17.66	0.07
OGLE-LMC-RRLYR-19522	VMC83.747175	69.387300	83.747175	-69.387300	RRab	18.773	19.429	0.656644300	6.0E-7	2167.40515	18.10	0.04
OGLE-LMC-RRLYR-20103	VMC84.145230	69.388500	84.145230	-69.388500	RRab	18.533	19.967	0.612116100	2.0E-6	2187.76041	17.75	0.05
OGLE-LMC-RRLYR-18732	VMC83.239020	69.385600	83.239020	-69.385600	RRc	19.015	19.466	0.295578300	5.0E-7	2167.68219	18.41	0.04
OGLE-LMC-RRLYR-21259	VMC85.062645	69.388710	85.062645	-69.388710	RRab	18.298	18.785	0.626123300	1.8E-6	2187.47668	17.66	0.02
OGLE-LMC-RRLYR-18817	VMC83.287230	69.389500	83.287230	-69.389500	RRab	19.220	19.883	0.510168100	8.0E-7	2167.65261	18.33	0.03
OGLE-LMC-RRLYR-20942	VMC84.778755	69.391210	84.778755	-69.391210	RRc	19.254	19.899	0.298194400	7.0E-7	2187.75991	18.53	0.05
OGLE-LMC-RRLYR-21788	VMC85.533720	69.387700	85.533720	-69.387700	RRab	18.787	19.318	0.512275000	7.0E-7	2187.43515	18.09	0.04
OGLE-LMC-RRLYR-18437	VMC83.063100	69.390720	83.063100	-69.390720	RRab	18.843	19.178	0.330669600	8.0E-7	2167.79963	18.39	0.04
OGLE-LMC-RRLYR-19542	VMC83.758305	69.394360	83.758305	-69.394360	RRab	18.990	19.693	0.636006000	3.5E-6	2167.70571	18.02	0.03
OGLE-LMC-RRLYR-19994	VMC84.076095	69.395610	84.076095	-69.395610	RRab	18.868	19.455	0.557741000	8.0E-7	2187.60153	18.02	0.03
OGLE-LMC-RRLYR-21366	VMC85.139145	69.395290	85.139145	-69.395290	RRc	18.659	19.239	0.395096400	1.1E-6	2187.50956	17.95	0.03
OGLE-LMC-RRLYR-21238	VMC85.038705	69.398180	85.038705	-69.398180	RRc	18.967	19.332	0.298505400	1.1E-6	2187.65044	18.09	0.05
OGLE-LMC-RRLYR-19136	VMC83.485320	69.399170	83.485320	-69.399170	RRab	18.823	-99.99	0.601844900	1.7E-6	2248.19936	18.01	0.03
OGLE-LMC-RRLYR-20068	VMC84.127725	69.385460	84.127725	-69.385460	RRab	18.773	19.434	0.663688900	1.7E-6	2187.15358	17.84	0.04
OGLE-LMC-RRLYR-19456	VMC83.701650	69.393490	83.701650	-69.393490	RRab	19.268	19.726	0.373043000	3.0E-7	2167.79387	18.54	0.10
OGLE-LMC-RRLYR-21564	VMC85.308105	69.402440	85.308105	-69.402440	RRc	19.351	20.065	0.307710100	2.0E-6	2193.76293	18.62	0.04
OGLE-LMC-RRLYR-19208	VMC83.530095	69.406280	83.530095	-69.406280	RRab	19.209	19.886	0.489128300	1.0E-6	2167.61607	18.56	0.04
OGLE-LMC-RRLYR-18799	VMC83.277045	69.404990	83.277045	-69.404990	RRab	18.869	19.616	0.612156800	1.0E-6	2167.53845	18.07	0.03
OGLE-LMC-RRLYR-21471	VMC85.221810	69.405190	85.221810	-69.405190	RRab	19.300	20.010	0.486916200	1.3E-6	2187.66128	18.27	0.04
OGLE-LMC-RRLYR-20636	VMC84.545820	69.408620	84.545820	-69.408620	RRab	19.043	19.769	0.551028800	1.6E-6	2187.39738	17.94	0.03
OGLE-LMC-RRLYR-19140	VMC83.488095	69.408490	83.488095	-69.408490	RRab	18.768	19.310	0.534141900	7.0E-7	2167.44764	17.97	0.03
OGLE-LMC-RRLYR-20736	VMC84.633930	69.410100	84.633930	-69.410100	RRab	19.125	-99.99	0.584687900	6.1E-6	2187.57820	18.16	0.04
OGLE-LMC-RRLYR-21496	VMC85.246080	69.407560	85.246080	-69.407560	RRab	19.053	19.815	0.585193900	1.3E-6	2187.50184	18.16	0.04
OGLE-LMC-RRLYR-19002	VMC83.407200	69.409090	83.407200	-69.409090	RRc	19.408	19.233	0.289506500	8.0E-7	2167.69656	18.18	0.04

130 Data analysis, and first results for RR Lyrae stars from the VMC survey

OGLE-LMC-RRLYR-20047	VMC84.114240	69.411150	84.114240	-69.411150	RRab	18.892	19.413	0.483944900	8.0E-7	2187.52660	18.16	0.03
OGLE-LMC-RRLYR-19065	VMC83.444940	69.413950	83.444940	-69.413950	RRab	19.007	19.517	0.480258000	4.0E-7	2167.60434	18.31	0.04
OGLE-LMC-RRLYR-21689	VMC85.430895	69.409240	85.430895	-69.409240	RRab	19.068	19.818	0.622468600	2.4E-6	2187.17275	17.85	0.05
OGLE-LMC-RRLYR-19800	VMC83.936730	69.410330	83.936730	-69.410330	RRab	19.012	19.464	0.322801800	1.0E-6	2187.45360	18.41	0.05
OGLE-LMC-RRLYR-21736	VMC85.483920	69.413090	85.483920	-69.413090	RRab	18.690	19.304	0.577655400	9.0E-7	2187.62405	17.99	0.03
OGLE-LMC-RRLYR-20422	VMC84.377715	69.415730	84.377715	-69.415730	RRab	18.673	19.191	0.503412300	8.0E-7	2187.74744	18.00	0.03
OGLE-LMC-RRLYR-18877	VMC83.330865	69.416540	83.330865	-69.416540	RRab	18.681	19.233	0.549522000	7.0E-7	2167.50823	17.84	0.05
OGLE-LMC-RRLYR-20826	VMC84.690465	69.419660	84.690465	-69.419660	RRab	20.040	21.180	0.453302300	1.9E-6	2187.43913	18.90	0.04
OGLE-LMC-RRLYR-20855	VMC84.709815	69.423290	84.709815	-69.423290	RRab	19.963	21.181	0.568335200	3.0E-6	2187.68165	18.34	0.03
OGLE-LMC-RRLYR-18295	VMC82.991490	69.420970	82.991490	-69.420970	RRab	18.869	19.306	0.329605500	3.0E-7	455.54581	18.35	0.03
OGLE-LMC-RRLYR-20567	VMC84.487050	69.426240	84.487050	-69.426240	RRab	18.806	19.477	0.613993100	1.6E-6	2193.43192	17.96	0.03
OGLE-LMC-RRLYR-19124	VMC83.478375	69.421500	83.478375	-69.421500	RRab	18.864	19.410	0.467395700	3.0E-7	2167.86132	17.98	0.05
OGLE-LMC-RRLYR-20014	VMC84.086880	69.424370	84.086880	-69.424370	RRab	18.959	19.482	0.501810300	5.0E-7	2187.64397	18.33	0.03
OGLE-LMC-RRLYR-21372	VMC85.143675	69.425530	85.143675	-69.425530	RRab	19.006	19.633	0.514599600	1.3E-6	2187.57029	18.28	0.03
OGLE-LMC-RRLYR-19450	VMC83.696685	69.428530	83.696685	-69.428530	RRab	18.841	19.387	0.488239000	1.9E-6	2167.67739	18.24	0.04
OGLE-LMC-RRLYR-20733	VMC84.631425	69.428620	84.631425	-69.428620	RRab	19.682	99.99	0.576951500	3.9E-5	2250.64030	18.17	0.03
OGLE-LMC-RRLYR-20166	VMC84.191550	69.432790	84.191550	-69.432790	RRab	18.980	19.603	0.561303100	2.0E-6	2187.61223	18.14	0.04
OGLE-LMC-RRLYR-18505	VMC83.101380	69.428250	83.101380	-69.428250	RRab	18.576	19.127	0.585810200	3.0E-7	455.68042	17.87	0.04
OGLE-LMC-RRLYR-18362	VMC83.024865	69.424560	83.024865	-69.424560	RRab	18.766	19.246	0.525071400	2.0E-7	455.36602	18.05	0.03
OGLE-LMC-RRLYR-19125	VMC83.478780	69.432630	83.478780	-69.432630	RRe	19.135	19.550	0.272139200	1.0E-6	2167.83458	18.68	0.04
OGLE-LMC-RRLYR-21754	VMC85.501095	69.429520	85.501095	-69.429520	RRab	18.860	19.508	0.557439800	1.5E-6	2187.68720	18.00	0.04
OGLE-LMC-RRLYR-20434	VMC84.385395	69.434840	84.385395	-69.434840	RRab	18.643	19.360	0.700666400	1.8E-6	2187.70877	17.78	0.03
OGLE-LMC-RRLYR-18835	VMC83.302290	69.433540	83.302290	-69.433540	RRab	18.982	19.514	0.511058300	4.0E-7	2167.82138	18.30	0.04
OGLE-LMC-RRLYR-18491	VMC83.092830	69.430360	83.092830	-69.430360	RRab	19.018	19.608	0.446083200	2.0E-7	455.41208	18.39	0.06
OGLE-LMC-RRLYR-21547	VMC85.294995	69.433790	85.294995	-69.433790	RRab	18.967	19.522	0.467858500	5.0E-7	2187.55638	18.17	0.04
OGLE-LMC-RRLYR-20618	VMC84.532845	69.438620	84.532845	-69.438620	RRc	18.466	18.954	0.422715500	1.0E-6	2187.61577	17.80	0.03
OGLE-LMC-RRLYR-19766	VMC83.910885	69.439180	83.910885	-69.439180	RRab	18.802	19.393	0.532757200	2.1E-6	2187.26756	18.27	0.03
OGLE-LMC-RRLYR-19276	VMC83.574915	69.437490	83.574915	-69.437490	RRab	18.829	19.315	0.502674200	5.0E-7	2167.52928	18.15	0.03
OGLE-LMC-RRLYR-18981	VMC83.396610	69.437460	83.396610	-69.437460	RRab	19.092	19.746	0.557207400	3.8E-6	2167.36751	18.20	0.03
OGLE-LMC-RRLYR-20165	VMC84.189465	69.443480	84.189465	-69.443480	RRab	18.716	19.235	0.633420300	3.2E-6	2187.16114	17.93	0.03
OGLE-LMC-RRLYR-20905	VMC84.746370	69.444250	84.746370	-69.444250	RRab	18.798	19.588	0.742462900	2.1E-6	2187.54214	17.72	0.03
OGLE-LMC-RRLYR-21082	VMC84.897285	69.445150	84.897285	-69.445150	RRc	18.675	19.186	0.400535600	1.7E-6	2187.48710	18.14	0.03
OGLE-LMC-RRLYR-19330	VMC83.607345	69.444490	83.607345	-69.444490	RRc	19.000	19.390	0.296607500	6.0E-7	2167.83569	17.74	0.08
OGLE-LMC-RRLYR-20922	VMC84.760575	69.447130	84.760575	-69.447130	RRab	19.080	19.648	0.481913800	8.0E-7	2187.66379	18.36	0.03
OGLE-LMC-RRLYR-20481	VMC84.425280	69.448710	84.425280	-69.448710	RRc	19.021	19.576	0.323523900	1.1E-6	2187.75702	18.60	0.07
OGLE-LMC-RRLYR-20788	VMC84.667980	69.448900	84.667980	-69.448900	RRc	19.066	19.599	0.309506500	8.0E-7	2187.73430	18.40	0.06
OGLE-LMC-RRLYR-18212	VMC82.969635	69.443870	82.969635	-69.443870	RRab	18.603	19.122	0.401648100	4.0E-7	455.40111	17.92	0.04
OGLE-LMC-RRLYR-20421	VMC84.377235	69.450070	84.377235	-69.450070	RRab	18.949	19.616	0.630091400	2.6E-6	2187.68775	17.97	0.03
OGLE-LMC-RRLYR-19114	VMC83.475135	69.450200	83.475135	-69.450200	RRab	18.922	19.493	0.507752500	6.0E-7	2167.52305	18.17	0.03
OGLE-LMC-RRLYR-19678	VMC83.843565	69.446500	83.843565	-69.446500	RRab	18.639	19.271	0.608577800	1.1E-6	2167.33973	17.78	0.04
OGLE-LMC-RRLYR-18233	VMC82.976865	69.450530	82.976865	-69.450530	RRab	18.713	19.242	0.592934100	2.0E-7	455.54874	18.11	0.03
OGLE-LMC-RRLYR-20267	VMC84.264840	69.455980	84.264840	-69.455980	RRab	19.280	20.007	0.488273200	1.2E-6	2187.50967	18.28	0.04
OGLE-LMC-RRLYR-21540	VMC85.288755	69.454700	85.288755	-69.454700	RRe	19.286	19.849	0.267070400	1.2E-6	2187.66916	18.50	0.05
OGLE-LMC-RRLYR-19640	VMC83.820120	69.458050	83.820120	-69.458050	RRc	19.058	19.499	0.281793800	4.0E-7	2167.82023	18.32	0.04
OGLE-LMC-RRLYR-19061	VMC83.442285	69.458330	83.442285	-69.458330	RRab	18.957	19.483	0.493544200	4.0E-7	2167.49471	18.30	0.04
OGLE-LMC-RRLYR-21455	VMC85.209915	69.458930	85.209915	-69.458930	RRc	19.521	19.947	0.409514500	2.6E-6	2187.51599	19.01	0.06
OGLE-LMC-RRLYR-21436	VMC85.199130	69.459390	85.199130	-69.459390	RRab	18.959	19.711	0.492684900	4.0E-7	2187.71214	17.81	0.05
OGLE-LMC-RRLYR-20504	VMC84.446820	69.461890	84.446820	-69.461890	RRab	19.059	19.796	0.553237400	1.7E-6	2187.67015	17.80	0.06
OGLE-LMC-RRLYR-18823	VMC83.288475	69.463470	83.288475	-69.463470	RRab	18.899	19.488	0.559140800	7.0E-7	2167.63032	18.05	0.03
OGLE-LMC-RRLYR-18484	VMC83.086185	69.462780	83.086185	-69.462780	RRab	18.788	19.418	0.610020400	3.0E-7	455.30629	18.08	0.03
OGLE-LMC-RRLYR-17975	VMC83.931915	69.467190	83.931915	-69.467190	RRab	18.748	19.165	0.450602300	6.0E-7	2187.58378	18.19	0.04
OGLE-LMC-RRLYR-20169	VMC84.193770	69.468380	84.193770	-69.468380	RRab	19.089	19.662	0.458053200	5.0E-7	2187.61666	18.39	0.03
OGLE-LMC-RRLYR-19656	VMC83.827545	69.470010	83.827545	-69.470010	RRc	18.973	19.507	0.354633000	7.0E-7	2167.53634	18.44	0.04
OGLE-LMC-RRLYR-19776	VMC83.920005	69.469210	83.920005	-69.469210	RRab	18.801	19.341	0.571782600	9.0E-7	2187.45644	17.96	0.03
OGLE-LMC-RRLYR-20614	VMC84.529140	69.470320	84.529140	-69.470320	RRab	19.183	20.097	0.746826100	6.1E-6	2187.30663	17.94	0.03
OGLE-LMC-RRLYR-19877	VMC83.992860	69.471020	83.992860	-69.471020	RRab	19.056	19.834	0.594987000	2.3E-6	2187.51845	18.12	0.04
OGLE-LMC-RRLYR-18454	VMC83.072640	69.467080	83.072640	-69.467080	RRe	19.008	19.340	0.271429600	4.0E-7	455.51020	18.77	0.07
OGLE-LMC-RRLYR-21567	VMC85.309950	69.472060	85.309950	-69.472060	RRc	19.225	19.891	0.345137600	1.2E-6	2187.64703	18.40	0.05

5.6 RR Lyrae stars in the 30 Dor region

131

OGLE-LMC-RRLYR-18992	VMC83.402010	69.473620	83.402010	-69.473620	RRab	18.734	19.218	0.610378400	1.3E-6	2167.32444	17.45	0.05
OGLE-LMC-RRLYR-21349	VMC85.129335	69.473240	85.129335	-69.473240	RRab	18.521	19.036	0.614473600	6.0E-7	2187.70861	17.83	0.03
OGLE-LMC-RRLYR-18335	VMC83.005005	69.473100	83.005005	-69.473100	RRab	18.605	19.202	0.610227100	4.0E-7	455.67412	17.86	0.03
OGLE-LMC-RRLYR-19077	VMC83.454765	69.474060	83.454765	-69.474060	RRab	18.858	19.310	0.492017500	5.8E-6	2167.50770	18.04	0.04
OGLE-LMC-RRLYR-21308	VMC85.092735	69.463380	85.092735	-69.463380	RRab	19.010	19.747	0.610148300	1.6E-6	2187.33661	18.05	0.03
OGLE-LMC-RRLYR-18758	VMC83.253315	69.475870	83.253315	-69.475870	RRab	18.514	18.813	0.570659600	1.5E-6	2167.50052	16.59	0.03
OGLE-LMC-RRLYR-19072	VMC83.450190	69.477310	83.450190	-69.477310	RRe	19.105	19.581	0.292712200	8.0E-7	2167.71843	18.69	0.06
OGLE-LMC-RRLYR-18580	VMC83.139165	69.476100	83.139165	-69.476100	RRab	18.750	19.334	0.573889700	2.0E-7	455.50380	18.06	0.04
OGLE-LMC-RRLYR-20127	VMC84.162465	69.479830	84.162465	-69.479830	RRab	18.903	19.534	0.556355400	1.6E-6	2187.31592	18.18	0.03
OGLE-LMC-RRLYR-21625	VMC85.365765	69.476710	85.365765	-69.476710	RRab	18.908	19.618	0.575331100	9.0E-7	2187.55649	17.98	0.03
OGLE-LMC-RRLYR-18656	VMC83.192610	69.477660	83.192610	-69.477660	RRab	18.905	19.357	0.349730700	9.0E-7	2167.60310	18.24	0.04
OGLE-LMC-RRLYR-20482	VMC84.425910	69.481780	84.425910	-69.481780	RRab	19.064	19.681	0.478289100	1.7E-6	2187.51931	17.76	0.04
OGLE-LMC-RRLYR-21221	VMC85.024770	69.478770	85.024770	-69.478770	RRab	18.465	19.044	0.642005600	8.0E-7	2187.34678	17.64	0.03
OGLE-LMC-RRLYR-21315	VMC85.095180	69.480380	85.095180	-69.480380	RRe	18.949	19.549	0.484683900	8.0E-7	2187.45997	18.25	0.03
OGLE-LMC-RRLYR-18427	VMC83.054970	69.478100	83.054970	-69.478100	RRe	18.753	19.147	0.288382300	2.0E-7	455.52555	18.21	0.04
OGLE-LMC-RRLYR-21985	VMC85.741470	69.476460	85.741470	-69.476460	RRab	18.535	19.090	0.643022200	1.4E-6	2187.16291	17.73	0.03
OGLE-LMC-RRLYR-19701	VMC83.858100	69.485370	83.858100	-69.485370	RRab	18.709	19.358	0.633612300	1.6E-6	2167.40626	17.89	0.03
OGLE-LMC-RRLYR-21930	VMC85.685475	69.479300	85.685475	-69.479300	RRab	18.966	19.743	0.603831600	2.2E-6	2187.50963	18.09	0.03
OGLE-LMC-RRLYR-18520	VMC83.108430	69.482970	83.108430	-69.482970	RRab	18.740	19.326	0.568642500	3.0E-7	455.54977	17.82	0.03
OGLE-LMC-RRLYR-22025	VMC85.782645	69.479630	85.782645	-69.479630	RRc	19.267	20.085	0.312354500	1.2E-6	2187.69520	18.44	0.04
OGLE-LMC-RRLYR-21048	VMC84.870990	69.487140	84.870990	-69.487140	RRc	19.322	19.882	0.275190800	8.0E-7	2187.69942	18.68	0.05
OGLE-LMC-RRLYR-20406	VMC84.367350	69.487920	84.367350	-69.487920	RRab	19.042	19.790	0.633124000	1.9E-6	2187.36917	18.11	0.04
OGLE-LMC-RRLYR-19032	VMC83.426280	69.487840	83.426280	-69.487840	RRab	18.752	19.385	0.613908400	7.0E-7	2167.76293	17.98	0.04
OGLE-LMC-RRLYR-21559	VMC85.303830	69.486800	85.303830	-69.486800	RRab	19.205	19.867	0.480403800	5.0E-7	2187.32898	18.43	0.04
OGLE-LMC-RRLYR-21143	VMC84.948795	69.488930	84.948795	-69.488930	RRc	19.330	20.297	0.403838000	3.7E-6	2187.58346	17.97	0.04
OGLE-LMC-RRLYR-18355	VMC83.019735	69.487010	83.019735	-69.487010	RRab	18.723	19.282	0.638756700	3.0E-7	455.60513	18.05	0.03
OGLE-LMC-RRLYR-19555	VMC83.764590	69.494750	83.764590	-69.494750	RRab	18.681	19.337	0.632338800	2.0E-6	2167.66947	17.93	0.03
OGLE-LMC-RRLYR-21498	VMC85.246200	69.494240	85.246200	-69.494240	RRab	18.766	19.471	0.576193700	4.6E-6	2187.56451	17.87	0.03
OGLE-LMC-RRLYR-20070	VMC84.129285	69.496060	84.129285	-69.496060	RRab	19.093	19.757	0.486218600	1.2E-6	2187.30089	18.41	0.04
OGLE-LMC-RRLYR-21791	VMC85.535235	69.491370	85.535235	-69.491370	RRab	18.878	19.634	0.606266200	2.3E-6	2187.60529	17.93	0.03
OGLE-LMC-RRLYR-21805	VMC85.547175	69.492710	85.547175	-69.492710	RRab	18.549	19.164	0.710427400	1.6E-6	2187.27342	17.80	0.03
OGLE-LMC-RRLYR-20006	VMC84.082950	69.499970	84.082950	-69.499970	RRab	18.704	19.211	0.574689400	1.0E-6	2187.61444	17.98	0.04
OGLE-LMC-RRLYR-18691	VMC83.210310	69.494190	83.210310	-69.494190	RRab	18.708	19.274	0.561063700	7.0E-7	2167.38946	18.00	0.03
OGLE-LMC-RRLYR-18808	VMC83.280645	69.501940	83.280645	-69.501940	RRab	18.947	19.528	0.557848800	6.0E-7	2167.69639	18.12	0.03
OGLE-LMC-RRLYR-18419	VMC83.051220	69.490520	83.051220	-69.490520	RRab	18.672	19.308	0.672972600	1.2E-6	455.33677	17.80	0.03
OGLE-LMC-RRLYR-19286	VMC83.582415	69.503550	83.582415	-69.503550	RRab	18.849	19.492	0.612046100	1.4E-6	2167.36804	18.13	0.03
OGLE-LMC-RRLYR-19738	VMC83.890545	69.504610	83.890545	-69.504610	RRab	18.639	19.215	0.592092600	1.0E-6	2187.74478	17.91	0.03
OGLE-LMC-RRLYR-20270	VMC84.268230	69.507640	84.268230	-69.507640	RRe	18.750	19.175	0.291095800	8.0E-7	2187.50032	18.29	0.03
OGLE-LMC-RRLYR-20311	VMC84.294945	69.508180	84.294945	-69.508180	RRc	18.678	19.100	0.406336400	3.1E-6	2187.70967	17.91	0.03
OGLE-LMC-RRLYR-20179	VMC84.199125	69.492240	84.199125	-69.492240	RRab	18.810	19.518	0.624264400	2.9E-6	2187.56846	18.08	0.03
OGLE-LMC-RRLYR-20578	VMC84.492015	69.510560	84.492015	-69.510560	RRc	19.085	19.691	0.338144200	1.4E-6	2187.46568	18.40	0.04
OGLE-LMC-RRLYR-21152	VMC84.958125	69.510670	84.958125	-69.510670	RRe	18.810	19.309	0.3060623400	9.0E-7	2187.67868	18.27	0.04
OGLE-LMC-RRLYR-19407	VMC83.665995	69.510660	83.665995	-69.510660	RRe	19.663	20.323	0.284580900	1.4E-6	2167.63886	18.67	0.04
OGLE-LMC-RRLYR-20100	VMC84.144285	69.512980	84.144285	-69.512980	RRab	19.036	19.649	0.548607600	1.5E-6	2187.24237	18.29	0.03
OGLE-LMC-RRLYR-21599	VMC85.343925	69.509340	85.343925	-69.509340	RRab	19.118	19.931	0.58226800	1.6E-6	2187.34483	18.16	0.03
OGLE-LMC-RRLYR-18570	VMC83.134425	69.511100	83.134425	-69.511100	RRab	18.543	19.096	0.592500900	3.0E-7	455.35994	17.77	0.03
OGLE-LMC-RRLYR-21741	VMC85.494090	69.509580	85.494090	-69.509580	RRc	19.050	19.623	0.327988700	1.1E-6	2187.65659	18.29	0.03
OGLE-LMC-RRLYR-20489	VMC84.436140	69.514080	84.436140	-69.514080	RRab	18.589	19.220	0.643781200	3.6E-6	2187.50168	17.78	0.03
OGLE-LMC-RRLYR-21400	VMC85.168665	69.512270	85.168665	-69.512270	RRe	19.257	19.994	0.347315100	1.3E-6	2187.60084	18.29	0.04
OGLE-LMC-RRLYR-22029	VMC85.785225	69.507750	85.785225	-69.507750	RRab	19.022	19.781	0.477961100	6.0E-7	2187.51714	18.14	0.03
OGLE-LMC-RRLYR-20176	VMC84.198210	69.515610	84.198210	-69.515610	RRc	18.640	19.226	0.455743100	3.7E-6	2187.75141	18.04	0.03
OGLE-LMC-RRLYR-20149	VMC84.176865	69.516780	84.176865	-69.516780	RRab	18.746	19.392	0.602829400	1.6E-6	2187.76738	17.92	0.03
OGLE-LMC-RRLYR-18818	VMC83.287545	69.510440	83.287545	-69.510440	RRab	18.694	19.339	0.633899200	1.9E-6	2167.26673	18.02	0.03
OGLE-LMC-RRLYR-19354	VMC83.620635	69.514810	83.620635	-69.514810	RRab	18.653	19.293	0.657061900	1.0E-6	2167.49026	17.94	0.04
OGLE-LMC-RRLYR-20168	VMC84.191985	69.520030	84.191985	-69.520030	RRab	18.699	19.295	0.559149400	7.0E-7	2187.48768	18.06	0.04
OGLE-LMC-RRLYR-18790	VMC83.270655	69.519350	83.270655	-69.519350	RRab	18.884	19.374	0.531622200	1.1E-6	2167.42628	18.24	0.03
OGLE-LMC-RRLYR-20232	VMC84.241530	69.522270	84.241530	-69.522270	RRc	19.018	19.501	0.326834200	7.0E-7	2187.66947	18.44	0.05
OGLE-LMC-RRLYR-21721	VMC85.465050	69.518370	85.465050	-69.518370	RRc	19.110	19.791	0.361955200	1.0E-6	2187.63865	18.23	0.03

132 Data analysis, and first results for RR Lyrae stars from the VMC survey

OGLE-LMC-RRLYR-21156	VMC84.960645_-69.522560	84.960645	-69.522560	RRab	19.911	20.908	0.580764200	3.1E-6	2187.69176	18.27	0.04
OGLE-LMC-RRLYR-20558	VMC84.481845_-69.525210	84.481845	-69.525210	RRab	18.694	19.275	0.557826500	7.0E-7	2187.42179	18.03	0.03
OGLE-LMC-RRLYR-21910	VMC85.665210_-69.519500	85.665210	-69.519500	RRab	18.887	19.531	0.584263900	1.9E-6	2187.70765	17.96	0.03
OGLE-LMC-RRLYR-19472	VMC83.713440_-69.528000	83.713440	-69.528000	RRab	19.254	19.991	0.534126600	8.0E-7	2167.73697	18.23	0.03
OGLE-LMC-RRLYR-21762	VMC85.511565_-69.526340	85.511565	-69.526340	RRc	19.151	19.824	0.333039200	1.3E-6	2187.66342	18.30	0.03
OGLE-LMC-RRLYR-21070	VMC84.887235_-69.530060	84.887235	-69.530060	RRe	19.110	19.524	0.264065200	1.6E-6	2187.72807	18.59	0.05
OGLE-LMC-RRLYR-19843	VMC83.966640_-69.533680	83.966640	-69.533680	RRab	18.597	19.210	0.626539300	2.0E-6	2187.57277	17.92	0.03
OGLE-LMC-RRLYR-19144	VMC83.489715_-69.532570	83.489715	-69.532570	RRc	18.799	19.316	0.367440400	9.0E-7	2167.72501	18.18	0.03
OGLE-LMC-RRLYR-18439	VMC83.063350_-69.530240	83.063350	-69.530240	RRe	18.995	19.416	0.273984000	5.0E-7	455.49184	18.61	0.05
OGLE-LMC-RRLYR-21456	VMC85.209915_-69.532630	85.209915	-69.532630	RRc	19.654	20.604	0.338146800	2.3E-6	2187.51540	18.32	0.04
OGLE-LMC-RRLYR-20187	VMC84.212685_-69.536270	84.212685	-69.536270	RRab	18.817	19.446	0.573008300	1.3E-6	2187.54758	17.98	0.03
OGLE-LMC-RRLYR-19053	VMC83.439870_-69.534550	83.439870	-69.534550	RRab	18.628	19.346	0.753716400	0.1E-5	2167.48155	17.76	0.03
OGLE-LMC-RRLYR-19515	VMC83.741760_-69.534350	83.741760	-69.534350	RRe	18.987	19.372	0.261687100	6.0E-7	2167.73730	18.56	0.04
OGLE-LMC-RRLYR-21057	VMC84.877395_-69.534900	84.877395	-69.534900	RRab	18.420	19.082	0.724855700	1.4E-6	2187.23229	17.58	0.03
OGLE-LMC-RRLYR-18438	VMC83.063325_-69.534290	83.063325	-69.534290	RRab	18.804	19.417	0.563223100	2.0E-7	455.41772	17.99	0.03
OGLE-LMC-RRLYR-18574	VMC83.136225_-69.533650	83.136225	-69.533650	RRab	18.809	19.295	0.542525000	2.0E-7	455.54044	17.34	0.07
OGLE-LMC-RRLYR-21181	VMC84.984135_-69.536840	84.984135	-69.536840	RRab	19.054	19.885	0.562316600	1.8E-6	2187.37315	18.06	0.04
OGLE-LMC-RRLYR-21765	VMC85.515870_-69.533650	85.515870	-69.533650	RRab	18.743	19.444	0.678663100	8.3E-6	2187.64510	17.88	0.03
OGLE-LMC-RRLYR-20509	VMC84.450570_-69.539170	84.450570	-69.539170	RRab	18.771	19.419	0.700537800	2.0E-6	2187.57045	17.91	0.03
OGLE-LMC-RRLYR-19281	VMC83.577480_-69.538380	83.577480	-69.538380	RRab	19.494	20.236	0.477206000	6.0E-7	2167.75745	18.41	0.04
OGLE-LMC-RRLYR-21925	VMC85.677960_-69.534540	85.677960	-69.534540	RRab	18.972	19.625	0.538176100	1.1E-6	2187.34215	18.12	0.03
OGLE-LMC-RRLYR-18394	VMC83.040945_-69.537100	83.040945	-69.537100	RRab	18.773	19.299	0.496332700	2.0E-7	455.28277	18.00	0.04
OGLE-LMC-RRLYR-21842	VMC85.582545_-69.537120	85.582545	-69.537120	RRab	19.046	19.650	0.504553300	1.4E-6	2187.55915	18.33	0.04
OGLE-LMC-RRLYR-19015	VMC83.416785_-69.542280	83.416785	-69.542280	RRab	19.039	19.626	0.474261200	4.0E-7	2167.55337	18.42	0.05
OGLE-LMC-RRLYR-19123	VMC83.477820_-69.542990	83.477820	-69.542990	RRc	18.877	19.369	0.340796900	6.0E-7	2167.62923	18.22	0.03
OGLE-LMC-RRLYR-20023	VMC84.094065_-69.545680	84.094065	-69.545680	RRab	18.947	19.433	0.452966400	3.0E-7	2187.51182	18.33	0.03
OGLE-LMC-RRLYR-19552	VMC83.763360_-69.547090	83.763360	-69.547090	RRe	19.241	19.893	0.370311600	7.0E-7	2167.69892	18.21	0.03
OGLE-LMC-RRLYR-18961	VMC83.388045_-69.546310	83.388045	-69.546310	RRab	18.694	19.377	0.667550200	9.0E-7	2167.74752	17.83	0.03
OGLE-LMC-RRLYR-19669	VMC83.838510_-69.549430	83.838510	-69.549430	RRab	18.912	19.540	0.546935600	6.0E-7	2167.39400	18.20	0.03
OGLE-LMC-RRLYR-18862	VMC83.197305_-69.547060	83.197305	-69.547060	RRab	19.002	19.640	0.523757700	5.0E-7	2167.44483	17.97	0.03
OGLE-LMC-RRLYR-21386	VMC85.153875_-69.546470	85.153875	-69.546470	RRab	19.084	19.951	0.618440500	1.2E-6	2187.62601	17.97	0.03
OGLE-LMC-RRLYR-19149	VMC83.492910_-69.547960	83.492910	-69.547960	RRab	18.765	19.390	0.578968600	1.1E-6	2167.37530	17.94	0.03
OGLE-LMC-RRLYR-18234	VMC82.977390_-69.548910	82.977390	-69.548910	RRab	18.853	19.381	0.535680300	2.0E-7	455.36166	18.13	0.03
OGLE-LMC-RRLYR-22004	VMC85.759125_-69.547880	85.759125	-69.547880	RRc	18.973	19.527	0.353864200	1.0E-6	2187.63936	18.40	0.03
OGLE-LMC-RRLYR-21802	VMC85.546710_-69.550560	85.546710	-69.550560	RRab	19.344	20.293	0.548051800	8.0E-7	2187.32879	18.07	0.03
OGLE-LMC-RRLYR-21722	VMC85.469205_-69.551660	85.469205	-69.551660	RRab	18.533	19.086	0.622004900	1.4E-6	2187.69972	17.85	0.02
OGLE-LMC-RRLYR-18333	VMC83.004750_-69.552720	83.004750	-69.552720	RRab	18.955	19.449	0.505912100	2.0E-7	455.21873	18.26	0.03
OGLE-LMC-RRLYR-18795	VMC83.271570_-69.558850	83.271570	-69.558850	RRab	18.661	19.283	0.599672400	8.0E-7	2167.55330	17.99	0.03
OGLE-LMC-RRLYR-18719	VMC83.228295_-69.559310	83.228295	-69.559310	RRab	18.881	19.504	0.526953400	2.4E-6	2167.77963	18.20	0.04
OGLE-LMC-RRLYR-20125	VMC84.161925_-69.563660	84.161925	-69.563660	RRab	18.642	19.305	0.782180300	2.1E-6	2187.41353	17.79	0.03
OGLE-LMC-RRLYR-19735	VMC83.886585_-69.564030	83.886585	-69.564030	RRab	18.753	19.429	0.653313600	2.5E-6	2167.89110	18.04	0.04
OGLE-LMC-RRLYR-19874	VMC83.988229_-69.564590	83.988229	-69.564590	RRe	18.882	19.211	0.318036100	7.0E-7	2187.52589	18.35	0.04
OGLE-LMC-RRLYR-19453	VMC83.700435_-69.566460	83.700435	-69.566460	RRab	19.324	19.955	0.479549700	6.0E-7	2167.49191	18.43	0.05
OGLE-LMC-RRLYR-19078	VMC83.454945_-69.568410	83.454945	-69.568410	RRab	18.961	19.602	0.577477400	9.0E-7	2167.49297	18.05	0.03
OGLE-LMC-RRLYR-21797	VMC85.543185_-69.569730	85.543185	-69.569730	RRab	18.927	19.673	0.609267400	3.0E-6	2187.29380	17.99	0.03
OGLE-LMC-RRLYR-20581	VMC84.493230_-69.572890	84.493230	-69.572890	RRc	18.613	18.965	0.304455900	2.7E-6	2187.47555	18.25	0.04
OGLE-LMC-RRLYR-19308	VMC83.594385_-69.576040	83.594385	-69.576040	RRab	18.818	19.409	0.563233900	7.0E-7	2167.88393	18.16	0.03
OGLE-LMC-RRLYR-19416	VMC83.673015_-69.576270	83.673015	-69.576270	RRab	18.519	19.139	0.722468600	3.0E-6	2167.74884	17.78	0.03
OGLE-LMC-RRLYR-20849	VMC84.705225_-69.577120	84.705225	-69.577120	RRab	18.683	19.269	0.662088200	1.5E-6	2187.41522	17.81	0.03
OGLE-LMC-RRLYR-18445	VMC83.065815_-69.574910	83.065815	-69.574910	RRab	18.845	19.319	0.469893400	2.0E-7	455.51870	18.26	0.04
OGLE-LMC-RRLYR-19003	VMC83.407425_-69.577370	83.407425	-69.577370	RRe	19.011	19.601	0.342961000	1.0E-6	2167.85120	18.10	0.03
OGLE-LMC-RRLYR-20730	VMC84.629895_-69.580870	84.629895	-69.580870	RRab	18.829	19.442	0.533023100	1.2E-6	2187.56516	17.84	0.05
OGLE-LMC-RRLYR-19478	VMC83.716785_-69.582950	83.716785	-69.582950	RRab	19.354	19.931	0.477685000	7.0E-7	2167.52015	18.58	0.06
OGLE-LMC-RRLYR-21149	VMC84.953550_-69.583120	84.953550	-69.583120	RRab	18.584	19.218	0.685559200	3.7E-6	2187.29704	17.79	0.03
OGLE-LMC-RRLYR-18405	VMC83.045550_-69.581340	83.045550	-69.581340	RRab	18.911	19.481	0.526087300	2.0E-7	455.26900	18.19	0.03
OGLE-LMC-RRLYR-19968	VMC84.057300_-69.582050	84.057300	-69.582050	RRe	19.059	19.479	0.297798300	7.0E-7	2187.67715	18.44	0.05
OGLE-LMC-RRLYR-21485	VMC85.238040_-69.581950	85.238040	-69.581950	RRab	18.998	19.738	0.565901500	1.3E-6	2187.66657	18.02	0.04
OGLE-LMC-RRLYR-21474	VMC85.224705_-69.583210	85.224705	-69.583210	RRc	19.294	19.856	0.310207600	1.9E-6	2187.65788	18.53	0.05

5.6 RR Lyrae stars in the 30 Dor region

133

OGLE-LMC-RRLYR-19971	VMC84.058185	69.587580	84.058185	-69.587580	RRab	18.822	19.348	0.506939500	8.0E-7	2187.57395	18.21	0.04
OGLE-LMC-RRLYR-18941	VMC83.376900	69.586710	83.376900	-69.586710	RRab	18.801	19.385	0.583312200	6.0E-7	2167.32108	18.19	0.04
OGLE-LMC-RRLYR-19494	VMC83.730240	69.588230	83.730240	-69.588230	RRab	18.893	19.606	0.650464300	2.9E-6	2167.78550	17.96	0.03
OGLE-LMC-RRLYR-19949	VMC84.043365	69.588820	84.043365	-69.588820	RRab	18.715	19.275	0.556453000	8.0E-7	2187.50161	18.00	0.03
OGLE-LMC-RRLYR-19513	VMC83.740215	69.589990	83.740215	-69.589990	RRab	18.742	19.312	0.556523600	6.0E-7	2167.40589	18.04	0.03
OGLE-LMC-RRLYR-21773	VMC85.520565	69.582220	85.520565	-69.582220	R Rc	19.048	19.777	0.364411500	1.9E-6	2187.47591	18.16	0.03
OGLE-LMC-RRLYR-19156	VMC83.496435	69.591330	83.496435	-69.591330	RRab	18.787	19.398	0.534289400	1.7E-6	2167.81140	18.16	0.03
OGLE-LMC-RRLYR-18529	VMC83.115855	69.589190	83.115855	-69.589190	RRab	18.872	19.594	0.612508500	5.0E-7	455.21153	18.20	0.04
OGLE-LMC-RRLYR-21430	VMC85.193640	69.589400	85.193640	-69.589400	RRab	19.462	20.565	0.556615200	1.4E-6	2187.22849	18.13	0.04
OGLE-LMC-RRLYR-19714	VMC83.874195	69.592820	83.874195	-69.592820	RRab	18.691	19.259	0.563112200	7.0E-7	2167.76385	17.97	0.04
OGLE-LMC-RRLYR-21811	VMC85.555290	69.589410	85.555290	-69.589410	RRab	18.959	19.674	0.524715500	1.1E-6	2187.66910	18.17	0.03
OGLE-LMC-RRLYR-20712	VMC84.617880	69.594530	84.617880	-69.594530	RRab	19.868	21.119	0.568812100	8.9E-6	2187.73957	18.49	0.04
OGLE-LMC-RRLYR-19051	VMC83.439150	69.593590	83.439150	-69.593590	RRab	18.962	19.745	0.620595100	3.0E-6	2167.46027	18.04	0.03
OGLE-LMC-RRLYR-19007	VMC83.409810	69.595260	83.409810	-69.595260	RRab	19.082	19.830	0.589131200	7.0E-7	2167.55569	18.13	0.03
OGLE-LMC-RRLYR-18480	VMC83.083770	69.594680	83.083770	-69.594680	RRab	18.824	19.385	0.536039600	3.0E-7	455.34646	18.19	0.03
OGLE-LMC-RRLYR-20976	VMC84.814185	69.598240	84.814185	-69.598240	RRab	20.436	21.642	0.508931600	2.6E-6	2187.69729	18.59	0.03
OGLE-LMC-RRLYR-20221	VMC84.233715	69.599510	84.233715	-69.599510	RRab	18.845	19.380	0.535586900	4.0E-7	2187.61494	18.15	0.04
OGLE-LMC-RRLYR-20954	VMC84.790290	69.600450	84.790290	-69.600450	RRab	18.634	19.131	0.578089100	1.2E-6	2187.40467	18.01	0.03
OGLE-LMC-RRLYR-21766	VMC85.516605	69.596690	85.516605	-69.596690	RRab	18.790	19.547	0.657067700	1.1E-6	2187.43861	17.89	0.03
OGLE-LMC-RRLYR-20116	VMC84.154530	69.600250	84.154530	-69.600250	RRab	18.807	19.417	0.573615800	7.0E-7	2187.33791	18.16	0.03
OGLE-LMC-RRLYR-21276	VMC85.071090	69.600930	85.071090	-69.600930	RRab	19.210	20.039	0.535407300	1.5E-6	2187.50725	17.64	0.06
OGLE-LMC-RRLYR-19958	VMC84.048300	69.603700	84.048300	-69.603700	RRab	19.143	19.810	0.562130700	7.0E-7	2187.23364	18.26	0.04
OGLE-LMC-RRLYR-21960	VMC85.714890	69.597150	85.714890	-69.597150	RRab	18.768	19.272	0.608620900	1.1E-6	2187.71358	17.67	0.04
OGLE-LMC-RRLYR-18501	VMC83.099040	69.602580	83.099040	-69.602580	R Rc	18.859	19.250	0.305103500	8.0E-7	455.52352	18.42	0.04
OGLE-LMC-RRLYR-22095	VMC85.860195	69.598420	85.860195	-69.598420	RRab	18.875	19.397	0.499240500	6.0E-7	2187.73820	18.04	0.03
OGLE-LMC-RRLYR-19955	VMC84.046305	69.605500	84.046305	-69.605500	RRab	18.900	19.487	0.611215200	1.7E-6	2187.70003	18.15	0.04
OGLE-LMC-RRLYR-20396	VMC84.361695	69.606120	84.361695	-69.606120	RRab	18.553	19.012	0.472058300	1.5E-6	2187.70366	17.79	0.04
OGLE-LMC-RRLYR-21626	VMC85.366185	69.601490	85.366185	-69.601490	RRab	18.848	19.470	0.580995400	1.8E-6	2187.25724	17.98	0.04
OGLE-LMC-RRLYR-19174	VMC83.506620	69.606660	83.506620	-69.606660	R Rc	18.623	19.220	0.330903100	9.0E-7	2167.71646	17.51	0.06
OGLE-LMC-RRLYR-18829	VMC83.295765	69.606700	83.295765	-69.606700	RRab	18.990	19.480	0.312966600	1.1E-6	2167.84860	18.46	0.04
OGLE-LMC-RRLYR-18709	VMC83.218845	69.605250	83.218845	-69.605250	RRab	18.936	19.561	0.538889400	1.2E-6	2167.77593	18.13	0.04
OGLE-LMC-RRLYR-19069	VMC83.446710	69.607040	83.446710	-69.607040	RRab	19.271	20.000	0.564325200	1.6E-6	2167.67065	18.12	0.04
OGLE-LMC-RRLYR-20410	VMC84.372480	69.611080	84.372480	-69.611080	RRab	18.749	19.415	0.583716600	1.0E-6	2187.38643	18.09	0.03
OGLE-LMC-RRLYR-21484	VMC85.237785	69.610070	85.237785	-69.610070	RRab	19.860	20.802	0.481323200	2.2E-6	2187.54029	18.57	0.04
OGLE-LMC-RRLYR-18381	VMC83.031285	69.608290	83.031285	-69.608290	RRab	18.943	19.655	0.603496200	4.0E-7	455.26818	18.13	0.03
OGLE-LMC-RRLYR-21201	VMC85.006905	69.606850	85.006905	-69.606850	RRab	19.562	20.582	0.619869200	3.6E-6	2187.39938	18.46	0.05
OGLE-LMC-RRLYR-20400	VMC84.363795	69.616010	84.363795	-69.616010	RRab	18.541	19.125	0.735082700	2.3E-6	2187.05451	16.88	0.05
OGLE-LMC-RRLYR-18957	VMC83.387115	69.615580	83.387115	-69.615580	R Rc	19.048	19.534	0.296915400	6.0E-7	2167.71237	18.34	0.04
OGLE-LMC-RRLYR-19418	VMC83.673705	69.616060	83.673705	-69.616060	RRab	18.681	19.329	0.690786100	1.9E-6	2167.53113	17.98	0.03
OGLE-LMC-RRLYR-20264	VMC84.263805	69.620040	84.263805	-69.620040	R Rc	18.838	19.257	0.305861700	6.0E-7	2187.62345	18.33	0.03
OGLE-LMC-RRLYR-21534	VMC85.282325	69.614180	85.282325	-69.614180	RRab	18.933	19.694	0.591204000	2.1E-6	2187.24315	17.73	0.04
OGLE-LMC-RRLYR-19705	VMC83.859675	69.621120	83.859675	-69.621120	RRab	18.924	19.375	0.579749000	1.2E-6	2167.81132	17.59	0.05
OGLE-LMC-RRLYR-19589	VMC83.784345	69.622870	83.784345	-69.622870	RRab	18.736	19.369	0.626270100	1.7E-6	2167.60215	17.97	0.03
OGLE-LMC-RRLYR-19317	VMC83.599740	69.627100	83.599740	-69.627100	R Rc	19.077	19.650	0.340059600	7.0E-7	2167.88085	18.47	0.05
OGLE-LMC-RRLYR-20263	VMC84.262755	69.629080	84.262755	-69.629080	RRab	19.029	19.651	0.531805200	1.1E-6	2187.26022	18.28	0.03
OGLE-LMC-RRLYR-21961	VMC85.716660	69.624630	85.716660	-69.624630	RRab	18.847	19.474	0.579759200	1.6E-6	2187.37987	17.97	0.03
OGLE-LMC-RRLYR-21423	VMC85.187235	69.628640	85.187235	-69.628640	RRab	19.258	99.99	0.673185700	4.9E-6	2187.62189	17.79	0.04
OGLE-LMC-RRLYR-21887	VMC85.641615	69.627220	85.641615	-69.627220	RRab	18.512	19.053	0.639858800	7.0E-7	2187.74721	17.83	0.03
OGLE-LMC-RRLYR-19730	VMC83.888135	69.634410	83.888135	-69.634410	RRab	19.223	19.801	0.461863900	1.0E-6	2167.68048	18.45	0.04
OGLE-LMC-RRLYR-21447	VMC85.204500	69.633080	85.204500	-69.633080	R Rc	19.259	19.807	0.293578100	7.0E-7	2187.53796	18.64	0.04
OGLE-LMC-RRLYR-19771	VMC83.913870	69.637000	83.913870	-69.637000	RRab	19.065	19.770	0.572170600	1.2E-6	2167.54876	18.10	0.03
OGLE-LMC-RRLYR-19960	VMC84.048960	69.638470	84.048960	-69.638470	R Rc	18.968	19.318	0.271653400	1.4E-6	2187.60165	18.63	0.04
OGLE-LMC-RRLYR-21334	VMC85.112370	69.637260	85.112370	-69.637260	R Rc	19.327	19.775	0.276988800	1.3E-6	2187.62589	18.79	0.05
OGLE-LMC-RRLYR-22077	VMC85.840890	69.631540	85.840890	-69.631540	R Rc	18.755	19.134	0.311803800	4.0E-7	2187.52613	18.19	0.03
OGLE-LMC-RRLYR-19295	VMC83.586405	69.642270	83.586405	-69.642270	RRab	18.983	19.593	0.487861000	2.0E-7	456.41949	18.19	0.03
OGLE-LMC-RRLYR-21739	VMC85.490010	69.639020	85.490010	-69.639020	RRab	18.812	19.448	0.612839600	1.5E-6	2187.26744	17.99	0.03
OGLE-LMC-RRLYR-22070	VMC85.834095	69.637480	85.834095	-69.637480	RRab	18.885	19.486	0.525190200	9.0E-7	2187.62464	18.32	0.04
OGLE-LMC-RRLYR-21521	VMC85.273200	69.640700	85.273200	-69.640700	RRab	18.984	19.564	0.531432000	5.0E-7	2187.67864	18.02	0.03

134Data analysis, and first results for RR Lyrae stars from the VMC survey

OGLE-LMC-RRLYR-21700	VMC85.441350	69.640250	85.441350	-69.640250	RRab	18.858	19.497	0.647971800	3.7E-6	2187.25866	18.05	0.03
OGLE-LMC-RRLYR-21669	VMC85.414065	69.638890	85.414065	-69.638890	RRc	18.847	19.343	0.354395100	1.1E-6	2187.75494	18.27	0.03
OGLE-LMC-RRLYR-19712	VMC83.867400	69.642560	83.867400	-69.642560	RRc	18.885	19.370	0.335391100	7.0E-7	2167.80364	18.40	0.04
OGLE-LMC-RRLYR-20511	VMC84.450885	69.648390	84.450885	-69.648390	RRab	19.175	19.889	0.521562000	8.0E-7	2187.45658	18.34	0.05
OGLE-LMC-RRLYR-18397	VMC83.042310	69.644050	83.042310	-69.644050	RRab	18.826	19.505	0.560906800	2.0E-7	455.37974	18.09	0.03
OGLE-LMC-RRLYR-18608	VMC83.166090	69.647080	83.166090	-69.647080	RRab	18.918	19.475	0.532005800	4.0E-7	456.35216	18.09	0.04
OGLE-LMC-RRLYR-19055	VMC83.440860	69.649000	83.440860	-69.649000	RRe	19.102	19.568	0.292002600	9.0E-7	456.51254	18.42	0.05
OGLE-LMC-RRLYR-20402	VMC84.364920	69.650450	84.364920	-69.650450	RRab	19.544	20.295	0.498958800	2.0E-6	2187.70649	18.53	0.05
OGLE-LMC-RRLYR-19488	VMC83.724960	69.651570	83.724960	-69.651570	RRab	18.634	19.193	0.565695800	3.0E-7	456.19507	17.82	0.03
OGLE-LMC-RRLYR-18545	VMC83.120610	69.650400	83.120610	-69.650400	RRc	18.862	19.428	0.326557700	3.0E-7	455.42173	18.14	0.03
OGLE-LMC-RRLYR-18572	VMC83.135460	69.648360	83.135460	-69.648360	RRab	18.734	19.350	0.612755900	3.0E-7	455.50850	17.97	0.03
OGLE-LMC-RRLYR-19605	VMC83.797065	69.652760	83.797065	-69.652760	RRab	18.836	19.446	0.765745800	2.9E-6	2167.78803	17.90	0.03
OGLE-LMC-RRLYR-21743	VMC85.495305	69.650110	85.495305	-69.650110	RRab	18.806	19.390	0.612098900	1.2E-6	2187.29200	17.68	0.05
OGLE-LMC-RRLYR-20702	VMC84.609360	69.655200	84.609360	-69.655200	RRc	19.284	19.997	0.337584600	1.2E-6	2187.53974	18.44	0.06
OGLE-LMC-RRLYR-20651	VMC84.560685	69.655710	84.560685	-69.655710	RRe	19.170	19.667	0.309831000	6.0E-7	2187.62976	18.50	0.04
OGLE-LMC-RRLYR-21590	VMC85.333995	69.652830	85.333995	-69.652830	RRab	18.837	19.409	0.552175800	7.0E-7	2187.51853	18.01	0.04
OGLE-LMC-RRLYR-21391	VMC85.157055	69.653470	85.157055	-69.653470	RRab	18.923	19.493	0.524737600	1.5E-6	2187.61195	18.27	0.03
OGLE-LMC-RRLYR-19011	VMC83.413455	69.658000	83.413455	-69.658000	RRc	19.504	20.074	0.310840900	4.0E-7	456.63216	18.93	0.05
OGLE-LMC-RRLYR-20414	VMC84.373305	69.660920	84.373305	-69.660920	RRab	19.038	19.526	0.479090900	1.8E-6	2187.36361	18.05	0.04
OGLE-LMC-RRLYR-20778	VMC84.663345	69.663570	84.663345	-69.663570	RRab	19.134	19.995	0.629414800	2.7E-6	2187.31413	18.01	0.03
OGLE-LMC-RRLYR-20061	VMC84.122910	69.665180	84.122910	-69.665180	RRab	18.720	19.379	0.639051700	3.2E-6	2187.28669	17.92	0.03
OGLE-LMC-RRLYR-20763	VMC84.652905	69.665090	84.652905	-69.665090	RRab	19.515	20.526	0.559273200	1.1E-6	2187.37904	18.52	0.04
OGLE-LMC-RRLYR-22076	VMC85.840875	69.655460	85.840875	-69.655460	RRab	19.026	19.599	0.468623200	1.3E-6	2187.66724	18.25	0.05
OGLE-LMC-RRLYR-21785	VMC85.529610	69.662200	85.529610	-69.662200	RRab	18.845	19.517	0.650519900	3.2E-6	2187.63232	18.00	0.03
OGLE-LMC-RRLYR-18751	VMC83.248635	69.665060	83.248635	-69.665060	RRab	18.854	19.498	0.565610500	6.0E-7	456.38975	18.08	0.04
OGLE-LMC-RRLYR-20456	VMC84.403140	69.666800	84.403140	-69.666800	RRab	18.889	19.507	0.531347800	7.0E-7	2187.52377	17.96	0.05
OGLE-LMC-RRLYR-19037	VMC83.431980	69.668900	83.431980	-69.668900	RRab	18.782	19.363	0.612251300	6.0E-7	456.28784	18.08	0.04
OGLE-LMC-RRLYR-19497	VMC83.732370	69.673670	83.732370	-69.673670	RRab	19.059	19.816	0.588639100	4.0E-7	456.62578	18.12	0.03
OGLE-LMC-RRLYR-19863	VMC83.977875	69.674910	83.977875	-69.674910	RRab	18.743	19.205	0.564972500	7.0E-7	2187.48618	17.65	0.08
OGLE-LMC-RRLYR-18620	VMC83.172030	69.674140	83.172030	-69.674140	RRab	18.730	19.349	0.586992940	3.0E-7	456.27100	18.06	0.03
OGLE-LMC-RRLYR-21071	VMC84.889980	69.675710	84.889980	-69.675710	RRab	19.001	19.738	0.603032400	2.2E-6	2187.66462	18.12	0.03
OGLE-LMC-RRLYR-20783	VMC84.664200	69.674730	84.664200	-69.674730	RRab	18.994	19.724	0.597993700	1.5E-6	2187.62427	17.92	0.04
OGLE-LMC-RRLYR-18566	VMC83.131995	69.670470	83.131995	-69.670470	RRab	19.178	19.788	0.423186800	2.0E-7	455.52431	18.50	0.04
OGLE-LMC-RRLYR-20197	VMC84.218985	69.674820	84.218985	-69.674820	RRab	18.780	19.219	0.554683200	6.0E-7	2187.32772	17.78	0.04
OGLE-LMC-RRLYR-18326	VMC83.002875	69.675380	83.002875	-69.675380	RRab	18.820	19.478	0.592322500	6.0E-7	455.66084	18.08	0.03
OGLE-LMC-RRLYR-18769	VMC83.257230	69.677950	83.257230	-69.677950	RRe	19.206	19.718	0.296007800	5.0E-7	455.41033	18.67	0.04
OGLE-LMC-RRLYR-20603	VMC84.515025	69.680200	84.515025	-69.680200	RRab	19.092	19.825	0.556062200	9.0E-7	2187.69621	18.14	0.03
OGLE-LMC-RRLYR-18664	VMC83.198025	69.683550	83.198025	-69.683550	RRab	18.691	19.175	0.538663300	5.7E-6	455.5151	17.94	0.03
OGLE-LMC-RRLYR-18383	VMC83.032230	69.683010	83.032230	-69.683010	RRab	18.782	19.378	0.621794500	6.0E-7	455.45882	18.04	0.03
OGLE-LMC-RRLYR-19931	VMC84.031845	69.681820	84.031845	-69.681820	RRab	18.717	19.273	0.611428200	9.0E-7	2187.34144	18.05	0.03
OGLE-LMC-RRLYR-20227	VMC84.239115	69.687220	84.239115	-69.687220	RRab	19.263	19.999	0.627557400	8.6E-6	2222.53707	18.01	0.03
OGLE-LMC-RRLYR-20564	VMC84.483840	69.688990	84.483840	-69.688990	RRab	18.932	19.999	0.569199800	3.7E-6	2260.23830	18.17	0.04
OGLE-LMC-RRLYR-18964	VMC83.388750	69.687980	83.388750	-69.687980	RRab	18.895	19.444	0.505439300	2.0E-7	455.40070	18.60	0.07
OGLE-LMC-RRLYR-21699	VMC85.440045	69.681910	85.440045	-69.681910	RRab	18.759	19.387	0.642617500	2.3E-6	2187.33158	17.93	0.03
OGLE-LMC-RRLYR-18673	VMC83.202075	69.685590	83.202075	-69.685590	RRc	18.831	19.466	0.339399100	5.0E-7	455.41898	18.06	0.04
OGLE-LMC-RRLYR-19873	VMC83.987685	69.681760	83.987685	-69.681760	RRab	19.492	20.313	0.533241600	1.1E-6	2187.76152	18.31	0.03
OGLE-LMC-RRLYR-20328	VMC84.310215	69.679210	84.310215	-69.679210	RRab	18.996	19.651	0.585350200	2.7E-6	2187.51016	17.88	0.05
OGLE-LMC-RRLYR-18379	VMC83.029860	69.688140	83.029860	-69.688140	RRab	18.848	19.237	0.562611100	2.0E-7	455.58906	17.63	0.03
OGLE-LMC-RRLYR-19791	VMC83.930235	69.691980	83.930235	-69.691980	RRab	18.752	19.303	0.518580200	1.0E-6	726.66349	17.78	0.05
OGLE-LMC-RRLYR-21145	VMC84.949860	69.687650	84.949860	-69.687650	RRab	19.046	19.999	0.472952000	2.6E-6	2222.74237	18.20	0.04
OGLE-LMC-RRLYR-21839	VMC85.580100	69.690170	85.580100	-69.690170	RRc	18.760	19.262	0.361855100	7.0E-7	2187.43880	18.13	0.03
OGLE-LMC-RRLYR-19205	VMC83.527725	69.697020	83.527725	-69.697020	RRab	18.967	19.584	0.527220400	6.0E-7	455.41475	18.29	0.03
OGLE-LMC-RRLYR-21473	VMC85.224345	69.692640	85.224345	-69.692640	RRab	18.839	19.413	0.503534200	6.0E-7	2187.63515	18.11	0.03
OGLE-LMC-RRLYR-21718	VMC85.462890	69.696240	85.462890	-69.696240	RRe	18.930	19.418	0.339869400	1.0E-6	2187.56553	18.32	0.03
OGLE-LMC-RRLYR-19141	VMC83.488470	69.698340	83.488470	-69.698340	RRe	19.063	19.453	0.253287200	2.0E-7	455.63310	18.45	0.04
OGLE-LMC-RRLYR-21452	VMC85.207230	69.698690	85.207230	-69.698690	RRab	19.485	20.427	0.517663700	1.2E-6	2187.73058	18.19	0.03
OGLE-LMC-RRLYR-20106	VMC84.147375	69.703520	84.147375	-69.703520	RRc	18.896	20.658	0.291316000	5.0E-7	726.59408	18.89	0.05
OGLE-LMC-RRLYR-21587	VMC85.331775	69.699600	85.331775	-69.699600	RRab	19.015	19.533	0.463729600	5.0E-7	2187.49025	18.10	0.06

5.6 RR Lyrae stars in the 30 Dor region

135

OGLE-LMC-RRLYR-20188	VMC84.212745	-69.705900	84.212745	-69.705900	RRab	19.236	19.992	0.540591300	4.0E-7	726.40634	18.30	0.03
OGLE-LMC-RRLYR-20345	VMC84.321795	-69.704400	84.321795	-69.704400	RRab	19.351	20.240	0.555803900	6.0E-7	726.60473	18.19	0.03
OGLE-LMC-RRLYR-22111	VMC85.873620	-69.698330	85.873620	-69.698330	RRab	18.618	19.188	0.566775400	6.0E-7	2187.27818	17.98	0.03
OGLE-LMC-RRLYR-20412	VMC84.372855	-69.706330	84.372855	-69.706330	RRab	19.104	19.973	0.627752100	6.0E-7	726.23220	18.18	0.04
OGLE-LMC-RRLYR-19529	VMC83.748705	-69.708760	83.748705	-69.708760	RRab	18.730	19.275	0.409358600	4.0E-7	455.62775	17.95	0.03
OGLE-LMC-RRLYR-18344	VMC83.014470	-69.703020	83.014470	-69.703020	RRab	18.775	19.207	0.479610200	2.0E-7	455.57989	18.21	0.03
OGLE-LMC-RRLYR-18469	VMC83.079150	-69.704260	83.079150	-69.704260	RRab	18.714	19.407	0.652128900	1.1E-6	455.60963	17.71	0.04
OGLE-LMC-RRLYR-21368	VMC85.140840	-69.708380	85.140840	-69.708380	RRc	18.846	19.301	0.313632700	5.0E-7	2187.68912	18.40	0.04
OGLE-LMC-RRLYR-21189	VMC84.992805	-69.708970	84.992805	-69.708970	RRab	19.170	20.072	0.752155200	2.7E-5	2187.18932	17.93	0.04
OGLE-LMC-RRLYR-19278	VMC83.575755	-69.709910	83.575755	-69.709910	RRab	18.717	19.246	0.549089400	2.0E-7	455.53171	18.13	0.04
OGLE-LMC-RRLYR-18370	VMC83.027640	-69.706910	83.027640	-69.706910	RRab	18.830	19.283	0.523025700	4.0E-7	455.29615	18.07	0.04
OGLE-LMC-RRLYR-21213	VMC85.019880	-69.710540	85.019880	-69.710540	RRab	19.436	19.947	0.358494900	1.6E-6	2187.70675	18.66	0.05
OGLE-LMC-RRLYR-18257	VMC82.982400	-69.709040	82.982400	-69.709040	RRab	18.826	19.284	0.521167800	2.0E-7	455.25854	18.07	0.04
OGLE-LMC-RRLYR-19784	VMC83.926095	-69.712840	83.926095	-69.712840	RRab	19.045	19.747	0.550895300	2.0E-7	726.67604	18.24	0.05
OGLE-LMC-RRLYR-18976	VMC83.393610	-69.712590	83.393610	-69.712590	RRab	18.824	19.398	0.587151400	4.0E-7	455.61211	18.04	0.03
OGLE-LMC-RRLYR-21798	VMC85.543770	-69.709170	85.543770	-69.709170	RRab	18.806	19.457	0.553898100	7.0E-7	2187.61362	17.71	0.09
OGLE-LMC-RRLYR-21642	VMC85.385670	-69.710840	85.385670	-69.710840	RRab	18.819	19.384	0.569320900	8.0E-7	2187.65779	17.83	0.04
OGLE-LMC-RRLYR-18771	VMC83.258865	-69.710530	83.258865	-69.710530	RRc	18.779	19.389	0.410654600	8.0E-7	455.51904	18.17	0.03
OGLE-LMC-RRLYR-20026	VMC84.095895	-69.717950	84.095895	-69.717950	RRc	19.137	19.689	0.294476200	3.0E-7	726.72019	18.76	0.06
OGLE-LMC-RRLYR-19748	VMC83.898885	-69.718170	83.898885	-69.718170	RRab	18.632	19.212	0.639370700	4.0E-7	726.79731	17.89	0.03
OGLE-LMC-RRLYR-21417	VMC85.181160	-69.717110	85.181160	-69.717110	RRc	19.601	20.644	0.312884600	1.4E-6	2187.74646	18.40	0.04
OGLE-LMC-RRLYR-20140	VMC84.169245	-69.719290	84.169245	-69.719290	RRc	18.631	19.166	0.385329600	8.0E-7	726.81190	17.96	0.03
OGLE-LMC-RRLYR-22092	VMC85.858965	-69.715890	85.858965	-69.715890	RRab	19.205	20.315	0.638332800	5.4E-6	2187.71975	18.02	0.03
OGLE-LMC-RRLYR-21730	VMC85.482000	-69.717450	85.482000	-69.717450	RRab	18.860	19.371	0.512881500	6.0E-7	2187.39620	18.23	0.03
OGLE-LMC-RRLYR-20466	VMC84.410865	-69.723910	84.410865	-69.723910	RRc	19.531	20.367	0.334787200	8.0E-7	726.76740	18.45	0.04
OGLE-LMC-RRLYR-20630	VMC84.543165	-69.723730	84.543165	-69.723730	RRab	19.033	19.790	0.588010200	1.8E-6	2187.45390	17.94	0.05
OGLE-LMC-RRLYR-18453	VMC83.072505	-69.721610	83.072505	-69.721610	RRab	18.704	19.232	0.548498000	6.0E-7	455.34849	17.72	0.05
OGLE-LMC-RRLYR-19558	VMC83.766375	-69.725630	83.766375	-69.725630	RRab	19.039	19.608	0.525451500	4.0E-7	455.35194	18.38	0.04
OGLE-LMC-RRLYR-18765	VMC83.255850	-69.721230	83.255850	-69.721230	RRab	18.951	19.562	0.549932800	4.0E-7	455.63485	18.43	0.04
OGLE-LMC-RRLYR-18778	VMC83.263995	-69.722990	83.263995	-69.722990	RRab	18.511	18.850	0.695893900	9.0E-7	455.44490	17.62	0.03
OGLE-LMC-RRLYR-20683	VMC84.592530	-69.722200	84.592530	-69.722200	RRab	19.119	19.775	0.548011600	1.5E-6	2187.69771	18.11	0.03
OGLE-LMC-RRLYR-19102	VMC83.468910	-69.722310	83.468910	-69.722310	RRab	18.630	19.036	0.375915200	1.1E-6	455.43941	18.09	0.03
OGLE-LMC-RRLYR-19957	VMC84.048075	-69.728080	84.048075	-69.728080	RRab	18.761	19.414	0.661394700	1.9E-6	726.72565	18.00	0.04
OGLE-LMC-RRLYR-21387	VMC85.154100	-69.726880	85.154100	-69.726880	RRab	19.448	20.438	0.627258700	2.1E-6	2187.22750	18.14	0.04
OGLE-LMC-RRLYR-18369	VMC83.027415	-69.728390	83.027415	-69.728390	RRab	18.872	19.417	0.519211500	2.0E-7	455.34173	18.34	0.04
OGLE-LMC-RRLYR-22006	VMC85.760145	-69.725780	85.760145	-69.725780	RRab	19.222	20.001	0.547579200	1.2E-6	2187.50103	18.23	0.03
OGLE-LMC-RRLYR-20012	VMC84.086055	-69.731710	84.086055	-69.731710	RRab	19.103	19.766	0.491957800	2.0E-7	726.38152	18.12	0.04
OGLE-LMC-RRLYR-19365	VMC83.628390	-69.732600	83.628390	-69.732600	RRab	18.718	19.339	0.626064100	4.0E-7	455.47302	17.99	0.04
OGLE-LMC-RRLYR-21919	VMC85.673235	-69.728360	85.673235	-69.728360	RRab	19.053	19.871	0.634019900	1.7E-6	2187.25810	18.05	0.03
OGLE-LMC-RRLYR-20927	VMC84.766890	-69.733920	84.766890	-69.733920	RRc	19.192	19.758	0.300887000	8.0E-7	2187.76540	18.45	0.04
OGLE-LMC-RRLYR-19663	VMC83.832990	-69.733000	83.832990	-69.733000	RRab	19.102	19.696	0.524575700	4.0E-7	726.51630	18.42	0.04
OGLE-LMC-RRLYR-21747	VMC85.496580	-69.733620	85.496580	-69.733620	RRab	18.732	19.257	0.515246800	7.0E-7	2187.38400	18.00	0.03
OGLE-LMC-RRLYR-22057	VMC85.826175	-69.731870	85.826175	-69.731870	RRab	18.708	19.317	0.577003700	8.0E-7	2187.29804	17.88	0.03
OGLE-LMC-RRLYR-19847	VMC83.969115	-69.739600	83.969115	-69.739600	RRab	19.188	19.925	0.558837700	6.0E-7	726.81255	18.29	0.03
OGLE-LMC-RRLYR-21237	VMC85.037085	-69.739300	85.037085	-69.739300	RRc	18.858	19.786	0.356067600	3.0E-6	2187.53282	17.44	0.02
OGLE-LMC-RRLYR-21284	VMC85.074315	-69.739670	85.074315	-69.739670	RRab	18.793	19.382	0.553133300	7.0E-7	2187.45546	17.90	0.03
OGLE-LMC-RRLYR-20658	VMC84.573750	-69.742790	84.573750	-69.742790	RRab	19.043	19.967	0.760583600	9.3E-6	2187.72849	17.95	0.02
OGLE-LMC-RRLYR-19355	VMC83.621025	-69.742980	83.621025	-69.742980	RRab	18.910	19.573	0.578060900	7.0E-7	455.56928	18.28	0.04
OGLE-LMC-RRLYR-19163	VMC83.500320	-69.744700	83.500320	-69.744700	RRab	18.786	19.335	0.551811500	2.0E-7	455.16594	18.18	0.03
OGLE-LMC-RRLYR-20611	VMC84.524400	-69.746230	84.524400	-69.746230	RRc	19.360	19.982	0.304751900	1.3E-6	2187.76799	18.87	0.05
OGLE-LMC-RRLYR-19160	VMC83.498250	-69.745600	83.498250	-69.745600	RRab	18.880	19.425	0.508030100	2.0E-7	455.42271	18.26	0.03
OGLE-LMC-RRLYR-18513	VMC83.105265	-69.743980	83.105265	-69.743980	RRab	18.937	19.610	0.642766600	1.3E-6	455.26412	18.01	0.04
OGLE-LMC-RRLYR-21101	VMC84.911955	-69.740510	84.911955	-69.740510	RRc	18.749	19.120	0.351167500	8.0E-7	2187.55731	17.92	0.05
OGLE-LMC-RRLYR-20086	VMC84.136650	-69.749340	84.136650	-69.749340	RRab	19.000	19.727	0.552563200	4.0E-7	726.71347	18.19	0.03
OGLE-LMC-RRLYR-19927	VMC84.028905	-69.750130	84.028905	-69.750130	RRab	18.768	19.314	0.551053700	4.0E-7	726.53031	18.11	0.03
OGLE-LMC-RRLYR-20739	VMC84.636585	-69.750360	84.636585	-69.750360	RRab	18.933	19.622	0.576238300	1.0E-6	2187.38183	18.14	0.03
OGLE-LMC-RRLYR-20364	VMC84.338685	-69.749770	84.338685	-69.749770	RRab	19.411	20.331	0.487577100	3.0E-7	726.49189	18.34	0.03
OGLE-LMC-RRLYR-18854	VMC83.317995	-69.749230	83.317995	-69.749230	RRe	18.201	18.212	0.286473700	6.0E-7	455.53905	18.20	0.04

136 Data analysis, and first results for RR Lyrae stars from the VMC survey

OGLE-LMC-RRLYR-18704	VMC83.217210	69.743200	83.217210	-69.743200	RRab	18.691	19.319	0.592128100	3.0E-7	455.48895	17.75	0.04
OGLE-LMC-RRLYR-21865	VMC85.606335	69.745170	85.606335	-69.745170	RRab	18.716	19.323	0.563064900	1.1E-6	2187.63346	17.87	0.03
OGLE-LMC-RRLYR-21812	VMC85.557285	69.745260	85.557285	-69.745260	RRab	18.907	19.442	0.479509800	7.0E-7	2187.53085	18.22	0.04
OGLE-LMC-RRLYR-19352	VMC83.620065	69.748270	83.620065	-69.748270	RRab	18.795	19.417	0.579655200	3.0E-7	455.28283	18.14	0.04
OGLE-LMC-RRLYR-21843	VMC85.585110	69.748600	85.585110	-69.748600	RRab	18.944	19.532	0.516924000	4.0E-7	2187.60251	18.44	0.04
OGLE-LMC-RRLYR-19315	VMC83.598735	69.756080	83.598735	-69.756080	R Rc	18.855	19.404	0.396497200	6.0E-7	455.62297	18.25	0.03
OGLE-LMC-RRLYR-19348	VMC83.618265	69.756270	83.618265	-69.756270	RRab	18.850	19.376	0.367949400	4.0E-7	455.67866	18.22	0.04
OGLE-LMC-RRLYR-18697	VMC83.213850	69.755050	83.213850	-69.755050	RRab	18.927	19.603	0.629352300	9.0E-7	455.57487	18.17	0.03
OGLE-LMC-RRLYR-18866	VMC83.325750	69.760120	83.325750	-69.760120	RRab	18.587	19.174	0.580332200	4.0E-7	455.28814	17.79	0.03
OGLE-LMC-RRLYR-20613	VMC84.525360	69.762040	84.525360	-69.762040	RRab	19.191	19.967	0.582558800	1.5E-6	2187.59901	18.15	0.03
OGLE-LMC-RRLYR-18173	VMC82.950495	69.755840	82.950495	-69.755840	RRab	18.770	19.412	0.593782800	7.0E-7	455.55236	18.02	0.04
OGLE-LMC-RRLYR-19757	VMC83.905620	69.765090	83.905620	-69.765090	RRab	18.608	19.226	0.652045800	4.0E-7	726.57868	17.96	0.03
OGLE-LMC-RRLYR-21264	VMC85.065480	69.763520	85.065480	-69.763520	RRab	19.104	19.875	0.465595400	7.0E-7	2187.39389	18.15	0.03
OGLE-LMC-RRLYR-19147	VMC83.491725	69.763920	83.491725	-69.763920	RRab	18.438	19.082	0.780936100	2.8E-6	455.45774	17.53	0.03
OGLE-LMC-RRLYR-18763	VMC83.255160	69.764670	83.255160	-69.764670	RRab	18.724	19.177	0.553127000	2.0E-7	455.27871	17.91	0.04
OGLE-LMC-RRLYR-21502	VMC85.250415	69.765020	85.250415	-69.765020	RRab	18.854	19.605	0.596208100	1.4E-6	2187.35888	17.58	0.06
OGLE-LMC-RRLYR-19521	VMC83.747160	69.768940	83.747160	-69.768940	R Rc	18.674	19.529	0.319459300	4.0E-7	726.60135	17.88	0.04
OGLE-LMC-RRLYR-21853	VMC85.597215	69.765240	85.597215	-69.765240	RRab	18.833	19.433	0.585710700	1.7E-6	2187.24206	17.95	0.03
OGLE-LMC-RRLYR-21421	VMC85.183845	69.763850	85.183845	-69.763850	RRab	19.365	99.99	0.612821100	2.0E-6	2187.59881	17.26	0.09
OGLE-LMC-RRLYR-18754	VMC83.249745	69.770880	83.249745	-69.770880	RRab	18.988	19.796	0.666125200	4.0E-7	455.27137	17.94	0.03
OGLE-LMC-RRLYR-18204	VMC82.967310	69.769660	82.967310	-69.769660	RRab	19.166	19.842	0.545211500	2.0E-7	455.24373	18.34	0.04
OGLE-LMC-RRLYR-19839	VMC83.960100	69.775210	83.960100	-69.775210	RRab	19.084	19.798	0.514121600	4.0E-7	726.48513	18.00	0.06
OGLE-LMC-RRLYR-20710	VMC84.616635	69.775730	84.616635	-69.775730	RRab	18.849	19.526	0.624987000	1.1E-6	2187.66247	17.92	0.04
OGLE-LMC-RRLYR-21321	VMC85.102605	69.775730	85.102605	-69.775730	RRab	19.051	19.724	0.491292200	4.0E-7	2187.49795	18.22	0.04
OGLE-LMC-RRLYR-21734	VMC85.483815	69.772810	85.483815	-69.772810	R Rc	19.230	19.785	0.305065400	8.0E-7	2187.47773	18.49	0.05
OGLE-LMC-RRLYR-20691	VMC84.600270	69.776540	84.600270	-69.776540	RRab	19.554	20.463	0.551247800	4.1E-6	2187.68012	18.54	0.05
OGLE-LMC-RRLYR-18289	VMC82.989825	69.775640	82.989825	-69.775640	RRab	18.849	19.386	0.524173500	2.0E-7	455.17774	18.18	0.04
OGLE-LMC-RRLYR-21737	VMC85.486965	69.774770	85.486965	-69.774770	RRab	18.841	19.436	0.583427500	9.0E-7	2187.66656	18.07	0.03
OGLE-LMC-RRLYR-20751	VMC84.646965	69.780080	84.646965	-69.780080	RRab	18.477	19.011	0.644630800	5.0E-7	2187.38003	17.65	0.03
OGLE-LMC-RRLYR-19567	VMC83.769720	69.780990	83.769720	-69.780990	RRab	18.751	19.405	0.607959500	8.0E-7	455.59976	17.86	0.03
OGLE-LMC-RRLYR-20576	VMC84.491655	69.781690	84.491655	-69.781690	R Rc	19.089	19.727	0.330475300	1.0E-6	2187.74356	18.02	0.04
OGLE-LMC-RRLYR-19578	VMC83.778570	69.777580	83.778570	-69.777580	RRab	19.064	19.758	0.546648500	4.0E-7	455.16873	18.06	0.03
OGLE-LMC-RRLYR-20379	VMC84.346935	69.786110	84.346935	-69.786110	RRab	19.810	20.950	0.539316700	7.0E-7	726.73022	18.35	0.03
OGLE-LMC-RRLYR-20045	VMC84.111300	69.784970	84.111300	-69.784970	RRab	19.249	20.223	0.738833700	3.7E-6	726.59152	17.89	0.03
OGLE-LMC-RRLYR-21395	VMC85.161555	69.786090	85.161555	-69.786090	RRab	19.157	19.914	0.571204000	2.0E-6	2187.51133	18.18	0.03
OGLE-LMC-RRLYR-21472	VMC85.224105	69.790600	85.224105	-69.790600	RRab	19.465	20.484	0.579536400	2.0E-6	2187.58943	18.26	0.03
OGLE-LMC-RRLYR-19545	VMC83.760975	69.789120	83.760975	-69.789120	RRab	18.792	19.376	0.559871100	2.0E-7	455.60392	18.16	0.03
OGLE-LMC-RRLYR-19349	VMC83.618895	69.792260	83.618895	-69.792260	R Rc	18.953	19.392	0.303837300	3.0E-7	455.58665	18.55	0.05
OGLE-LMC-RRLYR-18892	VMC83.343315	69.788850	83.343315	-69.788850	RRab	19.011	19.716	0.621094600	1.3E-6	455.37556	17.92	0.05
OGLE-LMC-RRLYR-18687	VMC83.208840	69.790950	83.208840	-69.790950	RRab	18.812	19.467	0.624974500	1.0E-6	455.62631	18.03	0.03
OGLE-LMC-RRLYR-19128	VMC83.479800	69.791530	83.479800	-69.791530	RRab	18.747	19.288	0.605138700	3.0E-7	455.41531	18.12	0.03
OGLE-LMC-RRLYR-21814	VMC85.558185	69.790330	85.558185	-69.790330	RRab	18.905	19.443	0.517321500	1.3E-6	2187.44669	18.24	0.03
OGLE-LMC-RRLYR-20681	VMC84.591540	69.795940	84.591540	-69.795940	RRab	18.846	19.562	0.656909900	5.3E-6	2187.66645	17.96	0.03
OGLE-LMC-RRLYR-18896	VMC83.344695	69.802450	83.344695	-69.802450	R Rc	18.818	19.302	0.354180900	1.1E-6	455.58309	18.22	0.04
OGLE-LMC-RRLYR-20425	VMC84.378900	69.806200	84.378900	-69.806200	RRab	19.592	20.845	0.561129300	7.0E-7	726.52190	18.16	0.03
OGLE-LMC-RRLYR-20358	VMC84.333705	69.806840	84.333705	-69.806840	RRab	19.576	20.678	0.488860100	5.0E-7	726.82267	17.68	0.04
OGLE-LMC-RRLYR-19240	VMC83.552415	69.805980	83.552415	-69.805980	RRab	18.977	19.753	0.672490200	8.0E-7	456.19065	18.11	0.03
OGLE-LMC-RRLYR-19775	VMC83.919195	69.806540	83.919195	-69.806540	RRab	18.842	19.571	0.615988400	5.0E-7	726.67900	18.04	0.03
OGLE-LMC-RRLYR-20229	VMC84.239775	69.808410	84.239775	-69.808410	RRab	18.451	19.119	0.755386500	9.0E-7	726.45269	17.60	0.03
OGLE-LMC-RRLYR-18408	VMC83.047995	69.806660	83.047995	-69.806660	RRab	19.105	19.606	0.428174400	2.0E-7	455.65508	18.41	0.03
OGLE-LMC-RRLYR-20016	VMC84.087555	69.808680	84.087555	-69.808680	RRab	18.923	19.465	0.518857700	3.0E-7	726.60768	18.29	0.03
OGLE-LMC-RRLYR-21612	VMC85.352445	69.799130	85.352445	-69.799130	RRab	19.406	19.932	0.508986600	2.0E-6	2187.71837	18.64	0.04
OGLE-LMC-RRLYR-21583	VMC85.328865	69.808450	85.328865	-69.808450	RRab	19.510	20.450	0.602398900	2.9E-6	2187.67292	18.15	0.03
OGLE-LMC-RRLYR-18348	VMC83.016465	69.807440	83.016465	-69.807440	R Rc	18.828	19.342	0.355733700	4.0E-7	455.44041	18.00	0.03
OGLE-LMC-RRLYR-20510	VMC84.450660	69.813110	84.450660	-69.813110	R Rc	19.054	19.734	0.357058500	7.0E-7	726.64130	18.39	0.04
OGLE-LMC-RRLYR-21424	VMC85.187550	69.812950	85.187550	-69.812950	RRab	19.689	20.683	0.318481000	1.4E-6	2187.48957	18.48	0.04
OGLE-LMC-RRLYR-20479	VMC84.424215	69.816090	84.424215	-69.816090	RRab	18.882	19.547	0.540847900	3.0E-7	726.50966	17.99	0.03
OGLE-LMC-RRLYR-19814	VMC83.948655	69.819220	83.948655	-69.819220	R Rc	18.758	19.263	0.355872600	3.0E-7	726.48302	17.97	0.03

5.6 RR Lyrae stars in the 30 Dor region

137

OGLE-LMC-RRLYR-18870	VMC83.327985	69.813560	83.327985	-69.813560	RRc	18.915	19.393	0.318512900	3.0E-7	455.43451	18.45	0.03
OGLE-LMC-RRLYR-20831	VMC84.693780	69.820860	84.693780	-69.820860	RRab	19.040	19.652	0.508578500	3.0E-7	726.59762	18.21	0.04
OGLE-LMC-RRLYR-22002	VMC85.757745	69.815300	85.757745	-69.815300	RRab	19.159	19.911	0.567584700	1.6E-6	2187.33625	18.16	0.04
OGLE-LMC-RRLYR-19075	VMC83.452890	69.817170	83.452890	-69.817170	RRab	19.019	19.803	0.580979400	4.0E-7	455.67855	18.19	0.04
OGLE-LMC-RRLYR-19239	VMC83.551755	69.821220	83.551755	-69.821220	RRab	19.061	19.825	0.588855200	7.0E-7	456.39940	18.33	0.05
OGLE-LMC-RRLYR-19082	VMC83.456655	69.821270	83.456655	-69.821270	RRab	18.468	19.044	0.606470500	2.0E-7	455.59494	17.80	0.03
OGLE-LMC-RRLYR-18623	VMC83.172525	69.819670	83.172525	-69.819670	RRab	19.043	19.598	0.496626000	4.0E-7	455.68368	18.25	0.04
OGLE-LMC-RRLYR-20577	VMC84.491850	69.825000	84.491850	-69.825000	RRab	19.093	19.589	0.469548600	2.0E-7	726.64561	18.37	0.04
OGLE-LMC-RRLYR-19862	VMC83.975355	69.825040	83.975355	-69.825040	RRe	19.576	20.031	0.22527900	4.0E-7	726.81151	19.23	0.09
OGLE-LMC-RRLYR-18493	VMC83.094105	69.820140	83.094105	-69.820140	RRc	18.820	19.230	0.350782800	7.0E-7	455.50053	18.18	0.03
OGLE-LMC-RRLYR-20262	VMC84.262425	69.822320	84.262425	-69.822320	RRab	19.188	20.149	0.632352800	1.4E-6	726.55826	18.07	0.03
OGLE-LMC-RRLYR-20201	VMC84.224085	69.825500	84.224085	-69.825500	RRab	19.112	19.969	0.541253800	3.0E-7	726.50759	18.05	0.04
OGLE-LMC-RRLYR-19703	VMC83.858850	69.827140	83.858850	-69.827140	RRab	19.045	19.762	0.569479600	3.0E-7	726.43579	18.19	0.03
OGLE-LMC-RRLYR-19759	VMC83.906475	69.826410	83.906475	-69.826410	RRab	19.012	19.600	0.495096600	2.0E-7	726.66792	18.20	0.03
OGLE-LMC-RRLYR-20087	VMC84.136740	69.829260	84.136740	-69.829260	RRab	18.780	19.239	0.590565700	8.0E-7	726.61962	16.91	0.04
OGLE-LMC-RRLYR-20292	VMC84.283020	69.828990	84.283020	-69.828990	RRab	19.278	20.165	0.564464500	5.0E-7	726.50303	18.26	0.03
OGLE-LMC-RRLYR-18481	VMC83.084640	69.826750	83.084640	-69.826750	RRab	18.658	19.333	0.641868700	8.0E-7	455.10981	18.08	0.03
OGLE-LMC-RRLYR-19901	VMC84.009765	69.834260	84.009765	-69.834260	RRab	18.836	19.535	0.646936100	5.0E-7	726.32662	18.04	0.03
OGLE-LMC-RRLYR-22125	VMC85.892835	69.825840	85.892835	-69.825840	RRab	18.944	19.638	0.564646000	7.0E-7	2187.48558	18.25	0.03
OGLE-LMC-RRLYR-20742	VMC84.637755	69.837110	84.637755	-69.837110	RRc	19.253	19.792	0.271386100	3.0E-7	726.67670	18.69	0.04
OGLE-LMC-RRLYR-19334	VMC83.611290	69.837380	83.611290	-69.837380	RRab	19.098	19.872	0.647521400	1.4E-6	455.11800	18.05	0.03
OGLE-LMC-RRLYR-18916	VMC83.360235	69.831830	83.360235	-69.831830	RRab	18.823	19.527	0.634512800	1.3E-6	455.62351	17.89	0.03
OGLE-LMC-RRLYR-20762	VMC84.652485	69.834060	84.652485	-69.834060	RRab	19.314	20.122	0.354203900	2.0E-6	726.49752	18.46	0.04
OGLE-LMC-RRLYR-21099	VMC84.910665	69.839930	84.910665	-69.839930	RRc	19.193	19.414	0.336962900	1.1E-6	726.66886	17.91	0.06
OGLE-LMC-RRLYR-19721	VMC83.877555	69.842230	83.877555	-69.842230	RRab	18.485	19.104	0.705742500	4.0E-7	726.37315	17.66	0.03
OGLE-LMC-RRLYR-20557	VMC84.481455	69.845000	84.481455	-69.845000	RRab	18.548	19.197	0.724680800	1.0E-6	726.74826	17.56	0.03
OGLE-LMC-RRLYR-20041	VMC84.107835	69.848290	84.107835	-69.848290	RRe	19.476	19.881	0.247755100	4.0E-7	726.63404	19.02	0.05
OGLE-LMC-RRLYR-19005	VMC83.407950	69.847140	83.407950	-69.847140	RRab	18.986	19.659	0.523465200	3.0E-7	455.47900	18.47	0.04
OGLE-LMC-RRLYR-20820	VMC84.687090	69.841900	84.687090	-69.841900	RRab	19.419	20.081	0.587034600	1.1E-6	726.32483	17.99	0.04
OGLE-LMC-RRLYR-21025	VMC84.855060	69.848230	84.855060	-69.848230	RRab	19.218	20.087	0.548441100	1.7E-6	726.37283	18.12	0.03
OGLE-LMC-RRLYR-20182	VMC84.203205	69.850980	84.203205	-69.850980	RRab	18.758	19.372	0.625826800	8.0E-7	726.48512	17.93	0.03
OGLE-LMC-RRLYR-18377	VMC83.029470	69.844830	83.029470	-69.844830	RRab	18.764	19.206	0.547653700	2.0E-7	455.43524	18.05	0.03
OGLE-LMC-RRLYR-18214	VMC82.970415	69.843600	82.970415	-69.843600	RRab	18.682	19.187	0.564651300	2.0E-7	455.45351	17.80	0.05
OGLE-LMC-RRLYR-19657	VMC83.827875	69.853320	83.827875	-69.853320	RRab	18.687	19.500	0.839594400	1.9E-6	726.41027	17.69	0.02
OGLE-LMC-RRLYR-19001	VMC83.406990	69.851550	83.406990	-69.851550	RRab	18.662	19.226	0.598744400	4.0E-7	455.31659	18.10	0.03
OGLE-LMC-RRLYR-20200	VMC84.223470	69.854910	84.223470	-69.854910	RRab	18.845	19.503	0.562713100	4.0E-7	726.46898	17.92	0.04
OGLE-LMC-RRLYR-19611	VMC83.802960	69.855990	83.802960	-69.855990	RRab	19.437	20.429	0.565717300	1.3E-6	726.54055	18.20	0.03
OGLE-LMC-RRLYR-22110	VMC85.872345	69.847320	85.872345	-69.847320	RRab	18.670	19.298	0.618954900	2.1E-6	2187.56411	17.88	0.03
OGLE-LMC-RRLYR-19870	VMC83.982360	69.856180	83.982360	-69.856180	RRab	18.971	19.539	0.465149400	7.0E-7	726.81466	18.33	0.03
OGLE-LMC-RRLYR-21994	VMC85.750050	69.849570	85.750050	-69.849570	RRab	18.442	18.972	0.510484200	4.0E-7	2187.35071	17.74	0.03
OGLE-LMC-RRLYR-19161	VMC83.498565	69.856850	83.498565	-69.856850	RRab	19.102	19.902	0.563206600	3.0E-7	455.17703	18.25	0.03
OGLE-LMC-RRLYR-20144	VMC84.174450	69.857280	84.174450	-69.857280	RRc	18.846	19.267	0.300103500	4.0E-7	726.80218	18.37	0.03
OGLE-LMC-RRLYR-21896	VMC85.653375	69.853430	85.653375	-69.853430	RRab	18.076	18.529	0.662613900	4.0E-6	2187.55522	17.55	0.03
OGLE-LMC-RRLYR-19404	VMC83.662770	69.859140	83.662770	-69.859140	RRab	18.973	19.488	0.456243600	3.0E-7	455.26726	18.38	0.03
OGLE-LMC-RRLYR-22096	VMC85.860765	69.851360	85.860765	-69.851360	RRc	18.999	19.622	0.341981400	1.0E-6	2187.68206	18.41	0.03
OGLE-LMC-RRLYR-21449	VMC85.205025	69.852970	85.205025	-69.852970	RRab	18.619	19.213	0.652459900	2.8E-6	2187.69031	17.88	0.03
OGLE-LMC-RRLYR-19103	VMC83.470005	69.860840	83.470005	-69.860840	RRab	18.621	19.460	0.759015800	1.7E-6	455.00094	17.57	0.03
OGLE-LMC-RRLYR-20066	VMC84.124635	69.862950	84.124635	-69.862950	RRab	19.102	19.929	0.623734100	1.9E-6	726.24076	18.07	0.03
OGLE-LMC-RRLYR-19482	VMC83.720355	69.864500	83.720355	-69.864500	RRe	19.086	19.625	0.297571600	5.0E-7	455.69637	18.46	0.05
OGLE-LMC-RRLYR-20015	VMC84.087480	69.863570	84.087480	-69.863570	RRab	18.953	19.450	0.485577000	1.0E-6	726.66959	18.26	0.04
OGLE-LMC-RRLYR-18207	VMC82.968240	69.859750	82.968240	-69.859750	RRab	18.703	19.221	0.560011600	6.0E-7	455.29203	18.19	0.04
OGLE-LMC-RRLYR-22061	VMC85.828005	69.857970	85.828005	-69.857970	RRab	18.993	19.641	0.448866000	8.0E-7	2193.83513	18.21	0.03
OGLE-LMC-RRLYR-20449	VMC84.392805	69.859880	84.392805	-69.859880	RRab	19.107	19.545	0.449035100	2.0E-7	726.67865	18.14	0.04
OGLE-LMC-RRLYR-20843	VMC84.699525	69.867710	84.699525	-69.867710	RRab	19.765	20.537	0.543774600	6.0E-7	726.79405	17.87	0.04
OGLE-LMC-RRLYR-21463	VMC85.216410	69.867140	85.216410	-69.867140	RRab	18.717	19.368	0.611589400	1.5E-6	2187.62351	17.92	0.03
OGLE-LMC-RRLYR-19940	VMC84.037035	69.867010	84.037035	-69.867010	RRab	18.660	19.209	0.536057600	3.0E-7	726.30699	18.09	0.03
OGLE-LMC-RRLYR-18356	VMC83.019765	69.869730	83.019765	-69.869730	RRab	18.819	19.425	0.609177700	3.0E-7	455.39589	18.35	0.03
OGLE-LMC-RRLYR-21325	VMC85.103730	69.870810	85.103730	-69.870810	RRab	20.083	21.763	0.470508600	2.3E-6	2187.38084	18.55	0.03

138Data analysis, and first results for RR Lyrae stars from the VMC survey

OGLE-LMC-RRLYR-19290	VMC83.585010	69.875920	83.585010	-69.875920	RRab	18.946	19.697	0.638813300	7.0E-7	455.65716	18.03	0.03
OGLE-LMC-RRLYR-18802	VMC83.278410	69.875560	83.278410	-69.875560	RRab	18.456	19.048	0.672313800	6.0E-7	455.04219	17.77	0.03
OGLE-LMC-RRLYR-18929	VMC83.368425	69.878560	83.368425	-69.878560	RRab	19.542	20.318	0.490573900	3.0E-7	455.26030	18.31	0.05
OGLE-LMC-RRLYR-21723	VMC85.471335	69.876220	85.471335	-69.876220	RRab	18.751	19.260	0.348357800	1.0E-6	2187.54403	18.27	0.03
OGLE-LMC-RRLYR-19633	VMC83.816475	69.881290	83.816475	-69.881290	RRab	18.662	19.200	0.556892900	4.0E-7	726.61101	17.89	0.03
OGLE-LMC-RRLYR-22050	VMC85.813125	69.871520	85.813125	-69.871520	RRab	18.914	19.630	0.611218000	9.0E-7	2187.45300	18.01	0.04
OGLE-LMC-RRLYR-21904	VMC85.658775	69.876950	85.658775	-69.876950	RRab	18.895	19.415	0.470435300	1.0E-6	2187.45067	18.34	0.03
OGLE-LMC-RRLYR-18726	VMC83.234160	69.881970	83.234160	-69.881970	RRab	18.626	19.305	0.687437000	3.4E-6	455.34899	17.95	0.03
OGLE-LMC-RRLYR-19203	VMC83.523960	69.879560	83.523960	-69.879560	RRab	19.055	19.854	0.610510800	7.0E-7	455.33006	18.15	0.03
OGLE-LMC-RRLYR-19405	VMC83.663550	69.886620	83.663550	-69.886620	RRab	18.970	19.685	0.625824300	8.0E-7	455.63778	18.09	0.03
OGLE-LMC-RRLYR-21924	VMC85.677570	69.881870	85.677570	-69.881870	RRab	19.026	19.722	0.577155600	1.8E-6	2187.26568	18.29	0.04
OGLE-LMC-RRLYR-19921	VMC84.023625	69.888890	84.023625	-69.888890	RRab	18.620	19.243	0.703752000	1.3E-6	726.16934	17.86	0.03
OGLE-LMC-RRLYR-18258	VMC82.983570	69.885010	82.983570	-69.885010	RRab	18.697	19.263	0.583438100	3.0E-7	455.33071	18.16	0.04
OGLE-LMC-RRLYR-19277	VMC83.575395	69.890620	83.575395	-69.890620	RRab	18.929	19.597	0.618362400	6.0E-7	455.33413	17.90	0.03
OGLE-LMC-RRLYR-18432	VMC83.057640	69.888630	83.057640	-69.888630	RRab	18.814	19.249	0.324752800	3.0E-7	455.49026	18.37	0.04
OGLE-LMC-RRLYR-20118	VMC84.155310	69.891700	84.155310	-69.891700	RRab	18.644	19.287	0.606401400	8.0E-7	726.52682	17.95	0.03
OGLE-LMC-RRLYR-18551	VMC83.125125	69.889350	83.125125	-69.889350	RRab	18.880	19.551	0.569303000	2.0E-7	455.22226	18.20	0.03
OGLE-LMC-RRLYR-20307	VMC84.293670	69.892700	84.293670	-69.892700	RRab	18.797	19.621	0.682137400	1.0E-6	726.73164	17.78	0.03
OGLE-LMC-RRLYR-19573	VMC83.777085	69.894100	83.777085	-69.894100	RRC	19.029	19.485	0.326457800	3.0E-7	455.43950	18.59	0.04
OGLE-LMC-RRLYR-20861	VMC84.713535	69.889670	84.713535	-69.889670	RRab	18.833	19.614	0.716369300	1.2E-6	726.82436	17.77	0.03
OGLE-LMC-RRLYR-21989	VMC85.747650	69.890990	85.747650	-69.890990	RRC	19.102	19.668	0.317366500	1.2E-6	2187.63482	18.44	0.03
OGLE-LMC-RRLYR-21085	VMC84.899235	69.897210	84.899235	-69.897210	RRab	19.630	20.846	0.639254200	3.4E-6	726.41085	18.10	0.03
OGLE-LMC-RRLYR-20921	VMC84.759960	69.897810	84.759960	-69.897810	RRab	19.279	20.170	0.612672100	1.0E-6	726.77930	18.20	0.03
OGLE-LMC-RRLYR-20960	VMC84.798285	69.900840	84.798285	-69.900840	RRab	19.762	21.012	0.512878400	5.0E-7	726.76193	18.43	0.04
OGLE-LMC-RRLYR-19789	VMC83.929380	69.898840	83.929380	-69.898840	RRab	18.808	19.438	0.595922700	5.0E-7	726.56344	18.08	0.04
OGLE-LMC-RRLYR-20767	VMC84.655230	69.901700	84.655230	-69.901700	RRe	18.920	19.185	0.222790800	5.0E-7	726.82845	18.55	0.05
OGLE-LMC-RRLYR-20432	VMC84.384735	69.896040	84.384735	-69.896040	RRab	19.474	20.371	0.584386700	1.4E-6	726.32677	18.32	0.03
OGLE-LMC-RRLYR-18943	VMC83.377680	69.900110	83.377680	-69.900110	RRab	18.832	19.477	0.655071600	1.3E-6	455.07477	18.03	0.04
OGLE-LMC-RRLYR-19452	VMC83.699940	69.899100	83.699940	-69.899100	RRe	19.238	19.845	0.269105600	5.0E-7	455.49487	18.56	0.03
OGLE-LMC-RRLYR-22117	VMC85.877610	69.899690	85.877610	-69.899690	Rrab	18.540	19.081	0.546169700	5.0E-7	2187.49227	17.89	0.03
OGLE-LMC-RRLYR-19332	VMC83.610165	69.908620	83.610165	-69.908620	RRab	19.073	19.771	0.541093000	3.0E-7	455.50213	18.26	0.04
OGLE-LMC-RRLYR-19852	VMC83.972385	69.907980	83.972385	-69.907980	RRab	18.779	19.334	0.581711400	4.0E-7	726.58225	17.90	0.03
OGLE-LMC-RRLYR-21330	VMC85.108560	69.906330	85.108560	-69.906330	RRab	18.967	19.640	0.531957300	1.0E-6	2187.36761	18.24	0.03
OGLE-LMC-RRLYR-21818	VMC85.563960	69.903420	85.563960	-69.903420	RRab	18.865	19.621	0.624837800	1.7E-6	2187.69385	16.77	0.03
OGLE-LMC-RRLYR-19480	VMC83.717460	69.910130	83.717460	-69.910130	RRab	18.673	19.268	0.622000200	6.0E-7	455.40490	18.03	0.03
OGLE-LMC-RRLYR-20483	VMC84.426090	69.910210	84.426090	-69.910210	RRab	19.149	20.273	0.494247000	2.0E-7	726.44355	18.10	0.04
OGLE-LMC-RRLYR-18486	VMC83.090985	69.910280	83.090985	-69.910280	RRab	18.830	19.222	0.651752000	9.0E-7	455.58633	17.83	0.03
OGLE-LMC-RRLYR-19829	VMC83.954265	69.909420	83.954265	-69.909420	RRC	18.541	18.959	0.353211000	1.2E-6	726.64527	18.26	0.03
OGLE-LMC-RRLYR-19058	VMC83.441355	69.913480	83.441355	-69.913480	RRab	18.779	19.047	0.511983700	2.0E-7	455.69773	17.97	0.05
OGLE-LMC-RRLYR-21397	VMC85.163790	69.911000	85.163790	-69.911000	RRe	18.898	19.285	0.273164600	1.5E-6	2187.62983	18.33	0.04
OGLE-LMC-RRLYR-18702	VMC83.216565	69.913710	83.216565	-69.913710	RRC	19.037	19.574	0.335212700	4.0E-7	455.67338	18.61	0.04
OGLE-LMC-RRLYR-19288	VMC83.583345	69.914330	83.583345	-69.914330	RRe	19.109	19.509	0.272846700	3.0E-7	455.49417	18.65	0.04
OGLE-LMC-RRLYR-20247	VMC83.249975	69.918160	84.249975	-69.918160	RRab	18.852	19.607	0.586845600	5.0E-7	726.65069	18.02	0.03
OGLE-LMC-RRLYR-18588	VMC83.147025	69.912050	83.147025	-69.912050	RRC	18.916	19.245	0.280121200	2.0E-7	455.64801	18.09	0.06
OGLE-LMC-RRLYR-20703	VMC83.611400	69.920730	84.611400	-69.920730	RRab	19.360	20.316	0.653578200	4.1E-6	726.22218	18.04	0.03
OGLE-LMC-RRLYR-20160	VMC84.185130	69.921260	84.185130	-69.921260	RRC	19.073	19.671	0.335050400	4.0E-7	739.64061	18.43	0.04
OGLE-LMC-RRLYR-18309	VMC82.996755	69.918040	82.996755	-69.918040	RRab	18.806	19.115	0.291213600	2.0E-7	455.57877	18.08	0.05
OGLE-LMC-RRLYR-18826	VMC83.290800	69.923840	83.290800	-69.923840	RRC	18.644	19.174	0.349618000	4.0E-7	455.65327	18.14	0.03
OGLE-LMC-RRLYR-20359	VMC83.334365	69.927290	84.334365	-69.927290	RRab	19.183	20.152	0.631715000	1.3E-6	726.24824	18.02	0.03
OGLE-LMC-RRLYR-21597	VMC85.339080	69.923710	85.339080	-69.923710	RRab	18.269	18.861	0.836161200	2.2E-6	2187.00871	17.46	0.03
OGLE-LMC-RRLYR-18735	VMC83.240475	69.926530	83.240475	-69.926530	RRab	18.800	19.492	0.632234800	8.0E-7	455.51813	18.15	0.04
OGLE-LMC-RRLYR-20318	VMC83.303450	69.929360	84.303450	-69.929360	RRab	19.413	20.566	0.617363200	1.2E-6	726.47797	18.06	0.03
OGLE-LMC-RRLYR-21646	VMC85.390530	69.926480	85.390530	-69.926480	RRab	18.985	19.786	0.613207300	1.9E-6	2187.24717	18.03	0.03
OGLE-LMC-RRLYR-20013	VMC84.086670	69.928520	84.086670	-69.928520	RRC	19.070	19.638	0.300353600	4.0E-7	726.69656	18.26	0.05
OGLE-LMC-RRLYR-19210	VMC83.530125	69.923350	83.530125	-69.923350	RRab	18.760	19.357	0.563832200	3.0E-7	455.47681	18.11	0.03
OGLE-LMC-RRLYR-19807	VMC83.942055	69.925720	83.942055	-69.925720	RRab	18.948	19.497	0.466720300	4.0E-7	726.73099	18.25	0.03
OGLE-LMC-RRLYR-19934	VMC84.033465	69.930780	84.033465	-69.930780	RRab	18.843	19.386	0.489216700	4.0E-7	726.54487	18.04	0.03
OGLE-LMC-RRLYR-19551	VMC83.761890	69.929740	83.761890	-69.929740	RRab	19.146	19.421	0.427560500	2.0E-7	455.37099	18.27	0.06

5.6 RR Lyrae stars in the 30 Dor region

139

OGLE-LMC-RRLYR-18384	VMC83.032485	69.930640	83.032485	-69.930640	RRab	18.830	19.487	0.587671500	3.0E-7	455.52708	18.20	0.03
OGLE-LMC-RRLYR-18425	VMC83.053830	69.930860	83.053830	-69.930860	RRc	18.940	19.407	0.319099200	2.0E-7	455.52355	18.36	0.04
OGLE-LMC-RRLYR-20445	VMC84.391500	69.933520	84.391500	-69.933520	RRab	19.470	20.265	0.519582900	4.0E-7	726.77403	18.34	0.04
OGLE-LMC-RRLYR-18918	VMC83.361555	69.933580	83.361555	-69.933580	RRab	18.432	19.024	0.791871900	8.0E-7	455.51307	17.66	0.03
OGLE-LMC-RRLYR-19460	VMC83.704995	69.930780	83.704995	-69.930780	RRab	18.631	19.197	0.599184700	5.0E-7	455.64139	17.64	0.06
OGLE-LMC-RRLYR-21525	VMC85.276950	69.927060	85.276950	-69.927060	RRc	19.021	19.637	0.342766500	1.0E-6	2187.76744	18.19	0.04
OGLE-LMC-RRLYR-19530	VMC83.748720	69.938260	83.748720	-69.938260	RRab	18.687	19.232	0.554377900	3.0E-7	455.26155	18.02	0.03
OGLE-LMC-RRLYR-21643	VMC85.386075	69.933810	85.386075	-69.933810	RRab	18.910	19.449	0.491954400	4.0E-7	2187.63836	18.33	0.03
OGLE-LMC-RRLYR-20572	VMC84.489495	69.938300	84.489495	-69.938300	RRab	19.362	20.332	0.591965700	1.5E-6	726.50939	18.04	0.04
OGLE-LMC-RRLYR-19265	VMC83.569275	69.935790	83.569275	-69.935790	RRab	18.631	19.195	0.573641400	4.0E-7	455.48143	18.00	0.05
OGLE-LMC-RRLYR-19101	VMC83.468175	69.935500	83.468175	-69.935500	RRc	19.061	19.568	0.353957900	5.0E-7	455.49986	18.39	0.04
OGLE-LMC-RRLYR-19105	VMC83.471085	69.940160	83.471085	-69.940160	RRc	18.714	19.108	0.369656500	3.0E-7	455.67536	17.98	0.03
OGLE-LMC-RRLYR-22075	VMC85.839240	69.932110	85.839240	-69.932110	RRc	18.986	19.404	0.303790000	6.0E-7	2187.65413	18.56	0.04
OGLE-LMC-RRLYR-21401	VMC85.169625	69.940940	85.169625	-69.940940	RRc	19.222	19.884	0.334256500	1.0E-6	2187.75335	17.94	0.06
OGLE-LMC-RRLYR-22103	VMC85.866360	69.935730	85.866360	-69.935730	RRc	18.601	18.984	0.318580200	1.0E-6	2187.70891	18.10	0.03
OGLE-LMC-RRLYR-21172	VMC84.977580	69.941900	84.977580	-69.941900	RRab	19.225	20.257	0.745185100	3.0E-6	726.55421	18.00	0.03
OGLE-LMC-RRLYR-21490	VMC85.241235	69.939840	85.241235	-69.939840	RRc	18.891	19.449	0.350480100	9.0E-7	2187.74509	18.19	0.04
OGLE-LMC-RRLYR-19641	VMC83.820135	69.942970	83.820135	-69.942970	RRab	18.826	19.355	0.528162100	2.0E-7	726.75597	18.19	0.03
OGLE-LMC-RRLYR-18607	VMC83.165550	69.942570	83.165550	-69.942570	RRab	18.872	19.499	0.574056100	8.0E-7	455.61913	18.12	0.04
OGLE-LMC-RRLYR-19664	VMC83.833905	69.947490	83.833905	-69.947490	RRab	18.847	19.106	0.525540100	4.0E-7	726.40118	17.57	0.04
OGLE-LMC-RRLYR-18860	VMC83.321805	69.947090	83.321805	-69.947090	RRab	18.475	19.158	0.839598900	1.0E-6	455.00071	17.76	0.03
OGLE-LMC-RRLYR-21347	VMC85.126890	69.946090	85.126890	-69.946090	RRab	18.841	19.502	0.567557900	7.0E-7	726.77972	17.86	0.03
OGLE-LMC-RRLYR-18595	VMC83.152380	69.947080	83.152380	-69.947080	RRab	18.801	19.555	0.463131100	2.0E-7	455.46151	17.83	0.04
OGLE-LMC-RRLYR-19867	VMC83.980635	69.949770	83.980635	-69.949770	RRc	19.019	19.502	0.311640300	6.0E-7	726.67254	18.70	0.06
OGLE-LMC-RRLYR-18699	VMC83.214390	69.946610	83.214390	-69.946610	RRab	18.901	19.505	0.524385100	2.0E-7	455.23043	18.38	0.04
OGLE-LMC-RRLYR-20211	VMC84.227115	69.952530	84.227115	-69.952530	RRab	19.238	20.073	0.588014400	8.0E-7	726.39338	18.12	0.04
OGLE-LMC-RRLYR-19018	VMC83.417625	69.952020	83.417625	-69.952020	RRab	18.971	19.604	0.612061600	8.0E-7	455.37388	18.20	0.04
OGLE-LMC-RRLYR-22015	VMC85.767090	69.948160	85.767090	-69.948160	RRab	18.863	19.410	0.515186700	4.0E-7	2187.64240	18.24	0.03
OGLE-LMC-RRLYR-20793	VMC84.670350	69.955730	84.670350	-69.955730	RRab	18.774	19.413	0.580842900	4.0E-7	726.28921	17.97	0.03
OGLE-LMC-RRLYR-18571	VMC83.134455	69.960520	83.134455	-69.960520	RRab	18.531	18.856	0.619662600	6.0E-7	455.19080	17.82	0.03
OGLE-LMC-RRLYR-18281	VMC82.989315	69.958180	82.989315	-69.958180	RRab	18.650	19.418	0.584840800	3.0E-7	455.41779	17.21	0.05
OGLE-LMC-RRLYR-19429	VMC83.679240	69.966270	83.679240	-69.966270	RRab	19.070	19.597	0.496066300	9.0E-7	455.44952	18.43	0.04
OGLE-LMC-RRLYR-19668	VMC83.836830	69.966050	83.836830	-69.966050	RRab	19.000	19.661	0.490961900	6.0E-7	726.48454	18.39	0.04
OGLE-LMC-RRLYR-21028	VMC84.856815	69.966850	84.856815	-69.966850	RRc	18.900	19.346	0.339785800	4.0E-7	726.62689	18.26	0.03
OGLE-LMC-RRLYR-21815	VMC85.559625	69.961800	85.559625	-69.961800	RRab	19.067	19.641	0.470844900	2.0E-7	726.44073	18.26	0.03
OGLE-LMC-RRLYR-20773	VMC84.659280	69.968030	84.659280	-69.968030	RRab	19.102	19.952	0.653455900	5.0E-7	726.76673	18.06	0.03
OGLE-LMC-RRLYR-21510	VMC85.263555	69.968860	85.263555	-69.968860	RRab	19.068	19.909	0.627729800	8.0E-7	726.80309	18.11	0.03
OGLE-LMC-RRLYR-19836	VMC83.954970	69.974780	83.954970	-69.974780	RRab	18.912	19.682	0.625063100	1.1E-6	726.77751	18.08	0.03
OGLE-LMC-RRLYR-19609	VMC83.800650	69.975120	83.800650	-69.975120	RRab	18.560	19.047	0.592321100	2.0E-7	726.48277	18.02	0.04
OGLE-LMC-RRLYR-18924	VMC83.365020	69.967830	83.365020	-69.967830	RRc	18.951	19.437	0.338865600	3.0E-7	455.62838	18.01	0.06
OGLE-LMC-RRLYR-20128	VMC84.162570	69.977280	84.162570	-69.977280	RRe	19.398	20.108	0.280868400	5.0E-7	726.64830	18.55	0.04
OGLE-LMC-RRLYR-20327	VMC84.309000	69.979490	84.309000	-69.979490	RRab	19.191	20.091	0.650235800	2.3E-6	726.52651	17.91	0.03
OGLE-LMC-RRLYR-18282	VMC82.989375	69.976920	82.989375	-69.976920	RRab	18.697	19.232	0.603456200	6.0E-7	455.18747	17.95	0.03
OGLE-LMC-RRLYR-20062	VMC84.123345	69.980660	84.123345	-69.980660	RRab	19.292	19.981	0.456117000	3.0E-7	726.55159	18.04	0.04
OGLE-LMC-RRLYR-21062	VMC84.878910	69.980230	84.878910	-69.980230	RRab	19.540	20.080	0.519359400	5.0E-7	726.79511	17.99	0.04
OGLE-LMC-RRLYR-18776	VMC83.263230	69.981080	83.263230	-69.981080	RRab	18.756	19.376	0.575850700	4.0E-7	455.31580	17.96	0.03
OGLE-LMC-RRLYR-20772	VMC84.658770	69.984130	84.658770	-69.984130	RRab	19.194	20.105	0.592727900	5.0E-7	726.66925	17.87	0.05
OGLE-LMC-RRLYR-21539	VMC85.286760	69.981850	85.286760	-69.981850	RRc	19.047	19.660	0.350539600	6.0E-7	726.67065	18.35	0.03
OGLE-LMC-RRLYR-20337	VMC84.314130	69.970120	84.314130	-69.970120	RRab	19.170	20.090	0.535294900	4.0E-7	726.37004	17.15	0.05
OGLE-LMC-RRLYR-19320	VMC83.600880	69.985880	83.600880	-69.985880	RRab	18.637	19.189	0.582536100	7.0E-7	455.21683	18.04	0.03
OGLE-LMC-RRLYR-22151	VMC85.919430	69.980230	85.919430	-69.980230	RRab	18.717	19.325	0.596724400	1.5E-6	2187.30003	18.04	0.03
OGLE-LMC-RRLYR-20347	VMC84.323670	69.990020	84.323670	-69.990020	RRc	19.133	19.657	0.286871600	3.0E-7	726.76782	18.36	0.04
OGLE-LMC-RRLYR-18774	VMC83.262135	69.984410	83.262135	-69.984410	RRab	18.737	19.276	0.576399800	4.0E-7	455.60095	18.19	0.04
OGLE-LMC-RRLYR-21926	VMC85.678275	69.984660	85.678275	-69.984660	RRab	18.695	19.359	0.606612000	8.0E-7	2187.52078	17.58	0.03
OGLE-LMC-RRLYR-18945	VMC83.378940	69.986040	83.378940	-69.986040	RRc	18.618	19.421	0.352805100	5.0E-7	455.43441	16.88	0.03
OGLE-LMC-RRLYR-21576	VMC85.320810	69.989030	85.320810	-69.989030	RRc	19.011	19.775	0.450381200	1.6E-6	726.63044	18.00	0.04
OGLE-LMC-RRLYR-20362	VMC84.336945	69.994050	84.336945	-69.994050	RRc	19.235	19.869	0.394017600	2.5E-6	726.68536	18.20	0.04
OGLE-LMC-RRLYR-19688	VMC83.850195	69.992610	83.850195	-69.992610	RRe	18.979	19.458	0.275825300	3.0E-7	726.70550	18.36	0.04

140Data analysis, and first results for RR Lyrae stars from the VMC survey

OGLE-LMC-RRLYR-21627	VMC85.366365	69.993440	85.366365	-69.993440	RRab	18.800	19.318	0.572049500	5.0E-7	726.74737	18.08	0.03
OGLE-LMC-RRLYR-18729	VMC83.237490	69.994430	83.237490	-69.994430	RRab	18.703	19.266	0.518801200	4.0E-7	455.49943	18.10	0.03
OGLE-LMC-RRLYR-20320	VMC84.303885	69.999150	84.303885	-69.999150	RRab	19.109	19.941	0.616125800	1.1E-6	726.47342	18.05	0.03
OGLE-LMC-RRLYR-21577	VMC85.321740	69.996090	85.321740	-69.996090	RRab	18.530	19.168	0.700934000	1.4E-6	726.77460	17.72	0.03
OGLE-LMC-RRLYR-20516	VMC84.454455	70.001200	84.454455	-70.001200	RRab	18.930	19.531	0.569994200	3.0E-7	726.50662	18.13	0.03
OGLE-LMC-RRLYR-21701	VMC85.441620	69.998230	85.441620	-69.998230	RRe	18.808	19.188	0.298159500	5.0E-7	726.81051	18.35	0.04
OGLE-LMC-RRLYR-20853	VMC84.707070	70.002500	84.707070	-70.002500	RRc	19.165	19.815	0.350246000	8.0E-7	726.80791	18.47	0.03
OGLE-LMC-RRLYR-20779	VMC84.663360	70.004120	84.663360	-70.004120	RRab	18.907	19.624	0.600291000	4.0E-7	726.42925	18.07	0.03
OGLE-LMC-RRLYR-22108	VMC85.870605	69.999560	85.870605	-69.999560	RRab	18.946	19.592	0.513562900	1.0E-6	2187.74306	17.97	0.03
OGLE-LMC-RRLYR-19878	VMC83.993445	70.007500	83.993445	-70.007500	RRab	19.143	20.092	0.650047100	1.5E-6	726.54955	18.15	0.04
OGLE-LMC-RRLYR-21327	VMC85.105065	70.005040	85.105065	-70.005040	RRab	19.391	20.370	0.540755100	4.0E-7	726.35320	18.46	0.03
OGLE-LMC-RRLYR-18921	VMC83.364150	70.003840	83.364150	-70.003840	RRc	18.957	19.396	0.317210300	3.0E-7	455.54081	18.33	0.04
OGLE-LMC-RRLYR-18614	VMC83.170845	70.008140	83.170845	-70.008140	RRab	18.744	19.344	0.554027700	5.0E-7	455.58511	18.22	0.04
OGLE-LMC-RRLYR-19338	VMC83.612700	70.009130	83.612700	-70.009130	RRab	18.709	19.365	0.598832600	4.0E-7	455.15490	17.93	0.03
OGLE-LMC-RRLYR-22129	VMC85.895715	70.004090	85.895715	-70.004090	RRab	18.670	19.310	0.637227600	8.0E-7	2187.55515	17.79	0.03
OGLE-LMC-RRLYR-19025	VMC83.420340	70.010940	83.420340	-70.010940	RRe	18.954	19.426	0.331924000	3.0E-7	455.70071	18.62	0.06
OGLE-LMC-RRLYR-21155	VMC84.959940	70.011150	84.959940	-70.011150	RRab	19.633	20.613	0.506917000	5.0E-7	726.51332	18.15	0.03
OGLE-LMC-RRLYR-20866	VMC84.716805	70.012790	84.716805	-70.012790	RRab	19.064	19.783	0.520728500	4.0E-7	726.40352	18.18	0.04
OGLE-LMC-RRLYR-19856	VMC83.973915	70.014190	83.973915	-70.014190	RRab	18.944	19.570	0.557306300	3.0E-7	726.29044	17.44	0.10
OGLE-LMC-RRLYR-19780	VMC83.923305	70.013900	83.923305	-70.013900	RRab	19.188	20.012	0.519737400	9.0E-7	726.39810	18.20	0.04
OGLE-LMC-RRLYR-19528	VMC83.748660	70.012750	83.748660	-70.012750	RRab	18.686	19.359	0.632795900	6.0E-7	455.19888	17.99	0.03
OGLE-LMC-RRLYR-19106	VMC83.471520	70.013870	83.471520	-70.013870	RRc	19.093	19.650	0.295501800	4.0E-7	455.46961	18.73	0.05
OGLE-LMC-RRLYR-20338	VMC84.314385	70.018340	84.314385	-70.018340	RRab	18.894	21.201	0.564232300	1.2E-6	726.42552	18.43	0.04
OGLE-LMC-RRLYR-22062	VMC85.828365	70.010970	85.828365	-70.010970	RRab	18.744	19.392	0.601249900	2.6E-6	2187.67268	17.78	0.04
OGLE-LMC-RRLYR-20548	VMC84.476775	70.019230	84.476775	-70.019230	RRe	19.091	19.556	0.276118000	7.0E-7	726.61604	18.60	0.04
OGLE-LMC-RRLYR-19112	VMC83.474280	70.021190	83.474280	-70.021190	RRab	18.920	19.490	0.516630200	4.0E-7	455.26213	18.38	0.04
OGLE-LMC-RRLYR-21750	VMC85.499190	70.016800	85.499190	-70.016800	RRab	18.773	19.391	0.617544200	8.0E-7	726.60523	18.06	0.04
OGLE-LMC-RRLYR-21691	VMC85.432320	70.020970	85.432320	-70.020970	RRab	18.648	19.414	0.719367700	2.0E-6	748.38863	17.87	0.03
OGLE-LMC-RRLYR-20361	VMC84.335325	70.026750	84.335325	-70.026750	RRc	19.104	19.769	0.330997200	6.0E-7	726.69623	18.22	0.04
OGLE-LMC-RRLYR-22126	VMC85.893405	70.019910	85.893405	-70.019910	RRab	19.513	20.087	0.351105000	3.0E-7	2187.47530	19.00	0.07
OGLE-LMC-RRLYR-21199	VMC85.006440	70.026300	85.006440	-70.026300	RRab	19.128	20.074	0.631919100	8.0E-7	726.23641	18.08	0.03
OGLE-LMC-RRLYR-19302	VMC83.589015	70.028830	83.589015	-70.028830	RRab	18.897	19.463	0.512089300	2.0E-7	455.34348	18.17	0.04
OGLE-LMC-RRLYR-19698	VMC83.857380	70.033600	83.857380	-70.033600	RRe	19.143	19.906	0.351144700	1.1E-6	726.80537	18.50	0.05
OGLE-LMC-RRLYR-20357	VMC84.333195	70.034090	84.333195	-70.034090	RRab	18.802	19.505	0.704224200	8.0E-7	726.48782	18.06	0.04
OGLE-LMC-RRLYR-19250	VMC83.560665	70.033150	83.560665	-70.033150	RRe	18.308	18.726	0.356017200	3.0E-7	455.66933	17.96	0.04
OGLE-LMC-RRLYR-21890	VMC85.645800	70.029030	85.645800	-70.029030	RRab	19.010	19.703	0.550514800	5.0E-7	726.71166	18.27	0.03
OGLE-LMC-RRLYR-22120	VMC85.887975	70.027980	85.887975	-70.027980	RRe	19.710	20.384	0.402190200	3.3E-6	2187.50920	19.07	0.09
OGLE-LMC-RRLYR-19360	VMC83.626335	70.033800	83.626335	-70.033800	RRab	18.869	19.525	0.600719400	3.0E-7	455.69290	18.03	0.03
OGLE-LMC-RRLYR-20105	VMC84.147045	70.032090	84.147045	-70.032090	RRab	19.250	20.071	0.477368300	7.0E-7	726.69404	18.48	0.04
OGLE-LMC-RRLYR-20756	VMC84.649260	70.035660	84.649260	-70.035660	RRab	19.142	20.016	0.600851600	6.0E-7	726.73402	18.16	0.03
OGLE-LMC-RRLYR-18287	VMC82.989690	70.030300	82.989690	-70.030300	RRab	18.607	19.151	0.532368500	2.0E-7	455.49836	18.12	0.03
OGLE-LMC-RRLYR-18989	VMC83.405895	70.028230	83.405895	-70.028230	RRab	18.728	19.213	0.560333300	3.0E-7	455.53209	18.28	0.04
OGLE-LMC-RRLYR-21195	VMC85.000785	70.041140	85.000785	-70.041140	RRab	19.287	20.102	0.539678400	3.0E-7	726.77385	18.18	0.03
OGLE-LMC-RRLYR-19820	VMC83.950680	70.040080	83.950680	-70.040080	RRe	19.400	19.970	0.281789700	6.0E-7	726.74346	18.91	0.05
OGLE-LMC-RRLYR-21064	VMC84.881085	70.043720	84.881085	-70.043720	RRab	19.486	20.400	0.519432100	4.0E-7	726.63447	18.48	0.04
OGLE-LMC-RRLYR-19819	VMC83.950005	70.049190	83.950005	-70.049190	RRab	19.106	19.898	0.539747100	3.0E-7	726.53028	18.21	0.03
OGLE-LMC-RRLYR-21823	VMC85.567335	70.046160	85.567335	-70.046160	RRe	18.590	19.124	0.612064100	4.0E-7	726.50552	17.96	0.03
OGLE-LMC-RRLYR-18500	VMC83.098785	70.046270	83.098785	-70.046270	RRe	18.902	19.301	0.271831000	8.0E-7	455.69041	18.38	0.04
OGLE-LMC-RRLYR-18712	VMC83.220240	70.048580	83.220240	-70.048580	RRab	18.605	19.123	0.577915400	2.0E-7	455.56300	18.08	0.03
OGLE-LMC-RRLYR-20331	VMC84.311130	70.054240	84.311130	-70.054240	RRab	18.569	19.141	0.585712000	3.0E-7	726.29493	17.88	0.03
OGLE-LMC-RRLYR-21923	VMC85.677510	70.049990	85.677510	-70.049990	RRab	18.584	19.209	0.634958800	2.4E-6	2187.36084	17.82	0.03
OGLE-LMC-RRLYR-21197	VMC85.005210	70.059110	85.005210	-70.059110	RRab	19.001	19.717	0.598061400	4.0E-7	726.51096	18.13	0.04
OGLE-LMC-RRLYR-22102	VMC85.866105	70.055650	85.866105	-70.055650	RRab	18.965	19.697	0.545805000	9.0E-7	2187.74601	18.20	0.03
OGLE-LMC-RRLYR-22084	VMC85.851465	70.059230	85.851465	-70.059230	RRab	18.608	19.257	0.727180000	9.6E-6	2187.63676	17.84	0.03
OGLE-LMC-RRLYR-20180	VMC84.199830	70.064930	84.199830	-70.064930	RRab	18.688	19.225	0.563164300	3.0E-7	726.68065	18.17	0.03
OGLE-LMC-RRLYR-19194	VMC83.518830	70.066300	83.518830	-70.066300	RRab	18.841	19.465	0.635867000	9.0E-7	455.18929	17.58	0.04
OGLE-LMC-RRLYR-20957	VMC84.794010	70.062730	84.794010	-70.062730	RRe	19.091	19.406	0.230712700	3.0E-7	726.80817	18.26	0.07
OGLE-LMC-RRLYR-21188	VMC84.992610	70.065860	84.992610	-70.065860	RRab	18.574	19.124	0.571897600	7.0E-7	726.45735	17.91	0.03

5.6 RR Lyrae stars in the 30 Dor region

141

OGLE-LMC-RRLYR-19945	VMC84.039675	70.070610	84.039675	-70.070610	RRab	18.892	19.468	0.573776100	4.0E-7	726.49454	18.12	0.03
OGLE-LMC-RRLYR-19677	VMC83.842050	70.071730	83.842050	-70.071730	RRc	19.101	19.755	0.360196500	6.0E-7	726.82632	18.47	0.05
OGLE-LMC-RRLYR-18431	VMC83.057595	70.065960	83.057595	-70.065960	RRc	18.764	19.255	0.329418200	2.0E-7	455.46946	18.29	0.05
OGLE-LMC-RRLYR-20593	VMC84.507615	70.072870	84.507615	-70.072870	RRab	18.881	19.508	0.502730700	1.5E-6	726.74313	18.29	0.04
OGLE-LMC-RRLYR-20162	VMC84.187110	70.075670	84.187110	-70.075670	RRab	19.022	19.739	0.598546900	8.0E-7	726.33913	18.13	0.03
OGLE-LMC-RRLYR-20771	VMC84.658020	70.073360	84.658020	-70.073360	RRab	19.093	19.884	0.446337900	5.0E-7	726.62888	17.94	0.05
OGLE-LMC-RRLYR-21302	VMC85.087290	70.075160	85.087290	-70.075160	RRc	19.363	20.119	0.325584500	4.0E-7	726.52440	18.44	0.04
OGLE-LMC-RRLYR-18183	VMC82.956720	70.072890	82.956720	-70.072890	RRab	18.673	19.244	0.553222800	2.0E-7	455.32984	18.17	0.03
OGLE-LMC-RRLYR-20164	VMC84.188655	70.078920	84.188655	-70.078920	RRab	18.817	19.420	0.596857000	5.0E-7	726.57556	18.08	0.04
OGLE-LMC-RRLYR-19667	VMC83.834760	70.078690	83.834760	-70.078690	RRab	18.762	19.590	0.506383700	2.0E-7	726.56542	17.78	0.04
OGLE-LMC-RRLYR-21613	VMC85.353990	70.075940	85.353990	-70.075940	RRc	19.064	19.614	0.327279200	8.0E-7	726.77010	18.22	0.04
OGLE-LMC-RRLYR-19729	VMC83.882895	70.075360	83.882895	-70.075360	RRab	18.700	19.427	0.701129800	9.0E-7	726.62190	17.94	0.03
OGLE-LMC-RRLYR-19724	VMC83.881230	70.072400	83.881230	-70.072400	RRab	18.793	19.194	0.497527500	2.0E-7	726.45549	18.02	0.03
OGLE-LMC-RRLYR-18811	VMC83.281260	70.075570	83.281260	-70.075570	RRab	18.503	19.074	0.606021700	4.0E-7	455.25588	17.87	0.03
OGLE-LMC-RRLYR-20283	VMC84.277110	70.079120	84.277110	-70.079120	RRc	18.739	19.222	0.366736600	1.6E-6	726.80337	17.96	0.03
OGLE-LMC-RRLYR-21461	VMC85.215990	70.078030	85.215990	-70.078030	RRe	19.219	19.731	0.269496000	6.0E-7	726.66308	18.51	0.04
OGLE-LMC-RRLYR-20735	VMC84.633390	70.085570	84.633390	-70.085570	RRab	18.654	19.313	0.641559000	6.0E-7	726.32935	17.80	0.03
OGLE-LMC-RRLYR-19913	VMC84.020835	70.083270	84.020835	-70.083270	RRc	18.560	19.178	0.446550800	7.0E-7	726.80044	17.83	0.03
OGLE-LMC-RRLYR-20210	VMC84.226665	70.083680	84.226665	-70.083680	RRab	18.868	19.452	0.524432100	2.0E-7	726.33845	18.06	0.03
OGLE-LMC-RRLYR-19397	VMC83.656860	70.088650	83.656860	-70.088650	RRab	18.537	20.202	0.540054200	2.0E-7	455.40907	17.65	0.07
OGLE-LMC-RRLYR-18723	VMC83.231550	70.087560	83.231550	-70.087560	RRab	18.742	19.319	0.583049300	6.0E-7	455.46069	18.28	0.03
OGLE-LMC-RRLYR-21296	VMC85.084215	70.088100	85.084215	-70.088100	RRab	18.900	19.435	0.530419000	3.0E-7	726.62018	18.24	0.03
OGLE-LMC-RRLYR-19753	VMC83.903160	70.089790	83.903160	-70.089790	RRc	19.108	19.617	0.293010100	3.0E-7	726.55996	18.06	0.06
OGLE-LMC-RRLYR-22055	VMC85.824285	70.085830	85.824285	-70.085830	RRc	18.912	19.440	0.327029800	1.1E-6	2187.47623	18.28	0.04
OGLE-LMC-RRLYR-19812	VMC83.947440	70.094260	83.947440	-70.094260	RRab	18.851	19.627	0.657308000	7.0E-7	726.47935	17.62	0.04
OGLE-LMC-RRLYR-21027	VMC84.856320	70.091240	84.856320	-70.091240	RRc	19.451	19.856	0.418123500	1.7E-6	726.75380	19.08	0.05
OGLE-LMC-RRLYR-21291	VMC85.080480	70.093680	85.080480	-70.093680	RRc	18.776	19.227	0.336960200	4.0E-7	726.79356	18.28	0.03
OGLE-LMC-RRLYR-18210	VMC82.969080	70.090990	82.969080	-70.090990	RRc	19.013	19.439	0.288800900	2.0E-7	455.55371	18.90	0.06
OGLE-LMC-RRLYR-20067	VMC84.125430	70.098150	84.125430	-70.098150	RRc	18.827	18.857	0.329536700	4.0E-7	726.78736	18.14	0.04
OGLE-LMC-RRLYR-21522	VMC85.274010	70.095160	85.274010	-70.095160	RRc	19.072	19.622	0.326366300	7.0E-7	726.83190	18.45	0.03
OGLE-LMC-RRLYR-19158	VMC83.497890	70.097190	83.497890	-70.097190	RRab	18.791	19.296	0.563487700	3.0E-7	455.59496	18.00	0.03
OGLE-LMC-RRLYR-18850	VMC83.312790	70.096790	83.312790	-70.096790	RRab	17.836	18.022	0.615608000	3.0E-7	455.64331	17.61	0.03
OGLE-LMC-RRLYR-19505	VMC83.737125	70.099110	83.737125	-70.099110	RRc	18.719	19.301	0.405818300	9.0E-7	455.52001	18.25	0.05
OGLE-LMC-RRLYR-19100	VMC83.468160	70.098150	83.468160	-70.098150	RRab	18.735	19.354	0.648996300	1.3E-6	455.24532	18.02	0.04
OGLE-LMC-RRLYR-20491	VMC84.436305	70.100620	84.436305	-70.100620	RRc	19.240	19.771	0.281646300	4.0E-7	726.75905	18.70	0.05
OGLE-LMC-RRLYR-20222	VMC84.233745	70.097640	84.233745	-70.097640	RRab	18.886	19.567	0.620856900	1.1E-6	726.59914	18.26	0.04
OGLE-LMC-RRLYR-20977	VMC84.814500	70.100970	84.814500	-70.100970	RRab	18.788	19.409	0.637839600	3.0E-7	726.62934	18.04	0.03
OGLE-LMC-RRLYR-18354	VMC83.019255	70.099130	83.019255	-70.099130	RRc	18.911	19.366	0.296019700	2.0E-7	455.47410	18.58	0.05
OGLE-LMC-RRLYR-19734	VMC83.886570	70.100720	83.886570	-70.100720	RRab	18.636	19.302	0.717487100	9.0E-7	726.40287	17.91	0.03
OGLE-LMC-RRLYR-21480	VMC85.232340	70.101690	85.232340	-70.101690	RRab	18.550	19.163	0.807633300	1.1E-6	726.05129	17.71	0.03
OGLE-LMC-RRLYR-19902	VMC84.010410	68.789620	84.010410	-68.789620	RRab	18.878	19.478	0.595411000	1.0E-6	2187.29304	17.97	0.03
OGLE-LMC-RRLYR-18359	VMC83.023275	68.879310	83.023275	-68.879310	RRab	18.903	19.500	0.538687700	5.0E-7	2167.85107	18.16	0.04
OGLE-LMC-RRLYR-21775	VMC85.520970	69.001690	85.520970	-69.001690	RRc	19.057	19.540	0.292558400	8.0E-7	2187.73742	18.38	0.03
OGLE-LMC-RRLYR-21927	VMC85.678500	69.031430	85.678500	-69.031430	RRab	19.409	20.406	0.466404700	4.0E-7	2187.58154	18.39	0.04
OGLE-LMC-RRLYR-19642	VMC83.820495	69.133530	83.820495	-69.133530	RRab	20.948	-99.99	0.506663400	3.0E-6	2167.71746	18.72	0.06
OGLE-LMC-RRLYR-21819	VMC85.564440	69.154800	85.564440	-69.154800	RRe	19.455	20.430	0.637086200	2.2E-6	2187.71885	18.00	0.03
OGLE-LMC-RRLYR-19897	VMC84.006390	69.161500	84.006390	-69.161500	RRab	18.577	19.053	0.577290300	7.0E-7	2187.19737	17.74	0.04
OGLE-LMC-RRLYR-19907	VMC84.015255	69.344950	84.015255	-69.344950	RRab	18.837	19.347	0.468069400	4.0E-7	2187.53285	18.34	0.03
OGLE-LMC-RRLYR-18756	VMC83.252490	69.346080	83.252490	-69.346080	RRab	18.867	19.494	0.636845400	2.9E-6	2167.54695	17.61	0.05
OGLE-LMC-RRLYR-21131	VMC84.935085	69.486650	84.935085	-69.486650	RRab	19.530	20.289	0.465428500	8.0E-7	2187.32803	18.48	0.04
OGLE-LMC-RRLYR-19950	VMC84.044865	69.531780	84.044865	-69.531780	RRab	19.099	19.900	0.610635500	2.1E-6	2187.63763	18.16	0.03
OGLE-LMC-RRLYR-20167	VMC84.191955	69.553530	84.191955	-69.553530	RRc	18.783	19.285	0.381338600	1.2E-6	2187.64413	18.04	0.04
OGLE-LMC-RRLYR-19739	VMC83.890830	69.555860	83.890830	-69.555860	RRe	19.175	19.561	0.271107500	9.0E-7	2167.85589	18.59	0.04
OGLE-LMC-RRLYR-21376	VMC85.146510	69.574770	85.146510	-69.574770	RRab	19.369	20.030	0.510776700	7.0E-7	2187.37050	18.28	0.04
OGLE-LMC-RRLYR-20102	VMC84.145080	69.584490	84.145080	-69.584490	RRab	19.137	19.937	0.646178400	3.5E-6	2187.19907	18.10	0.03
OGLE-LMC-RRLYR-20239	VMC84.247290	69.586120	84.247290	-69.586120	RRc	18.996	19.490	0.326591700	7.0E-7	2187.70737	18.24	0.05
OGLE-LMC-RRLYR-19727	VMC83.882265	69.595110	83.882265	-69.595110	RRab	18.761	19.392	0.667246400	2.3E-6	2167.37151	17.88	0.03
OGLE-LMC-RRLYR-21241	VMC85.042695	69.675480	85.042695	-69.675480	RRab	18.752	19.306	0.617993100	1.6E-6	2187.27347	17.44	0.04

OGLE-LMC-RRLYR-21069	VMC84.887145	69.692930	84.887145	-69.692930	RRab	19.505	20.345	0.566264400	2.0E-6	2187.59937	18.24	0.04
OGLE-LMC-RRLYR-21103	VMC84.912195	69.803940	84.912195	-69.803940	RRab	20.295	21.556	0.480494600	2.7E-6	2187.68118	18.79	0.04
OGLE-LMC-RRLYR-20597	VMC84.510825	69.866540	84.510825	-69.866540	RRab	18.855	19.440	0.543809600	7.0E-7	726.62412	18.07	0.03
OGLE-LMC-RRLYR-19769	VMC83.913240	69.873340	83.913240	-69.873340	RRab	18.864	19.492	0.609469200	5.0E-7	726.69028	17.76	0.04
OGLE-LMC-RRLYR-19756	VMC83.905590	69.949190	83.905590	-69.949190	RRc	18.832	19.280	0.333571400	4.0E-7	726.68591	18.15	0.04
OGLE-LMC-RRLYR-21720	VMC85.463370	69.954380	85.463370	-69.954380	RRab	18.980	19.745	0.606700400	1.1E-6	726.76901	18.23	0.03
OGLE-LMC-RRLYR-20440	VMC84.388065	69.965810	84.388065	-69.965810	RRab	19.149	20.046	0.610235000	6.0E-7	726.36313	18.03	0.03
OGLE-LMC-RRLYR-21132	VMC84.935610	70.038750	84.935610	-70.038750	RRab	19.243	20.127	0.634055600	3.9E-6	726.48290	17.86	0.04
OGLE-LMC-RRLYR-19122	VMC83.477460	70.065250	83.477460	-70.065250	RRab	18.762	19.363	0.593087900	4.0E-7	455.52114	18.09	0.03
OGLE-LMC-RRLYR-21481	VMC85.232610	70.080580	85.232610	-70.080580	RRab	19.160	19.795	0.494338100	3.0E-7	726.79429	18.08	0.04
OGLE-LMC-RRLYR-18390	VMC83.038725	68.957060	83.038725	-68.957060	RRab	19.344	20.245	0.590197700	1.4E-6	2167.87924	18.21	0.04
OGLE-LMC-RRLYR-20029	VMC84.097995	68.975130	84.097995	-68.975130	RRab	19.414	20.370	0.613943000	2.2E-6	2187.74795	18.19	0.03
OGLE-LMC-RRLYR-21224	VMC85.026120	69.007190	85.026120	-69.007190	RRe	19.182	19.805	0.290408500	1.6E-6	2187.50271	18.55	0.04
OGLE-LMC-RRLYR-20313	VMC84.296295	69.359520	84.296295	-69.359520	RRab	18.706	19.185	0.540636400	8.0E-7	2187.30773	17.90	0.04
OGLE-LMC-RRLYR-19556	VMC83.765025	69.446560	83.765025	-69.446560	RRc	19.023	19.523	0.294396800	5.0E-7	2167.72577	18.54	0.03
OGLE-LMC-RRLYR-20042	VMC84.107835	69.452950	84.107835	-69.452950	RRab	18.869	19.395	0.539172900	7.0E-7	2187.69069	18.09	0.03
OGLE-LMC-RRLYR-20279	VMC84.274575	69.461300	84.274575	-69.461300	RRc	18.908	19.334	0.292694300	1.3E-6	2187.56767	18.42	0.03
OGLE-LMC-RRLYR-18886	VMC83.334675	69.517360	83.334675	-69.517360	RRab	18.999	19.626	0.547445600	9.0E-7	2167.40949	18.11	0.04
OGLE-LMC-RRLYR-18676	VMC83.202615	69.592060	83.202615	-69.592060	RRab	18.754	19.392	0.615660400	1.3E-6	2167.52881	18.05	0.03
OGLE-LMC-RRLYR-18328	VMC83.003310	69.705330	83.003310	-69.705330	RRab	18.824	19.411	0.606289300	3.0E-7	455.10417	17.88	0.04
OGLE-LMC-RRLYR-20271	VMC84.268365	69.732370	84.268365	-69.732370	RRab	20.025	21.331	0.551163900	8.0E-7	726.58406	18.24	0.03
OGLE-LMC-RRLYR-21016	VMC84.850185	69.815990	84.850185	-69.815990	RRc	19.247	19.839	0.298570000	4.0E-7	726.66659	18.61	0.04
OGLE-LMC-RRLYR-19347	VMC83.617230	69.912980	83.617230	-69.912980	RRab	18.981	19.680	0.506211300	1.3E-6	455.23954	18.22	0.03
OGLE-LMC-RRLYR-20685	VMC84.597015	69.918960	84.597015	-69.918960	RRab	19.225	20.052	0.581219300	7.0E-7	726.53144	17.90	0.04
OGLE-LMC-RRLYR-20022	VMC84.093600	70.025790	84.093600	-70.025790	RRab	19.035	19.801	0.566133800	6.0E-7	726.32421	17.74	0.06

Table 5.7: Properties of RR Lyrae stars in the 30 Dor field. Column 1: OGLE III id of the star; Column 2: VMC id; Columns 3,4: RA,DEC from the OGLE III catalogue; Column 5: RR type; Column 6, 7: OGLE III I , V mean magnitudes; Column 8: period from OGLE III; Column 9: error in the period; Column 10: time of maximum light from OGLE III; Column 11: $\langle K_S \rangle$ magnitudes obtained by simply intensity-averaging the time-series data; Column 12: error in $\langle K_S \rangle$.

Chapter 6

First results for Classical Cepheids from the VMC survey

In this Chapter we present results for the Classical Cepheids contained in the SEP field and in the 30 Dor star forming region of the Large Magellanic Cloud (LMC).

6.1 VMC data for the Cepheids

As a result of the matching procedure between the VMC and the optical survey catalogues described in the previous sections, we found 12 and 326 Classical Cepheids in the SEP and 30 Dor fields, respectively.

Periods available from EROS-2 for the SEP Cepheids, and from OGLE-III for the 30 Dor variables, were used to fold the K_S -band light curves produced by the VMC observations, and derive average K_S magnitudes.

Examples of the VMC K_S -band light curves of Cepheids in the SEP and 30 Dor regions are shown in Figs. 6.1 and 6.2, respectively. Error bars of the individual K_S measurements are shown in the figures, they are of the same size of the data-points.

The Cepheid light curves are very well sampled and nicely shaped (see Figs. 6.1 and 6.2). To derive the (intensity) average $\langle K_S \rangle$ values we simply used custom software written in “c” language, that performs a spline interpolation to the data. Final $\langle K_S \rangle$ values are provided in Tabs. 6.1 and 6.2, for SEP and 30 Dor Cepheids, respectively, along with the star main characteristics (Id, coordinates, period, pulsation mode, time of maximum light, average magnitude, K -band amplitude and reddening). An “a” in the last column of Tab. 6.2 flags objects that were not used in the derivation of the PLK relations.

The very small number of Cepheids in the SEP field is consistent with the very

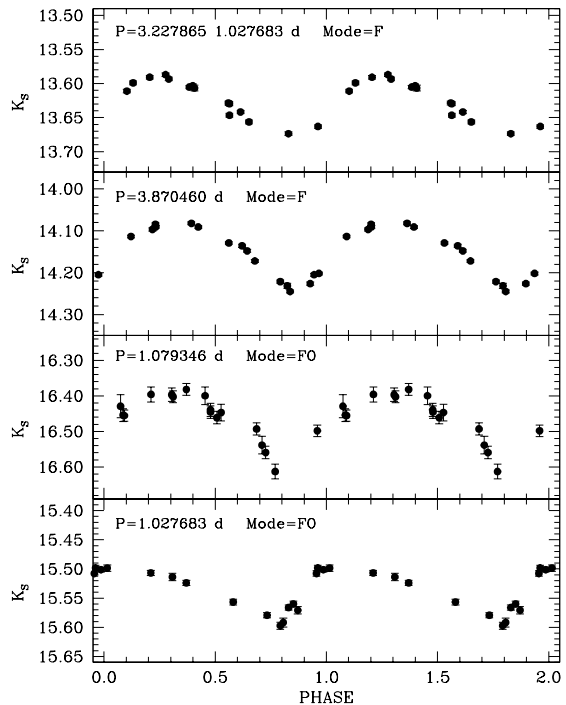


Figure 6.1: K_S -band light curves for a sample of Cepheids in the SEP field. Typical errors of the individual data points are of the order of 0.01–0.02 mag. F and FO stand for fundamental and first overtone pulsators, respectively. Note the nice light curve of a faint FO Cepheid (third panel from the top). Periods used to fold the light curves are taken from the EROS-2 catalogue.

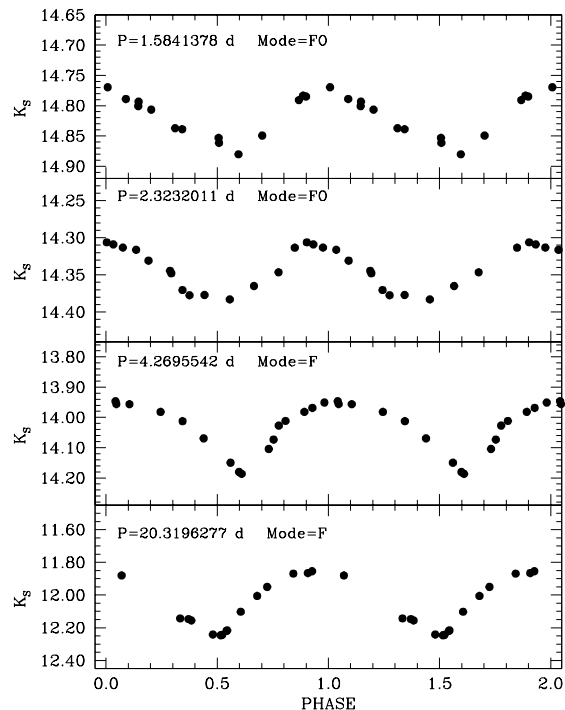


Figure 6.2: Same as Fig 6.1, but for Cepheids in the in the 30 Dor field. Typical errors of the individual data points are of the order of 0.01-0.02 mag, hence have same size as the data points plotted in the figure. Periods used to fold the light curves are taken form the OGLE-III catalogue.

Table 6.1: Results for Classical Cepheids in the SEP field of the LMC.

ID	RA J2000	DEC J2000	M	$\langle V_{EROS-2} \rangle$ mag	Period d	$\langle K_S \rangle$ mag	$A(K_S)$ mag	$\sigma_{\langle K_S \rangle}$ mag
VMC89.1490000	65.7950600	89.14900	-65.79506	FO	16.596	1.188733	15.264	0.09
VMC89.2963600	65.8544800	89.29636	-65.85448	FO	16.561	1.044436	15.284	0.10
VMC89.1597100	66.0507000	89.15971	-66.05070	FO	16.640	1.214786	15.338	0.08
VMC88.8761500	66.0993300	88.87615	-66.09933	F	15.785	3.870460	14.145	0.15
VMC89.0557000	66.3761100	89.05570	-66.37611	FO	16.944	1.027683	15.533	0.10
VMC89.8533000	66.4916700	89.85330	-66.49167	F	16.844	1.238489	15.681	0.09
VMC90.8548300	66.5234800	90.85483	-66.52348	FO	16.677	1.277076	15.224	0.14
VMC90.8282200	66.8789600	90.82822	-66.87896	FO	15.096	3.227865	13.631	0.09
VMC90.3222800	66.8888500	90.32228	-66.88885	F	5.986	4.085779	13.900	0.03
VMC89.8422000	66.9526700	89.84220	-66.95267	FO	16.100	1.683674	14.788	0.11
VMC88.8976100	67.0381800	88.89761	-67.03818	F	17.009	3.902331	14.130	0.02
VMC89.9288900	67.0630000	89.92889	-67.06300	FO	15.767	1.907595	14.515	0.09
								0.0023

peripheral location of this region, that is very far from the LMC bar/s, where most of the Classical Cepheids are located. It is also remarkable the predominance of first overtone (FO; 8) with respect to fundamental-mode (F; 4) pulsators, as well as the lack of Cepheids with periods longer than 4 d, in the SEP. This is likely related to the specific star formation history occurred in the SEP region.

6.1 VMC data for the Cepheids

147

Table 6.2: Results for Classical Cepheids in the 30 Dor field of the LMC

ID	RA J2000	DEC J2000	M	$I_{OGLEIII}$ mag	$V_{OGLEIII}$ mag	Period d	T_0^{MAX} d	$\langle K_S \rangle$ mag	A(K) mag	r.m.s. mag	E(V-I) mag	Notes
VMC82.7029600	69.8133300	82.70296	-69.81333	F	15.354	16.105	3.240862	452.93897	14.353	0.22	0.006	0.08
VMC82.7478300	69.5920000	82.74783	-69.59200	F	14.89	15.693	4.656827	452.97342	13.917	0.22	0.008	0.09
VMC82.7537900	69.7590000	82.75379	-69.75900	F	14.724	15.453	4.874545	454.84077	13.775	0.23	0.004	0.08
VMC82.7542900	69.1084200	82.75429	-69.10842	F	15.779	16.722	3.130618	2165.82771	14.589	0.12	0.007	0.12
VMC82.7570800	69.1059700	82.75708	-69.10597	F	15.993	17.003	2.908321	2166.54407	14.694	0.2	0.010	0.12
VMC82.7624600	69.5353300	82.76246	-69.53533	F	14.816	15.547	4.641402	451.31822	13.957	0.25	0.009	0.09
VMC82.8027900	70.0742500	82.80279	-70.07425	F	14.949	15.679	4.226975	452.86098	14.041	0.22	0.008	0.02
VMC82.8228700	69.9078600	82.82287	-69.90786	F	14.357	15.133	5.976499	450.5059	13.388	0.21	0.004	0.1
VMC82.8262500	69.6073300	82.82625	-69.60733	F	14.875	15.716	4.83438	451.16849	13.833	0.14	0.008	0.1
VMC82.8433700	69.8897200	82.84337	-69.88972	F	15.058	15.643	3.408864	454.04755	14.12	0.19	0.009	0.1
VMC82.8970400	69.3185600	82.89704	-69.31856	F	14.202	15.019	7.809176	2166.03299	13.147	0.22	0.004	0.05
VMC82.9099600	69.9482500	82.90996	-69.94825	F	15.24	16.081	3.880888	455.22749	14.151	0.18	0.015	0.09
VMC82.9115800	69.9783300	82.91158	-69.97833	F	14.792	15.497	4.628197	455.39739	13.842	0.25	0.012	0.09
VMC82.9222500	69.9534200	82.92225	-69.95342	F	15.24	15.956	3.307002	454.00423	14.057	0.27	0.022	0.09
VMC82.9345000	69.9698300	82.93450	-69.96983	F	15.163	15.879	3.380503	453.92686	14.305	0.25	0.075	0.09
VMC82.9505800	70.0242500	82.95058	-70.02425	F	14.861	15.62	4.132642	454.15633	13.873	0.2	0.020	0.07
VMC82.9544600	70.1484200	82.95446	-70.14842	F	15.621	16.331	2.524455	454.17488	14.811	0.19	0.020	0.05
VMC82.9601700	69.9160000	82.96017	-69.91600	F	15.072	15.762	3.768631	453.80204	14.165	0.23	0.009	0.05
VMC82.9845000	69.2427800	82.98450	-69.24278	F	14.04	14.808	9.215951	2160.38653	12.974	0.06	0.008	0.09
VMC83.0042500	69.7980600	83.00425	-69.79806	F	15.458	16.184	2.971145	455.46278	14.484	0.18	0.009	0.1
VMC83.0105800	69.6372800	83.01058	-69.63728	F	15.155	15.915	3.712696	453.56871	14.195	0.22	0.007	0.11
VMC83.0204600	69.3491900	83.02046	-69.34919	F	15.375	16.027	2.911571	2167.13778	14.5	0.2	0.006	0.06
VMC83.0499200	70.0052800	83.04992	-70.00528	F	14.984	15.708	3.775564	454.9026	14.102	0.19	0.009	0.08
VMC83.0516700	69.9766700	83.05167	-69.97667	F	15.26	15.88	2.942559	452.84633	14.453	0.19	0.014	0.09
VMC83.0650800	70.0321700	83.06508	-70.03217	F	15.044	15.793	4.296477	454.18056	11.766	0.00	0.015	0.08
VMC83.0945800	69.0350000	83.09458	-69.03500	F	15.007	15.885	4.937826	2163.3717	13.896	0.25	0.004	0.16
VMC83.0973300	68.9955300	83.09733	-68.99553	F	13.973	15.076	14.190111	2156.10073	12.546	0.3	0.043	0.16
VMC83.1038300	69.9773100	83.10383	-69.97731	F	14.597	15.39	5.737309	450.71813	13.579	0.21	0.012	0.05
VMC83.1105400	69.7727500	83.11054	-69.77275	F	15.258	15.998	3.343827	453.71576	14.31	0.23	0.004	0.13
VMC83.1372500	69.9969700	83.13725	-69.99697	F	14.869	15.625	4.654957	451.95253	13.878	0.25	0.009	0.03
VMC83.1579200	70.0825600	83.15792	-70.08256	F	15.026	15.776	4.015951	454.02541	14.014	0.14	0.016	0.02
VMC83.2432500	69.8655000	83.24325	-69.86550	F	15.222	16.154	4.800791	455.577	13.891	0.15	0.012	0.08
VMC83.2438700	69.0845600	83.24387	-69.08456	F	14.568	15.58	7.671496	2161.27411	13.284	0.14	0.004	0.19
VMC83.2781200	68.7574400	83.27812	-68.75744	F	14.882	15.632	4.431046	2166.06131	13.857	0.27	0.010	0.09
VMC83.3068700	69.9155800	83.30687	-69.91558	F	15.162	16.017	4.154816	452.58024	14.056	0.19	0.010	0.1
VMC83.3183700	70.0649400	83.31837	-70.06494	F	14.675	15.41	4.995947	454.73076	13.727	0.22	0.014	0.05
VMC83.3449600	69.9555300	83.34496	-69.95553	F	15.066	15.853	4.291601	452.2075	13.945	0.22	0.014	0.09
VMC83.3741200	69.6191700	83.37412	-69.61917	F	15.484	16.335	3.472105	2167.04769	14.404	0.11	0.008	0.1
VMC83.3812100	69.0147500	83.38121	-69.01475	F	15.406	16.237	3.448526	2166.74453	14.402	0.21	0.008	0.17
VMC83.4026700	69.7548600	83.40267	-69.75486	F	15.069	15.873	4.236821	452.173	13.845	0.12	0.008	0.09
VMC83.4186200	69.8830800	83.41862	-69.88308	F	15.731	17.133	5.261907	450.9101	13.936	0.24	0.012	0.1
VMC83.4523300	69.7535300	83.45233	-69.75353	F	15.269	15.953	3.310933	455.13602	14.347	0.21	0.009	0.09
VMC83.4768300	70.0486400	83.47683	-70.04864	F	14.28	14.7	5.064058	450.68856	13.528	0.19	0.008	0.08
VMC83.4896200	69.5662200	83.48962	-69.56622	F	15.074	16.141	6.532017	2166.25924	13.658	0.11	0.004	0.11
VMC83.4912500	70.1128100	83.49125	-70.11281	F	15.045	15.845	4.517043	451.75529	13.943	0.09	0.037	0.08
VMC83.5038800	68.6811900	83.50388	-68.68119	F	14.683	15.539	5.798564	2163.85837	13.612	0.08	0.006	0.12
VMC83.5165000	68.6531400	83.51650	-68.65314	F	14.927	15.722	4.659693	2163.29992	13.957	0.24	0.007	0.08
VMC83.5265000	69.6099400	83.52650	-69.60994	F	15.121	15.96	4.261772	2165.91166	14.064	0.15	0.006	0.11
VMC83.5314600	68.7268600	83.53146	-68.72686	F	14.942	15.754	4.174311	2164.31609	13.904	0.2	0.004	0.12
VMC83.6161200	69.8171700	83.61612	-69.81717	F	15.352	16.107	3.117261	454.70285	14.393	0.18	0.009	0.11
VMC83.6361700	69.3217200	83.63617	-69.32172	F	15.738	16.446	2.369933	2166.20817	14.865	0.21	0.013	0.12
VMC83.6375400	68.8372200	83.63754	-68.83722	F	14.341	15.344	8.967181	2159.60105	13.123	0.03	0.004	0.17
VMC83.6635800	70.0731100	83.66358	-70.07311	F	15.254	16.051	3.555175	453.55441	14.225	0.2	0.013	0.1
VMC83.6650800	68.8100000	83.66508	-68.81000	F	15.189	16.266	5.076578	2164.42413	13.797	0.17	0.006	0.11
VMC83.6732100	68.6906700	83.67321	-68.69067	F	14.381	15.147	6.540879	2165.68434	13.383	0.27	0.004	0.11

a

a

a

VMC83.6879200	69.9888100	83.68792	-69.98881	F	15.568	16.193	2.618309	454.53154	14.618	0.21	0.011	0.1
VMC83.6975800	-69.9143100	83.69758	-69.91431	F	14.773	15.471	4.657003	452.43129	13.85	0.23	0.009	0.1
VMC83.7161700	-69.4016900	83.71617	-69.40169	F	14.28	15.192	8.257998	2159.98882	13.162	0.08	0.005	0.12
VMC83.7576700	-69.6168600	83.75767	-69.61686	F	16.126	16.911	1.851911	2167.22731	15.129	0.11	0.006	0.11
VMC83.7945000	-69.6170390	83.79450	-69.61703	F	14.855	15.682	4.920229	2163.68721	13.81	0.16	0.005	0.11
VMC83.7973700	-69.9630300	83.79737	-69.96303	F	15.291	16.016	3.221109	724.54147	14.324	0.23	0.019	0.1
VMC83.8090400	-70.1044700	83.80904	-70.10447	F	15.324	15.986	2.839646	726.54495	14.521	0.29	0.012	0.13
VMC83.8416700	-69.9688900	83.84167	-69.96889	F	15.521	16.283	2.942805	725.77439	14.552	0.18	0.006	0.1
VMC83.8513300	-69.9568900	83.85133	-69.95689	F	15.097	15.972	4.519293	725.80223	14.001	0.11	0.009	0.1
VMC83.8562500	-68.7750300	83.85625	-68.77503	F	15.115	15.868	3.618613	2185.22198	14.172	0.26	0.004	0.13
VMC83.8781700	-69.9682500	83.87817	-69.96825	F	15.616	16.914	4.225043	724.59231	14.102	0.25	0.005	0.1
VMC83.8824600	-69.7228300	83.88246	-69.72283	F	14.294	15.084	6.935845	722.70818	13.259	0.21	0.007	0.12
VMC83.8926200	-70.0995300	83.89262	-70.09953	F	15.256	16.046	3.64626	726.36329	14.202	0.17	0.005	0.16
VMC83.8953700	-70.0903300	83.89537	-70.09033	F	15.226	16.072	3.200247	724.05297	14.134	0.14	0.009	0.16
VMC83.8958800	-69.5750300	83.89588	-69.57503	F	14.647	15.466	6.136573	2162.85028	13.643	0.15	0.012	0.09
VMC83.9537900	-69.9442500	83.95379	-69.94425	F	15.154	15.903	3.66089	723.69615	14.19	0.22	0.009	0.1
VMC83.9659600	-70.0671900	83.96596	-70.06719	F	15.253	16.088	3.882611	724.2457	13.988	0.21	0.012	0.16
VMC83.9744600	-68.6594400	83.97446	-68.65944	F	14.428	15.292	6.480397	2222.22239	13.448	0.15	0.002	0.11
VMC83.9817900	-68.9933900	83.98179	-68.99339	F	15.239	16.252	4.880068	2185.5541	13.916	0.18	0.004	0.33
VMC83.9966300	-70.0736700	83.99663	-70.07367	F	15.214	16.179	4.324082	725.21517	13.984	0.23	0.011	0.16
VMC84.0283300	-68.8203900	84.02833	-68.82039	F	13.222	14.123	18.715996	2179.63811	12.025	0.49	0.008	0.14
VMC84.0371200	-69.8349200	84.03712	-69.83492	F	15.255	16.013	3.618591	726.23757	14.256	0.22	0.013	0.14
VMC84.0705800	-69.9042500	84.07058	-69.90425	F	13.91	14.718	9.610902	717.35084	12.867	0.26	0.002	0.13
VMC84.0774200	-70.0115800	84.07742	-70.01158	F	15.513	16.71	4.302878	726.00968	14.094	0.27	0.007	0.16
VMC84.0896200	-70.1105300	84.08962	-70.11053	F	14.857	15.567	4.427445	725.14397	13.938	0.25	0.007	0.16
VMC84.0957500	-68.8169400	84.09575	-68.81694	F	16.719	17.23	1.163712	2187.16311	15.45	0.09	0.009	0.15
VMC84.0961200	-70.0687200	84.09612	-70.06872	F	15.515	16.277	2.91712	724.32914	14.492	0.23	0.002	0.16
VMC84.1130000	-69.6797800	84.11300	-69.67978	F	15.362	16.115	3.318209	2185.86737	14.406	0.21	0.009	0.11
VMC84.1175000	-69.8208900	84.11750	-69.82089	F	13.861	14.75	10.071731	723.75258	12.774	0.09	0.005	0.14
VMC84.1188300	-69.6737500	84.11883	-69.67375	F	16.323	17.394	2.908452	2186.32344	14.767	0.22	0.005	0.11
VMC84.1256200	-69.9641900	84.12562	-69.96419	F	14.984	15.867	4.851802	724.59013	13.828	0.23	0.008	0.13
VMC84.1427900	-70.0890000	84.14279	-70.08900	F	15.054	15.896	4.416394	723.96114	14.0	0.23	0.003	0.16
VMC84.2236700	-70.1067500	84.22367	-70.10675	F	14.746	15.504	4.888984	722.05615	13.743	0.22	0.012	0.11
VMC84.2276700	-69.9407200	84.22767	-69.94072	F	15.861	16.854	2.830581	725.0778	14.616	0.2	0.005	0.21
VMC84.2641300	-70.0760600	84.26413	-70.07606	F	15.029	15.77	3.929258	725.38678	14.075	0.22	0.006	0.11
VMC84.2751200	-69.9433300	84.27512	-69.94333	F	15.37	16.315	3.59175	724.45749	14.231	0.24	0.012	0.21
VMC84.3236700	-68.6712200	84.32367	-68.67122	F	14.558	15.343	6.337916	2182.40849	13.514	0.07	0.003	0.17
VMC84.3435400	-69.4831700	84.34354	-69.48317	F	13.478	14.398	14.216367	2174.35713	12.302	0.38	0.011	0.18
VMC84.3682500	-69.1951700	84.36825	-69.19517	F	17.007	18.404	2.389343	2187.68231	15.109	0.22	0.006	0.2
VMC84.3951700	-69.0917800	84.39517	-69.09178	F	15.983	17.02	3.133491	2187.30985	14.612	0.24	0.005	0.2
VMC84.4132100	-70.1085800	84.41321	-70.10858	F	14.296	15.399	4.109942	723.74314	12.698	0.05	0.012	0.12
VMC84.4258300	-69.9806700	84.42583	-69.98067	F	15.719	16.561	2.830818	725.09652	14.635	0.16	0.006	0.22
VMC84.4327100	-69.5863900	84.43271	-69.58639	F	15.683	17.174	6.856682	2182.67429	13.591	0.22	0.007	0.17
VMC84.4332900	-69.9852500	84.43329	-69.98525	F	14.465	15.298	5.950195	724.27584	13.392	0.24	0.008	0.22
VMC84.4707500	-70.0320300	84.47075	-70.03203	F	14.834	15.554	4.185139	725.96612	13.884	0.23	0.014	0.16
VMC84.4717500	-69.2077800	84.47175	-69.20778	F	16.21	17.449	2.947501	2186.21439	14.738	0.25	0.007	0.2
VMC84.5319200	-69.9396400	84.53192	-69.93964	F	15.352	16.291	3.627441	724.93703	14.207	0.15	0.008	0.24
VMC84.5323300	-69.1518100	84.53233	-69.15181	F	16.469	17.711	2.999089	2185.08407	14.798	0.23	0.006	0.2
VMC84.5394600	-69.7268900	84.53946	-69.72689	F	15.67	16.555	3.070851	2186.04468	14.551	0.21	0.006	0.21
VMC84.5694600	-69.7201100	84.56946	-69.72011	F	15.537	16.338	3.097344	2187.76931	14.501	0.23	0.015	0.21
VMC84.5818300	-69.1553600	84.58183	-69.15536	F	16.154	17.319	3.452496	2185.95731	14.593	0.22	0.006	0.2
VMC84.6056200	-68.6574700	84.60562	-68.65747	F	16.284	19.999	4.269554	2185.03076	14.032	0.24	0.004	0.2
VMC84.6248300	-70.0906400	84.62483	-70.09064	F	15.211	16.415	5.61994	721.73745	13.716	0.22	0.013	0.2
VMC84.6292100	-69.4912800	84.62921	-69.49128	F	16.044	19.999	3.010677	2190.95985	14.745	0.23	0.005	0.2
VMC84.6906700	-69.8426400	84.69067	-69.84264	F	15.096	16.099	4.851884	726.48961	13.92	0.15	0.004	0.27
VMC84.7067900	-70.0194700	84.70679	-70.01947	F	15.374	16.249	3.444329	726.55227	14.276	0.22	0.006	0.2
VMC84.7255800	-69.7144200	84.72558	-69.71442	F	16.188	17.558	4.358595	2184.31101	14.317	0.24	0.006	0.19
VMC84.7745400	-69.1263600	84.77454	-69.12636	F	15.951	17.136	3.514661	2184.902	14.464	0.22	0.006	0.17
VMC84.8131700	-69.3275600	84.81317	-69.32756	F	13.335	14.58	23.1107	2173.78238	11.735	0.41	0.021	0.2

a

a

a

6.1 VMC data for the Cepheids

149

VMC84.8607500	69.2553600	84.86075	-69.25536	F	16.706	18.381	3.47036	2185.71285	14.647	0.17	0.006	0.2
VMC84.8947100	69.1663900	84.89471	-69.16639	F	16.83	18.183	2.27171	2186.80757	15.087	0.21	0.005	0.17
VMC84.9115000	70.0420600	84.91150	-70.04206	F	14.702	15.792	7.192972	722.48232	13.301	0.25	0.011	0.13
VMC84.9425400	69.7910000	84.94254	-69.79100	F	15.577	16.454	3.106948	2186.61457	14.438	0.2	0.009	0.15
VMC84.9472500	70.0213300	84.94725	-70.02133	F	14.952	15.782	4.812791	726.51845	13.855	0.27	0.006	0.13
VMC84.9483300	70.0651700	84.94833	-70.06517	F	15.085	16.035	4.91727	723.59123	13.808	0.23	0.004	0.13
VMC84.9702100	70.0807200	84.97021	-70.08072	F	14.918	15.752	4.863336	722.44955	13.856	0.22	0.006	0.13
VMC84.9925000	69.0057500	84.99250	-69.00575	F	15.79	16.743	3.09562	2185.19882	14.55	0.2	0.005	0.27
VMC85.0200000	69.3711100	85.02000	-69.37111	F	15.499	16.363	3.385188	2186.5575	14.423	0.14	0.006	0.22
VMC85.0496700	69.3818300	85.04967	-69.38183	F	15.001	15.942	5.30412	2187.59537	13.756	0.24	0.003	0.22
VMC85.0534200	69.6355800	85.05342	-69.63558	F	16.191	17.524	4.364797	2185.81355	14.323	0.23	0.004	0.26
VMC85.0762100	68.7064700	85.07621	-68.70647	F	15.542	16.292	2.89419	2185.66511	14.536	0.2	0.004	0.17
VMC85.1030400	69.8720800	85.10304	-69.87208	F	14.823	15.84	6.27001	2185.45129	13.553	0.11	0.010	0.18
VMC85.1324600	68.7918100	85.13246	-68.79181	F	14.549	15.428	6.349792	2182.45427	13.396	0.23	0.002	0.15
VMC85.1391700	70.0307200	85.13917	-70.03072	F	15.606	16.444	3.206093	726.68396	14.515	0.19	0.004	0.13
VMC85.1434200	69.5984700	85.14342	-69.59847	F	16.052	17.174	3.493634	2186.2858	14.489	0.25	0.006	0.21
VMC85.1466300	69.0992800	85.14663	-69.09928	F	16.022	17.039	2.897505	2193.79171	14.667	0.18	0.003	0.27
VMC85.1826200	69.6577800	85.18262	-69.65778	F	15.873	16.704	2.42071	2187.62677	14.772	0.23	0.006	0.21
VMC85.1870000	69.4558600	85.18700	-69.45586	F	15.184	16.089	4.320914	2183.58395	14.015	0.16	0.004	0.22
VMC85.1913300	68.7347500	85.19133	-68.73475	F	14.706	15.46	5.322229	2183.34374	13.662	0.17	0.004	0.17
VMC85.1959600	69.9339700	85.19596	-69.93397	F	15.202	16.224	4.794257	2185.15372	13.924	0.18	0.006	0.18
VMC85.2872900	69.6189700	85.28729	-69.61897	F	14.732	15.662	7.323349	2185.26855	13.516	0.09	0.004	0.13
VMC85.2963700	69.5409400	85.29637	-69.54094	F	15.46	16.323	3.34595	2185.03397	14.406	0.2	0.006	0.19
VMC85.3070800	69.0644200	85.30708	-69.06442	F	13.731	14.541	11.446018	2178.50937	12.602	0.24	0.012	0.23
VMC85.3625000	69.1712200	85.36250	-69.17122	F	14.703	15.737	6.60688	2181.59574	13.412	0.24	0.004	0.23
VMC85.3720400	69.9175000	85.37204	-69.91750	F	15.136	15.974	4.133014	2184.17821	14.098	0.14	0.006	0.11
VMC85.3815000	68.7943900	85.38150	-68.79439	F	15.244	16.184	4.370518	2187.75876	14.034	0.22	0.009	0.17
VMC85.4010000	69.6936400	85.40100	-69.69364	F	13.349	14.307	20.319628	2181.0316	12.007	0.39	0.008	0.09
VMC85.4522100	68.6878100	85.45221	-68.68781	F	13.047	14.089	19.222249	2184.34941	11.77	0.45	0.033	0.17
VMC85.4641700	69.4034400	85.46417	-69.40344	F	15.471	16.259	3.199973	2185.06565	14.44	0.23	0.004	0.19
VMC85.4680000	69.8270300	85.46800	-69.82703	F	15.117	15.823	3.650866	2184.57804	14.117	0.21	0.004	0.09
VMC85.5329600	69.0053600	85.53296	-69.00536	F	14.476	15.339	7.7875625	2181.14918	13.222	0.21	0.009	0.2
VMC85.5381200	69.2079400	85.53812	-69.20794	F	15.292	16.208	4.080749	2184.50894	14.042	0.17	0.007	0.2
VMC85.5497100	68.8388600	85.54971	-68.83886	F	15.164	15.93	3.913076	2187.51653	14.146	0.28	0.006	0.17
VMC85.5718700	69.9954200	85.57187	-69.99542	F	15.927	16.655	2.01031	725.30076	14.965	0.18	0.006	0.1
VMC85.6621700	68.6706700	85.66217	-68.67067	F	14.422	15.479	5.406423	2183.38487	12.991	0.1	0.004	0.17
VMC85.7302500	69.9308100	85.73025	-69.93081	F	14.767	15.498	4.630885	2186.52603	13.818	0.25	0.006	0.12
VMC85.7748700	69.4906900	85.77487	-69.49069	F	14.253	15.116	8.558805	2179.84056	13.128	0.19	0.005	0.15
VMC85.7879200	69.6108100	85.78792	-69.61081	F	15.577	16.413	3.013363	2187.37171	14.541	0.18	0.004	0.11
VMC85.7937100	69.4696700	85.79371	-69.46967	F	14.756	15.535	4.783125	2186.84477	13.806	0.17	0.006	0.15
VMC85.8988300	69.1297200	85.89883	-69.12972	F	16.256	17.131	1.986145	2186.36341	15.138	0.12	0.009	0.18
VMC86.0109600	68.8207800	86.01096	-68.82078	F	15.922	16.801	2.31295	2186.59283	14.84	0.17	0.010	0.15
VMC86.0410400	69.2085300	86.04104	-69.20853	F	14.671	15.45	5.208322	2186.87375	13.676	0.23	0.002	0.16
VMC86.0615400	69.8610800	86.06154	-69.86108	F	16.023	16.967	2.586469	2186.24343	14.82	0.3	0.013	0.11
VMC86.0699200	69.8645600	86.06992	-69.86456	F	16.315	17.456	2.704462	2186.36035	14.874	0.13	0.017	0.11
VMC86.0700800	69.3040800	86.07008	-69.30408	F	13.832	14.819	12.090312	2178.40575	12.548	0.26	0.006	0.15
VMC86.1144600	69.5258900	86.11446	-69.52589	F	14.731	15.51	4.297464	2187.02142	13.584	0.15	0.007	0.15
VMC82.7496700	69.8211900	82.74967	-69.82119	F/FO	14.994	15.758	3.685621	452.48892	13.963	0.09	0.024	0.1
VMC82.7868700	70.0875000	82.78687	-70.08750	F/FO	15.015	15.647	3.446745	454.34056	14.21	0.13	0.024	0.03
VMC83.4140800	69.9152800	83.41408	-69.91528	F/FO	15.369	16.099	2.937016	453.37663	14.464	0.14	0.033	0.1
VMC83.4864200	68.8912800	83.48642	-68.89128	F/FO	16.103	16.825	1.884077	2167.17594	15.102	0.03	0.028	0.11
VMC83.9859600	70.0809400	83.98596	-70.08094	F/FO	15.36	16.175	3.455079	723.47457	14.279	0.12	0.001	0.16
VMC84.1307500	69.4714200	84.13075	-69.47142	F/FO	15.597	16.392	2.726671	2185.78771	14.684	0.06	0.030	0.11
VMC84.5965000	69.8935000	84.59650	-69.89350	F/FO	15.433	16.233	3.209915	726.43209	14.381	0.04	0.030	0.24
VMC85.1482100	69.7457200	85.14821	-69.74572	F/FO	16.575	17.422	1.498688	2187.06732	15.543	0.1	0.029	0.17
VMC82.6971200	69.7617200	82.69712	-69.76172	FO	14.534	15.201	3.267083	454.30735	13.75	0.08	0.003	0.07
VMC82.7020000	69.4541700	82.70200	-69.45417	FO	15.051	15.694	2.417794	453.87777	14.293	0.08	0.020	0.07
VMC82.7167100	69.9463900	82.71671	-69.94639	FO	14.895	15.563	2.312054	455.48636	13.959	0.09	0.012	0.07

a

a

a

VMC82.7201700	69.7738100	82.72017	-69.77381	FO	14.025	14.731	5.27263	452.33337	13.14	0.07	0.006	0.1
VMC82.7613800 ^a	69.9533600	82.76138	-69.95336	FO	14.802	15.503	3.048261	454.14719	13.917	0.1	0.016	0.06
VMC82.8040800 ^a	69.4331900	82.80408	-69.43319	FO	14.869	15.425	2.529597	454.06467	14.163	0.05	0.002	0.06
VMC82.8215400 ^a	70.0583100	82.82154	-70.05831	FO	15.074	15.728	2.248646	454.18552	14.289	0.07	0.009	0.06
VMC82.8303700 ^a	70.0498100	82.83037	-70.04981	FO	15.378	16.015	1.823699	454.42274	14.618	0.06	0.010	0.06
VMC82.8427900 ^a	70.0593900	82.84279	-70.05939	FO	15.325	15.905	1.829813	455.40677	14.564	0.1	0.011	0.06
VMC82.8526300 ^a	70.0991900	82.85263	-70.09919	FO	15.59	16.302	1.892952	454.23771	14.754	0.06	0.013	0.02
VMC82.8530000 ^a	69.2881400	82.85300	-69.28814	FO	16.882	17.476	0.722922	2167.51188	16.146	0.11	0.020	0.06
VMC82.8918300 ^a	69.0518300	82.89183	-69.05183	FO	16.673	17.331	0.960143	2167.53206	15.821	0.14	0.014	0.12
VMC82.8985800 ^a	70.0948300	82.89858	-70.09483	FO	18.417	18.987	0.269772	455.45924	17.48	0.07	0.064	0.05
VMC82.9025800 ^a	69.9453600	82.90258	-69.94536	FO	14.677	15.339	3.23636	454.99413	13.809	0.06	0.014	0.09
VMC82.9203300 ^a	69.7508600	82.92033	-69.75086	FO	16.258	17.001	1.309066	454.51366	15.276	0.07	0.010	0.13
VMC82.9310800 ^a	70.0262200	82.93108	-70.02622	FO	15.049	15.672	2.314595	2167.16066	14.276	0.09	0.010	0.07
VMC82.9357500 ^a	70.1480800	82.93575	-70.14808	FO	16.706	17.293	0.804268	455.52268	15.964	0.08	0.010	0.05
VMC82.9483300 ^a	69.9617800	82.94833	-69.96178	FO	15.047	15.673	2.455287	454.34384	14.206	0.1	0.017	0.09
VMC82.9832100 ^a	69.6821400	82.98321	-69.68214	FO	15.168	15.738	2.215576	453.54064	14.364	0.06	0.007	0.11
VMC83.0513300 ^a	69.0021700	83.05133	-69.00217	FO	15.156	15.949	2.737257	2165.62617	14.129	0.09	0.002	0.16
VMC83.0785000 ^a	69.7777200	83.07850	-69.77772	FO	14.737	15.498	3.50861	453.00126	13.698	0.08	0.006	0.12
VMC83.1158700 ^a	69.5715000	83.11587	-69.57150	FO	16.396	17.086	1.271329	454.43027	14.952	0.05	0.009	0.13
VMC83.1515800 ^a	69.9600000	83.15158	-69.96000	FO	14.973	15.635	2.699998	453.456	14.085	0.08	0.009	0.05
VMC83.1669600 ^a	69.3166700	83.16696	-69.31667	FO	14.913	15.608	2.678595	2167.78835	14.056	0.07	0.006	0.08
VMC83.1920000 ^a	69.8714700	83.19200	-69.87147	FO	15.718	16.493	1.83664	454.01813	14.685	0.07	0.005	0.07
VMC83.1937100 ^a	69.3731400	83.19371	-69.37314	FO	14.872	15.463	2.65946	2166.23215	14.098	0.08	0.003	0.08
VMC83.1975000 ^a	69.4250000	83.19750	-69.42500	FO	15.405	16.136	2.138465	2165.91871	14.531	0.06	0.009	0.09
VMC83.2232500 ^a	68.7091400	83.22325	-68.70914	FO	16.676	17.343	0.844755	2167.48821	15.761	0.16	0.009	0.09
VMC83.2953700 ^a	68.9160300	83.29537	-68.91603	FO	14.767	15.649	4.096914	2164.35521	13.651	0.13	0.004	0.13
VMC83.2962100 ^a	69.9728100	83.29621	-69.97281	FO	18.092	18.627	0.30217	455.56882	17.766	0.08	0.077	0.08
VMC83.3579600 ^a	69.6324400	83.35796	-69.63244	FO	15.212	15.878	2.323201	454.69593	14.346	0.08	0.004	0.1
VMC83.3607900 ^a	69.9425300	83.36079	-69.94253	FO	15.114	15.758	2.361496	454.13708	14.082	0.06	0.004	0.09
VMC83.3764600 ^a	68.7891100	83.37646	-68.78911	FO	16.246	17.02	1.250556	2167.5369	15.257	0.11	0.004	0.14
VMC83.3947900 ^a	68.6766100	83.39479	-68.67661	FO	16.447	17.162	1.038564	2167.4122	15.569	0.09	0.006	0.14
VMC83.4035000 ^a	69.9046700	83.40350	-69.90467	FO	15.197	15.816	2.162023	455.32129	14.265	0.07	0.005	0.1
VMC83.4157500 ^a	69.9050800	83.41575	-69.90508	FO	15.365	16.071	2.203441	454.05352	14.391	0.06	0.016	0.1
VMC83.4238700 ^a	68.8728300	83.42387	-68.87283	FO	14.972	15.622	2.473558	2166.42877	14.16	0.04	0.004	0.11
VMC83.4291700 ^a	69.8537200	83.42917	-69.85372	FO	15.627	16.379	1.889387	454.28337	14.61	0.11	0.025	0.1
VMC83.4454200 ^a	69.9095800	83.44542	-69.90958	FO	15.245	15.989	2.284975	453.72226	14.323	0.06	0.012	0.1
VMC83.4624600 ^a	69.2014200	83.46246	-69.20142	FO	15.889	16.73	1.690023	2167.32138	14.843	0.07	0.007	0.22
VMC83.4802100 ^a	69.9122200	83.48021	-69.91222	FO	15.382	16.034	2.134265	455.11862	14.398	0.07	0.008	0.1
VMC83.5097500 ^a	69.4123300	83.50975	-69.41233	FO	16.278	16.995	1.178909	2167.27495	14.992	0.05	0.009	0.1
VMC83.5650400 ^a	69.5732800	83.56504	-69.57328	FO	15.213	15.92	2.286305	2165.95711	14.365	0.08	0.005	0.1
VMC83.5775400 ^a	69.8940600	83.57754	-69.89406	FO	15.061	15.816	2.675345	454.10811	14.102	0.09	0.006	0.11
VMC83.5815400 ^a	70.0000800	83.58154	-70.00008	FO	16.01	16.58	1.21637	455.64199	15.272	0.1	0.008	0.1
VMC83.5856700 ^a	69.1230800	83.58567	-69.12308	FO	17.188	18.042	0.766376	2167.65798	16.162	0.07	0.010	0.22
VMC83.6169200 ^a	69.9031400	83.61692	-69.90314	FO	15.342	16.131	2.332323	454.01032	14.337	0.08	0.009	0.11
VMC83.6435400 ^a	69.9017800	83.64354	-69.90178	FO	15.144	15.811	2.292384	454.3579	14.262	0.03	0.005	0.11
VMC83.6604600 ^a	70.0788600	83.66046	-70.07886	FO	15.196	15.874	2.232129	453.51255	14.259	0.07	0.002	0.1
VMC83.6857100 ^a	68.7021900	83.68571	-68.70219	FO	14.586	15.359	3.981786	2167.21095	13.586	0.05	0.004	0.11
VMC83.6878300 ^a	69.2335300	83.68783	-69.23353	FO	14.679	15.395	3.261288	2167.61024	13.766	0.02	0.003	0.26
VMC83.7338300 ^a	69.6795000	83.73383	-69.67950	FO	16.86	17.518	0.73489	454.97274	16.091	0.12	0.010	0.11
VMC83.7495400 ^a	69.8999200	83.74954	-69.89992	FO	15.129	15.737	2.209189	453.83482	14.322	0.07	0.005	0.1
VMC83.7593700 ^a	69.5858300	83.75937	-69.58583	FO	16.747	17.413	0.844367	2167.44356	15.907	0.09	0.012	0.11
VMC83.7986700 ^a	68.7629400	83.79867	-68.76294	FO	16.244	17.049	0.960528	2187.50814	15.091	0.05	0.007	0.09
VMC83.8355000 ^a	69.9861100	83.83550	-69.98611	FO	14.938	15.655	2.811448	724.10267	14.035	0.1	0.006	0.1
VMC83.8537900 ^a	68.6836700	83.85379	-68.68367	FO	15.001	15.798	3.070689	2185.73675	13.93	0.08	0.004	0.13
VMC83.8737100 ^a	70.0695600	83.87371	-70.06956	FO	15.399	15.914	1.975942	726.60706	14.382	0.06	0.005	0.16
VMC83.8763300 ^a	69.0235000	83.87633	-69.02350	FO	17.533	18.538	0.737576	2187.65845	16.298	0.07	0.006	0.34
VMC83.9102500 ^a	69.7253600	83.91025	-69.72536	FO	15.579	16.261	1.857334	726.07069	14.683	0.09	0.008	0.12
VMC83.9239200 ^a	69.0846900	83.92392	-69.08469	FO	17.213	17.664	0.4651	2187.64608	16.79	0.1	0.026	0.33
VMC83.9515400 ^a	70.0641900	83.95154	-70.06419	FO	15.358	16.16	2.265118	725.68269	14.39	0.08	0.010	0.16

a

a

a

6.1 VMC data for the Cepheids

VMC83.9726200	70.0343600	83.97262	-70.03436	FO	16.507	17.517	1.340417	726.77725	15.262	0.07	0.010	0.16
VMC83.9807500	-70.0081100	83.98075	-70.00811	FO	14.703	15.532	3.695331	724.31683	13.686	0.07	0.006	0.16
VMC84.0166200	-69.5241900	84.01662	-69.52419	FO	15.922	16.599	1.565745	2187.68567	15.033	0.12	0.006	0.1
VMC84.0186700	-70.0321100	84.01867	-70.03211	FO	15.743	17.297	2.035364	725.39411	13.725	0.03	0.010	0.16
VMC84.0221700	-70.0742800	84.02217	-70.07428	FO	15.176	15.981	2.628979	726.01851	14.137	0.09	0.006	0.16
VMC84.0501200	-69.3625000	84.05012	-69.36250	FO	14.944	15.687	2.910257	2186.48061	14.038	0.08	0.007	0.15
VMC84.0555400	-69.4420000	84.05554	-69.44200	FO	15.359	16.006	2.026425	2185.98961	14.48	0.02	0.007	0.11
VMC84.0585000	-69.9390000	84.05850	-69.93900	FO	15.749	16.925	2.25822	724.73196	14.362	0.06	0.011	0.13
VMC84.0965400	-70.0520600	84.09654	-70.05206	FO	15.28	16.11	2.581354	725.29979	14.221	0.09	0.008	0.16
VMC84.0993700	-69.9015600	84.09937	-69.90156	FO	15.39	16.106	2.065799	725.88851	14.521	0.08	0.006	0.13
VMC84.1065000	-70.0901900	84.10650	-70.09019	FO	15.593	16.399	2.000805	725.93043	14.586	0.08	0.007	0.16
VMC84.1946200	-69.3700600	84.19462	-69.37006	FO	15.916	16.648	1.589839	2187.32214	14.986	0.09	0.005	0.18
VMC84.1963700	-69.2367200	84.19637	-69.23672	FO	17.629	18.611	0.410356	2187.75837	15.851	0.03	0.021	0.28
VMC84.2167100	-69.3695000	84.21671	-69.36950	FO	15.385	16.058	1.958458	2185.95189	14.534	0.08	0.010	0.18
VMC84.2262900	-69.9856100	84.22629	-69.98561	FO	15.883	16.747	1.804941	726.4283	14.819	0.05	0.006	0.21
VMC84.2327900	-69.9218900	84.23279	-69.92189	FO	15.62	16.563	2.145398	726.07603	14.484	0.09	0.008	0.21
VMC84.2467900	-69.9540800	84.24679	-69.95408	FO	15.688	16.616	1.973307	726.80329	14.564	0.06	0.008	0.21
VMC84.2650800	-70.0643900	84.26508	-70.06439	FO	15.695	16.533	1.893779	726.50448	14.594	0.07	0.017	0.11
VMC84.2947100	-69.9484700	84.29471	-69.94847	FO	16.996	17.885	0.883266	726.16631	15.919	0.09	0.010	0.21
VMC84.2958300	-69.3602500	84.29583	-69.36025	FO	14.935	15.722	3.163767	2186.62043	13.969	0.09	0.015	0.18
VMC84.3185000	-69.9013900	84.31850	-69.90139	FO	15.643	16.689	2.40556	726.24905	14.285	0.09	0.004	0.21
VMC84.3577900	-70.0804200	84.35779	-70.08042	FO	15.092	15.74	2.264897	725.77867	14.272	0.06	0.006	0.12
VMC84.3698700	-69.9333100	84.36987	-69.93331	FO	15.638	16.566	2.112169	725.99354	14.496	0.06	0.009	0.22
VMC84.3867100	-68.7111100	84.38671	-68.71111	FO	15.106	16.044	3.228755	2185.0128	13.908	0.08	0.005	0.17
VMC84.3916200	-69.6746900	84.39162	-69.67469	FO	16.062	16.79	1.316338	2187.67108	15.152	0.1	0.004	0.17
VMC84.3976700	-70.0986400	84.39767	-70.09864	FO	15.248	15.816	1.894534	725.68038	14.502	0.05	0.008	0.12
VMC84.4121300	-69.9761900	84.41213	-69.97619	FO	15.133	15.909	2.541628	725.68883	14.146	0.07	0.005	0.22
VMC84.4355000	-69.2457200	84.43550	-69.24572	FO	16.094	17.128	1.928963	2187.43048	14.781	0.1	0.037	0.2
VMC84.4957100	-69.9243300	84.49571	-69.92433	FO	15.283	16.175	2.478877	724.38577	14.179	0.07	0.010	0.24
VMC84.5000800	-69.2817800	84.50008	-69.28178	FO	16.86	17.885	1.200558	2186.81002	15.559	0.09	0.008	0.18
VMC84.5173300	-69.9514200	84.51733	-69.95142	FO	15.428	16.174	1.990272	725.30922	14.49	0.04	0.006	0.24
VMC84.5540400	-69.8775600	84.55404	-69.87756	FO	16.824	17.769	0.969189	726.37487	15.38	0.06	0.006	0.24
VMC84.6319200	-69.9920000	84.63192	-69.99200	FO	14.779	15.655	3.571087	723.63484	13.744	0.1	0.008	0.27
VMC84.6545000	-69.5729200	84.65450	-69.57292	FO	16.711	18.111	1.950142	2187.599	14.876	0.09	0.008	0.32
VMC84.6687900	-70.1106400	84.66879	-70.11064	FO	15.907	17.004	1.953709	726.05477	14.652	0.08	0.006	0.2
VMC84.6926200	-69.9358600	84.69262	-69.93586	FO	15.76	17.04	2.782939	725.77121	14.21	0.05	0.006	0.27
VMC84.6940000	-69.6885800	84.69400	-69.68858	FO	16.853	19.999	1.322446	2249.60191	15.297	0.07	0.006	0.19
VMC84.7540400	-69.8597500	84.75404	-69.85975	FO	16.586	17.549	1.320541	726.25262	15.372	0.1	0.007	0.27
VMC84.8200400	-70.1099700	84.82004	-70.10997	FO	15.794	16.545	1.587184	725.3721	14.868	0.11	0.010	0.12
VMC84.8294600	-70.0746700	84.82946	-70.07467	FO	16.721	18.169	1.96575	726.72225	14.835	0.07	0.002	0.12
VMC84.8302500	-70.0923600	84.83025	-70.09236	FO	15.468	16.368	2.537675	725.09722	14.333	0.07	0.005	0.12
VMC84.8335400	-69.5571100	84.83354	-69.55711	FO	15.827	16.543	1.641313	2187.16355	14.766	0.02	0.015	0.2
VMC84.8459200	-69.3685800	84.84592	-69.36858	FO	15.117	15.902	2.911248	2185.33494	14.079	0.07	0.0097	0.2
VMC84.8606200	-70.0388900	84.86062	-70.03889	FO	15.235	16.023	2.503442	724.37086	14.229	0.07	0.0060	0.12
VMC84.8607500	-69.6172200	84.86075	-69.61722	FO	18.094	20.255	2.183252	2185.9854	15.031	0.06	0.0043	0.2
VMC84.8612900	-69.8994700	84.86129	-69.89947	FO	16.322	17.283	1.413235	726.61113	15.085	0.09	0.0064	0.28
VMC84.9244600	-69.6139700	84.92446	-69.61397	FO	16.27	17.477	2.089392	2186.88295	14.666	0.08	0.0058	0.26
VMC84.9412500	-69.9014200	84.94125	-69.90142	FO	15.541	16.41	2.2143	725.78707	14.445	0.09	0.0083	0.17
VMC85.0190400	-68.8521700	85.01904	-68.85217	FO	16.646	17.46	1.055513	2187.69114	15.468	0.03	0.0171	0.18
VMC85.0530000	-69.9610800	85.05300	-69.96108	FO	16.063	17.155	1.844226	725.40332	14.738	0.06	0.0064	0.17
VMC85.0706700	-70.0889700	85.07067	-70.08897	FO	17.252	17.972	0.580853	726.49325	15.981	0.07	0.0115	0.13
VMC85.0858300	-69.3965300	85.08583	-69.39653	FO	15.626	16.28	1.584138	2186.67939	14.823	0.1	0.0045	0.22
VMC85.1360400	-70.0261900	85.13604	-70.02619	FO	15.81	16.653	1.848191	725.75518	14.733	0.07	0.0045	0.13
VMC85.1580000	-69.9266400	85.15800	-69.92664	FO	15.401	16.191	2.176327	2185.74512	14.396	0.06	0.0048	0.18
VMC85.2967900	-69.5427800	85.29679	-69.54278	FO	15.418	16.14	2.001621	2187.28077	14.523	0.09	0.0046	0.19
VMC85.3102100	-68.9213900	85.31021	-68.92139	FO	16.995	17.774	0.785469	2187.6721	16.013	0.04	0.0056	0.17
VMC85.3533300	-68.7182200	85.35333	-68.71822	FO	17.212	18.002	0.675793	2187.13439	16.217	0.09	0.0059	0.17
VMC85.3631700	-69.8885800	85.36317	-69.88858	FO	15.726	16.503	1.778921	2186.54678	14.702	0.11	0.0055	0.11
VMC85.5175800	-70.1026900	85.51758	-70.10269	FO	15.568	16.376	1.925496	725.3601	14.558	0.09	0.0149	0.14

a

a

VMC85.5237900	68.8817500	85.52379	-68.88175	FO	14.622	15.625	4.737597	2183.49648	13.369	0.09	0.0077	0.17
VMC85.5661700	-70.0946400	85.56617	-70.09464	FO	17.476	18.21	0.495666	726.40479	16.61	0.05	0.0185	0.14
VMC85.5958300	-69.8561400	85.59583	-69.85614	FO	15.15	15.788	2.205867	2187.07406	14.331	0.1	0.0092	0.1
VMC85.6187100	-69.7823300	85.61871	-69.78233	FO	15.844	16.435	1.285872	2186.88561	15.067	0.11	0.0060	0.1
VMC85.6227100	-69.9661100	85.62271	-69.96611	FO	14.785	15.633	3.928321	725.21854	13.66	0.03	0.0056	0.1
VMC85.6272500	-70.0772800	85.62725	-70.07728	FO	17.429	17.87	0.415751	726.5859	16.678	0.11	0.0241	0.14
VMC85.6607100	-70.0928900	85.66071	-70.09289	FO	15.671	16.589	2.036236	725.61624	14.456	0.07	0.0036	0.13
VMC85.7250000	-69.7336900	85.72500	-69.73369	FO	16.122	17.068	1.839786	2187.20841	14.765	0.07	0.0076	0.13
VMC85.8637900	-69.6055300	85.86379	-69.60553	FO	16.17	17.02	1.477193	2187.75508	15.137	0.08	0.0046	0.1
VMC85.8915000	-69.3112800	85.89150	-69.31128	FO	14.543	15.736	3.083662	2185.09123	12.941	0.03	0.0053	0.15
VMC85.9160400	-69.7380300	85.91604	-69.73803	FO	16.36	17.069	1.094458	2187.04359	15.465	0.09	0.0143	0.14
VMC85.9932900	-68.9028100	85.99329	-68.90281	FO	15.567	16.253	1.811681	2187.35588	14.64	0.06	0.0071	0.15
VMC85.9952500	-69.4873600	85.99525	-69.48736	FO	15.432	16.258	2.033228	2186.83039	14.429	0.11	0.0047	0.15
VMC85.9990400	-68.8570800	85.99904	-68.85708	FO	15.191	15.939	2.326961	2186.61535	14.245	0.05	0.0045	0.15
VMC86.0872900	-69.8647500	86.08729	-69.86475	FO	17.811	18.134	0.308278	2187.62609	17.431	0.06	0.0463	0.11
VMC86.1035400	-69.9754700	86.10354	-69.97547	FO	15.534	16.112	1.563193	2187.29978	14.746	0.08	0.0087	0.11
VMC86.1356300	-70.0256700	86.13563	-70.02567	FO	16.13	16.917	1.341401	2186.54489	15.151	0.06	0.0098	0.11
VMC86.1700800	-69.9203100	86.17008	-69.92031	FO	15.457	16.156	1.911485	2186.3996	14.499	0.09	0.0079	0.11
VMC83.2077900	-70.0708900	83.20779	-70.07089	FO/SO	16.296	16.851	0.951998	455.62868	15.416	0.08	0.0407	0.05
VMC83.3057900	-69.8713100	83.30579	-69.87131	FO/SO	17.148	17.793	0.628968	455.6168	16.317	0.1	0.0148	0.08
VMC83.5200400	-68.6412800	83.52004	-68.64128	FO/SO	16.423	17.054	0.914905	2167.85454	15.683	0.11	0.0151	0.08
VMC83.5680800	-69.8773900	85.56808	-69.87739	FO/SO	16.132	16.806	1.236071	2187.59048	15.015	0.07	0.0076	0.1
VMC83.6328300	-69.7541100	83.63283	-69.75411	FO/SO	16.746	17.322	0.749803	455.44006	15.95	0.13	0.0103	0.11
VMC84.0779600	-69.6683100	84.07796	-69.66831	FO/SO	16.826	17.434	0.73008	2187.37178	16.047	0.1	0.0093	0.11
VMC82.8781200	-69.7410300	82.87812	-69.74103	FO/SO	16.265	16.971	1.186461	455.20008	15.382	0.08	0.0182	0.13
VMC85.4944200	-69.3631100	85.49442	-69.36311	FO/SO	17.578	18.123	0.416365	2187.60105	16.862	0.05	0.0131	0.15
VMC84.4185000	-68.8450600	84.41850	-68.84506	FO/SO	17.214	17.949	0.668873	2187.13918	16.231	0.07	0.0193	0.17
VMC84.7129200	-69.8227200	84.71292	-69.82272	FO/SO	17.111	17.763	0.611007	726.69542	16.295	0.08	0.0153	0.19
VMC83.6123300	-69.0424200	83.61233	-69.04242	FO/SO	17.798	18.609	0.498891	2167.4803	16.762	0.08	0.0144	0.21
VMC83.6189200	-68.9502800	83.61892	-68.95028	FO/SO	16.737	17.379	0.791267	2167.09583	15.921	0.1	0.0138	0.21
VMC84.4010000	-69.7390600	84.40100	-69.73906	FO/SO	16.599	17.674	1.353017	726.18634	15.26	0.07	0.0081	0.23
VMC85.2746300	-69.0552200	85.27463	-69.05522	FO/SO	16.513	17.295	1.011729	2186.89479	15.552	0.08	0.0076	0.23
VMC84.7009200	-69.5859400	84.70092	-69.58594	FO/SO	18.167	19.622	0.833525	2187.07298	16.186	0.1	0.0133	0.32

Table 6.3: PL, Wesenheit and PLC relations for F and FO Classical Cepheids in the 30 Dor field. The Wesenheit function is defined as: $W(V, K_S) = K_S - 0.13*(V - K_S)$.

Mode	α	σ_α	β	σ_β	γ	σ_γ	r.m.s.
$K_S^0 = \alpha + \beta \log P$							
F	16.070	0.017	-3.295	0.018			0.102
FO	15.580	0.012	-3.471	0.035			0.099
$W(V, K_S) = \alpha + \beta \log P$							
F	15.870	0.013	-3.325	0.014			0.078
FO	15.400	0.008	-3.530	0.025			0.070
$K_S^0 = \alpha + \beta \log P + \gamma(V - K_S)_0$							
F	15.740	0.073	-3.346	0.013	0.216	0.014	0.073
FO	15.355	0.070	-3.545	0.026	0.163	0.014	0.070

6.2 Classical Cepheids in the 30 Dor field

The 30 Dor field contains 164 fundamental mode (F), 139 first overtone (FO), 8 F/FO, and 15 FO/SO (SO stands for second overtone) pulsators. The PLK relations of the 172 fundamental mode and the 154 first overtone¹ Classical Cepheids analysed in the 30 Dor field are shown in Fig. 6.3. Since the saturation level of the VMC survey in K_S limits the length of the periods we are able to measure to a maximum value of about 15-20 days, we complemented our data with the sample of Persson et al. (2004) that includes 84 F-mode Cepheids with periods mainly ranging between 10 and 100 days. To merge the two samples we first transformed Persson et al.'s original photometry from the LCO to the 2MASS system, using the relations by Carpenter (2001). These data are shown as light blue circles in Fig. 6.3. To account for the variable reddening that characterizes the 30 Dor region, we adopted the recent reddening evaluations by Haschke et al. (2011) (reported in column 12 of Table 6.2), while to correct Persson et al. (2004) dataset we adopted the reddening values provided by the Authors.

Finally, we performed least-square fits to the data of F- and FO-modes variables separately, adopting an equation of the form $K_S^0 = \alpha + \beta \log P$. The coefficients derived from the fits are provided in the first portion of Table 6.3.

In addition to the PLK_S relation we also considered the Period-Wesenheit (PW)

¹Double mode pulsators F/FO and FO/SO were included in the F and FO samples, respectively.

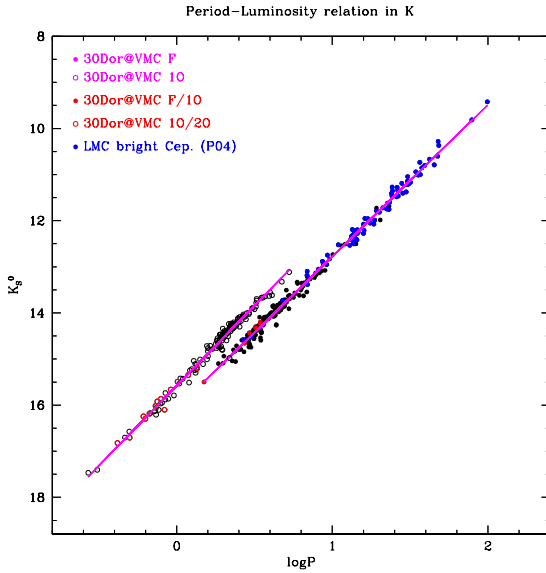


Figure 6.3: K_S -band PL relation for Cepheids in the 30 Dor field. Black open and filled circles show FO- and F-mode pulsators, respectively. Light blue filled circles show the F-mode Cepheid sample by Persson et al. (2004). Solid lines are the result of the least square fit to the data (see text for details).

and the Period-Luminosity-Color (PLC) relations. These relations are widely used in the literature and are particularly useful to study the 3D structure of the Magellanic System, as they have much smaller dispersions than a simple PLK_S relation.

The PW and PLC relations are usually calculated using the $(V - I)$ color. However, given the data available to us we decided to build our PW and PLC relations using the $V - K_S$. As far as we know, this is the first empirical PW using Near-IR colors. Following Cardelli et al. (1989) the Wesenheit function is defined as $W(V, K_S) = K_S - 0.13*(V - K_S)$ and the equation we want to fit has the form: $W(V, K_S) = \alpha + \beta \log P$. Similarly, we will adopt a PLC relation of the form $K_S^0 = \alpha + \beta \log P + \gamma(V - K_S)_0$.

Results from such a procedure are shown in Figs. 6.4 and 6.5, for the PW, and PLC relations, respectively. Coefficients of the PW and PLC equations derived with this procedure are provided in the middle and lower portions of Table 6.3.

We can now compare our results with previous studies. Literature values for the coefficients of the PL, PW, and PLC relations are summarized in Table 6.4. The first three rows of the table report the empirical results for the PLK_S of fundamental mode pulsators by Groenewegen (2000); Persson et al. (2004); Testa et

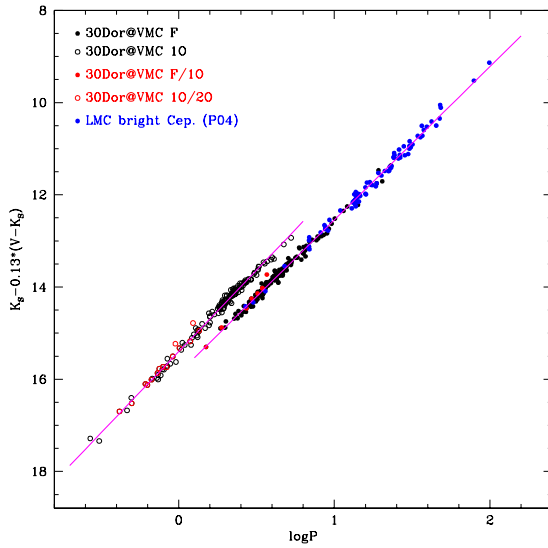


Figure 6.4: Period-Wesenheit relation for Cepheids in the 30 Dor field. Black open and filled circles show FO- and F-mode pulsators, respectively. Light blue filled circles show the F-mode Cepheid sample by Persson et al. (2004). Solid lines are the result of the least square fit to the data (see text for details).

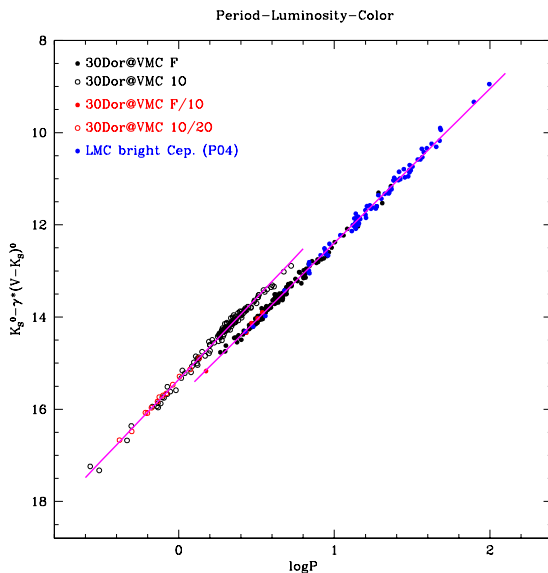


Figure 6.5: Period-Luminosity-Color relation for Cepheids in the 30 Dor field. Black open and filled circles show FO- and F-mode pulsators, respectively. Light blue filled circles show the F-mode Cepheid sample by Persson et al. (2004). Solid lines are the result of the least square fit to the data (see text for details).

al. (2007), whereas the fourth row shows the theoretical result by Caputo et al. (2000a). Similarly, rows 5-6 display the empirical results by Groenewegen (2000) and the semiempirical results by Bono et al. (2002). A comparison between Tab. 6.3 and Tab. 6.4 reveals that for the PLK_S relation of the F-mode pulsators, there is general agreement within the errors between our results and Groenewegen (2000); Persson et al. (2004); Storm et al. (2011a) (only slope for the latter). Only marginal agreement is found instead with Testa et al. (2007), whose results are based on the Persson et al. (2004) sample complemented at shorter periods with Cepheids belonging to the LMC clusters NGC1866 and NGC2031. As for the comparison with theory, we find that there is a satisfactory agreement between our slope and the slope predicted by pulsation models for the LMC chemical composition (Caputo et al., 2000a). The errors in the coefficients of our PLK_S relation are smaller than in previous studies. This is due to the large range in period spanned by the Cepheids in our sample, including for the first time a significant number of objects with near-infrared photometry and periods smaller than 5 days. In the case of the FO pulsators the agreement with Groenewegen (2000) is not as good as for F-mode Cepheids, this may be an effect of the deeper magnitude limit achieved by the VMC survey (Groenewegen, 2000, relies on 2MASS and DENIS data), that allowed us to reach the fainter FO-Cepheids populating the low-period tail of the PLK_S relation.

Since there are no empirical Wesenheit and the PLC relations in K available the literature we can only compare our PW and PLC relations with the theoretical results by Caputo et al. (2000a). The slope of our $W(V, K_S)$ relation is in agreement with the theoretical value, while a significant discrepancy is found between period and color-term coefficients.

The SEP Cepheids are too few to define independent PL, PW, and PLC relations. When plotted on the relations defined by the 30 Dor Cepheids (see Fig. 6.4) they show some scatter. However, it is not clear whether the scatter is due to them defining different relationships, or to projection effects.

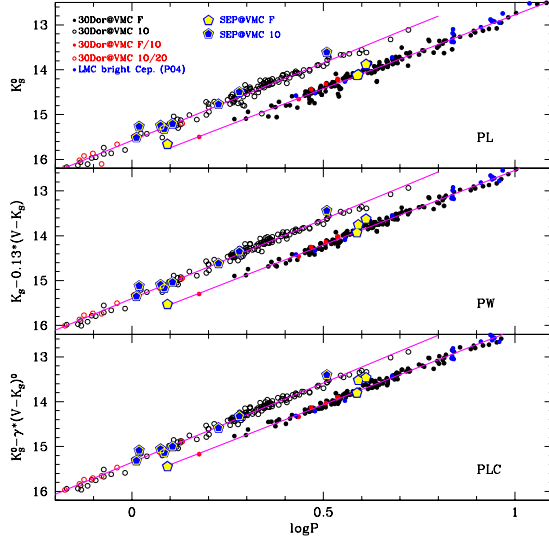


Figure 6.6: Cepheids in the SEP (blue and yellow pentagons for F and FO pulsators, respectively) field overplotted on the PL, PW and PLC relationships defined by the 30 Dor Cepheids.

Table 6.4: Literature values for the coefficients of the PL, Wesenheit and PLC relations for F and FO Classical Cepheids. As before, the Wesenheit function is defined as: $W(V, K_S) = K_S - 0.13 * (V - K_S)$. The photometry of previous studies was converted to the 2MASS system, to be consistent with our results.

Mode	α	σ_α	β	σ_β	γ	σ_γ	r.m.s.	Source
$K_S^0 = \alpha + \beta \log P$								
F	16.032	0.025	-3.246	0.036			0.168	Groenewegen (2000)
F	16.051	0.05	-3.281	0.040			0.108	Persson et al. (2004)
F	15.945	0.040	-3.19	0.040				Testa et al. (2007)
F	-2.36	0.04	-3.28	0.09			0.21	Storm et al. (2011b)
F	-2.65	0.01	-3.23	0.01			0.07	Caputo et al. (2000a)
FO	15.533	0.032	-3.381	0.076			0.137	Groenewegen (2000)
FO	15.62	0.13	-3.57	0.03			0.14	Bono et al. (2002)
$W(V, K_S) = \alpha + \beta \log P$								
F	-2.92	0.09	-3.21	0.04			0.09	Caputo et al. (2000a)
$K_S^0 = \alpha + \beta \log P + \gamma(V - K_S)_0$								
F	-3.37	0.04	-3.60	0.03	1.61	0.03	0.03	Caputo et al. (2000a)

6.3 Zero point of the PW and PLC relations, and distance to the LMC

Our main goal is to use the Cepheids (along with the RR Lyrae stars) to map the 3D geometry of the Magellanic System. However, this is not yet feasible with the few VMC tiles observed so far. Still, we can use the PL, PW and PLC relations derived in the previous section to estimate an absolute distance to the LMC, but need to calibrate their zero points. In the following we shall use mainly the PW and PLC relations, as they appear to be less dispersed than the PL, and will rely only on “direct” measurements of their zero points, based on the trigonometric parallaxes of Galactic Cepheids, and the Baade-Wesselink method applied to LMC Cepheids.

6.3.1 Zero points from the parallax of Galactic Cepheids

Accurate parallaxes for Galactic Cepheids are available for less than 20 objects, from observations with the Hipparcos satellite (van Leeuwen et al., 2007), and the Hubble Space Telescope (Benedict et al., 2007). From van Leeuwen et al. (2007) and Benedict et al. (2007) samples we only retained stars with most accurate parallax ($\delta\pi/\pi \leq 0.2$). Photometric data (including K -band photometry) and individual reddening values for these stars were taken from Fouqué et al. (2007), while for the Lutz-Kelker corrections we followed Benedict et al. (2007). We then computed the PL, PW and PLC relations. The color term in the PLC relation turned out to be not significant, thus the PL and PLC are identical and equal to: $K_S^0 = -2.44 \pm 0.12 - (3.20 \pm 0.14)\log P$. Similarly, for the Wesenheit function we have: $W(V, K_S) = -2.61 \pm 0.12 - (3.28 \pm 0.13)\log P$. Although rather uncertain the slopes of these relations are in good agreement with our results from the 30 Dor Cepheids within the errors. We thus adopted our slopes from the 30 Dor Cepheids for the PL and PW relations and derived their zero points:

$$K_S^0(F) = -2.36 \pm 0.05 - (3.295 \pm 0.018)\log P \quad (6.1)$$

$$W(V, K_S)(F) = -2.57 \pm 0.05 - (3.325 \pm 0.014)\log P \quad (6.2)$$

where we used a weighted average and the error on the zero point is the standard

6.3 Zero point of the PW and PLC relations, and distance to the LMC159

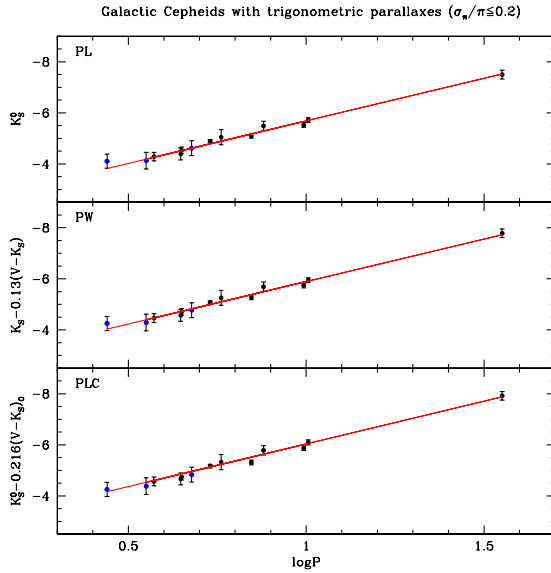


Figure 6.7: *PL*, *PW* and *PLC* relation for galactic Cepheids with accurate trigonometric parallaxes.

deviation of the mean. Similarly, by adopting our value of 0.216 for the $(V - K_S)$ color coefficient in the the PLC, we obtained: $W(V, K_S)(F) = -2.68 \pm 0.12 - (3.36 \pm 0.14)\log P + (0.216 \pm 0.014)(V - K_S)_0$.

Since, also the term in $\log P$ is virtually identical to our result for the LMC (-3.346 ± 0.013), we used this value to obtain the final zero point of the PLC by following the same procedure applied for the PW:

$$K_S^0(F) = -2.69 \pm 0.05 - (3.346 \pm 0.013)\log P + (0.216 \pm 0.014)(V - K_S)_0 \quad (6.3)$$

Here the errors on the zero points, as well as an estimate of the systematic errors due to the adoption of the same slope for the Galactic and LMC Cepheids, are based on the theoretical work by Caputo et al. (2000a). The PL, PW and PLC relations obtained with this procedure are shown in Fig. 6.7. By comparing Eq. 6.2 and 6.3 with the results in Tab. 6.3, we obtain distances to the LMC based on the F-mode Cepheids of: $(m - M)_0^{TRIG}(PW) = 18.44 \pm 0.05$, and $(m - M)_0^{TRIG}(PLC) = 18.43 \pm 0.05$, respectively.

6.3.2 Zero points from the IRSB Baade-Wesselink method

Recently, Storm et al. (2011a,b) have applied the InfraRed Surface Brightness modification of the Baade-Wesselink technique to a sample of Galactic and LMC Cepheids (36 objects in the LMC). We used their absolute magnitudes in K^2 and V to calibrate the zero points of the PW and PLC relations. As done with the Galactic Cepheids, we adopted our slopes for the PW and PLC relations and determined the zero points. The assumption is well justified in this case as both our and Storm et al. (2011b) Cepheids belong to the LMC. As a result we obtain:

$$K_S^0(F) = -2.40 \pm 0.07 - (3.295 \pm 0.018)\log P \quad (6.4)$$

$$W(V, K_S)(F) = -2.60 \pm 0.07 - (3.325 \pm 0.014)\log P \quad (6.5)$$

$$K_S^0(F) = -2.72 \pm 0.07 - (3.346 \pm 0.013)\log P + (0.216 \pm 0.014)(V - K_S)_0 \quad (6.6)$$

where the errors on the zero points include the dispersion of the measures, as well as the estimate of the systematic error due to the uncertainty on the “p-factor” (see e.g. Storm et al., 2011a, and references therein). The new zero points are in excellent agreement with those derived from the Galactic Cepheids. These relations lead to distance moduli for the LMC of: $(m - M)_0^{IRSB}(PW) = 18.46 \pm 0.07$, and $(m - M)_0^{IRSB}(PLC) = 18.46 \pm 0.07$, respectively.

6.3.3 Zero points from the CORS Baade-Wesselink method

A different implementation of the Baade-Wesselink technique, the so-called CORS method (see e.g. Caccin et al., 1981; Ripepi et al., 1997; Molinaro et al., 2011), has been applied by Molinaro et al. (2012) to 9 Cepheids (7 F- and 2 FO-mode) belonging to NGC1866, a populous young cluster in the LMC, deriving for the cluster a distance modulus of: $(m - M)_0(NGC1866) = 18.51 \pm 0.03$. This value can be used to calibrate the PW and PLC relations following the same procedure described

²Note that these K magnitudes were transformed to the 2MASS K_S system and referred to the center of LMC using the corrections by Storm et al. (2011b).

6.3 Zero point of the PW and PLC relations, and distance to the LMC161

in the previous sections, and with the advantage that we can now calibrate also the relation for the FO-mode pulsators (although only on two stars). In this case we obtain:

$$K_S^0(F) = -2.44 \pm 0.07 - (3.295 \pm 0.018) \log P \quad (6.7)$$

$$K_S^0(FO) = -2.94 \pm 0.07 - (3.471 \pm 0.035) \log P \quad (6.8)$$

$$W(V, K_S)(F) = -2.62 \pm 0.07 - (3.325 \pm 0.014) \log P \quad (6.9)$$

$$W(V, K_S)(FO) = -3.10 \pm 0.07 - (3.530 \pm 0.025) \log P \quad (6.10)$$

$$K_S^0(F) = -2.74 \pm 0.07 - (3.346 \pm 0.013) \log P + (0.216 \pm 0.014)(V - K_S)_0 \quad (6.11)$$

$$K_S^0(FO) = -3.15 \pm 0.07 - (3.545 \pm 0.026) \log P + (0.163 \pm 0.014)(V - K_S)_0 \quad (6.12)$$

Here, as in the previous section the errors in the zero points include both the dispersion of the measures, and the uncertainty in the “p-factor”. Averaging the results for F- and FO-mode Cepheids, we obtain distance moduli of: $(m - M)_0^{CORS}(PW) = 18.49 \pm 0.07$, and $(m - M)_0^{CORS}(PLC) = 18.49 \pm 0.07$. The -0.02 mag difference with Molinaro et al. (2012) is likely due to the distance between NGC1866 and the LMC center.

Summary and Conclusions

In this thesis we have used pulsating stars such as the RR Lyrae stars and the Cepheids as probes of the extended structure of galaxies, their formation and evolution history, by exploiting the potential of these variables as distance indicators and stellar population tracers.

We have first focused on the study of the pulsating variable stars in two “ultra-faint” new satellites of the Milky Way, namely, Leo IV and Hercules. Our main results are:

- the discovery of pulsating stars in both systems: Leo IV hosts 3 RR Lyrae stars and one SX Phoenicis, while Hercules hosts 9 RR Lyrae stars and one Anomalous Cepheid;
- the pulsation properties of the RR Lyrae stars in both systems are consistent with the Oosterhoff dichotomy observed in the Milky Way, and qualify both Leo IV and Hercules as Oosterhoff type II systems;
- the first $V, B - V$ color-magnitude diagram (CMD) of the Leo IV dwarf, and for Hercules the deepest $V, V - I$ CMD ever obtained;
- the measure of metallicities, from the Fourier analysis of the RR Lyrae light curves, in agreement with the spectroscopic estimates: $\langle [Fe/H]_{C09}^{Her} \rangle = -2.30 \pm 0.15$ dex; $\langle [Fe/H]_{C09}^{Leo\,IV} \rangle = -2.27$ dex.
- accurate distances for both systems from the RR Lyrae stars: $\mu_0^{Leo\,IV} = 20.99 \pm 0.07$ mag ($d = 158 \pm 5$ kpc), and $\mu_0^{Her} = 20.63 \pm 0.08$ mag ($d = 134 \pm 5$ kpc), for $M_V = 0.54$ at $[Fe/H] = -1.5$ dex;
- the discovery in both galaxies of RR Lyrae stars that lie well outside the galaxy half-light radius but perfectly fall on the Horizontal Branch of the

respective CMDs, thus suggesting that these galaxies are highly likely due to the interaction with the MW.

The second part of the thesis was focused on the analysis of the RR Lyrae stars and Classical Cepheids located in the South Ecliptic Pole (SEP) field and in the 30 Doradus (30 Dor) star forming region of the LMC, on the basis of the infrared K_S time series photometry obtained by the VMC survey of the Magellanic System. Our main results in thi spart of the thesis are:

- the classification of 11 Classical Cepheids and 106 RR Lyrae stars (76 RR_{ab} and 30 RR_c) in the SEP field, where no public variable stars catalogues are currently available and construction of the K_S light curves;
- measure of photometric metallicities, from the Fourier analysis of the light curves, for the RR Lyrae in the SEP field where no spectroscopic metallicity estimates are available;
- the K band average magnitudes for RR Lyrae stars and Classical Cepheids in both in the SEP and the 30 Dor fields;
- the PL_K relation for RR Lyrae stars in both fields:

$$k_0^{SEP} = (17.351 \pm 0.035) - 2.450 \pm 0.133 \times \log P \quad (6.13)$$

with r.m.s.=0.082; and

$$k_0^{30Dor} = (17.454 \pm 0.019) - 2.51 \pm 0.067 \times \log P \quad (6.14)$$

with a r.m.s. of 0.181.

- the distance estimate for the SEP field using several PL_K relations present in literature: $\mu_0 = 18.58 \pm 0.03$ mag; and a very preliminary distance estimate also estimate for the 30 Dor field using the same method: $\mu_0 \sim 18.7$ mag
- the PL_K , PL_{KC} and Wesenheit relations for Fundamental mode and First Overtone Classical Cepheids in the 30 Dor field;
- the distance estimate for the 30 Dor field using the Classical Cepheids and a number of different methods to calibrate the zero point of the PL_{KC} and Wesenheit relations ($\mu_0 = 18.46 \pm 0.07$).

6.3 Zero point of the PW and PLC relations, and distance to the LMC165

From these results obtained for Leo IV and Hercules, we can conclude that the ultra-faint dwarf galaxies are confirmed to be best candidates of the building blocks that may have contributed to the formation of the external Galactic halo.

For what concerns the geometrical structure of the LMC is clearly not yet possible to have a comprehensive view, given the very limited number of fields available so far. However, the data quality of the VMC survey was proved to be excellent for Classical Cepheids stars and very good for RR Lyrae stars. According to our preliminary results the Classical Cepheids are confirmed to be excellent distance indicators and population tracers in the central, more crowded regions of the LMC, while the RR Lyrae stars remain best probes of in the external regions, where the crowding is not an issue and Classical Cepheids are not available. The very preliminary results from the RR Lyrae in the 30 Dor field are very puzzling and need to be understood. The zero point of the RR Lyrae magnitude-metallicity relation still remains a controversial issue, thus using the PL_K relation seems the right direction to go.

Bibliography

- Abbe, C. 1867, MNRAS , 27, 257
- Adén, D., Wilkinson, M. I., Read, J. I., et al. 2009, ApJL , 706, L150
- Adén, D., Eriksson, K., Feltzing, S., et al. 2011, A& A , 525, A153
- Alcock, C., et al. 2000, ApJ , 542, 281
- Alcock, C., Allsman, R. A., Alves, D. R., et al. 1998, AJ , 115, 1921
- Alibert, Y., Baraffe, I., Hauschildt, P., & Allard, F. 1999, A& A , 344, 551
- Ansari, R., Cavalier, F., Moniez, M., et al. 1996, A& A , 314, 94
- Arnaboldi, M., Dietrich, J., Hatziminaoglou, E., et al. 2008, The Messenger, 134, 42
- Baade, W., & Swope, H. H. 1961, AJ , 66, 300
- Baade, W. 1952, *Trans. I.A.U.*, 8, 397
- Bailey, S. I. 1902, Annals of Harvard College Observatory, 38, 1
- Baird S.R., 1981, ApJ, 245, 208
- Battinelli, P., & Demers, S. 1992, AJ , 104, 1458
- Beaulieu, J. P., Grison, P., Tobin, W., et al. 1995, A& A , 303, 137
- Bell, E. F., Slater, C. T., & Martin, N. F. 2011, ApJL , 742, L15
- Belokurov, V., Zucker, D. B., Evans, N. W., et al. 2006, ApJL , 647, L111
- Belokurov, V., Zucker, D. B., Evans, N. W., et al. 2007, ApJ , 654, 897

- Belokurov, V., Walker, M. G., Evans, N. W., et al. 2008, ApJL , 686, L83
- Belokurov, V., Walker, M. G., Evans, N. W., et al. 2009, MNRAS , 397, 1748
- Belokurov, V., Walker, M. G., Evans, N. W., et al. 2010, ApJL , 712, L103
- Benedict, G. F., McArthur, B. E., Fredrick, L. W., et al. 2002, AJ , 123, 473
- Benedict, G. F., McArthur, B. E., Feast, M. W., et al. 2007, AJ , 133, 1810
- Benedict, G. F., McArthur, B. E., Feast, M. W., et al. 2011, AJ , 142, 187
- Bertin, E., & Arnouts, S. 1996, A& A Supp. , 117, 393
- Besla, G., Kallivayalil, N., Hernquist, L., et al. 2007, ApJ , 668, 949
- Besla, G., Kallivayalil, N., Hernquist, L., et al. 2010, ApJL , 721, L97
- Bland-Hawthorn, J., Sutherland, R., Agertz, O., & Moore, B. 2007, ApJL , 670, L109
- Blažko, S. 1907, Astronomische Nachrichten, 175, 325
- Blumenthal, G. R., Faber, S. M., Primack, J. R., & Rees, M. J. 1984, Nature , 311, 517
- Bonnarel, F., Fernique, P., Bienaymé, O., et al. 2000, A& A Supp. , 143, 33
- Bono, G., Caputo, F., Castellani, V., & Marconi, M. 1996, ApJL , 471, L33
- Bono, G., Caputo, F., Santolamazza, P., Cassisi, S., & Piersimoni, A. 1997, AJ , 113, 2209
- Bono, G., Caputo, F., Castellani, V., Marconi, M., & Storm, J. 2001, MNRAS , 326, 1183
- Bono, G., Groenewegen, M. A. T., Marconi, M., & Caputo, F. 2002, ApJL , 574, L33
- Bono, G., Caputo, F., Castellani, V., Marconi, M., Storm, J., & Degl'Innocenti, S. 2003, MNRAS , 344, 1097

- Bono, G., Marconi, M., Cassisi, S., et al. 2005, *ApJ* , 621, 966
- Borissova, J., Minniti, D., Rejkuba, M., et al. 2004, *A& A* , 423, 97
- Borissova, J., Minniti, D., Rejkuba, M., & Alves, D. 2006, *A& A* , 460, 459
- Borissova, J., Rejkuba, M., Minniti, D., Catelan, M., & Ivanov, V. D. 2009, *A& A* , 502, 505
- Bragaglia, A., Gratton, R. G., Carretta, E., et al. 2001, *AJ* , 122, 207
- Braun, R., & Thilker, D. A. 2004, *A& A* , 417, 421
- Brüns, C., Kerp, J., Staveley-Smith, L., et al. 2005, *A& A* , 432, 45
- Buonanno, R., Corsi, C., Bellazzini, M., Ferraro, F. R., Fusi Pecci, 1997, *AJ*, 113, 706
- Cacciari, C., Corwin, T. M., & Carney, B. W. 2005, *AJ* , 129, 267
- Cacciari, C., & Clementini, G. 2003, Stellar Candles for the Extragalactic Distance Scale, 635, 105
- Caccin, R., Onnembo, A., Russo, G., & Sollazzo, C. 1981, *A& A* , 97, 104
- Capaccioli, M., Mancini, D., & Sedmak, G. 2005, *The Messenger*, 120, 10
- Caputo, F., & degl’Innocenti, S. 1995, *A& A* , 298, 833
- Caputo, F. 1998, *A&ARv*, 9, 33
- Caputo, F., Marconi, M., & Musella, I. 2000, *A& A* , 354, 610
- Caputo, F., Castellani, V., Marconi, M., & Ripepi, V. 2000, *MNRAS* , 316, 819
- Caputo, F., Castellani, V., Degl’Innocenti, S., Fiorentino, G., & Marconi, M. 2004, *A& A* , 424, 927
- Cardelli, J. A., Clayton, G. C., & Mathis, J. S. 1989, *ApJ* , 345, 245
- Carpenter, J. M. 2001, *AJ* , 121, 2851

- Carollo, D., Beers, T. C., Lee, Y. S., et al. 2007, *Nature* , 450, 1020
- Carretta, E., & Gratton, R. G. 1997, *A& A Supp.* , 121, 95
- Carretta, E., Bragaglia, A., Gratton, R. G., et al. 2009, *A& A* , 505, 117
- Cassisi, S., Castellani, M., Caputo, F., & Castellani, V. 2004, *A& A* , 426, 641
- Catelan, M., Pritzl, B. J., & Smith, H. A. 2004, *Astrop. J. Supp.* , 154, 633
- Catelan, M. 2009, *Ap& SS* , 320, 261
- Chiba, M., & Beers, T. C. 2000, *AJ* , 119, 2843
- Cioni, M.-R., Loup, C., Habing, H. J., et al. 2000, *A& A Supp.* , 144, 235
- Cioni, M.-R. L., van der Marel, R. P., Loup, C., & Habing, H. J. 2000, *A& A* , 359, 601
- Cioni, M.-R. L., Clementini, G., Girardi, L., et al. 2011, *A& A* , 527, A116
- Clement, C. M., & Rowe, J. 2000, *AJ* , 120, 2579
- Clement, C. M., Muzzin, A., Dufton, Q., et al. 2001, *AJ* , 122, 2587
- Clementini, G., Di Tomaso, S., Di Fabrizio, L., et al. 2000, *AJ* , 120, 2054
- Clementini, G., Gratton, R., Bragaglia, A., et al. 2003, *AJ* , 125, 1309
- Clementini, G. 2010, Variable Stars, the Galactic halo and Galaxy Formation, Eds. N. Samus, C. Sterken, L. Szabados, Sternberg Astronomical Institute Publications, p. 111, (arXiv:1002.1575)
- Clementini, G. 2011, EAS Publications Series, 45, 267
- Cole, S., Aragon-Salamanca, A., Frenk, C. S., Navarro, J. F., & Zepf, S. E. 1994, *MNRAS* , 271, 781
- Coleman, M. G., de Jong, J. T. A., Martin, N. F., et al. 2007, *ApJL* , 668, L43
- Connors, T. W., Kawata, D., & Gibson, B. K. 2006, *MNRAS* , 371, 108

- Coppola, G., Dall’Ora, M., Ripepi, V., et al. 2011, MNRAS , 416, 1056
- Correnti, M., Bellazzini, M., Ibata, R. A., Ferraro, F. R., & Varghese, A. 2010, ApJ , 721, 329
- Cox, J. P., & Whitney, C. 1958, ApJ , 127, 561
- Cross, N. J. G., Collins, R. S., Hambly, N. C., et al. 2009, MNRAS , 399, 1730
- Da Costa, G. S., & Armandroff, T. E. 1995, AJ , 109, 2533
- Dall’Ora, M., Ripepi, V., Caputo, F., et al. 2003, AJ , 126, 197
- Dall’Ora, M., et al. 2004, ApJ , 610, 269
- Dall’Ora, M., Clementini, G., Kinemuchi, K., et al. 2006, ApJL , 653, L109
- Dall’Ora et al. in preparation
- Dalton, G. B., Caldwell, M., Ward, A. K., et al. 2006, Proc. SPIE , 6269,
- Davis, M., Efstathiou, G., Frenk, C. S., & White, S. D. M. 1985, ApJ , 292, 371
- Del Principe, M., Piersimoni, A. M., Storm, J., et al. 2006, ApJ , 652, 362
- Demers, S., & Harris, W. E. 1974, AJ , 79, 627
- Di Criscienzo, M., Marconi, M., & Caputo, F. 2004, ApJ , 612, 1092
- Di Criscienzo, M., Caputo, F., Marconi, M., & Cassisi, S. 2007, A& A , 471, 893
- Di Fabrizio, L., Clementini, G., Maio, M., Bragaglia, A., Carretta, E., Gratton, R., Montegriffo, P., & Zoccali, M. 2005, A& A , 430, 603
- Dolphin, A. E. 2000, PASP , 112, 1383
- Durrell, P. R., & Harris, W. E. 1993, AJ , 105, 1420
- Eddington, A. S. 1926, The Observatory, 49, 88
- Efremov, Y. N. 2003, Astronomy Reports, 47, 1000
- Eggen, O. J., Lynden-Bell, D., & Sandage, A. R. 1962, ApJ , 136, 748

- Emerson, J. P. 2001, The New Era of Wide Field Astronomy, 232, 339
- Elmegreen, B. G., & Efremov, Y. N. 1996, ApJ , 466, 802
- Emerson, J., McPherson, A., & Sutherland, W. 2006, The Messenger, 126, 41
- Epchtein, N., Deul, E., Derriere, S., et al. 1999, A& A , 349, 236
- Ferguson, A. M. N., Chapman, S., Ibata, R., et al. 2006, Planetary Nebulae Beyond the Milky Way, 286
- Fernley, J., Skillen, I., Carney, B. W., Cacciari, C., & Janes, K. 1998, MNRAS , 293, L61
- Ferraro, F. R., Paltrinieri, B., Fusi Pecci, F., et al. 1997, ApJL , 484, L145
- Fiorentino, G., & Monelli, M. 2012, arXiv:1202.2752
- Fouqué, P., Arriagada, P., Storm, J., et al. 2007, A& A , 476, 73
- Frebel, A., Johnson, J. L., & Bromm, V. 2009, MNRAS , 392, L50
- Freedman, W. L., & Madore, B. F. 1990, ApJ , 365, 186
- Freedman, W. L., Madore, B. F., Gibson, B. K., et al. 2001, ApJ , 553, 47
- Gardiner, L. T., & Noguchi, M. 1996, MNRAS , 278, 191
- Gingold, R. A. 1976, ApJ , 204, 116
- Graham, J. A. 1975, PASP , 87, 641
- Gratton, R. G., Bragaglia, A., Clementini, G., Carretta, E., Di Fabrizio, L., Maio, M., & Taribello, E. 2004, A& A , 421, 937
- Gratton, R. G., Carretta, E., Bragaglia, A., Lucatello, S., D’Orazi,V. 2010, A&A, 517, 81
- Grebel, E. K. 2005, IAU Colloq. 198: Near-fields cosmology with dwarf elliptical galaxies, 1
- Greco, C., Dall’Ora, M., Clementini, G., et al. 2008, ApJL , 675, L73

- Grillmair, C. J. 2006, ApJL , 645, L37
- Grillmair, C. J. 2009, ApJ , 693, 1118
- Groenewegen, M. A. T. 2000, A& A , 363, 901
- Groenewegen, M. A. T., & Oudmaijer, R. D. 2000, A& A , 356, 849
- Guhathakurta, P., & Reitzel, D. B. 1998, Galactic Halos, 136, 22
- Gullieuszik, M., Groenewegen, M. A. T., Cioni, M. - L., et al. 2011, arXiv:1110.4497
- Hacking P. et al., 1985, PASP, 97, 616
- Hambly, N. C., Collins, R. S., Cross, N. J. G., et al. 2008, MNRAS , 384, 637
- Harris, J. 2007, ApJ , 658, 345
- Haschke, R., Grebel, E. K., & Duffau, S. 2011, AJ , 141, 158
- Hayashi, E., Navarro, J. F., Taylor, J. E., Stadel, J., & Quinn, T. 2003, ApJ , 584, 541
- Heitsch, F., & Putman, M. E. 2009, ApJ , 698, 1485
- Helmi, A., Irwin, M. J., Tolstoy, E., et al. 2006, ApJL , 651, L121
- Hubble, E. P. 1936, Realm of the Nebulae, by E.P. Hubble. New Haven: Yale University Press, 1936. ISBN 9780300025002,
- Ibata, R. A., Gilmore, G., & Irwin, M. J. 1994, Nature , 370, 194
- Ibata, R. A., Gilmore, G., & Irwin, M. J. 1995, MNRAS , 277, 781
- Ibata, R., Irwin, M., Lewis, G., Ferguson, A. M. N., & Tanvir, N. 2001, Nature , 412, 49
- Irwin, M. J., Kunkel, W. E., & Demers, S. 1985, Nature , 318, 160
- Irwin, M., & Hatzidimitriou, D. 1995, MNRAS , 277, 1354
- Irwin, M. J., Lewis, J., Hodgkin, S., et al. 2004, Proc. SPIE , 5493, 411

- Irwin, M. J., Belokurov, V., Evans, N. W., et al. 2007, ApJL , 656, L13
- Johnson, J. A., & Bolte, M. 1998, ApJ, 115, 693
- Johnson, J. A., & Bolte, M. 1998, AJ , 115, 693
- Jones, R. V., Carney, B. W., & Fulbright, J. P. 1996, PASP , 108, 877
- Jurcsik, J. 1995, Acta Astron. , 45, 653
- Jurcsik, J., & Kovacs, G. 1996, A& A , 312, 111
- Kallivayalil, N., van der Marel, R. P., & Alcock, C. 2006, ApJ , 652, 1213
- Kallivayalil, N., van der Marel, R. P., Alcock, C., et al. 2006, ApJ , 638, 772
- Kaluzny, J., Kubiak, M., Szymanski, M., et al. 1997, A& A Supp. , 125, 343
- Kaluzny, J., Mochnacki, S., & Rucinski, S. M. 2006, AJ , 131, 407
- Kapakos, E., Hatzidimitriou, D., & Soszyński, I. 2011, MNRAS , 415, 1366
- Kauffmann, G., & White, S. D. M. 1993, MNRAS , 261, 921
- Kauffmann, G., & et al. 1999, Evolution of Large Scale Structure : From Recombination to Garching, 307
- Kereš, D., & Hernquist, L. 2009, ApJL , 700, L1
- King, D. S., & Cox, J. P. 1968, PASP , 80, 365
- Kirby, E. N., Simon, J. D., Geha, M., Guhathakurta, P., & Frebel, A. 2008, ApJL , 685, L43
- Kirby, E. N., Guhathakurta, P., Bolte, M., Sneden, C., & Geha, M. C. 2009, ApJ , 705, 328
- Kirby, E. N., Guhathakurta, P., Simon, J. D., et al. 2010, Astrop. J. Supp. , 191, 352
- Koch, A., McWilliam, A., Grebel, E. K., Zucker, D. B., & Belokurov, V. 2008, ApJL , 688, L13

- Kovács, G., & Walker, A. R. 2001, *A& A* , 371, 579
- Kraft, R. P., & Schmidt, M. 1963, *ApJ* , 137, 249
- Kravtsov, A. V., Klypin, A. A., Bullock, J. S., & Primack, J. R. 1998, *ApJ* , 502, 48
- Kubiak, M., & Udalski, A. 2003, *Acta Astron.* , 53, 117
- Kuehn, C., Kinemuchi, K., Ripepi, V., et al. 2008, *ApJL* , 674, L81
- Landolt, A. U. 1992, *AJ* , 104, 340
- Laney, C. D., & Stobie, R. S. 1986, *MNRAS* , 222, 449
- Laney, C. D., & Stobie, R. S. 1994, *MNRAS* , 266, 441
- Lasker, B. M., Lattanzi, M. G., McLean, B. J., et al. 2008, *AJ* , 136, 735
- Leavitt, H. S., & Pickering, E. C. 1912, *Harvard College Observatory Circular*, 173, 1
- Lee, Y.-W., Demarque, P., & Zinn, R. 1994, *ApJ* , 423, 248
- Liu, T., & Janes, K. A. 1990, *ApJ* , 354, 273
- Lindgren, L., & Perryman, M. A. C. 1996, *A& A Supp.* , 116, 579
- Lindgren, L. 2010, *IAU Symposium*, 261, 296
- Longmore, A. J., Fernley, J. A., & Jameson, R. F. 1986, *MNRAS* , 220, 279
- Madore, B. F., & Freedman, W. L. 1991, *PASP* , 103, 933
- Madore, B. F., & Freedman, W. L. 2012, *ApJ* , 744, 132
- Marconi, M., Fiorentino, G., & Caputo, F. 2004, *A& A* , 417, 1101
- Marconi, M., Musella, I., & Fiorentino, G. 2005, *ApJ* , 632, 590
- Marconi, M., Bono, G., Caputo, F., et al. 2006, *Mem. S.A.It.*, 77, 67
- Marconi, M., & Di Criscienzo, M. 2007, *A& A* , 467, 223

- Marquette, J. B. 1999, New Views of the Magellanic Clouds, 190, 523
- Martin, N. F., Ibata, R. A., Bellazzini, M., et al. 2004, MNRAS , 348, 12
- Martin, N. F., de Jong, J. T. A., & Rix, H.-W. 2008, ApJ , 684, 1075
- Mastropietro, C., Moore, B., Mayer, L., Wadsley, J., & Stadel, J. 2005, MNRAS , 363, 509
- Mastropietro, C. 2009, IAU Symposium, 256, 117
- Mateo, M. L. 1998, AR&A, 36, 435
- Mathewson, D. S., Cleary, M. N., & Murray, J. D. 1974, ApJ , 190, 291
- Matsunaga, N., Fukushi, H., Nakada, Y., et al. 2006, MNRAS , 370, 1979
- Matsunaga, N., Kawadu, T., Nishiyama, S., et al. 2011, Nature , 477, 188
- McConnachie, A. W., Irwin, M. J., Ibata, R. A., et al. 2003, MNRAS , 343, 1335
- McGonegal, R., McAlary, C. W., Madore, B. F., & McLaren, R. A. 1982, ApJL , 257, L33
- McClure-Griffiths, N. M., Pisano, D. J., Calabretta, M. R., et al. 2009, Astrop. J. Supp. , 181, 398
- McNamara, D. H. 1995, AJ , 109, 2134
- McNamara, D. H., Clementini, G., & Marconi, M. 2007, AJ , 133, 2752
- Meylan, G., & Heggie, D. C. 1997, A&ARv, 8, 1
- Miszalski, B., Napiwotzki, R., Cioni, M.-R. L., et al. 2011, A& A , 531, A157
- Meschin, I., Gallart, C., Aparicio, A., Cassisi, S., & Rosenberg, A. 2009, AJ , 137, 3619
- Meylan, G., Sarajedini, A., Jablonka, P., et al. 2001, AJ , 122, 830
- Molinaro, R., Ripepi, V., Marconi, M., et al. 2011, MNRAS , 413, 942

- Molinaro, R., Ripepi, V., Marconi, M., et al. 2012, arXiv:1201.3478
- Moore, B., Ghigna, S., Governato, F., Lake, G., Quinn, T., Stadel, J., & Tozzi, P. 1999, ApJL , 524, L19
- Moretti, M. I., Dall’Ora, M., Ripepi, V., et al. 2009, ApJL , 699, L125
- Morgan, S. M., Wahl, J. N., & Wieckhorst, R. M. 2007, MNRAS , 374, 1421
- Morris, P. W., Reid, I. N., Griffiths, W. K., & Penny, A. J. 1994, MNRAS , 271, 852
- Musella, I., Ripepi, V., Clementini, G., et al. 2009, ApJL , 695, L83
- Musella et al. in preparation
- Newberg, H. J., Yanny, B., Rockosi, C., et al. 2002, ApJ , 569, 245
- Nemec, J. M., Nemec, A. F. L., & Lutz, T. E. 1994, AJ , 108, 222
- Nidever, D. L., Majewski, S. R., Butler Burton, W., & Nigra, L. 2010, ApJ , 723, 1618
- Norris, J., & Zinn, R. 1975, ApJ , 202, 335
- Oosterhoff, P. T. 1939, The Observatory, 62, 104
- Paczynski, B. 1986, ApJ , 304, 1
- Payne-Gaposchkin, C. H. 1971, Smithsonian Contributions to Astrophysics, 13,
- Persson, S. E., Madore, B. F., Krzeminski, W., et al. 2004, AJ , 128, 2239
- Petersen, J. O. 1973, A& A , 27, 89
- Piersimoni, A. M., Bono, G., & Ripepi, V. 2002, AJ , 124, 1528
- Piersimoni, A. M., Bono, G., & Ripepi, V. 2002, AJ , 124, 1528
- Pietrinferni, A., Cassisi, S., Salaris, M., & Castelli, F. 2006, ApJ , 642, 797
- Piatek, S., Pryor, C., & Olszewski, E. W. 2008, AJ , 135, 1024

- Pojmanski, G. 1997, *Acta Astron.* , 47, 467
- Poretti, E. 2003, *A& A* , 409, 1031
- Poretti, E., Clementini, G., Held, E. V., et al. 2008, *ApJ* , 685, 947
- Preston, G. W. 1959, *ApJ* , 130, 507
- Pritzl, B. J., Smith, H. A., Catelan, M., & Sweigart, A. V. 2002, *AJ* , 124, 949
- Pritzl, B. J., Smith, H. A., Stetson, P. B., et al. 2003, *AJ* , 126, 1381
- Putman, M. E., Staveley-Smith, L., Freeman, K. C., Gibson, B. K., & Barnes, D. G. 2003, *ApJ* , 586, 170
- Reid, M. J., Menten, K. M., Zheng, X. W., et al. 2009, *ApJ* , 700, 137
- Reitzel, D. B., & Guhathakurta, P. 2002, *AJ* , 124, 234
- Renault, C., Aubourg, E., Bareyre, P., et al. 1998, *A& A* , 329, 522
- Richardson, J. C., Irwin, M. J., McConnachie, A. W., et al. 2011, *ApJ* , 732, 76
- Ripepi, V., Barone, F., Milano, L., & Russo, G. 1997, *A& A* , 318, 797
- Rodríguez, E., & López-González, M. J. 2000, *A& A* , 359, 597
- Rubele, S., Kerber, L., Girardi, L., et al. 2011, arXiv:1110.5852
- Saha, A., Sandage, A., Tamman, G. A., et al. 2001, *ApJ* , 562, 314
- Sand, D. J., Olszewski, E. W., Willman, B., et al. 2009, *ApJ* , 704, 898
- Sandage, A. 1981, *ApJL* , 244, L23
- Sandage, A. 1981, *ApJ* , 248, 161
- Sandage, A. 1990, *J. Roy. Astron. Soc. Can.*, 84, 70
- Schlegel, D. J., Finkbeiner, D. P., & Davis, M. 1998, *ApJ* , 500, 525
- Schwarzenberg-Czerny, A. 1996, *ApJL* , 460, L107

- Searle, L., & Zinn, R. 1978, *ApJ* , 225, 357
- Shapley, H., & McKibben Nail, V. 1955, *Proceedings of the National Academy of Science*, 41, 829
- Shattow, G., & Loeb, A. 2009, *MNRAS* , 392, L21
- Schwarzschild, M., & Harm, R. 1970, *ApJ* , 160, 341
- Simon, J. D., & Geha, M. 2007, *ApJ* , 670, 313
- Simon, N. R., & Teays, T. J. 1982, *ApJ* , 261, 586
- Skillen, I., Fernley, J. A., Stobie, R. S., & Jameson, R. F. 1993, *MNRAS* , 265, 301
- Skrutskie, M. F., Cutri, R. M., Stiening, R., et al. 2006, *AJ* , 131, 1163
- Slater, C. T., Bell, E. F., & Martin, N. F. 2011, *ApJL* , 742, L14
- Smith, H. A., Silbermann, N. A., Baird, S. R., & Graham, J. A. 1992, *AJ* , 104, 1430
- Smith, H. A., & Wehlau, A. 1985, *ApJ* , 298, 572
- Sollima, A., Cacciari, C., & Valenti, E. 2006, *MNRAS* , 372, 1675
- Sollima, A., Cacciari, C., Arkharov, A. A. H., et al. 2008, *MNRAS* , 384, 1583
- Soszynski, I., Udalski, A., Szymanski, M., et al. 2002, *Acta Astron.* , 52, 369
- Soszyński, I., Poleski, R., Udalski, A., et al. 2008, *Acta Astron.* , 58, 163
- Soszyński, I., Udalski, A., Szymański, M. K., et al. 2008, *Acta Astron.* , 58, 293
- Soszyński, I., Udalski, A., Szymański, M. K., et al. 2009, *Acta Astron.* , 59, 1
- Soszyński, I., Poleski, R., Udalski, A., et al. 2010, *Acta Astron.* , 60, 17
- Soszyński, I., Udalski, A., Szymański, M. K., et al. 2010, *Acta Astron.* , 60, 165
- Soszyński, I., Udalski, A., Szymański, M. K., et al. 2010, *Acta Astron.* , 60, 91
- Stetson, P. B. 1987, *PASP* , 99, 191

- Stetson, P. B. 1994, PASP , 106, 250
- Storm, J., Gieren, W., Fouqué, P., et al. 2011, A& A , 534, A95
- Storm, J., Gieren, W., Fouqué, P., et al. 2011, A& A , 534, A94
- Stumpff, P. 1980, A& A Supp. , 41, 1
- Szewczyk, O., et al. 2008, AJ , 136, 272
- Szymanski, M. K. 2005, Acta Astron. , 55, 43
- Testa, V., Marconi, M., Musella, I., et al. 2007, A& A , 462, 599
- Tisserand, P., et al. 2007, A& A , 469, 387
- Toomre, A., & Toomre, J. 1972, ApJ , 178, 623
- Turon, C., Luri, X., & Masana, E. 2012, arXiv:1202.3645
- Udalski, A., Szymanski, M., Kaluzny, J., Kubiak, M., & Mateo, M. 1992, Acta Astron. , 42, 253
- Udalski, A., Szymanski, M., Kaluzny, J., et al. 1993, Acta Astron. , 43, 289
- Udalski, A., Kubiak, M., & Szymanski, M. 1997, Acta Astron. , 47, 319
- Udalski, A., Soszynski, I., Szymanski, M., et al. 1999, Acta Astron. , 49, 223
- Udalski, A., Soszynski, I., Szymanski, M., et al. 1999, Acta Astron. , 49, 437
- Udalski, A. 2003, Acta Astron. , 53, 291
- Udalski, A., Szymanski, M. K., Soszynski, I., & Poleski, R. 2008, Acta Astron. , 58, 69
- van Albada, T. S., & Baker, N. 1971, ApJ , 169, 311
- van den Bergh, S., & Mackey, A. D. 2004, MNRAS , 354, 713
- van der Marel, R. P., & Cioni, M.-R. L. 2001, AJ , 122, 1807

- van Leeuwen, F., Feast, M. W., Whitelock, P. A., & Laney, C. D. 2007, MNRAS , 379, 723
- Walker, A. R. 1994, AJ , 108, 555
- Wallerstein, G. 1970, ApJ , 160, 345
- Wallerstein, G. 2002, PASP , 114, 689
- Walsh, S. M., Jerjen, H., & Willman, B. 2007, ApJL , 662, L83
- Wechsler, R. H., Bullock, J. S., Primack, J. R., Kravtsov, A. V., & Dekel, A. 2002, ApJ , 568, 52
- Weiner, B. J., & Williams, T. B. 1996, AJ , 111, 1156
- Welch, D. L., Alcock, C., Allsman, R. A., et al. 1997, Variables Stars and the Astrophysical Returns of the Microlensing Surveys, 205
- Weldrake, D. T. F., Sackett, P. D., Bridges, T. J., & Freeman, K. C. 2004, AJ , 128, 736
- Westerlund, B. E. 1997, Book,,
- Willman, B., Blanton, M. R., West, A. A., et al. 2005, AJ , 129, 2692
- Willman, B., Dalcanton, J. J., Martinez-Delgado, D., et al. 2005, ApJL , 626, L85
- Woolley, R. V. D. R., Sandage, A. R., Eggen, O. J., et al. 1962, Royal Greenwich Observatory Bulletins, 58, 31
- Yanny, B., Newberg, H. J., Grebel, E. K., et al. 2003, ApJ , 588, 824
- York, D. G., Adelman, J., Anderson, J. E., Jr., et al. 2000, AJ , 120, 1579
- Zaritsky, D., Harris, J., Grebel, E. K., & Thompson, I. B. 2000, ApJL , 534, L53
- Zaritsky, D., & Harris, J. 2004, ApJ , 604, 167
- Zaritsky, D., Harris, J., Thompson, I. B., & Grebel, E. K. 2004, AJ , 128, 1606
- Zentner, A. R., & Bullock, J. S. 2003, ApJ , 598, 49

- Zhevakin, S. A. 1953, Astr. Zh. 30, 161
- Zinn, R., & Searle, L. 1976, ApJ , 209, 734
- Zinn, R. 1980, Globular Clusters, 191
- Zinn, R., & West, M. J. 1984, Astrop. J. Supp. , 55, 45
- Zucker, D. B., Belokurov, V., Evans, N. W., et al. 2006, ApJL , 643, L103
- Zucker, D. B., Belokurov, V., Evans, N. W., et al. 2006, ApJL , 650, L41